Characterising downwind particulate and sulfur dioxide air pollution from volcanic emissions

Rachel Cecilia Wallingford Whitty

Submitted in accordance with the requirements for the degree of
Doctor of Philosophy

The University of Leeds
School of Earth and Environment

September 2022

The candidate confirms that the work submitted is her own, except where work which has formed part of jointly authored publications has been included. The contribution of the candidate and the other authors to this work has been explicitly indicated below. The candidate confirms that appropriate credit has been given within the thesis where reference has been made to the work of others.

The work in Chapter 2 appears in the following publication:

Whitty, R. C. W., Ilyinskaya, E., Mason, E., Wieser, P. E., Liu, E. J., Schmidt, A., Roberts, T., Pfeffer, M. A., Brooks, B., Mather, T. A., Edmonds, M., Elias, T., Schneider, D. J., Oppenheimer, C., Dybwad, A., A, N. P., & Kern, C. (2020). Spatial and temporal variations in SO_2 and $PM_{2.5}$ levels around Kīlauea volcano, Hawai'i during 2007–2018 [DOI: https://doi.org/10.3389/feart.2020.00036]. *Frontiers in Earth Science*, *8*, 36

RW collated and processed the data from the air quality monitoring network and from the community-operated PurpleAir instruments, analysed the data, made the figures and wrote the first draft of the manuscript which was then edited from suggestions by co-authors. RW, EI, PW, EM and EL were involved in eruption-response fieldwork. EI was involved in discussions regarding the work, providing suggestions during the data processing and analysis. EI, AS, TR, MP, and TM contributed to data interpretation. The manuscript was edited in line with comments from two journal-appointed reviewers, Claudia Spinetti and Antonio Álvarez-Valero, and by the journal editor, Elisa Trasatti.

The work in Chapter 3 appears in the following publication:

Whitty, R., Pfeffer, M., Ilyinskaya, E., Roberts, T., Schmidt, A., Barsotti, S., Strauch, W., Crilley, L., Pope, F., Bellanger, H., Mendoza, E., Mather, T., Liu, E., Peters, N., Taylor, I., Francis, H., Hernández Leiva, X., Lynch, D., Nobert, S., & Baxter, P. (2022). Effectiveness of low-cost air quality monitors for identifying volcanic SO_2 and PM downwind from Masaya volcano, Nicaragua [DOI: https://doi.org/10.30909/vol.05.01.3359]. *Volcanica*, *5*(1), 33–59

RW collated and processed the data from the air quality monitoring network, analysed the data, made the figures and wrote the first draft of the manuscript which was then edited from suggestions by co-authors. MP and EI were involved in discussions regarding the work, providing suggestions during the data processing and analysis. EI,

HB, EM, NP, IT, PB, EL, TM and RW collected the field data through network set-up and maintenance. LC and FP contributed to PM humidity correction. SB and AS contributed to ECMWF forecast data. The manuscript was edited in line with comments from a journal-appointed reviewer, Peter Kelly.

Chapter 4 is a draft manuscript ready for submission. Therefore, the format of this thesis is in compliance with the requirements for thesis submission with the use of published material. Chapter 4 will be submitted to a journal with the following title and author list:

Whitty, R., Ilyinskaya, E., Barsotti, S., Pfeffer, M., Roberts, T., Schmidt, A., Jóhansson, Þ., Gilbert, G., Hjörvar, T., Þrastarson, R., Fecht, D., Sigurðsson, E., & Sæmundsson, G. (n.d.). SO_2 and PM air quality and Icelandic population exposure during the 2021 Fagradalsfjall eruption

RW collated and processed the data from the air quality monitoring network, analysed the data, made the figures and wrote the first draft of the manuscript which was then edited from suggestions by co-authors. IE and SB were involved in discussions regarding the work, providing suggestions during the data processing and analysis. SB provided CALPUFF model outputs and exposure probability data, which were then processed by RW to analyse population exposure, assisted by DF. RW and SB worked on the CALPUFF rescaling methodology. TH, GG and MP designed, built and maintained IMO's measurement and data systems. ÞJ contributed access to and information on the municipality AQ network. DF and RÞ assisted with ArcGIS ArcMap analysis methodology. GS supplied the data from footpath counters at the eruption site. ES facilitated use of satellite imagery. Kristín Björg Ólafsdóttir compiled wind data from the eruption site. All coauthors contributed to draft review and editing.

Rationale for Alternative Format

The rationale for the alternative format thesis is that each of the three projects uses different datasets, methods and analyses such that it is more appropriate to be presented as three separate papers rather than the traditional format of having separate methods, results and discussion chapters. Furthermore, with two published papers, the chapters meet the requirement for an alternative format thesis.

Chapter 2 and Chapter 3 are published manuscripts with the candidate as lead author and work in Chapter 4 is ready to submit with the candidate as the lead author. The chapters are the result of work from the candidate, with minor contributions of co-authors recognised earlier. These chapters meet the criteria for the alternative format thesis as described in the protocol for the submission of an alternative style doctoral thesis by the Faculty of Environment at the University of Leeds. A cohesive discussion on the main findings of the thesis and a general introduction is provided to add context to the work.

Acknowledgements

This PhD took 4 years, 5 months and 7 days from start to submission. The journey seemed long even before Coronavirus shut the world down, and then it seemed longer still. I'd like to thank all those who helped me along the way, especially those listed below.

To my supervisors Evgenia Ilyinskaya, Melissa Pfeffer, Tjarda Roberts and Anja Schmidt. Thank you for being there through it all, for advising me and for pushing opportunities into my path. Thank you also to Andy Hooper for keeping us on the right track. Evgenia, thanks for the impromptu field-trips - the 11-day notice before flying out to Nicaragua certainly set the PhD off to a whirlwind start!

A huge thank you goes to the IGT department. It makes such a difference to work in an environment that is welcoming and friendly. IGT coffee mornings, IGT monthly bakeoffs and IGT Friday beers were the perfect temporary distractions from work.

To the SEE badminton club. Turns out that whacking a shuttle as hard as you can is a great way to vent PhD frustration, even when the shuttle goes straight into the net.

One of the most positive things I've found on this PhD journey have been the friends I've made along the way, especially Thirze Hermans, Jamie Ward, Itahisa Gonzalez Alvarez, Maeve Murphy Quinlan, Edna Dualeh, Roxana Stanca and Iris van Zelst. Thank you so much for making these few years many times more enjoyable than they otherwise would have been, for all the laughter, tears, jokes, adventures and stories along the way.

To Matt Nesbitt, who made the last 16 months of my PhD possible, believing in me when I lacked belief in myself. Your wacky sense of humour and contagious laughter always make the world seem brighter.

To my brother William for software and coding advice. And for sending photos and news from exotic places during Covid lockdown - it was good to know that the world still existed beyond what I could see from my desk.

To my elder sister Harriet and my nieces Lena, Piroschka and Annie, and my nephew

Arthur. Thank you for reminding me that life goes on outside academia. And for all the drawings of me on a volcano you sent.

To my younger sister Rose for her endless advice and patience. For years of virtual movie nights, even before virtual movie nights were a thing. For making me laugh and supporting me when I cried.

To my parents, Marion and Tom, for always being there no matter what. Mum thank you for the countless haircuts and for always knowing how to cheer me up when I needed it. Dad thank you for reading all my papers, even when they must surely have sent you to sleep. You've both given me the determination to keep going with this PhD right to the end, and to laugh despite the difficulties.

And lastly, to Arthur, the cat.

Abstract

One of the hazards of volcanic eruptions is the emission of gas and aerosol into the atmosphere, which can cause damage to the environment and human health as well as impacting climate. Emissions from effusive volcanic eruptions and passively degassing volcanoes typically remain in the troposphere where they are advected by the wind and can cause deterioration to air quality across a downwind region. Of the emitted gases, sulfur dioxide (SO_2) is often highly concentrated with respect to the background atmosphere and has important air quality and environmental consequences. Over time after emission from the volcanic source, SO_2 may be converted to sulfate aerosols through atmospheric processes, leading to additional air quality concerns with an increase in fine particulate matter (PM).

This thesis aims to characterise the SO_2 and PM air quality in regions downwind of tropospheric volcanic emissions. Three study sites are examined; Kīlauea volcano on the Island of Hawai'i, Masaya volcano in Nicaragua and Fagradalsfjall volcano in Iceland. The SO_2 and PM concentrations in the downwind regions are monitored using highly-accurate reference-grade air quality instruments, and a variety of lower-cost miniaturised sensors. Low-cost sensors are increasingly used for air quality measurements, and in this thesis I investigate their effectiveness for monitoring in volcanic environments. Low-cost sensors are used at Masaya volcano as a first-attempt to establish an air quality monitoring network. At Kīlauea volcano, a long time-series of SO_2 and PM data is examined to determine air quality deterioration during a period of extremely heightened volcanic activity. At Fagradalsfjall volcano, the impact of a small eruption in proximity to densely-populated areas is examined and the population exposure to volcanic SO_2 is estimated using a plume dispersion model. These studies increase the knowledge of SO_2 and aerosol dispersal from volcanic sources, especially for those communities in the affected areas.

Contents

List of Figures

List of Tables

Nomenclature

Abbreviations and symbols

SO_2	Sulfur dioxide
SO_4	Sulfate aerosol
H_2SO_4	Sulfate aerosol
-OH	Hydroxyl radical
O_3	Ozone
H_2O_2	Hydrogen peroxide
PM	Particulate Matter
PM_1	PM with particle diameter $<$ 1 µm
$PM_{2.5}$	PM with particle diameter $<$ 2.5 µm
PM_{10}	PM with particle diameter $<$ 10 µm
RH	Relative humidity (%)
ppmv	Parts per million volume
ppbv	Parts per billion volume

Acronyms

VAP	Volcanic air pollution
VAPE	Volcanic air pollution episode
ERZ	East Rift Zone
LERZ	Lower East Rift Zone
HDOH	Hawai‘i Department of Health
NPS	National Park Service

IMO	Icelandic Meteorological Office
INETER	Instituto Nicaragüense de Estudios Territoriales
SINAPRED	National System for Disaster Prevention, Mitigation and Attention
UNRESP	"Unseen but not unfelt: resilience to persistent volcanic emissions" Global Challenges Research Fund
WHO	World Health Organisation
EC	European Commission
ID	Icelandic Directive
EPA	Environmental Protection Agency
NAAQS	National Ambient Air Quality Standards set by the EPA
FEM	EPA Forum for Environmental Measurements
NOAA	National Oceanic and Atmospheric Administration
CALPUFF	California Puff Model
HYSPLIT	Hybrid Single-Particle Lagrangian Intergrated Trajectory model
WRF-ARW	Weather Research and Forecasting Advanced Research numerical model
ECMWF	European Centre for Medium-Range Weather Forecasts

Instrument abbreviations

43i	Pulsed fluorescence spectroscopy SO_2 analyser, reference-grade
BAM	Beta attenuation monitor
BAM-1020	BAM instrument, reference-grade
OPC	Optical particle counter
OPC-N2	Low-cost optical particle counter model
Plantower PMS	Low-cost miniaturised particle counter model
SO2-B4	Low-cost electrochemical SO_2 sensor

Pollutant health thresholds

SO_2: 195 µg/m^3	EPA NAAQS for hourly exposure, 2010
SO_2: 366 µg/m^3	EPA threshold for 24-hour exposure (Hawai‘i), pre-2010
SO_2: 40 µg/m^3	WHO threshold for 24-hour exposure, 2021
SO_2: 125 µg/m^3	EC threshold for 24-hour exposure, 2018
SO_2: 350 µg/m^3	ID threshold for hourly exposure, 2016
$PM_{2.5}$: 35 µg/m^3	EPA NAAQS for 24-hour exposure, 2010
$PM_{2.5}$: 25 µg/m^3	WHO threshold for 24-hour exposure, 2005
$PM_{2.5}$: 15 µg/m^3	WHO threshold for 24-hour exposure, 2021
PM_{10}: 50 µg/m^3	ID threshold for 24-hour exposure, 2016

Mathematical notation

S_{gas}	Sulfur component of the volcanic SO_2 mass concentration (µg/m^3)
S_{total}	Sum of sulfur components of volcanic SO_4^{2-} and SO_2 mass concentrations (µg/m^3)
t	Age of the volcanic cloud (seconds)
$-k$	First-order decay constant
ρ_p	Density of the dry particles
a_w	water activity (RH/100)
κ	Particle hygroscopicity
m	Wet aerosol mass
m_0	Dry aerosol mass
C	Humidity correction factor
PM_{Corr}	Corrected aerosol mass
PM_{Raw}	Raw aerosol mass

Chapter 1

Introduction

This thesis focuses on particulate and sulfur dioxide (SO_2) air pollution from volcanic emissions, both during active volcanic eruptions and as a result of passive degassing. In order to give context to the work I present later, in this introductory chapter I discuss background information regarding volcanic emissions, conversion of SO_2 to sulfate aerosols and the health issues which can result from exposure to these pollutants [Sections 1.1 to 1.3]. I then discuss systems for monitoring of SO_2 and particulate concentrations, including recent developments in low-cost sensors and instrumentation [Sections 1.4 to 1.5]. Following this, I conclude with a brief overview of the three study sites to give a broader context for understanding Chapters 2, 3 and 4 [Sections 1.7 and 1.8] and a discussion of the novelty and scientific contribution of this thesis.

1.1 Volcanic pollutant emissions

One of the widespread hazards associated with active volcanoes and volcanic eruptions is the gases and aerosols which are emitted into the atmosphere. These emissions can lead to long-term climatic impacts (Langmann, 2014; Robock, 2000; von Glasow et al., 2009), damage to the environment (Delmelle et al., 2002; Martınez et al., 2000) and affect air quality and human health (Carlsen et al., 2021a; Carlsen et al., 2021b; Hansell and Oppenheimer, 2004; Longo et al., 2008) [Section 1.3]. The impact of these volcanic emissions is strongly influenced by their injection height into the atmosphere. Explosive volcanic eruptions can inject volcanic pollutants into the stratosphere, where they can have a significant impact on regional to global climate. One such example is the 1991 VEI 6 eruption of Pinatubo volcano in the Philippines, which released an estimated 20 million tons of SO_2 into the stratosphere with a plume height of 30 km (Bluth et al., 1992; McCormick et al., 1995). Volcanic aerosols and gases in the stratosphere can result in stratospheric warming via reflecting some of the incoming solar radiation, which in turn results in a cooling of the Earth's surface (Robock, 2000; Swingedouw et al., 2017;

Timmreck, 2012). In contrast, effusive volcanic eruptions typically produce emissions which remain in the troposphere where they can impact air quality and cause damage to the downwind environment and impact the health of exposed individuals. This thesis is concerned with the volcanic emissions from effusive eruptions and passively degassing volcanoes where the emissions remain in the troposphere.

Emissions from active volcanoes are typically a complex and evolving cocktail of gases, aerosols and ash (Langmann, 2014; Oppenheimer and McGonigle, 2004; Oppenheimer et al., 2010; Pfeffer et al., 2006b; von Glasow et al., 2009). Of the gases emitted (which commonly include H_2O, CO_2, SO_2, HCl, HF and H_2S), sulfur dioxide (SO_2) is often the focal point of volcanic gas monitoring due to its high concentration in volcanic plumes compared to the background atmosphere, as well as its importance with respect to environmental, climatic and air quality impacts (Cadle et al., 1971; Lambert et al., 1988; Loughlin et al., 2012; Schmidt et al., 2015). The mass of SO_2 emitted during volcanic eruptions can vary greatly, along with the size and style of the eruption. During the 2014 - 2015 Holuhraun eruption in Iceland, the total emitted SO_2 was estimated to be 9.6 Mt, which is between 1.5 to 2 times more than the total anthropogenic emissions from the European Economic Area in 2011 (Ilyinskaya et al., 2017). Fluxes of SO_2 in such magnitudes can have serious implications for air quality and human health, not just in the surrounding area but across many kilometers downwind of the eruption (Carlsen et al., 2021a; Carlsen et al., 2021b; Ilyinskaya et al., 2017; Schmidt et al., 2015).

Once SO_2 is emitted into the atmosphere, it begins to undergo chemical conversion through a variety of reaction pathways to form secondary aerosols such as sulfate aerosol, H_2SO_4 (Allen et al., 2002; Delmelle et al., 2002; Stockwell and Calvert, 1983; Tam et al., 2016) [Section 1.2]. Sulfate aerosols in volcanic plumes are found both as primary aerosols (Mather et al., 2003), emitted directly from the volcanic source, and secondary aerosols resulting from the chemical conversion of gaseous SO_2 (Allen et al., 2002; Cadle et al., 1971; Stockwell and Calvert, 1983). The conversion of SO_2 to sulfate aerosol leads to a contrast between a "primitive" plume, which is comprised of a high gas:aerosol ratio, and a "mature" plume which has a low gas:aerosol ratio (Carlsen et al., 2021a; Ilyinskaya et al., 2017) [Figure 1.1]. This contrast in plume characteristics with increasing time since emission from the source can lead to different air quality and health concerns across the dispersal distance from the volcano [Section 1.3].

1.2 SO_2 conversion to sulfate aerosols

Volcanic aerosols (aerosols are suspensions of fine solid or liquid droplets in gas) are released as primary aerosols at the volcanic vent and are also formed as secondary aerosols via the conversion of volcanic gases in the atmosphere (Allen et al., 2002; Cadle et al., 1971; Mather et al., 2003; Stockwell and Calvert, 1983). There are a variety of

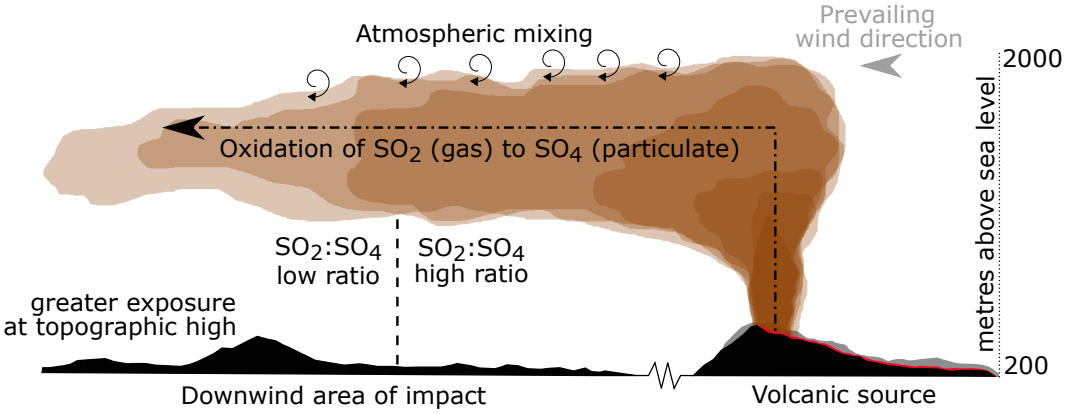

Figure 1.1: Schematic representation of the dispersal of volcanic pollutants following emission from source. Emission at source has a high ratio of gaseous SO_2 to sulfate aerosol (SO_4) and is considered a "primitive" volcanic plume. Chemical conversion of SO_2 to SO_4 during the exposure time in the atmosphere leads to a gradual transition to a low ratio of gaseous SO_2 to aerosol, at which point the plume is considered "mature". Dispersal of volcanic pollutants follows the wind direction, leading to exposure of a downwind area of impact. Regions with a higher topography downwind of the volcanic source are likely to be exposed to higher concentrations of pollutants. Note: not to scale.

species of volcanic aerosols, but here I discuss sulfate aerosols formed via the conversion of SO_2 gas, or released directly from the volcanic vent, which are the aerosols this thesis is primarily concerned with.

Once SO_2 is released into the atmosphere it is affected by both chemical and physical processes, including reactions with liquid- and solid-state suspended particles, leading to the conversion of SO_2 gas to sulfate aerosols (Allen et al., 2002; Stockwell and Calvert, 1983). In the stratosphere, the lifetime of SO_2 gas can extend to a year (Thomason and Peter, 2006). In the troposphere, the lifetime of SO_2 gas is generally considered to be several days to a week until the vast majority has been converted to sulfate aerosols or removed from the atmosphere via other pathways (Allen et al., 2002; Pattantyus et al., 2018; Pfeffer et al., 2006b; Rotstayn and Lohmann, 2002). In this thesis, I focus on volcanic emissions to the troposphere and, as such, the following discussion of the conversion of SO_2 gas to sulfate aerosols relates to tropospheric pathways. The rate of SO_2 conversion is dependent on the relative humidity and temperature of the atmosphere, as well as interactions with clouds and the availability of oxidants (Oppenheimer et al., 1998; Saxena and Seigneur, 1987). There are two main reaction pathways which gaseous SO_2 may undergo to convert to sulfate aerosol: the gas-phase route or the aqueous-phase route (Galeazzo et al., 2018; Pattantyus et al., 2018).

The gas-phase conversion route centres on the availability of the hydroxyl radical, -OH (Rattigan et al., 2000; Stockwell and Calvert, 1983). This oxidising agent is extremely reactive and is formed primarily via photolytic reactions with ozone (O_3),

meaning that it has diurnal and seasonal cycles depending on the availability of light (Kroll et al., 2015; Pattantyus et al., 2018). It has been estimated that the SO_2 conversion rate via the gas-phase pathways during daylight hours is 0.8 to 5% h^{-1}, two orders of magnitude higher than during the night when -OH is limited (Kroll et al., 2015; Pattantyus et al., 2018). In volcanic plumes the concentration of SO_2 is likely to be considerably higher than the concentration of -OH, and as a result the conversion rate will be limited by the availability of -OH (Galeazzo et al., 2018; Pattantyus et al., 2018). When there is a sufficient presence of the hydroxyl radical in the atmosphere, gaseous SO_2 may convert to the sulfate aerosol, H_2SO_4, via the following gas-phase reaction pathways (Cadle et al., 1971; Pattantyus et al., 2018; Stockwell and Calvert, 1983):

$$-OH + SO_2 \longrightarrow HOSO_2 \tag{1.1}$$

$$HOSO_2 + O_2 \longrightarrow SO_3 + HO_2 \tag{1.2}$$

$$SO_3 + H_2O \longrightarrow H_2SO_4 \tag{1.3}$$

Conversion can also occur when SO_2 in the atmosphere encounters a cloud, is dissolved into the water vapour and undergoes oxidation via aqueous-phase pathways (Monn and Schaeppi, 1993; Pattantyus et al., 2018). When SO_2 dissolves in water it forms a weak acid before undergoing dissociation to form either HSO_3 or SO_3 (Pattantyus et al., 2018). Aqueous sulfate formation may then occur as a result of the dissolved SO_2 undergoing hydrolysis and reacting with hydrogen peroxide (H_2O_2) or ozone, the two most likely oxidants for SO_2 in the aqueous phase, in one of the following reaction pathways (Green et al., 2019; Khoder, 2002; Saxena and Seigneur, 1987):

$$SO_3 + O_3 \longrightarrow SO_4 + 2\,H \tag{1.4}$$

$$HSO_3 + H_2O_2 \longrightarrow SO_4 + H \tag{1.5}$$

The pH of the water is a controlling factor as to which aqueous-phase reaction pathway is followed. O_3 becomes the leading oxidant at pH $>$ 5.5, whereas H_2O_2 reactions occur effectively at pH levels between 2 - 6 (Galeazzo et al., 2018; Green et al., 2019; Pattantyus et al., 2018). The solubility of SO_2 in water increases at lower temperatures and at neutral pH levels (Pattantyus et al., 2018). It has been estimated that the aqueous-phase conversion of SO_2 may be as high as 3 - 50% s^{-1}, though this

high conversion rate is unsustainable over time due to depletion of the limiting reactant and the parcel of air moving rapidly through and out of the cloud (Galeazzo et al., 2018; Pattantyus et al., 2018).

Both gas-phase and aqueous-phase oxidation pathways are important in the conversion of SO_2 to sulfate aerosols in the atmosphere (Saxena and Seigneur, 1987). Aqueous-phase reactions occur more readily under high-humidity conditions and dominate the sulfate formation process during nighttime when gas-phase pathways are reduced (McMurry and Wilson, 1982; Middleton et al., 1980).

1.3 Health impacts of volcanic emissions

Globally, over one billion people are estimated to live within 100 km of a volcano that has erupted in the Holocene (Freire et al., 2019). Among the hazards of active volcanoes are the emissions of gases and aerosols which can have far-reaching implications for human and animal health, the environment and agriculture (Carlsen et al., 2021a; Delmelle et al., 2002; Longo et al., 2008; Schmidt et al., 2011; Stewart et al., 2022). Large volcanic eruptions can release sufficient amounts of gases and aerosols to result in chronic hazards with long-lasting impacts to populations hundreds of km away from the source (Carlsen et al., 2021b; Schmidt et al., 2011). Here I will discuss some of the human health impacts which can occur following exposure to SO_2 gas and to sulfate aerosols.

SO_2 is considered an irritant gas in that it can cause inflammation of the eyes, throat, nose and lungs even at low concentrations (Miller, 2004; Williams-Jones and Rymer, 2015). Asthmatic individuals and those with pre-existing cardiac or respiratory health conditions are particularly vulnerable to exposure to SO_2 (ATSDR, 1998; CRI, 2004). Asthmatic individuals exposed to SO_2 mass concentrations at or above $1310\,\mu g/m^3$ for a three minute duration are likely to experience a respiratory attack (ATSDR, 1998; Balmes et al., 1987). In healthy adult individuals, exposure to high concentrations of SO_2 ($2620\,\mu g/m^3$) for greater than 10 minutes results in a 70 to 75% increase in breathing resistance and associated coughing (ATSDR, 1998; Frank et al., 1962). Concentrations of SO_2 at this level are commonly measured in proximity to active volcanic craters (D'Alessandro, 2006; Elias and Sutton, 2007; Ng'walali et al., 1999). Emissions of SO_2 in high concentrations at volcanic vents are dangerous to the millions of geotourists who visit volcanic sites each year (Heggie, 2009). At Mt Aso in Japan and at Hawaii Volcanoes National Park, the deaths of several visitors have occurred as a result of asthmatic or cardio-respiratory compromised individuals being exposed to SO_2 from volcanic vents (D'Alessandro, 2006; Heggie, 2009; Ng'walali et al., 1999). SO_2 can also have serious health implications to individuals living downwind of volcanic eruptions, with multiple studies indicating the effects of prolonged exposure to SO_2 even in dilute concentrations (Baxter et al., 1982; Carlsen et al., 2021b; Longo

et al., 2008; Longo, 2013; Mannino et al., 1996; Michaud et al., 2005; van Manen, 2014).

Exposure to sulfate aerosols can similarly result in irritation of the eyes and respiratory tract, as well as restricted lung action and aggravation of pre-existing respiratory conditions (Carlsen et al., 2021b; Hansell and Oppenheimer, 2004; Schlesinger, 1985; Williams-Jones and Rymer, 2015). Sulfate aerosols are a major component of volcanic particulate matter (PM) (Allen et al., 2002; Delmelle et al., 2002; Stockwell and Calvert, 1983; Tam et al., 2016). PM is commonly sub-divided into size categories of PM_1, $PM_{2.5}$ and PM_{10} (PM with particle diameters $<$1 µm, $<$2.5 µm and $<$10 µm, respectively). Particles sized between 2.5 to 10 µm are described as "coarse" PM and are generally deposited in the upper airways, whereas particles below 2.5 µm in size are termed "fine" and are capable of reaching the deepest parts of the lung (Quality of Urban Air Review Group, 1996). Volcanic aerosol is typically very fine ($<$1 µm diameter) (Ilyinskaya et al., 2021; Ilyinskaya et al., 2017; Martin et al., 2011; Mason et al., 2021) giving it the potential to reach deep into the lung once inhaled, though research into the physical impacts of volcanic aerosol are extremely limited (Schlesinger et al., 2006). PM is widely known to cause significant health issues, with the global burden of ambient $PM_{2.5}$ amounting to $>$ 3 million premature deaths each year (Lim et al., 2012). PM is especially linked to increased death from respiratory and cardiovascular diseases (Holgate, 2017) and recent studies have investigated a relationship between exposure to PM and a decline in short-term cognitive abilities (Gao et al., 2021; Shehab and Pope, 2019). Vulnerable populations particularly at risk to PM are children and elderly population groups, as well as those with pre-existing health conditions (Bateson and Schwartz, 2007; Bennett et al., 2007; Herbarth et al., 2001; World Health Organization, 2005).

As discussed in Sections 1.1 and 1.2, once released into the atmosphere, SO_2 gas will gradually undergo conversion to sulfate aerosols. Over time, the volcanic plume will undergo a transition from being predominantly composed of SO_2 gas to having a higher concentration of particulate components [Figure 1.1]. With this being the case, the health impacts of volcanic plumes can shift across the dispersal distance. Carlsen et al., 2021a and Carlsen et al., 2021b investigated the exposure of populated areas to primitive and mature volcanic plumes during the 2014 - 2015 Holuhraun eruption in Iceland, finding that the two plume types had independent effects on respiratory health outcomes in terms of uptake of asthma medication and emergency hospital visits for respiratory diseases. Chapter 2 discusses an example of plume dispersal causing exposure to varying pollutants across the downwind area. During the 2018 eruption of Kīlauea volcano on the Island of Hawai‘i, air quality stations between 40 to 100 km from the volcanic source recorded concentrations of SO_2 above health thresholds, and those stations further afield recorded concentrations of PM above health thresholds (Whitty et al., 2020).

To facilitate reducing the potential impacts of air quality on human health, govern-

ment agencies and health organisations around the world put forward recommendations for the maximum concentrations of pollutants which people may be exposed to (Icelandic Directive 2016; EPA, 2010; EPA, 2013; EC, 2018; WHO, 2021). For example, the World Health Organization (WHO) recommends a limit of $15\,\mu g/m^3$ as a daily-mean for $PM_{2.5}$ exposure, and a limit of $40\,\mu g/m^3$ as a daily-mean for SO_2 exposure (WHO, 2021). Recommended thresholds concerning SO_2 mainly relate to SO_2 from anthropogenic emissions, though the thresholds may also be exceeded during periods of volcanic unrest if volcanic emissions contribute significantly to the local or regional air pollution. These recommended thresholds for SO_2 and PM vary across countries, but offer a yardstick by which air quality can be compared spatially and temporally. When a volcanic eruption causes the air quality in an area to be consistently or sporadically above threshold values, there are potential mitigations which can be implemented to reduce health impacts. During the 2018 eruption of Kīlauea volcano, official government advice during periods of extreme degassing included remaining indoors, closing windows and recirculating air within buildings (Hawaii Emergency Management Agency, 2018). Where these steps are impractical (Horwell and Elias, 2020), mitigation advice may focus more on avoiding excess physical activity to reduce respiratory exposure to pollutants (Pohl 1998; Williams-Jones and Rymer 2015; IVHHN, 2020). Some arguments may be posed for distribution of face-masks during periods of extreme air pollution. However, face-masks come with additional complications associated with training the population in their use, the difficulties of effective distribution to communities, as well as the potential that those wearing face-masks may experience a false sense of security (McDonald et al., 2020). In environments were volcanic emissions form a significant contribution to the local or regional air quality, effective monitoring of the pollutants is a crucial step towards understanding and mitigating health impacts on exposed communities.

1.4 Monitoring of volcanic pollutants

Volcanic pollutants may be measured by a number of different techniques and approaches. SO_2 in volcanic plumes has been very successfully monitored via satellites (Carn et al., 2016; Carn et al., 2017; Krueger et al., 1990; Theys et al., 2013) [Section 1.6.2], via ultraviolet spectrometers such as the COSPEC (Elias et al., 2006; Stoiber and Jepsen, 1973; Sutton et al., 2001), FLYSPEC (Horton et al., 2006; Nadeau and Williams-Jones, 2009; Williams-Jones et al., 2006) and DOAS (Galle et al., 2003; Kern et al., 2020; McGonigle et al., 2002), as well as via SO_2 cameras (Burton et al., 2015; Kern et al., 2015a; Kern et al., 2015b; Mori and Burton, 2006). Measurements of volcanic aerosols and particulates have been successfully recorded using direct sampling instruments such as cascade impactors and filter packs (Ilyinskaya et al., 2021; Martin et al., 2011; Mason et al., 2021), as well as by aerosol spectrometers such as GRIMM

(Bukowiecki et al., 2011; Ilyinskaya et al., 2017; Martin et al., 2009).

In this thesis, highly accurate measurements of SO_2 and PM are made via reference-grade air quality instruments [Sections 1.4.1 and 1.4.2]. These instruments are used by government agencies and organisations around the world to monitor urban, industrial and volcanic ambient air quality. In the below sections [1.4.1 and 1.4.2] I will discuss reference-grade ground-based measurement systems which were used for data collection in the following chapters of this thesis, to provide an understanding of the instruments' operating principles and how they compare with respect to the lower-cost sensors.

1.4.1 Ground-based monitoring of SO_2

Pulsed fluorescence spectroscopy analysers are widely used to monitor concentrations of SO_2 in reference-grade air quality monitoring networks. The analysers operate on the principle that SO_2 molecules absorb ultraviolet (UV) light at one wavelength before reducing to a lower energy state where they emit UV light at a different wavelength (Mohn and Emmenegger 2001; Thermo Scientific, 2015). SO_2 molecules are excited by the radiation of a UV lamp, typically at a wavelength of between 190 to 230 nm (Luke 1997; Mohn and Emmenegger 2001; Thermo Scientific, 2015). As the energy levels of the excited SO_2 molecules decay, they emit UV light in a different wavelength, typically between 240 to 420 nm, with the amount of light emitted being proportional to the concentration of SO_2 present in the sampled air (Mohn and Emmenegger, 2001; Okabe et al., 1973). The UV light in the 240 to 420 nm range is detected by a photomultiplier tube and the concentration of SO_2 in the atmosphere is calculated (Thermo Scientific, 2015). Measurement interference from fluorescent hydrocarbons in the sampled air are removed by a hydrocarbon kicker in the sample inlet, which removes hydrocarbons but leaves SO_2 molecules untouched (Mohn and Emmenegger 2001; Thermo Scientific, 2015). This method provides very precise measurements of SO_2 down to very low concentrations in the ppbv range (parts per billion volume) (Thermo Scientific, 2010).

Thermo Fisher Scientific produce the 43i pulsed fluorescence spectroscopy analyser which has been FEM-designated by the EPA for measurements of SO_2 in the ambient atmosphere (Thermo Scientific, 2010; EPA, 2016). The FEM (Forum for Environmental Measurements) ensures that measurements are scientifically rigorous and recommends instruments which record data of a known and documented quality (EPA, 2016). A single pulsed fluorescence spectroscopy SO_2 analyser costs in the range of £8,000 to £12,000 ($\approx$ US$10,900 to US$16,300) depending on the configuration (quote from Thermo Fisher Scientific, 2021). The instrument weighs 21.8 kg with dimensions of 430 x 220 x 580 mm and must be kept in an air-conditioned enclosure with regular bi-annual multi-point calibration checks (Thermo Scientific, 2010).

1.4.2 Ground-based monitoring of particulates

Beta ray attenuation is a technique used frequently to measure particulates in reference-grade air quality monitoring networks. This method records the concentration of particulate in the atmosphere per cubic metre of air over a measurement period of one hour (Met One, 2008). At the beginning of the sample time, a carbon-14 element emits a source of constant high-energy electrons known as beta rays through to a small area onto a clean glass tape strip (Met One, 2013). To determine a zero particulate reading, the beta rays on the tape are detected and counted by a highly sensitive scintillation detector, commonly a photomultiplier tube (Gobeli et al. 2008; Met One, 2008). The glass tape is then advanced to an area where sampled ambient air is passed across it by means of an external pump, causing the tape to become loaded with particulate matter (Met One, 2013). Prior to reaching the glass tape, the sampled air is passed through size-selective inlets to ensure that only particles within the size-fraction of interest are sampled (Chung et al. 2001; Met One, 2013). After the sampling duration is complete, the glass tape is returned to the scintillation detector where the sampled particulate causes attenuation of the beta ray signal (Chung et al., 2001). The magnitude of ray attenuation increases with respect to the volume of particulate on the glass tape, allowing determination of the particulate mass concentration which was sampled during the measurement time (Gobeli et al. 2008; Met One, 2013).

When the sampling time occurs during periods of high humidity ($>$ 60% RH), beta attenuation monitors can over-read concentrations of particulate in the atmosphere by up to 20-50% as a result of accumulation of moisture on the glass tape (Gobeli et al., 2008). To prevent this occurring, Beta attenuation monitors (BAM) are fitted with heater systems which automatically warm the air when humidity exceeds a user-defined value (Chung et al., 2001; Gobeli et al., 2008). Heating of the air removes the moisture before it can accumulate on the glass tape, allowing BAM instruments to operate effectively even under high-humidity conditions (Chung et al. 2001; Met One, 2013). Baseline drift in BAM instruments is limited as the glass tape is advanced after each measurement period and a zero particulate reading is taken prior to the sample being exposed to the ambient air (Chung et al., 2001).

BAM instruments are widely used to measure particulate matter in the PM_1, $PM_{2.5}$ and PM_{10} size fractions (Schweizer et al., 2016). In particular, BAM-1020 (manufactured by Met One Instruments Inc) has been assigned by the EPA as a FEM-designated instrument to promote consistency in laboratory conditions and measurements, and to ensure that instruments are of reference-grade quality (EPA, 2016). In order to maintain long-term stability, BAM instruments are kept in air-conditioned enclosures and require a stable mains-power supply to operate (Met One, 2008). BAM-1020 instruments cost approximately £17,000 ($\approx$ US$23,200) (quote from Enviro Technology Services Ltd, 2021), and the instruments weigh 24.5 kg and measure 310 x 430 x 400 mm without

external attachments (Met One, 2013). As with pulsed fluorescence spectroscopy analysers [Section 1.4.1], the size, weight and required measurement infrastructure of the BAM-1020 limits the portability of the instrument. The combined cost of the instruments themselves and the costs associated with construction of monitoring enclosures gives both the BAM-1020 and the 43i spectroscopy analyser a high financial burden in comparison to low-cost monitoring systems [Section 1.5].

1.5 Low-cost monitoring systems

In this section I will discuss low-cost sensors and instruments which have been used by many studies, and in the following chapters of this thesis, as alternatives to the reference-grade instrumentation detailed in Section 1.4. In particular I will focus here on electrochemical sensors for the detection and monitoring of target gases, and miniaturised particle sensors for determining the concentration of particles of varying size modes. It should be noted that these low-cost instruments come with both advantages and disadvantages for monitoring air quality, and these shall also be discussed below.

1.5.1 Electrochemical gas sensors

Electrochemical gas sensors provide a method of gas monitoring that is low-cost as well as operating on low power requirements (Hagan et al., 2018; Mead et al., 2013; Popoola et al., 2016). Each sensor (approximately 32 mm in diameter) contains a porous membrane through which the target gas diffuses and enters a series of chambers containing electrolyte solution where the gas is oxidised or reduced depending on its chemical formula (Roberts et al., 2012) [Figure 1.2]. The resulting differences in the chemical potential, proportional to the concentration of the target gas diffused into the sensor, is detected by three electrodes which transmit the signal electronically to an external control system, such as a Raspberry Pi (Austin et al., 2006). The system is diffusion-controlled and the porous membrane must be exposed to flowing air, either to the atmosphere directly or via means of continuously-flowing sampled air pumped into a measurement chamber (Lewis et al., 2016; Roberts et al., 2012). As well as the target gas, other gases can diffuse into the electrochemical sensor. This results in an additional current response causing interference in the accuracy of the measurement and is known as cross-sensitivity (Austin et al., 2006; Hagan et al., 2018; Roberts et al., 2012; Roberts et al., 2014). Cross-sensitivies can result from gases to which the sensitivity is known and measured, but also to other atmospheric species to which the sensitivity is unknown and unmeasured (Alphasense, 2021; Lewis et al., 2016). Sensor performance can also be impacted by changes in temperature and humidity (Mead et al., 2013; Roberts et al., 2014), as well as a long-term drift in measurement accuracy related to the evaporation of the internal electrolyte solution (Hagan et al., 2018; Mead et al., 2013; Smith et al., 2017).

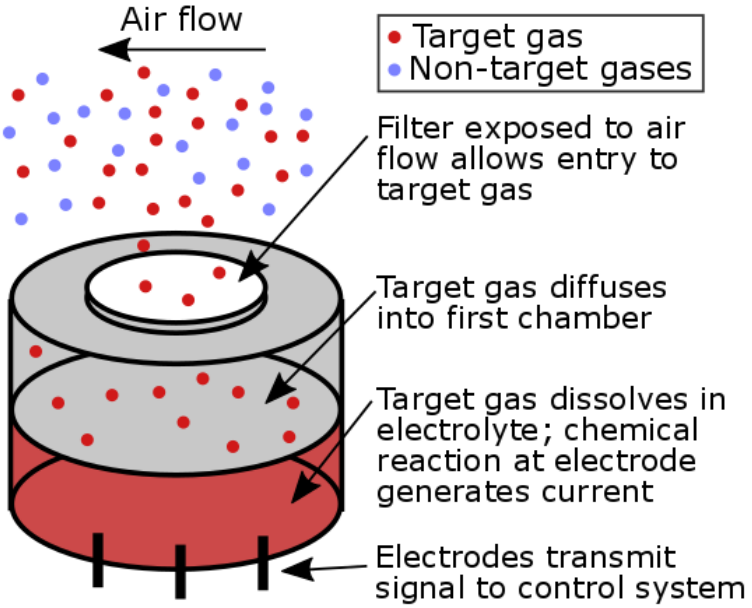

Figure 1.2: Schematic representation of an electrochemical gas sensor. Target gas diffuses through the filter which is exposed to the airflow. The target gas is dissolved into the electrolyte and causes chemical reactions which generate a current at the three electrodes (working, auxiliary and reference), which in turn pass the signal on to the measurement control system. Adapted from Roberts et al., 2012.

Electrochemical gas sensors were first patented at the end of the 20th Century (Miller, 2004), and have since been produced by a number of atmospheric-measurement companies, including the B4 series by Alphasense Ltd (Alphasense, 2021). They have been effectively used as monitoring systems for industrial and urban air quality (Austin et al., 2006; Cross et al., 2017; Mead et al., 2013). Electrochemical sensors were also incorporated into Multi-GAS (Multi-component Gas Analyzer System) for use in measuring the concentrations of gases at volcanic vents and fumaroles (Aiuppa et al., 2005; Shinohara, 2005). The Multi-GAS system has been successfully used at volcanoes around the globe to monitor gas concentrations in ppmv (parts per million volume) concentrations in near-source plumes (Aiuppa et al., 2007; Aiuppa et al., 2018; Roberts et al., 2012; Roberts et al., 2017; Shinohara et al., 2008; Witt et al., 2008). Electrochemical sensors have also been demonstrated to measure gases at sub-ppmv levels in more dilute atmospheric conditions (Hagan et al., 2018; Mead et al., 2013; Roberts et al., 2018).

Electrochemical sensors provide significant advantages for monitoring of air quality in compact systems. They are small and lightweight ($<$ 13 g per sensor) allowing use in portable systems, such as Multi-GAS, where ease of transportation is critical to reach remote or challenging measurement locations (Aiuppa et al., 2005; Shinohara, 2005). They are low-cost ($\approx$ £60 per sensor, 2022 quote from Alphasense Ltd.), reducing the infrastructure cost of air quality monitoring and allowing the potential for multiple sensor

deployment around an emission source at a relatively low financial burden. However, use of electrochemical sensors for air quality monitoring needs to be carefully approached as they can have issues associated with cross-sensitivities to non-target gases, accuracy reliance on stable temperature and humidity conditions, and long-term drift in the sensor baseline. Chapter 3 of this thesis investigates the efficacy of such low-cost electrochemical gas sensors for long-term volcanic pollutant monitoring.

1.5.2 Miniaturised particle sensors

As discussed in Section 1.4, monitoring of particulate matter may be successfully accomplished by use of reference-grade instrumentation which provides a high-accuracy of measurement but at a significant financial cost. In recent years, relatively low-cost instruments (in the range of £200 to £800) have become available on a commercial scale, providing user-friendly, off-the-shelf particulate monitoring. Examples include the OPC-N2 (produced by Alphasense Ltd) and the Plantower PMS sensor range. Because of their lower cost these particulate monitors present the opportunity for intensive air quality monitoring at a high spatial and temporal resolution, potentially to provide insight into pollution hot-spots or to investigate smaller-scale regional PM changes than would be feasible with their more expensive reference-grade counterparts (Zikova et al., 2017a; Zikova et al., 2017b).

The hallmark of these instruments is their low expense, which currently means that most are optical particle counters (OPCs), functioning using light-scattering operating principles which can be produced inexpensively (Manikonda et al., 2016; Wang et al., 2015). In this method, particles individually enter into the sensor and are illuminated by a light source, commonly a laser beam emitted from an infrared emitting diode (Alphasense, 2015; Rai et al., 2017). The particle scatters the light, which is then detected by a photodetector allowing the particle size to be determined and the number of particles over a sampling period to be counted (Kelly et al., 2017; Sayahi et al., 2019) [Figure 1.3A]. For particles with diameters > 0.3 µm, the scattered light is proportional to their size (Rai et al., 2017; Wang et al., 2015). Particles with diameters < 0.3 µm typically do not scatter sufficient light to allow them to be detected, and as such, OPCs are limited in the minimum size of particles which they can detect. One of the main issues with light-scattering in low-cost OPCs stems from the hygroscopicity of particles. All atmospheric particles are hygroscopic to some extent, in that they absorb moisture from the atmosphere. In high humidity conditions (> 60 % RH), water is often the dominant component of atmospheric particles, particularly for those particles which are mostly comprised of inorganic material (Crilley et al., 2018; Crilley et al., 2020; Gysel et al., 2007; McFiggans et al., 2005). In low-cost OPCs, the sampled air is not dried prior to entering the sensor, as this would require a heated inlet and result in increased production costs, enlarged instrument size and higher power requirements. In high

humidity conditions, the hygroscopic particles entering the sensor will bias the sensor accuracy by scattering the light disproportionately (Crilley et al., 2020) [Figure 1.3B, C]. As a consequence of this, particle mass concentrations reported by low-cost OPCs require correction for the effect of particle hygroscopic growth, using a correction factor such as discussed by Crilley et al., 2018 and Crilley et al., 2020. Inaccuracies can also occur with OPC instruments when they are used to sample particles that differ significantly in size, shape or composition to the particles used in their calibration, typically latex beads (Liu and Daum, 2000).

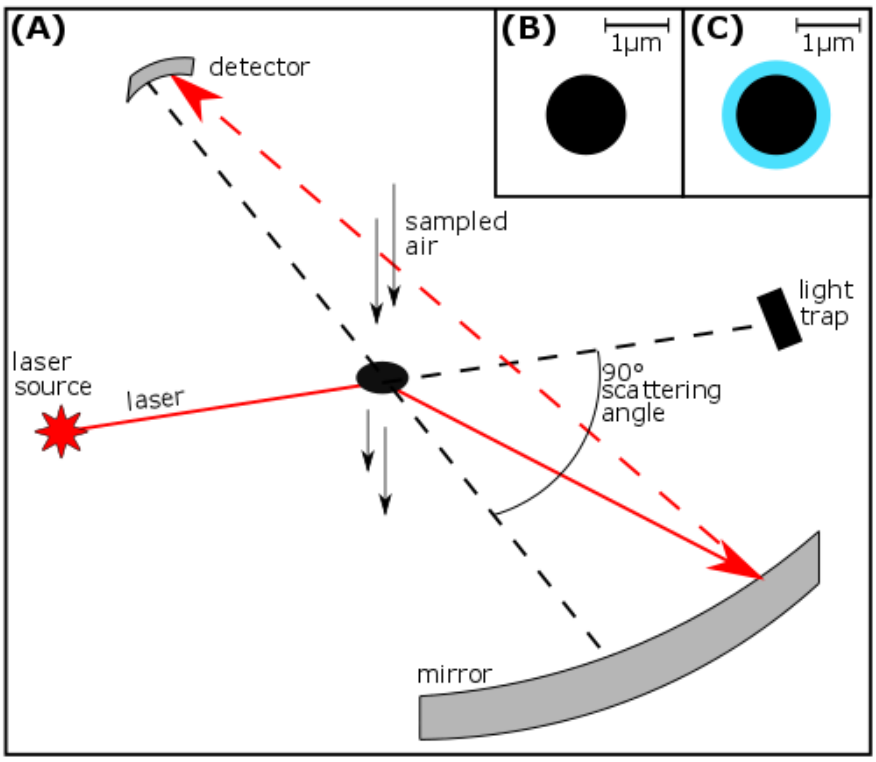

Figure 1.3: (A): Light-scattering principle used by the OPC-N2 low-cost particulate instrument. A laser at 658 nm wavelength passes through the particle (black circle) and is scattered towards an elliptical mirror. The reflected light (dashed red line) is detected by a dual-element photodetector allowing determination of particle size. Sampled air is introduced to the measurement chamber by means of a low power micro-fan. Adapted from Alphasense, 2015; Grimm and Eatough, 2012; Sousan et al., 2016 (B): Dry particle where the laser will be scattered from the surface of the particle itself. (C): Hygroscopic particle where a rim of water has accumulated around the particle, likely causing scattering not representative of the true particle size and density.

Low-cost OPC instruments provide many advantages in the field of particulate air quality monitoring. Their light-weight, compact and affordable nature makes them an inviting prospect for widening the scope of particulate monitoring, and their use has quickly become widespread in the air quality community (Alvarado et al., 2017; Crilley et al., 2018; Renard et al., 2016; Whitty et al., 2020; Zheng et al., 2018; Zikova et al., 2017b). However, it is important to remember that they are potentially limited in their

measurement accuracy, precision and reliability when compared to their reference-grade counterparts. Low-cost OPCs have been evaluated both under laboratory conditions (AQ-SPEC, 2022; Manikonda et al., 2016; Sousan et al., 2016; Wang et al., 2015) and in the field for monitoring of urban pollution (AQ-SPEC, 2022; Crilley et al., 2018; Crilley et al., 2020; Zikova et al., 2017b). In Chapter 2 of this thesis, we evaluate Plantower PMS low-cost particulate sensors for use in monitoring of dilute volcanic plumes, and compare them with reference-grade instrumentation. Chapter 3 of this thesis illustrates some of the issues which can occur when low-cost instruments are used in the field under sub-optimal environmental conditions.

1.6 Methods to determine plume transport direction

While this thesis is primarily concerned with monitoring of volcanic pollutants at ground-level via means of both reference-grade and low-cost instrumentation, some use is also made of other methods to trace volcanic plume dispersion. Here I will discuss use of plume dispersion models and satellite imagery to provide an understanding of how these techniques are used in the following chapters of this thesis.

1.6.1 Plume dispersion models

The use of numerical models to reproduce and examine the evolution of natural atmospheric processes is well established. With respect to the dispersion of volcanic emissions, numerical models have been developed and used successfully for modelling plume dispersion at volcanoes around the world. Significant examples include the NAME model (Heard et al., 2012; Jones et al., 2004; Schmidt et al., 2015), the PUFF model (Daniele et al., 2009; Searcy et al., 1998), the CANERM model (D'amours, 1998; Simpson et al., 2002), the REMOTE model (Langmann et al., 2009; Pfeffer et al., 2006a), the HYSPLIT model (Businger et al., 2015; Draxler and Hess, 1998; Ilyinskaya et al., 2021) and the CALPUFF model (Barsotti, 2020; Barsotti et al., 2004; Scire et al., 2000b).

Plume dispersion models are a very useful tool for hazard mitigation with respect to volcanic emissions and air pollutants. Depending on the model, they can forecast dispersion of volcanic SO_2 and sulfate aerosols through the atmosphere from the point of emission, indicating where and when there may be exposure of the ground surface to high concentrations of pollutants (Barsotti, 2020; Businger et al., 2015; Langmann et al., 2009). Model outputs can be used for operational forecasting of ground-level exposure, and can be used to estimate population exposure to volcanic air pollution. Furthermore, understanding of the interactions between atmospheric processes, meteorological processes and plume dynamics can be developed, and many plume dispersion models incorporate modules to describe chemical reactions such as the conversion of SO_2 gas to sulfate aerosols (Barsotti, 2020; Businger et al., 2015; Scire et al., 2000b).

In the following chapters of this thesis I make use of the HYSPLIT and CALPUFF plume dispersion models. I discuss below the details of these plume dispersion systems to provide context for the following chapters.

1.6.1.1 HYSPLIT plume dispersion model

The Hybrid Single-Particle Lagrangian Intergrated Trajectory (HYSPLIT) model was developed by the National Oceanic and Atmospheric Administration (NOAA). The HYSPLIT model is an atmospheric transport and dispersion model which has been successfully used for a multitude of applications, including tracking of wildfire smoke, anthropogenic pollution, radioactive material and volcanic emissions (Stein et al., 2015). The model uses a hybrid approach between Lagrangian methods which are concerned with the motion of specific fluid parcels, and Eulerian methods which use a three dimensional framework to compute air pollutant concentrations (Draxler and Hess, 1998).

The model operates by simulating the release of a pulse of pollutants, termed a puff, from the emission source (Draxler and Hess, 1997; Draxler and Hess, 1998). The puff is then advected both horizontally and vertically by the turbulent nature of the atmosphere, which is simulated by adding a random component to the motion (Draxler and Hess, 1997; Draxler and Hess, 1998). The dispersion rate of the puff is calculated by integrating the vertical diffusivity profile, horizontal deformation of the wind field and wind shear (Draxler and Hess, 1997; Draxler and Hess, 1998; Stein et al., 2015). Following the release of a pollutant puff, the HYSPLIT model calculates the first-guess position of the puff relative to the initial-position by computing the average of three-dimensional velocity vectors, which are linearly interpolated in both space and time (Draxler and Hess, 1997; Draxler and Hess, 1998). The model then iterates, determining the trajectory of the puff through time. Puff trajectories are terminated if they exit the top of the model, escaping beyond the top of the user-defined model boundaries, but where puffs are advected to intersect the ground-surface the trajectory will continue along the ground (Draxler and Hess, 1997). The HYSPLIT model operates a terrain-following coordinate system to determine the interaction of the puffs with the ground-surface (Draxler and Hess, 1997; Draxler and Hess, 1998). A further component of the HYSPLIT model is the potential for removal of pollutants from the system. Pollutants may be removed by dry deposition, either at a user-defined dry deposition velocity or computed by HYSPLIT with respect to the gravitational settling velocity (Draxler and Hess, 1997). Pollutants may also be removed through gaseous wet deposition via wet depletion, which is defined by a scavenging ratio and only applies for the portion of the puff below the cloud top (Draxler and Hess, 1997; Stein et al., 2015). The chemical formation and deposition of sulfate aerosols is incorporated into HYSPLIT by a dynamic particle partitioning algorithm including chemical processes between SO_2 gas and OH (Stein et al., 2015). The HYSPLIT model can incorporate

a variety of meteorological model data into its calculations, allowing optimisation of the model for different environmental settings (Stein et al., 2015). The model can also be used to calculate both forwards and backwards trajectories, allowing forecasting of where pollutants will be dispersed to, as well as examination of the origin of air masses containing pollutants (Draxler and Hess, 1998; Stein et al., 2015).

The HYSPLIT model has been in use on the Island of Hawai'i since 2010 to track the dispersal of volcanic pollutants from Kīlauea volcano (Pattantyus and Businger, 2014). In this setting, the model uses meteorological data from the Weather Research and Forecasting Advanced Research (WRF-ARW) numerical model, and the input of SO_2 emission rate is determined from observations at the volcanic source (Businger et al., 2015). The HYSPLIT model is run as ensemble forecasting, producing 60-hour forecasts twice daily for both SO_2 gas and sulfate aerosol concentrations at ground-level (Businger et al., 2015; Pattantyus and Businger, 2014). The output from the HYSPLIT model is made available to the public in real-time, providing information dissemination to the communities at risk of exposure to pollutants from Kīlauea volcano. During the 2018 lower East Rift Zone (LERZ) eruption, the HYSPLIT model's capability for back-trajectory simulations was used to allow determination of the age of the plume when it reached air quality stations in the downwind environment (Ilyinskaya et al., 2021; Whitty et al., 2020).

1.6.1.2 CALPUFF plume dispersion model

The California Puff (CALPUFF) model was developed by Earth Tech Inc in the 1990s and is a freely-available dispersion model (Exponent, 2022). The CALPUFF model has been used successfully for a variety of applications including tracking of anthropogenic emissions from cities and power plants as well as from volcanic eruptions (Barsotti, 2020; Levy et al., 2002; Tayanç and Berçin, 2007; Yim et al., 2010; Zhou et al., 2003). The Environmental Protection Agency (EPA) recommends CALPUFF for long-range transport modelling (EPA, 2000).

The set up of the CALPUFF model is complex and is comprised of a large number of processes linked together in a modular structure, allowing the configuration of the model to be defined for the required usage (Barsotti et al., 2008). The CALPUFF modelling system includes three main components - CALMET, CALPUFF and CALPOST. CALMET is a diagnostic processor which develops hourly temperature and wind conditions in a three-dimensional domain (Barsotti et al., 2004; Scire et al., 2000a). CALPUFF is a transport and dispersion model which computes the advection of pollutants through the atmosphere and simulates their distribution and chemical transformation through time and space, using inputs from the CALMET system (Scire et al., 2000b). CALPOST is the final system in the chain and is used to process the outputs from CALMET and CALPUFF, producing the result of the simulation (Scire et al., 2000b).

The CALPUFF model operates on a Lagrangian Gaussian method and treats pollutant emissions as a discrete series of particulate parcels, or puffs, which are advected by wind, according to the meteorological inputs, and diffuse into the atmosphere (Barsotti et al., 2004; Scire et al., 2000b). Typically a finite number of puffs are emitted across a simulated time period, and the user is able to define whether the output should be collected across a grid of receptors or at specific targeted points of interest across a spatial downwind area (Barsotti et al., 2004). As well as simulating the large-scale distribution of pollutant puffs, CALPUFF also contains algorithms to simulate complexities including the removal of pollutants, chemical transformations and the impact of vertical wind shear on the advection process (Scire et al., 2000b). The removal of pollutants can be by dry deposition, with user defined deposition velocities and the option for diurnal variability, and wet deposition using an empirical scavenging coefficient (Scire et al., 2000b). The CALPUFF model contains modules to describe chemical reactions which can be used to model the conversion of SO_2 gas to sulfate aerosols through time, and this can be incorporated into the plume dynamics within the model framework (Barsotti, 2020). Chemical transformation in the CALPUFF model operates as a pseudo-first-order process with user-defined rates and availability to vary the reaction rate across diurnal cycles (Scire et al., 2000b). The CALPUFF model also incorporates a complex terrain approach where elevation high points are evaluated with a dividing streamline to determine whether pollutant species should be advected over or around the high area (Scire et al., 2000b).

The CALPUFF model was used during the 2014 - 2015 Holuhraun eruption and the 2021 Fagradalsfjall eruption in Iceland for operational forecasting and probabilistic hazard mapping (Barsotti, 2020; Carlsen et al., 2021a).

1.6.2 Satellite imagery

Satellite observations and measurements provide significant advantages for monitoring of volcanoes and SO_2 emissions. They can be used to monitor emissions from volcanoes which are remote or difficult to access and those which are not actively monitored by ground-based instrumentation (Carn et al., 2017; Theys et al., 2013). During periods of volcanic unrest, satellites can be used to track the advection of volcanic plumes across local to global scales (Burton et al., 2021; Carboni et al., 2019; Krotkov et al., 2021). Satellite observations can also be used to determine the height of volcanic plumes in the atmosphere by determining the temperature of the plume-top in relation to the ambient temperature of the surrounding atmosphere (Corradini et al., 2010; Theys et al., 2013). However, satellite observations are not able to determine whether SO_2 in the atmospheric column is present at ground-level. Satellite observations are also limited by the temporal resolution over the target emission source and may be restricted during periods when meteorological clouds obscure the ground-surface from view.

In Chapters 3 and 4 of this thesis, satellite imagery is used as an independent proxy to determine the direction of plume advection and indicate whether SO_2 may be present at ground-level at air quality measurement stations. Here I will discuss some of the details of the satellite data used in the following chapters to provide context for the work.

1.6.2.1 Sentinel and Landsat imagery

In Chapter 3, satellite imagery was collected from the USGS Landlook Viewer (https://landlook.usgs.gov/) across the period of interest from the beginning of March until the end of August 2017 in the region around Masaya volcano, Nicaragua. The satellite imagery obtained was non-continuous across this period. Eleven images were obtained from the Landsat 7 satellite from the Enhanced Thematic Mapper Plus (ETM+), twelve images were obtained from the Landsat 8 satellite from the Operational Land Imager (OLI), and four images were obtained from the Sentinel-2 satellite from the Multispectral Instrument (MSI). Landsat 7 and Landsat 8 satellite imagery was at a 15 m spatial resolution using the panchromatic bands with a 16 day grounding track repeat cycle (NASA, 2022; Satellite Imaging Corporation, 2022). The Sentinel-2 satellite imagery was at a 10 m spatial resolution (Sentinel Online, 2022).

In Chapter 3, visible light satellite imagery was used as a means of determining the direction of plume movement away from the volcanic source point. The direction of plume advection from satellite imagery was used to estimate the likely height of the plume in the atmospheric column by comparison to the wind directions from forecast meteorological data. Of the twenty-seven satellite images which were collected (from Landsat 7 and 8 and from Sentinel-2), twelve could not be examined to determine plume advection due to a high extent of opaque cloud cover.

1.6.2.2 TROPOMI SO_2 satellite retrievals

In Chapter 4, satellite data from the Sentinel-5 Precursor satellite (Sentinel-5p) was used to determine the frequency with which SO_2 in the atmospheric column was measurable by ground-based instruments. The TROPOspheric Monitoring Instrument (TROPOMI) onboard Sentinel-5p measures ultraviolet radiance at a spatial resolution of 5.5 x 3.5 km^2 with a revisit time of one day (Romahn et al., 2022; Theys et al., 2017). The observed ultraviolet spectrum is used to derive a slant column density (SCD), representing the gas concentration along the light path through the atmospheric column (BIRA, 2022). The SCD is the converted into a vertical retrieval column by means of air mass factors (AMF), incorporating radiative transfers and accounting for clouds and surface properties (Theys et al. 2017, BIRA, 2022). The retrieval of the SO_2 vertical column is usually performed in near-real time (typically within three hours after measurement), allowing the data to be used operationally during periods of volcanic unrest

(Romahn et al., 2022).

In Chapter 4, pre-processed satellite imagery from Sentinel-5p TROPOMI was obtained from the Icelandic Meteorological Office (IMO) for a two-month sample period during the 2021 Fagradalsfjall eruption. The TROPOMI SO_2 vertical column data were used by the IMO during the eruption for operational hazard assessment. In Chapter 4, I analysed the TROPOMI satellite data in combination with a subset of the Icelandic reference-grade ground-based monitoring network to determine the frequency with which SO_2 in the atmospheric column reached ground level. This has important implications for use of satellite data for hazard assessment of potential exposure to volcanic pollutants at ground-level.

1.7 Thesis roadmap

- In **Chapter 2**, I discuss a study of SO_2 and PM measurements downwind from Kīlauea volcano, Hawai'i, during a large eruption event. I use data from a network of reference-grade instrumentation to determine a baseline of SO_2 and $PM_{2.5}$ concentrations during a period of comparatively low gas emissions and compare this to air quality during the period of increased volcanic activity. Using the reference-grade network, I give a first-order estimate of a conversion rate between SO_2 and sulfate aerosols. I also analyse data from a large network of low-cost community-operated particulate instruments and compare their accuracy with respect to the reference-grade air quality network.

- In **Chapter 3**, I discuss a study of SO_2 and PM measurements downwind from the passively degassing Masaya volcano in Nicaragua. I use data from low-cost instruments which were deployed in the field for six months as a first attempt at installing an air quality monitoring network in the area. I determine periods of volcanic pollution using the low-cost instruments and cross-reference with other methods of determining plume presence, including visual analysis of plume movement in satellite imagery and predicted plume movement from modelled meteorological data. I discuss the effectiveness of using low-cost instrumentation in the field for volcanic air quality measuring and suggest potential improvements for future use.

- In **Chapter 4**, I discuss a study of SO_2 and PM measurements from the 2021 Fagradalsfjall eruption in Iceland. I use data from a network of reference-grade air quality monitors and low-cost sensors to determine how air quality around the island was impacted during the eruption with respect to a pre-eruptive period. I use outputs from the CALPUFF dispersion model to estimate numbers of the population who may have been exposed to concentrations of SO_2 exceeding health guidelines. I use a point-analysis to determine the accuracy of the

CALPUFF dispersion model at predicting the presence of volcanic plume at an air quality station, and examine the frequency of plume grounding with regards to SO_2 visually apparent in satellite imagery.

1.8 Novelty and contribution

Each chapter of this thesis contributes to scientific knowledge differently, as each focuses on a specific study area and volcanic emission source. However, common themes are present throughout, providing insights into a variety of scientific areas. These include, among others, the deterioration to air quality that can result from volcanic emissions, challenges and successes in monitoring volcanic pollutants with low-cost instruments, and insights into the conversion of SO_2 gas into sulfate aerosols. Furthermore, as well as widening scientific knowledge, each chapter contributes to an understanding of the communities who are affected by the volcanic emissions in the specific study areas. In this section I will give a brief overview of the study sites presented in Chapter 2, Chapter 3 and Chapter 4 to give some background context to the volcanic systems and monitoring of volcanic pollutants in the area, and to briefly convey how the research of this thesis fits into existing work. The specific contributions of each chapter, and the novelty of the research therein, is also discussed below.

1.8.1 Chapter 2 - Kīlauea volcano

Kīlauea volcano on the Island of Hawai'i is one of the world's most active volcanoes, erupting near continuously between 1983 and 2018, and as such it has been very well studied (Andres and Kasgnoc, 1998; Beirle et al., 2014; Elias et al., 2018; Greenland, 1984; Kern et al., 2015b; Poland et al., 2008; Wilson et al., 2008). Up until 2018, activity was mostly concentrated at the summit and middle East Rift Zone (ERZ) where SO_2 emissions fluctuated across periods of volcanic activity (Elias and Sutton, 2007; Elias and Sutton, 2012). During 2018, the summit caldera collapsed and a large-scale eruption occurred along the lower East Rift Zone (LERZ) in a populated area, emitting an SO_2 flux an order of magnitude higher than that released during the previous decades (Kern et al., 2019; Neal et al., 2019).

Throughout the volcanic activity at Kīlauea, multiple studies have investigated the dispersal of volcanic air pollutants. The Island of Hawai'i provides a useful natural laboratory for studies of volcanic air quality as it has limited anthropogenic sources of pollution (Mather et al., 2012; Michaud et al., 2007; Tam et al., 2016). Movement of the trade winds during April to October each year causes the volcanic plume to move in a more linear, predictable pattern than would normally occur from a volcanic source, allowing the relationship between SO_2 and sulfate aerosols to be more readily quantifiable (Kroll et al., 2015; Porter et al., 2002). Kroll et al., 2015 investigated SO_2

conversion to sulfate aerosols using reference-grade SO_2 and particulate instrumentation located at sites near-field (3 km) and far-field (31 km) from the summit eruption plume. The concentrations of PM on the west coast of the island are increased during periods of intense volcanic degassing, in part due to high topographic areas in the centre of the island which cause an atmospheric gyre along the western coastline, allowing the volcanic plume to mature and continually return to the area (Ilyinskaya et al., 2021; Whitty et al., 2020).

The distribution of Kīlauea's volcanic pollutants around the Island of Hawai'i has been well documented. In the regions immediately downwind of the summit and ERZ (during the pre-2018 activity), high concentrations of SO_2 gas and sulfate aerosols were recorded (Longo et al., 2005). Individuals residing in those communities frequently exposed to Kīlauea's volcanic emissions were found to have a higher risk of acute bronchitis (Longo and Yang, 2008), increased prevalence of poor cardiorespiratory health (Longo et al., 2008; Longo, 2013) and a greater likelihood of suffering from acute respiratory illnesses (Longo et al., 2010). The city of Hilo, usually out of the dispersion area for Kīlauea's volcanic pollutants during trade wind conditions, was found to have a 15% increase in emergency department visits during periods when the trade winds weakened and the plume moved towards Hilo (Mannino et al., 1996). The effects of volcanic pollutants on the respiratory health of children across the Island of Hawai'i was investigated by Tam et al., 2016, who found that chronic exposure was associated with a decrease in lung function and increased prevalence of cough, but not with the prevalence of bronchitis or asthma.

As yet there has been no investigation to determine whether health issues increased in magnitude on the Island of Hawai'i resulting from the elevated SO_2 emissions during the LERZ eruption in 2018. However, in Chapter 2, I analyse SO_2 and $PM_{2.5}$ concentrations during this unprecedented eruption, comparing the air quality to a background period of lower volcanic activity. This chapter provides a study of downwind concentrations of SO_2 and PM on the Island of Hawai'i on a longer time-scale (12 years for SO_2 and 9 years for PM) than has previously been achieved. In this chapter I also examine data from a network of low-cost miniaturised particulate sensors and compare them to reference-grade BAM-1020 monitors to determine their reliability for volcanic PM monitoring in downwind environments. I estimate a first-order conversion rate for SO_2 to sulfate aerosols using the reference-grade air quality network and the HYSPLIT plume dispersal model, and achieve a value in the same order of magnitude as that calculated by Kroll et al., 2015 during the lower SO_2 emission period.

1.8.2 Chapter 3 - Masaya volcano

Masaya volcano in Nicaragua has a long history of degassing as far back as the 1500s (Rymer et al., 1998), with multiple cycles of increased SO_2 emissions, the latest of which

started in 1993 causing large fluxes of volcanic gas to be released into the atmosphere (Burton et al., 2000; Mather et al., 2006; Rymer et al., 1998; Williams-Jones et al., 2003). Masaya has frequently hosted an active lava lake over recent decades, and the persistent passive degassing at this volcano means it has been well-studied as an example of a volcanic SO_2 emission source (Mather et al., 2006; Mather et al., 2003; Nadeau and Williams-Jones, 2009; Pering et al., 2019; Stoiber et al., 1986; Williams-Jones et al., 2003).

Masaya volcano is relatively low-lying (635 m asl), which often results in the volcanic plume remaining trapped in the low atmosphere and frequently causes exposure of large areas downwind to high concentrations of SO_2 and PM (Delmelle et al., 2002; Nadeau and Williams-Jones, 2009). Prevailing winds cause the plume to predominantly be dispersed towards the west over an area higher than the volcanic crater, and the effects of the volcanic pollutants are distinctly noticeable in this region with sparse vegetation cover along the route of plume dispersion (Baxter et al., 1982; Delmelle et al., 2002; van Manen, 2014). In the affected downwind region, residents reported eye and skin irritation (Baxter et al., 1982), bronchitis and headache symptoms (Delmelle et al., 2002) and respiratory issues (van Manen, 2014). The dense plume from Masaya volcano also affects metal structures in the exposed downwind area, with metal building materials and communication infrastructure rapidly rusting and corroding (Baxter et al., 1982; Delmelle et al., 2002; Williams-Jones and Rymer, 2015).

Volcanic activity at Masaya volcano is monitored by Instituto Nicaragüense de Estudios Territoriales (INETER), but this does not include monitoring of air quality downwind of the crater. Nicaragua is an economically low-income country and one of the poorest in Latin America (World Food Programme, 2022). Installation of a network of reference-grade air quality monitoring stations in the region downwind of Masaya volcano would be significantly challenging due to the high financial burden and limited infrastructure for mains power. As such there has never been a permanent air quality monitoring network in the downwind region frequently exposed to the volcanic emissions. In Chapter 3, I analyse data from a six-month deployment of five low-cost air quality stations, comprising of electrochemical gas sensors and miniaturised particulate sensors, which were a first-attempt to monitor volcanic pollutants in the downwind region over a long time-scale. The stations were installed in communities in the affected downwind areas in an attempt to monitor the extent of volcanic pollutants that residents are exposed to, and to determine whether low-cost sensors could be used as a permanent system to monitor air quality in the region. Chapter 3 of this thesis is a study of the effectiveness of the low-cost sensors in this environment and uses a number of methods to assess whether these instruments are suitable for long-term downwind volcanic air quality monitoring. This chapter has implications for the future use of low-cost instruments in Nicaragua and in other similar volcanic areas and discusses the

practicalities and challenges of using such instrument systems.

1.8.3 Chapter 4 - Fagradalsfjall volcano

Iceland is an extremely volcanically active country with > 30 active volcanic systems (Sturkell et al., 2006; Thordarson and Larsen, 2007). Notable eruptions in recent decades include the 2010 eruption of Eyjafjallajökull and the 2014 - 15 eruption at Holuhraun, both of which had far-reaching implications in the northern hemisphere (Ilyinskaya et al., 2017; Langmann et al., 2012; Schmidt et al., 2015). The 2014 - 15 Holuhraun eruption released an estimated 9.6 Mt of SO_2 and caused widespread air quality deterioration around Iceland, with multiple occasions in the capital city of Reykjavík, 250 km from the eruption site, where SO_2 concentrations exceeded health guidelines (Gıślason et al., 2015). As discussed in Section 1.3, the Holuhraun eruption was the focus of two recent studies investigating the impact of large-scale volcanic emissions on health. Carlsen et al., 2021a and Carlsen et al., 2021b found that exposure of the population to high concentrations of SO_2 and PM can result in uptake in asthma medication and increased utilisation of health care for respiratory diseases.

The 2021 Fagradalsfjall eruption was on a much smaller-scale than the Holuhraun eruption, approximately 10 times smaller when considering both the volume of lava erupted and the total SO_2 emissions (IMO, 2021e, Pfeffer et al. 2018). However, the Fagradalsfjall eruption was the first to occur on the Reykjanes Peninsula in > 750 years, making it the first eruption in modern history to be located within 50 km of Reykjavík, the densest population centre in Iceland. This makes the Fagradalsfjall eruption an excellent opportunity to investigate the potential air quality impacts and population exposure to volcanic pollutants in a small-scale eruption which occurs in relative proximity to densely-populated areas. During the Fagradalsfjall eruption there was a very dense network of reference-grade air quality stations in Iceland, providing data on fluctuations in air quality with a fine spatial distribution, particularly in the areas with high population densities. In Chapter 4, I analyse data from the reference-grade air quality network across Iceland to determine the impact of the Fagradalsfjall eruption on SO_2 and PM concentrations with respect to background non-volcanic periods. I also analyse data from five eruption-response low-cost instruments within 3 km of the eruption site, providing measurements of near-field SO_2 concentrations which visitors to the eruption site may have been exposed to. Using the CALPUFF dispersion model and population distribution data, I estimate the number of Icelandic residents who may have been exposed to concentrations of SO_2 above health threshold levels during the course of the eruption. This chapter provides important insights into the air quality impact which can occur as a result of small-scale proximal volcanic eruptions.

The Fagradalsfjall eruption lasted for six months before activity ceased, but new eruptions are anticipated in the same region over the next century. Volcanic activity

on the Reykjanes Peninsula is cyclic, with periods of prolonged volcanism occurring approximately every 800 years (Björnsson et al., 2020; Hreinsdóttir et al., 2001; Pałgan et al., 2017). With this being the case, studies of the air quality impacts from such an eruption are important for future similar events in Iceland, as well as providing potential insights to other volcanic systems in densely-populated areas of the world.

References

Aiuppa, A., Bagnato, E., Witt, M., Mather, T., Parello, F., Pyle, D., & Martin, R. (2007). Real-time simultaneous detection of volcanic Hg and SO_2 at La Fossa Crater, Vulcano (Aeolian Islands, Sicily) [DOI: https://doi.org/10.1029/2007GL030762]. *Geophysical Research Letters*, *34*(21).

Aiuppa, A., Federico, C., Giudice, G., & Gurrieri, S. (2005). Chemical mapping of a fumarolic field: la Fossa crater, Vulcano Island (Aeolian Islands, Italy) [DOI: https://doi.org/10.1029/2005GL023207]. *Geophysical Research Letters*, *32*(13).

Aiuppa, A., de Moor, J. M., Arellano, S., Coppola, D., Francofonte, V., Galle, B., Giudice, G., Liuzzo, M., Mendoza, E., Saballos, A. et al. (2018). Tracking formation of a lava lake from ground and space: Masaya volcano (Nicaragua), 2014–2017 [DOI: https://agupubs.onlinelibrary.wiley.com/doi/full/10.1002/2017GC007227]. *Geochemistry, Geophysics, Geosystems*, *19*(2), 496–515.

Allen, A., Oppenheimer, C., Ferm, M., Baxter, P., Horrocks, L., Galle, B., McGonigle, A., & Duffell, H. (2002). Primary sulfate aerosol and associated emissions from Masaya Volcano, Nicaragua [DOI: https://doi.org/10.1029/2002JD002120]. *Journal of Geophysical Research: Atmospheres*, *107*(D23), ACH–5.

Alphasense. (2015). Alphasense User Manual OPC-N2 Optical Particle Counter [(Accessed 05/02/2020)]. *https://colandino.nl/wp-content/uploads/datasheet/072-0300_OPC-N2_manual_issue_3.pdf*.

Alphasense. (2021). SO2-B4 Sulfur Dioxide Sensor Data Sheet [(Accessed 05/02/2021)]. *https://www.alphasense.com/wp-content/uploads/2019/09/SO2-B4.pdf*.

Alvarado, M., Gonzalez, F., Erskine, P., Cliff, D., & Heuff, D. (2017). A methodology to monitor airborne pm_{10} dust particles using a small unmanned aerial vehicle [DOI: https://doi.org/10.3390/s17020343]. *Sensors*, *17*(2), 343.

Andres, R., & Kasgnoc, A. (1998). A time-averaged inventory of subaerial volcanic sulfur emissions [DOI: https://doi.org/10.1029/98JD02091]. *Journal of Geophysical Research: Atmospheres*, *103*(D19), 25251–25261.

AQ-SPEC. (2022). Air quality sensor performance evaluation centre [(Accessed 23/05/2022)]. *http://www.aqmd.gov/aq-spec/evaluations/summary-pm*.

ATSDR. (1998). Agency for Toxic Substances and Disease Registry; public health statement sulfur dioxide [Available at: https://www.atsdr.cdc.gov/ToxProfiles/tp116-c1-b.pdf]. *7446-09-5*.

Austin, C. C., Roberge, B., & Goyer, N. (2006). Cross-sensitivities of electrochemical detectors used to monitor worker exposures to airborne contaminants: False positive responses in the absence of target analytes [DOI: https://doi.org/10.1039/B510084D]. *Journal of Environmental Monitoring*, *8*(1), 161–166.

Balmes, J., Fine, J., & Sheppard, D. (1987). Symptomatic bronchoconstriction after short-term inhalation of sulfur dioxide [DOI: https://doi.org/10.1164/ajrccm/136.5.1117]. *American Review of Respiratory Disease*, *136*(5).

Barsotti, S., Neri, A., & Scire, J. (2008). The VOL-CALPUFF model for atmospheric ash dispersal: 1. Approach and physical formulation [DOI: https://doi.org/10.1029/2006JB004623]. *Journal of Geophysical Research: Solid Earth*, *113*(B3).

Barsotti, S. (2020). Probabilistic hazard maps for operational use: The case of SO2 air pollution during the Holuhraun eruption (Bárðarbunga, Iceland) in 2014–2015 [DOI: https://doi.org/10.1007/s00445-020-01395-3]. *Bulletin of Volcanology*, *82*(7), 1–15.

Barsotti, S., Neri, A., & Scire, J. (2004). Assessing volcanic ash hazard by using the CALPUFF system [Available at: https://www.researchgate.net/profile/A-Neri/publication/289122359_Assessing_the_volcanic_ash_hazard_by_using_the_CALPUFF_system/links/5689274c08ae1e63f1f8c5a7/Assessing-the-volcanic-ash-hazard-by-using-the-CALPUFF-system.pdf]. *2nd International Conference on Volcanic Ash and Aviation Safety*.

Bateson, T. F., & Schwartz, J. (2007). Children's response to air pollutants [DOI: https://doi.org/10.1080/15287390701598234]. *Journal of Toxicology and Environmental Health, Part A*, *71*(3), 238–243.

Baxter, P., Stoiber, R., & Williams, S. (1982). Volcanic gases and health: Masaya volcano, Nicaragua [DOI: https://doi.org/10.1016/S0140-6736(82)91109-6]. *The Lancet*.

Beirle, S., Hörmann, C., Penning de Vries, M., Dörner, S., Kern, C., & Wagner, T. (2014). Estimating the volcanic emission rate and atmospheric lifetime of SO2 from space: A case study for Kı¯lauea volcano, Hawai'i [DOI: https://doi.org/10.5194/acp-14-8309-2014]. *Atmospheric Chemistry and Physics*, *14*(16), 8309–8322.

Belgian Institute for Space Aeronomy. (2022). SP5/TROPOMI SO_2 ATBD. *S5P-BIRA-L2-400E-ATBD*, *CI-400E-ATBD*, 2.3.1.

Bennett, W. D., Zeman, K. L., & Jarabek, A. M. (2007). Nasal contribution to breathing and fine particle deposition in children versus adults [DOI: https://doi.org/10.1080/15287390701598200]. *Journal of Toxicology and Environmental Health, Part A*, *71*(3), 227–237.

Björnsson, S., Einarsson, P., Tulinius, H., & Hjartardóttir, Á. R. (2020). Seismicity of the Reykjanes Peninsula 1971–1976 [DOI: https://doi.org/10.1016/j.jvolgeores.2018.04.026]. *Journal of Volcanology and Geothermal Research*, *391*, 106369.

Bluth, G. J., Doiron, S. D., Schnetzler, C. C., Krueger, A. J., & Walter, L. S. (1992). Global tracking of the SO2 clouds from the June, 1991 Mount Pinatubo eruptions. *Geophysical Research Letters*, *19*(2), 151–154.

Bukowiecki, N., Zieger, P., Weingartner, E., Jurányi, Z., Gysel, M., Neininger, B., Schneider, B., Hueglin, C., Ulrich, A., Wichser, A. et al. (2011). Ground-based and airborne in-situ measurements of the Eyjafjallajökull volcanic aerosol plume in Switzerland in spring 2010 [DOI: https://doi.org/10.5194/acp-11-10011-2011]. *Atmospheric Chemistry and Physics*, *11*(19), 10011–10030.

Burton, M., Oppenheimer, C., Horrocks, L., & Francis, P. (2000). Remote sensing of CO2 and H2O emission rates from Masaya volcano, Nicaragua [DOI: https://doi.org/Doi10.1130/0091-7613(2000)28<915:Rsocah>2.0.Co;2]. *Geology*, *28*(10), 915–918.

Burton, M., Hayer, C., Miller, C., & Christenson, B. (2021). Insights into the 9 december 2019 eruption of Whakaari/White Island from analysis of TROPOMI SO2 imagery [DOI: https://www.science.org/doi/10.1126/sciadv.abg1218]. *Science Advances*, *7*(25), eabg1218.

Burton, M., Salerno, G., D'Auria, L., Caltabiano, T., Murè, F., & Maugeri, R. (2015). SO2 flux monitoring at Stromboli with the new permanent INGV SO_2 camera system: A comparison with the FLAME network and seismological data [DOI: https://doi.org/10.1016/j.jvolgeores.2015.02.006]. *Journal of volcanology and geothermal research*, *300*, 95–102.

Businger, S., Huff, R., Pattantus, A., Horton, K., Sutton, A., Elias, T., & Churubini, T. (2015). Observing and forecasting vog dispersion from Kı¯lauea Volcano, Hawai'i [DOI: https://doi.org/10.1175/BAMS-D-14-00150.1]. *American Meteorological Society*.

Cadle, R., Wartburg, A., & Grahek, P. (1971). The proportion of sulfate to sulfur dioxide in Kı¯lauea Volcano fume [DOI: https://doi.org/10.1016/0016-7037(71)90046-9]. *Geochimica et Cosmochimica Acta*, *35*(5), 503–507.

Carboni, E., Mather, T. A., Schmidt, A., Grainger, R. G., Pfeffer, M. A., Ialongo, I., & Theys, N. (2019). Satellite-derived sulfur dioxide (SO2) emissions from the 2014–2015 Holuhraun eruption (Iceland) [DOI: https://doi.org/10.5194/acp-19-4851-2019]. *Atmospheric Chemistry and Physics*, *19*(7), 4851–4862.

Carlsen, H. K., Ilyinskaya, E., Baxter, P., Schmidt, A., Thorsteinsson, T., Pfeffer, M., Barsotti, S., Dominici, F., Finnbjornsdottir, R. G., Jóhannsson, T., Aspelund, T., Gislason, T., Valdimarsdóttir, U., Briem, H., & Gudnason, T. (2021a). Increased respiratory morbidity associated with exposure to a mature volcanic plume from a large Icelandic fissure eruption [DOI: https://doi.org/10.1038/s41467-021-22432-5]. *Nature Communications*, *12*.

Carlsen, H. K., Valdimarsdóttir, U., Briem, H., Dominici, F., Finnbjornsdottir, R. G., Jóhannsson, T., Aspelund, T., Gislason, T., & Gudnason, T. (2021b). Severe

volcanic SO2 exposure and respiratory morbidity in the Icelandic population–a register study [DOI: https://doi.org/10.1186/s12940-021-00698-y]. *Environmental Health*, *20*(1), 1–12.

Carn, S., Clarisse, L., & Prata, A. J. (2016). Multi-decadal satellite measurements of global volcanic degassing [DOI: https://doi.org/10.1016/j.jvolgeores.2016.01.002]. *Journal of Volcanology and Geothermal Research*, *311*, 99–134.

Carn, S., Fioletov, V., McLinden, C., Li, C., & Krotkov, N. (2017). A decade of global volcanic SO2 emissions measured from space [DOI: https://doi.org/10.1038/srep44095]. *Scientific reports*, *7*(1), 1–12.

Chung, A., Chang, D. P., Kleeman, M. J., Perry, K. D., Cahill, T. A., Dutcher, D., McDougall, E. M., & Stroud, K. (2001). Comparison of real-time instruments used to monitor airborne particulate matter [DOI: https://doi.org/10.1080/10473289.2001.10464254]. *Journal of the Air & Waste Management Association*, *51*(1), 109–120.

Corradini, S., Merucci, L., Prata, A., & Piscini, A. (2010). Volcanic ash and SO2 in the 2008 Kasatochi eruption: Retrievals comparison from different IR satellite sensors [DOI: https://doi.org/10.1029/2009JD013634]. *Journal of Geophysical Research: Atmospheres*, *115*(D2).

CRI. (2004). The Centre for Research Information, health effects of project shad chemical agent: Sulfur dioxide [cas 7446-09-5]. *National Academies*.

Crilley, L. R., Shaw, M., Pound, R., Kramer, L. J., Price, R., Young, S., Lewis, A. C., & Pope, F. D. (2018). Evaluation of a low-cost optical particle counter (Alphasense OPC-N2) for ambient air monitoring [DOI: https://doi.org/10.5194/amt-11-709-2018]. *Atmospheric Measurement Techniques*, 709–720.

Crilley, L. R., Singh, A., Kramer, L. J., Shaw, M. D., Alam, M. S., Apte, J. S., Bloss, W. J., Hildebrandt Ruiz, L., Fu, P., Fu, W. et al. (2020). Effect of aerosol composition on the performance of low-cost optical particle counter correction factors [DOI: https://doi.org/10.5194/amt-13-1181-2020]. *Atmospheric Measurement Techniques*, *13*(3), 1181–1193.

Cross, E. S., Williams, L. R., Lewis, D. K., Magoon, G. R., Onasch, T. B., Kaminsky, M. L., Worsnop, D. R., & Jayne, J. T. (2017). Use of electrochemical sensors for measurement of air pollution: Correcting interference response and validating measurements [DOI: https://doi.org/10.5194/amt-10-3575-2017]. *Atmospheric Measurement Techniques*, *10*(9), 3575–3588.

D'Alessandro, W. (2006). Gas hazard: An often neglected natural risk in volcanic areas. *WIT Transactions on Ecology and the Environment*, *89*.

D'amours, R. (1998). Modeling the ETEX plume dispersion with the Canadian emergency response model [DOI: https://doi.org/10.1016/S1352-2310(98)00182-4]. *Atmospheric Environment*, *32*(24), 4335–4341.

Daniele, P., Lirer, L., Petrosino, P., Spinelli, N., & Peterson, R. (2009). Applications of the PUFF model to forecasts of volcanic clouds dispersal from Etna and Vesuvio [DOI: https://doi.org/10.1016/j.cageo.2008.06.002]. *Computers & geosciences*, *35*(5), 1035–1049.

Delmelle, P., Stix, J., Baxter, P., Garcia-Alvarez, J., & Barquero, J. (2002). Atmospheric dispersion, environmental effects and potential health hazard associated with the low-altitude gas plume of Masaya volcano, Nicaragua [DOI: https://doi.org/10.1007/s00445-002-0221-6]. *Bulletin of Volcanology*, *64*(6), 423–434.

Draxler, R. R., & Hess, G. (1997). Description of the HYSPLIT_4 modelling sysem [Available at: https://www.researchgate.net/publication/255682850_Description_of_the_HYSPLIT_4_modelling_system]. *NOAA Technical Memorandum, ERL ARL-224*.

Draxler, R. R., & Hess, G. (1998). An overview of the HYSPLIT_4 modelling system for trajectories [Available at: https://www.arl.noaa.gov/documents/reports/MetMag.pdf]. *Australian meteorological magazine*, *47*(4), 295–308.

Elias, T., Kern, C., Horton, K., Sutton, A. J., & Garbeil, H. (2018). Measuring SO2 emission rates at Kı¯lauea Volcano, Hawai'i USA, 2014-2017 [DOI: https://doi.org/10.3389/feart.2018.00214]. *Frontiers in Earth Science*, *6*, 214.

Elias, T., Sutton, A. J., Oppenheimer, C., Horton, K. A., Garbeil, H., Tsanev, V., McGonigle, A. J., & Williams-Jones, G. (2006). Comparison of COSPEC and two miniature ultraviolet spectrometer systems for SO_2 measurements using scattered sunlight [DOI: https://doi.org/10.1007/s00445-005-0026-5]. *Bulletin of Volcanology*, *68*(4), 313–322.

Elias, T., & Sutton, A. J. (2007). *Sulfur dioxide emission rates from Kı¯lauea Volcano, Hawai'i, an update: 2002-2006* [Available at: https://doi.org/10.3133/ofr20071114]. US Geological Survey.

Elias, T., & Sutton, A. J. (2012). *Sulfur dioxide emission rates from Kı¯lauea Volcano, Hawai'i, 2007–2010* (tech. rep.) [Available at: https://pubs.usgs.gov/of/2012/1107/of2012-1107_text.pdf]. US Geological Survey.

Environmental Protection Agency. (2000). Requirements for preparation, adoption, and submittal of state implementation plans (Guideline on Air Quality Models) [Available at: https://www.govinfo.gov/content/pkg/FR-2000-04-21/pdf/00-4235.pdf]. *Federal Register 65*, *78*, 21505–21546.

Environmental Protection Agency. (2010). Primary National Ambient Air Quality Standard for Sulfur Dioxide; Final Rule [(Accessed 15/1/2019)]. *https://www.govinfo.gov/content/pkg/FR-2010-06-22/pdf/2010-13947.pdf*, *40 CFR Parts 50, 53, and 58*.

Environmental Protection Agency. (2013). Federal and State Ambient Air Quality Standards [(Accessed 15/1/2019)]. *http://health.hawaii.gov/cab/files/2013/05/naaqs_jan_2013.pdf*.

Environmental Protection Agency. (2016). List of designated reference and equivalent methods [Available at: https://www.epa.gov/sites/production/files/2019-08/documents/designated_reference_and-equivalent_methods.pdf]. *National Exposure Research Laboratory*.

European Commission. (2018). Environment Air Quality Standards [(Accessed 21/1/2019)]. *http://ec.europa.eu/environment/air/quality/standards.htm*.

Exponent. (2022). CALPUFF Modeling System [Accessible at: http://www.src.com/]. *Engineering and Scientific Consulting*.

Frank, N. R., Amdur, M. O., Worcester, J., & Whittenberger, J. L. (1962). Effects of acute controlled exposure to SO2 on respiratory mechanics in healthy male adults [DOI: https://doi.org/10.1152/jappl.1962.17.2.252]. *Journal of applied physiology*, *17*(2), 252–258.

Freire, S., Florczyk, A. J., Pesaresi, M., & Sliuzas, R. (2019). An improved global analysis of population distribution in proximity to active volcanoes, 1975–2015 [DOI: https://doi.org/10.3390/ijgi8080341]. *ISPRS international journal of geo-information*, *8*(8), 341.

Galeazzo, T., Bekki, S., Martin, E., Savarino, J., & Arnold, S. R. (2018). Photochemical box modelling of volcanic SO2 oxidation: Isotopic constraints [DOI: https://doi.org/10.5194/acp-18-17909-2018]. *Atmospheric Chemistry and Physics*, *18*(24), 17909–17931.

Galle, B., Oppenheimer, C., Geyer, A., McGonigle, A. J., Edmonds, M., & Horrocks, L. (2003). A miniaturised ultraviolet spectrometer for remote sensing of SO2 fluxes: A new tool for volcano surveillance [DOI: https://doi.org/10.1016/S0377-0273(02)00356-6]. *Journal of Volcanology and Geothermal Research*, *119*(1-4), 241–254.

Gao, X., Coull, B., Lin, X., Vokonas, P., Spiro, A., Hou, L., Schwartz, J., & Baccarelli, A. A. (2021). Short-term air pollution, cognitive performance and nonsteroidal anti-inflammatory drug use in the veterans affairs normative aging study [DOI: https://doi.org/10.1038/s43587-021-00060-4]. *Nature Aging*, *1*(5), 430–437.

Gıślason, S. R., Stefansdottir, G., Pfeffer, M., Barsotti, S., Jóhannsson, T., Galeczka, I. M., Bali, E., Sigmarsson, O., Stefánsson, A., Keller, N. S. et al. (2015). Environmental pressure from the 2014–15 eruption of Bárðarbunga volcano, Iceland [DOI: https://hdl.handle.net/20.500.11815/447].

Gobeli, D., Schloesser, H., & Pottberg, T. (2008). Met one instruments BAM-1020 beta attenuation mass monitor US-EPA $PM_{2.5}$ federal equivalent method field test results [Available at: http://citeseerx.ist.psu.edu/viewdoc/download?doi=10.1.1.584.2489&rep=rep1&type=pdf]. *The Air & Waste Management Association (A&WMA) Conference, Kansas City, MO*, *2*(3).

Green, J. R., Fiddler, M. N., Holloway, J. S., Fibiger, D. L., McDuffie, E. E., Campuzano-Jost, P., Schroder, J. C., Jimenez, J. L., Weinheimer, A. J., Aquino, J. et al.

(2019). Rates of wintertime atmospheric SO2 oxidation based on aircraft observations during clear-sky conditions over the eastern United States [DOI: https://doi.org/10.1029/2018JD030086]. *Journal of Geophysical Research: Atmospheres*, *124*(12), 6630–6649.

Greenland, L. (1984). Gas composition of the January 1983 eruption of Kilauea volcano, Hawaii [DOI: https://doi.org/10.1016/0016-7037(84)90361-2]. *Geochimica et Cosmochimica Acta*, *48*(1), 193–195.

Grimm, H., & Eatough, D. (2012). Aerosol measurement: The use of optical light scattering for the determination of particulate size distribution, and particulate mass, including the semi-volatile fraction [DOI: https://doi.org/10.3155/1047-3289.59.1.101]. *Journal of the Air and Waste Management Association*.

Gysel, M., Crosier, J., Topping, D., Whitehead, J., Bower, K., Cubison, M., Williams, P., Flynn, M., McFiggans, G., & Coe, H. (2007). Closure study between chemical composition and hygroscopic growth of aerosol particles during TORCH2 [DOI: https://doi.org/10.5194/acp-7-6131-2007]. *Atmospheric Chemistry and Physics*, *7*(24), 6131–6144.

Hagan, D. H., Isaacman-VanWertz, G., Franklin, J. P., Wallace, L. M., Kocar, B. D., Heald, C. L., & Kroll, J. H. (2018). Calibration and assessment of electrochemical air quality sensors by co-location with regulatory-grade instruments [DOI: https://doi.org/10.5194/amt-11-315-2018]. *Atmospheric Measurement Techniques*, *11*(1), 315–328.

Hansell, A., & Oppenheimer, C. (2004). Health hazards from volcanic gases: A systematic literature review [DOI: https://doi.org/10.1080/00039890409602947]. *Archives of Environmental Health: An International Journal*, *59*(12), 628–639.

Hawaii Emergency Management Agency. (2018). How to cope with hazardous volcanic gas emissions [(Accessed 15/4/2021)]. *http://dod.hawaii.gov/hiema/how-to-cope-with-hazardous-volcanic-gas-emissions/*.

Heard, I. P., Manning, A. J., Haywood, J. M., Witham, C., Redington, A., Jones, A., Clarisse, L., & Bourassa, A. (2012). A comparison of atmospheric dispersion model predictions with observations of SO2 and sulphate aerosol from volcanic eruptions [DOI: https://doi.org/10.1029/2011JD016791]. *Journal of Geophysical Research: Atmospheres*, *117*(D20).

Heggie, T. W. (2009). Geotourism and volcanoes: Health hazards facing tourists at volcanic and geothermal destinations [DOI: https://doi.org/10.1016/j.tmaid.2009.06.002]. *Travel medicine and infectious disease*, *7*(5), 257–261.

Herbarth, O., Fritz, G., Krumbiegel, P., Diez, U., Franck, U., & Richter, M. (2001). Effect of sulfur dioxide and particulate pollutants on bronchitis in children — a risk analysis [DOI: https://doi.org/10.1002/tox.1033]. *Environmental Toxicology*, *16*(3), 269–276.

Holgate, S. (2017). "Every breath we take: the lifelong impact of air pollution" - a call for action [DOI: https://doi.org/10.7861/clinmedicine.17-1-8]. *Clinical Medicine*, *17*(1), 8–12.

Horton, K. A., Williams-Jones, G., Garbeil, H., Elias, T., Sutton, A. J., Mouginis-Mark, P., Porter, J. N., & Clegg, S. (2006). Real-time measurement of volcanic SO2 emissions: Validation of a new UV correlation spectrometer (FLYSPEC) [DOI: https://doi.org/10.1007/s00445-005-0014-9]. *Bulletin of volcanology*, *68*(4), 323–327.

Horwell, C. J., & Elias, T. (2020). 'This advice is absurd': issues with providing generic advice on community protection from chronic volcanic degassing [DOI: https://doi.org/10.5194/egusphere-egu2020-16190]. *EGU General Assembly Conference Abstracts*, 16190.

Hreinsdóttir, S., Einarsson, P., & Sigmundsson, F. (2001). Crustal deformation at the oblique spreading Reykjanes Peninsula, SW Iceland: GPS measurements from 1993 to 1998 [DOI: https://doi.org/10.1029/2001JB000428]. *Journal of Geophysical Research: Solid Earth*, *106*(B7), 13803–13816.

Icelandic Directive. (2016). Reglugerð um brennisteinsdíoxíð, köfnunarefnisdíoxíð og köfnunarefnisoxíð, bensen, kolsýring, svifryk og blý í andrúmsloftinu [Available at: https://www.reglugerd.is/reglugerdir/eftir-raduneytum/umhverfisraduneyti/nr/20277]. *B-deild*, *Nr.920*.

Icelandic Meteorological Office. (2021). "The small eruption" in Fagradalsfjall celebrates six months [(Accessed 27/10/2021)]. *https://en.vedur.is/about-imo/news/the-small-eruption-in-fagradalsfjall-celebrates-six-months*.

Ilyinskaya, E., Mason, E., Wieser, P., Holland, L., Liu, E., Mather, T., Edmonds, M., Whitty, R., Elias, T., Nadeau, P., Schneider, D., McQuaid, J., Allen, S., Harvey, J., Oppenheimer, C., Kern, C., & Damby, D. (2021). Rapid metal pollutant deposition from the volcanic plume of Kı¯lauea, Hawai'i [DOI: https://doi.org/10.1038/s43247-021-00146-2]. *Communications Earth and Environment*.

Ilyinskaya, E., Schmidt, A., Mather, T. A., Pope, F. D., Witham, C., Baxter, P., Jóhannsson, T., Pfeffer, M., Barsotti, S., Singh, A. et al. (2017). Understanding the environmental impacts of large fissure eruptions: Aerosol and gas emissions from the 2014–2015 Holuhraun eruption (Iceland) [DOI: https://doi.org/10.1016/j.epsl.2017.05.025]. *Earth and Planetary Science Letters*, *472*, 309–322.

International Volcanic Health Hazard Network. (2020). The health hazards of volcanic and geothermal gases: A guide for the public [(Accessed 12/4/2021)]. *https://www.ivhhn.org/information/health-impacts-volcanic-gases#Howtolivewithvolcanicemissions*.

Jones, A., Thomson, D., Hort, M., & Devenish, B. (2004). The UK Met Office's next-generation atmospheric dispersion model, NAME III [DOI: https://doi.org/10.1007/978-0-387-68854-1_62]. *Air Pollution Modeling and its Application XVII,*

Proceedings of the 27th NATO/CCMS International Technical Meeting on Air Pollution Modelling and its Application, 24–29.

Kelly, K., Whitaker, J., Petty, A., Widmer, C., Dybwad, A., Sleeth, D., Martin, R., & Butterfield, A. (2017). Ambient and laboratory evaluation of a low-cost particulate matter sensor [DOI: https://doi.org/10.1016/j.envpol.2016.12.039]. *Environmental Pollution*, *221*, 491–500.

Kern, C., Elias, T., Nadeau, P., Lerner, A., Werner, C., Cappos, M., Clor, L., Kelly, P., Realmuto, V., Theys, N., & Carn, S. (2019). Sulfur dioxide emissions associated with Kı¯lauea Volcano's 2018 fissure eruption; V43C-0209 [Available at: https://ui.adsabs.harvard.edu/abs/2019AGUFM.V43C0209L/abstract]. *American Geophysical Union Fall Meeting*.

Kern, C., Lerner, A. H., Elias, T., Nadeau, P. A., Holland, L., Kelly, P. J., Werner, C. A., Clor, L. E., & Cappos, M. (2020). Quantifying gas emissions associated with the 2018 rift eruption of Kı¯lauea Volcano using ground-based DOAS measurements [DOI: https://doi.org/10.1007/s00445-020-01390-8]. *Bulletin of Volcanology*, *82*(7), 1–24.

Kern, C., Lübcke, P., Bobrowski, N., Campion, R., Mori, T., Smekens, J.-F., Stebel, K., Tamburello, G., Burton, M., Platt, U. et al. (2015a). Intercomparison of SO2 camera systems for imaging volcanic gas plumes [DOI: https://doi.org/10.1016/j.jvolgeores.2014.08.026]. *Journal of Volcanology and Geothermal Research*, *300*, 22–36.

Kern, C., Sutton, J., Elias, T., Lee, L., Kamibayashi, K., Antolik, L., & Werner, C. (2015b). An automated SO2 camera system for continuous, real-time monitoring of gas emissions from Kı¯lauea Volcano's summit Overlook Crater [DOI: https://doi.org/10.1016/j.jvolgeores.2014.12.004]. *Journal of Volcanology and Geothermal Research*, *300*, 81–94.

Khoder, M. (2002). Atmospheric conversion of sulfur dioxide to particulate sulfate and nitrogen dioxide to particulate nitrate and gaseous nitric acid in an urban area [DOI: https://doi.org/10.1016/S0045-6535(02)00391-0]. *Chemosphere*, *49*(6), 675–684.

Kroll, J. H., Cross, E. S., Hunter, J. F., Pai, S., XII, T., XI, T., Wallace, L. M., Croteau, P. L., Jayne, J. T., Worsnop, D. R. et al. (2015). Atmospheric evolution of sulfur emissions from Kılauea: real-time measurements of oxidation, dilution, and neutralization within a volcanic plume [Available at: https://pubs.acs.org/doi/pdf/10.1021/es506119x]. *Environmental science & technology*, *49*(7), 4129–4137.

Krotkov, N., Realmuto, V., Li, C., Seftor, C., Li, J., Brentzel, K., Stuefer, M., Cable, J., Dierking, C., Delamere, J. et al. (2021). Day-night monitoring of volcanic SO2 and ash clouds for aviation avoidance at northern polar latitudes [DOI: https://doi.org/10.3390/rs13194003]. *Remote Sensing*, *13*(19), 4003.

Krueger, A. J., Walter, L. S., Schnetzler, C. C., & Doiron, S. D. (1990). TOMS measurement of the sulfur dioxide emitted during the 1985 Nevado del Ruiz eruptions [DOI: https://doi.org/10.1016/0377-0273(90)90081-P]. *Journal of Volcanology and Geothermal Research*, *41*(1-4), 7–15.

Lambert, G., Le Cloarec, M., & Pennisi, M. (1988). Volcanic output of SO2 and trace metals: A new approach [DOI: https://doi.org/10.1016/0016-7037(88)90054-3]. *Geochimica et Cosmochimica Acta*, *52*(1), 39–42.

Langmann, B. (2014). On the role of climate forcing by volcanic sulphate and volcanic ash [DOI: https://doi.org/10.1155/2014/340123]. *Advances in Meteorology*, *2014*, 1–17.

Langmann, B., Folch, A., Hensch, M., & Matthias, V. (2012). Volcanic ash over europe during the eruption of Eyjafjallajökull on Iceland, April–May 2010 [DOI: https://doi.org/10.1016/j.atmosenv.2011.03.054]. *Atmospheric Environment*, *48*, 1–8.

Langmann, B., Hort, M., & Hansteen, T. (2009). Meteorological influence on the seasonal and diurnal variability of the dispersion of volcanic emissions in Nicaragua: A numerical model study. *Journal of Volcanology and Geothermal Research*, *182*(1-2), 34–44.

Levy, J. I., Spengler, J. D., Hlinka, D., Sullivan, D., & Moon, D. (2002). Using CALPUFF to evaluate the impacts of power plant emissions in Illinois: model sensitivity and implications [DOI: https://doi.org/10.1016/S1352-2310(01)00493-9]. *Atmospheric Environment*, *36*(6), 1063–1075.

Lewis, A. C., Lee, J. D., Edwards, P. M., Shaw, M. D., Evans, M. J., Moller, S. J., Smith, K. R., Buckley, J. W., Ellis, M., Gillot, S. R. et al. (2016). Evaluating the performance of low cost chemical sensors for air pollution research [Available at: https://pubs.rsc.org/en/content/articlelanding/2016/FD/C5FD00201J]. *Faraday discussions*, *189*, 85–103.

Lim, S. S., Vos, T., Flaxman, A. D., Danaei, G., Shibuya, K., Adair-Rohani, H., AlMazroa, M. A., Amann, M., Anderson, H. R., Andrews, K. G. et al. (2012). A comparative risk assessment of burden of disease and injury attributable to 67 risk factors and risk factor clusters in 21 regions, 1990–2010: A systematic analysis for the Global Burden of Disease Study 2010 [DOI: https://doi.org/10.1016/S0140-6736(12)61766-8]. *The lancet*, *380*(9859), 2224–2260.

Liu, Y., & Daum, P. H. (2000). The effect of refractive index on size distributions and light scattering coefficients derived from optical particle counters [DOI: https://doi.org/10.1016/S0021-8502(99)00573-X]. *Journal of Aerosol Science*, *31*(8), 945–957.

Longo, B., Rossignol, A., & Green, J. (2008). Cardiorespiratory health effects associated with sulphurous volcanic air pollution [DOI: https://doi.org/10.1016/j.puhe.2007.09.017]. *Public Health*, *122*(8), 809–20.

Longo, B. M. (2013). Adverse health effects associated with increased activity at Kı¯lauea Volcano: A repeated population-based survey [DOI: https://doi.org/10.1155/2013/475962]. *ISRN Public Health*, *2013*.

Longo, B. M., Grunder, A., Chuan, R., & Rossignol, A. (2005). SO2 and fine aerosol dispersion from the Kı¯lauea plume, Kau district, Hawai'i, USA [DOI: https://doi.org/10.1130/G21167.1]. *Geology*, *33*(3), 217–220.

Longo, B. M., & Yang, W. (2008). Acute bronchitis and volcanic air pollution: A community-based cohort study at Kı¯lauea Volcano, Hawai'i, USA [DOI: https://doi.org/10.1080/15287390802414117]. *Journal of Toxicology and Environmental Health, Part A*, *71*(24), 1565–1571.

Longo, B. M., Yang, W., Green, J. B., Crosby, F. L., & Crosby, V. L. (2010). Acute health effects associated with exposure to volcanic air pollution (vog) from increased activity at Kı¯lauea Volcano in 2008 [DOI: https://doi.org/10.1080/15287394.2010.497440]. *Journal of Toxicology and Environmental Health, Part A*, *73*(20), 1370–1381.

Loughlin, S., Aspinall, W., Vye-Brown, C., Baxter, P., Braban, C., Hort, M., Schmidt, A., Thordarson, T., & Witham, C. (2012). Large-magnitude fissure eruptions in Iceland: Source characterisation [DOI: https://eprints.whiterose.ac.uk/80209/]. *BGS Open File Report*, *OR/12/098*.

Luke, W. T. (1997). Evaluation of a commercial pulsed fluorescence detector for the measurement of low-level SO_2 concentrations during the Gas-Phase Sulfur Intercomparison Experiment [DOI: https://doi.org/10.1029/96JD03347]. *Journal of Geophysical Research: Atmospheres*, *102*(D13), 16255–16265.

Manikonda, A., Zıḱová, N., Hopke, P. K., & Ferro, A. R. (2016). Laboratory assessment of low-cost PM monitors [DOI: https://doi.org/10.1016/j.jaerosci.2016.08.010]. *Journal of Aerosol Science*, *102*, 29–40.

Mannino, D. M., Ruben, S., Holschuh, F. C., Holschuh, T. C., Wilson, M. D., & Holschuh, T. (1996). Emergency department visits and hospitalizations for respiratory disease on the Island of Hawai'i, 1981 to 1991 [DOI: http://hdl.handle.net/10524/54120]. *Hawai'i medical journal*, *55*(3).

Martin, R. S., Ilyinskaya, E., Sawyer, G. M., Tsanev, V. I., & Oppenheimer, C. (2011). A re-assessment of aerosol size distributions from Masaya volcano (Nicaragua) [DOI: https://doi.org/10.1016/j.atmosenv.2010.10.049]. *Atmospheric Environment*, *45*(3), 547–560.

Martin, R., Mather, T., Pyle, D., Power, M., Tsanev, V., Oppenheimer, C., Allen, A., Horwell, C., & Ward, E. (2009). Size distributions of fine silicate and other particles in Masaya's volcanic plume [DOI: https://doi.org/10.1029/2008JD011211]. *Journal of Geophysical Research: Atmospheres*, *114*(D9).

Martınez, M., Fernández, E., Valdés, J., Barboza, V., Van der Laat, R., Duarte, E., Malavassi, E., Sandoval, L., Barquero, J., & Marino, T. (2000). Chemical evolu-

tion and volcanic activity of the active crater lake of Poás volcano, Costa Rica, 1993–1997 [DOI: https://doi.org/10.1016/S0377-0273(99)00165-1]. *Journal of Volcanology and Geothermal Research*, *97*(1-4), 127–141.

Mason, E., Wieser, P., Liu, E., Edmonds, M., Ilyinskaya, E., Whitty, R., Mather, T., Elias, T., Nadeau, P., Wilkes, T. et al. (2021). Volatile metal emissions from volcanic degassing and lava-seawater interactions at Kı¯lauea Volcano, Hawai'i [DOI: https://doi.org/10.1038/s43247-021-00145-3]. *Communications Earth and Environment*.

Mather, T. A., McCabe, J. R., Rai, V. K., Thiemens, M. H., Pyle, D. M., Heaton, T. H. E., Sloane, H. J., & Fern, G. R. (2006). Oxygen and sulfur isotopic composition of volcanic sulfate aerosol at the point of emission [DOI: https://doi.org/10.1029/2005JD006584]. *Journal of Geophysical Research*, *111*.

Mather, T. A., Witt, M., Pyle, D., Quayle, B., Aiuppa, A., Bagnato, E., Martin, R., Sims, K., Edmonds, M., Sutton, A. et al. (2012). Halogens and trace metal emissions from the ongoing 2008 summit eruption of Kı¯lauea volcano, Hawai'i [DOI: https://doi.org/10.1016/j.gca.2011.11.029]. *Geochimica et Cosmochimica Acta*, *83*, 292–323.

Mather, T., Allen, A., Oppenheimer, C., Pyle, D., & McGonigle, A. (2003). Size-resolved characterisation of soluble ions in the particles in the tropospheric plume of Masaya volcano, Nicaragua: origins and plume processing [DOI: https://doi.org/10.1023/A:1026327502060]. *Journal of Atmospheric Chemistry*, *46*(3), 207–237.

McCormick, M. P., Thomason, L. W., & Trepte, C. R. (1995). Atmospheric effects of the Mt Pinatubo eruption. *Nature*, *373*(6513), 399–404.

McDonald, F., Horwell, C. J., Wecker, R., Dominelli, L., Loh, M., Kamanyire, R., & Ugarte, C. (2020). Facemask use for community protection from air pollution disasters: An ethical overview and framework to guide agency decision making [DOI: https://doi.org/10.1016/j.ijdrr.2019.101376]. *International Journal of Disaster Risk Reduction*, *43*, 101376.

McFiggans, G., Alfarra, M. R., Allan, J., Bower, K., Coe, H., Cubison, M., Topping, D., Williams, P., Decesari, S., Facchini, C. et al. (2005). Simplification of the representation of the organic component of atmospheric particulates [DOI: https://doi.org/10.1039/B419435G]. *Faraday Discussions*, *130*, 341–362.

McGonigle, A., Oppenheimer, C., Galle, B., Mather, T., & Pyle, D. (2002). Walking traverse and scanning DOAS measurements of volcanic gas emission rates [DOI: https://doi.org/10.1029/2002GL015827]. *Geophysical Research Letters*, *29*(20), 46–1.

McMurry, P., & Wilson, J. (1982). Growth laws for the formation of secondary ambient aerosols: Implications for chemical conversion mechanisms [DOI: https://doi.

org/10.1016/0004-6981(82)90319-5]. *Atmospheric Environment (1967)*, *16*(1), 121–134.

Mead, M., Popoola, O., Stewart, G., Landshoff, P., Calleja, M., Hayes, M., Baldovi, J., McLeod, M., Hodgson, T., Dicks, J. et al. (2013). The use of electrochemical sensors for monitoring urban air quality in low-cost, high-density networks [DOI: https://doi.org/10.1016/j.atmosenv.2012.11.060]. *Atmospheric Environment*, *70*, 186–203.

Met One Instruments Inc. (2008). BAM 1020 particulate monitor operation manual [Available at: https://www.arb.ca.gov/airwebmanual/instrument_manuals/Documents/BAM-1020-9800_Manual_Rev_H.pdf]. *[BAM-1020-9800 Rev H]*.

Met One Instruments Inc. (2013). BAM-1020 [Available at: https://www.et.co.uk/assets/resources/files/bam-1020-product-datasheet-2019-1.pdf]. *Continuous Particulate Monitor*.

Michaud, J. D., Michaud, J.-P., & Krupitsky, D. (2007). Temporal variability in SO2 exposures at Hawai'i Volcanoes National Park, USA [DOI: 10.1007/S00254-006-0459-Y]. *Environmental geology*, *52*(1), 81–92.

Michaud, J.-P., Krupitsky, D., Grove, J. S., & Anderson, B. S. (2005). Volcano related atmospheric toxicants in Hilo and Hawai'i Volcanoes National Park: Implications for human health [DOI: https://doi.org/10.1016/j.neuro.2004.12.004]. *Neurotoxicology*, *26*(4), 555–563.

Middleton, P., Kiang, C., & Mohnen, V. A. (1980). Theoretical estimates of the relative importance of various urban sulfate aerosol production mechanisms [DOI: https://doi.org/10.1016/0004-6981(80)90211-5]. *Atmospheric Environment (1967)*, *14*(4), 463–472.

Miller, V. (2004). Health Effects of Project SHAD Chemical Agent: Sulfur Dioxide, Prepared for the National Academies by The Center for Research Information [Available at: https://paperzz.com/doc/8956749/health-effects-of-project-shad-chemical-agent]. *Contract No. IOM-2794-04-001*, 1–58.

Mohn, J., & Emmenegger, L. (2001). Determination of Sulphur Dioxide by Pulsed UV-Fluorescence [Available at: https://www.environmental-expert.com/articles/determination-of-sulphur-dioxide-by-pulsed-uv-fluorescence-840601]. *Swiss Federal Laboritories for Materials, Testing and Research*.

Monn, C., & Schaeppi, G. (1993). Concentrations of total suspended particulates, fine particles and their anionic compounds in ambient air and indoor air [DOI: https://doi.org/10.1080/09593339309385359]. *Environmental technology*, *14*(9), 869–875.

Mori, T., & Burton, M. (2006). The SO2 camera: A simple, fast and cheap method for ground-based imaging of SO2 in volcanic plumes [DOI: https://doi.org/10.1029/2006GL027916]. *Geophysical research letters*, *33*(24).

Nadeau, P. A., & Williams-Jones, G. (2009). Apparent downwind depletion of volcanic SO2 flux — lessons from Masaya Volcano, Nicaragua [DOI: https://doi.org/10.1007/s00445-008-0251-9]. *Bulletin of Volcanology*, *71*(4), 389–400.

NASA. (2022). Operational Land Imager [Available at: https://landsat.gsfc.nasa.gov/satellites/landsat-8/spacecraft-instruments/operational-land-imager/].

Neal, C., Brantley, S., Antolik, L., Babb, J., Burgess, M., Calles, K., Cappos, M., Chang, J., Conway, S., Desmither, L. et al. (2019). The 2018 rift eruption and summit collapse of Kı¯lauea Volcano [DOI: https://www.science.org/doi/10.1126/science.aav7046]. *Science*, *363*(6425), 367–374.

Ng'walali, P. M., Koreeda, A., Kibayashi, K., & Tsunenari, S. (1999). Fatalities by inhalation of volcanic gas at Mt. Aso crater in Kumamoto, Japan [DOI: https://doi.org/10.1016/S1344-6223(99)80034-0]. *Legal Medicine*, *1*(3), 180–184.

Okabe, H., Splitstone, P. L., & Ball, J. J. (1973). Ambient and source SO2 detector based on a fluorescence method [DOI: https://doi.org/10.1080/00022470.1973.10469797]. *Journal of the Air Pollution Control Association*, *23*(6), 514–516.

Oppenheimer, C., & McGonigle, J. (2004). Exploiting ground-based optical sensing technologies for volcanic gas surveillance [DOI: https://doi.org/10.4401/ag-3353]. *Annals Geophysics*, *47*(4).

Oppenheimer, C., Francis, P., & Stix, J. (1998). Depletion rates of sulfur dioxide in tropospheric volcanic plumes [DOI: https://doi.org/10.1029/98GL01988]. *Geophysical Research Letters*, *25*(14), 2671–2674.

Oppenheimer, C., Kyle, P., Eisele, F., Crawford, J., Huey, G., Tanner, D., Kim, S., Mauldin, L., Blake, D., Beyersdorf, A. et al. (2010). Atmospheric chemistry of an Antarctic volcanic plume [DOI: https://doi.org/10.1029/2009JD011910]. *Journal of Geophysical Research: Atmospheres*, *115*(D4).

Pałgan, D., Devey, C. W., & Yeo, I. A. (2017). Volcanism and hydrothermalism on a hotspot–influenced ridge: Comparing Reykjanes Peninsula and Reykjanes Ridge, Iceland [DOI: https://doi.org/10.1016/j.jvolgeores.2017.10.017]. *Journal of Volcanology and Geothermal Research*, *348*, 62–81.

Pattantyus, A. K., Businger, S., & Howell, S. G. (2018). Review of sulfur dioxide to sulfate aerosol chemistry at Kı¯lauea Volcano, Hawai'i [DOI: https://doi.org/10.1016/j.atmosenv.2018.04.055]. *Atmospheric Environment*, *185*, 262–271.

Pattantyus, A. K., & Businger, S. (2014). Ensemble forecasting of volcanic emissions in Hawai'i [DOI: https://doi.org/10.4401/ag-6607]. *Annals of Geophysics*, *57*.

Pering, T. D., Ilanko, T., Wilkes, T. C., England, R. A., Silcock, S. R., Stanger, L. R., Willmott, J. R., Bryant, R. G., & McGonigle, A. J. (2019). A rapidly convecting lava lake at Masaya Volcano, Nicaragua [DOI: https://doi.org/10.3389/feart.2018.00241]. *Frontiers in Earth Science*, *6*, 241.

Pfeffer, M. A., Bergsson, B., Barsotti, S., Stefánsdóttir, G., Galle, B., Arellano, S., Conde, V., Donovan, A., Ilyinskaya, E., Burton, M., Aiuppa, A., Whitty, R. C. W.,

Simmons, I. C., Arason, T., Jónasdóttir, E., Keller, N., Yeo, R. F., Arngrímsson, H., Jóhannsson, T., ... Mereu, L. (2018). Ground-based measurements of the 2014–2015 Holuhraun volcanic cloud (Iceland) [DOI: https://doi.org/10.3390/geosciences8010029]. *Geosciences*, *8*(1), 29.

Pfeffer, M., Langmann, B., & Graf, H.-F. (2006a). Atmospheric transport and deposition of Indonesian volcanic emissions [DOI: https://doi.org/10.5194/acp-6-2525-2006]. *Atmospheric Chemistry and Physics*, *6*(9), 2525–2537.

Pfeffer, M., Rietmeijer, F., Brearley, A., & Fischer, T. P. (2006b). Electron microbeam analyses of aerosol particles from the plume of Poás Volcano, Costa Rica and comparison with equilibrium plume chemistry modeling [DOI: https://doi.org/10.1016/j.jvolgeores.2005.10.009]. *Journal of volcanology and geothermal research*, *152*(1-2), 174–188.

Pohl, H. R. (1998). Toxicological profile for sulfur dioxide [Available at: https://www.atsdr.cdc.gov/toxprofiles/tp116.pdf]. *U.S. Department for Health and Human Services*.

Poland, M., Miklius, A., Orr, T., Sutton, J., Thornber, C., & Wilson, D. (2008). New episodes of volcanism at Kı¯lauea Volcano, Hawai'i [DOI: https://doi.org/10.1029/2008EO050001]. *Eos, Transactions American Geophysical Union*, *89*(5), 37–38.

Popoola, O. A., Stewart, G. B., Mead, M. I., & Jones, R. L. (2016). Development of a baseline-temperature correction methodology for electrochemical sensors and its implications for long-term stability [DOI: https://doi.org/10.1016/j.atmosenv.2016.10.024]. *Atmospheric Environment*, *147*, 330–343.

Porter, J. N., Horton, K. A., Mouginis-Mark, P. J., Lienert, B., Sharma, S. K., Lau, E., Sutton, A. J., Elias, T., & Oppenheimer, C. (2002). Sun photometer and lidar measurements of the plume from the Hawai'i Kı¯lauea Volcano, Hawai'i Volcano Pu'u 'Ō'ō vent: Aerosol flux and SO_2 lifetime [DOI: https://doi.org/10.1029/2002GL014744]. *Geophysical Research Letters*, *29*(16), 30–1.

Quality of Urban Air Review Group. (1996). *Airborne particulate matter in the United Kingdom* (Vol. 3). The Department.

Rai, A. C., Kumar, P., Pilla, F., Skouloudis, A. N., Di Sabatino, S., Ratti, C., Yasar, A., & Rickerby, D. (2017). End-user perspective of low-cost sensors for outdoor air pollution monitoring [DOI: https://doi.org/10.1016/j.scitotenv.2017.06.266]. *Science of The Total Environment*, *607*, 691–705.

Rattigan, O., Boniface, J., Swartz, E., Davidovits, P., Jayne, J., Kolb, C., & Worsnop, D. (2000). Uptake of gas-phase SO2 in aqueous sulfuric acid: Oxidation by H2O2, O3, and HONO [DOI: https://doi.org/10.1029/2000JD900372]. *Journal of Geophysical Research: Atmospheres*, *105*(D23), 29065–29078.

Renard, J.-B., Dulac, F., Berthet, G., Lurton, T., Vignelles, D., Jégou, F., Tonnelier, T., Jeannot, M., Couté, B., Akiki, R. et al. (2016). LOAC: a small aerosol optical

counter/sizer for ground-based and balloon measurements of the size distribution and nature of atmospheric particles–Part 1: Principle of measurements and instrument evaluation [DOI: https://doi.org/10.5194/amt-9-1721-2016]. *Atmospheric Measurement Techniques*, *9*(4), 1721–1742.

Roberts, T., Braban, C., Oppenheimer, C., Martin, R., Freshwater, R., Dawson, D., Griffiths, P., Cox, R., Saffell, J., & Jones, R. (2012). Electrochemical sensing of volcanic gases [DOI: https://doi.org/10.1016/j.chemgeo.2012.08.027]. *Chemical Geology*, *332*, 74–91.

Roberts, T., Saffell, J., Oppenheimer, C., & Lurton, T. (2014). Electrochemical sensors applied to pollution monitoring: Measurement error and gas ratio bias — a volcano plume case study [DOI: https://doi.org/10.1016/j.jvolgeores.2014.02.023]. *Journal of volcanology and geothermal research*, *281*, 85–96.

Roberts, T. J., Lurton, T., Giudice, G., Liuzzo, M., Aiuppa, A., Coltelli, M., Vignelles, D., Salerno, G., Couté, B., Chartier, M. et al. (2017). Validation of a novel Multi-Gas sensor for volcanic HCl alongside H_2S and SO_2 at Mt. Etna [DOI: https://doi.org/10.1007/s00445-017-1114-z]. *Bulletin of volcanology*, *79*(5), 36.

Roberts, T. J., Vignelles, D., Liuzzo, M., Giudice, G., Aiuppa, A., Coltelli, M., Salerno, G., Chartier, M., Couté, B., Berthet, G. et al. (2018). The primary volcanic aerosol emission from Mt Etna: Size-resolved particles with SO2 and role in plume reactive halogen chemistry [DOI: https://doi.org/10.1016/j.gca.2017.09.040]. *Geochimica et Cosmochimica Acta*, *222*, 74–93.

Robock, A. (2000). Volcanic eruptions and climate [DOI: https://doi.org/10.1029/1998RG000054]. *Reviews of geophysics*, *38*(2), 191–219.

Romahn, F., Pedergnana, M., Loyola, D., Apituley, A., Sneep, M., & Veefkind, J. (2022). Sentinel-5 precursor/TROPOMI Level 2 Product User Manual Sulphur Dioxide SO_2. *S5P-L2-DLR-PUM-400E*, 02.03.01.

Rotstayn, L. D., & Lohmann, U. (2002). Simulation of the tropospheric sulfur cycle in a global model with a physically based cloud scheme [DOI: https://doi.org/10.1029/2002JD002128]. *Journal of Geophysical Research: Atmospheres*, *107*(D21).

Rymer, H., de Vries, B. v. W., Stix, J., & Williams-Jones, G. (1998). Pit crater structure and processes governing persistent activity at Masaya Volcano, Nicaragua [DOI: https://doi.org/10.1007/s004450050196]. *Bulletin of Volcanology*, *59*(5), 345–355.

Satellite Imaging Corporation. (2022). Landsat 7 ETM+ Satellite Sensor [Available at: https://www.satimagingcorp.com/satellite-sensors/other-satellite-sensors/landsat/].

Saxena, P., & Seigneur, C. (1987). On the oxidation of SO2 to sulfate in atmospheric aerosols [DOI: https://doi.org/10.1016/0004-6981(87)90077-1]. *Atmospheric Environment (1967)*, *21*(4), 807–812.

Sayahi, T., Butterfield, A., & Kelly, K. (2019). Long-term field evaluation of the Plantower PMS low-cost particulate matter sensors [DOI: https://doi.org/10.1016/j.envpol.2018.11.065]. *Environmental Pollution*, *245*, 932–940.

Schlesinger, R., Kunzli, N., Hidy, G., Gotschi, T., & Jerrett, M. (2006). The health relevance of ambient particulate matter characteristics: Coherence of toxicological and epidemiological inferences [DOI: https://doi.org/10.1080/08958370500306016]. *Inhalation toxicology*, *18*(2), 95–125.

Schlesinger, R. B. (1985). Effects of inhaled acids on respiratory tract defense mechanisms [DOI: https://doi.org/10.1289/ehp.856325]. *Environmental health perspectives*, *63*, 25–38.

Schmidt, A., Leadbetter, S., Theys, N., Carboni, E., Witham, C., Stevenson, J., Birch, C., Thordarson, T., Turnock, S., Barsotti, S., Delaney, L., Feng, W., Grainger, R., Hort, M., Höskuldsson, Á., Ialongo, I., Ilyinskaya, E., Jóhannsson, T., Kenny, P., ... Shepherd, J. (2015). Satellite detection, long-range transport, and air quality impacts of volcanic sulfur dioxide from the 2014–2015 flood lava eruption at Bárðarbunga (Iceland) [DOI: https://doi.org/10.1002/2015JD023638]. *Journal of Geophysical Research: Atmospheres*, *120*(18), 9739–9757.

Schmidt, A., Ostro, B., Carslaw, K. S., Wilson, M., Thordarson, T., Mann, G. W., & Simmons, A. J. (2011). Excess mortality in Europe following a future Laki-style Icelandic eruption [DOI: https://doi.org/10.1073/pnas.1108569108]. *Proceedings of the National Academy of Sciences*, *108*(38), 15710–15715.

Schweizer, D., Cisneros, R., & Shaw, G. (2016). A comparative analysis of temporary and permanent beta attenuation monitors: The importance of understanding data and equipment limitations when creating $pm_{2.5}$ air quality health advisories [DOI: https://doi.org/10.1016/j.apr.2016.02.003]. *Atmospheric Pollution Research*, *7*(5), 865–875.

Scire, J. S., Robe, F. R., Fernau, M. E., & Yamartino, R. J. (2000a). A user's guide for the CALMET meteorological model [Available at: http://www.src.com/calpuff/download/CALMET_UsersGuide.pdf]. *Earth Tech, Inc.*

Scire, J. S., Strimaitis, D. G., Yamartino, R. J. et al. (2000b). A user's guide for the CALPUFF dispersion model [Available at: http://www.src.com/CALPUFF/download/CALPUFF_UsersGuide.pdf]. *Earth Tech, Inc*, *521*, 1–521.

Searcy, C., Dean, K., & Stringer, W. (1998). PUFF: A Lagrangian trajectory volcanic ash tracking model [DOI: https://doi.org/10.1016/S0377-0273(97)00037-1]. *Journal of Volcanology and Geothermal Research*, *80*(1), 16.

Sentinel Online. (2022). MultiSpectral Instrument (MSI) Overview [Available at: https://sentinels.copernicus.eu/web/sentinel/technical-guides/sentinel-2-msi/msi-instrument].

Shehab, M., & Pope, F. (2019). Effects of short-term exposure to particulate matter air pollution on cognitive performance [DOI: https://doi.org/10.1038/s41598-019-44561-0]. *Scientific reports*, *9*(1), 1–10.

Shinohara, H., Aiuppa, A., Giudice, G., Gurrieri, S., & Liuzzo, M. (2008). Variation of H2O/CO2 and CO2/SO2 ratios of volcanic gases discharged by continuous degassing of Mount Etna volcano, Italy [DOI: https://doi.org/10.1029/2007JB005185]. *Journal of Geophysical Research: Solid Earth*, *113*(B9).

Shinohara, H. (2005). A new technique to estimate volcanic gas composition: Plume measurements with a portable multi-sensor system [DOI: https://doi.org/10.1016/j.jvolgeores.2004.12.004]. *Journal of Volcanology and Geothermal Research*, *143*(4), 319–333.

Simpson, J. J., Berg, J. S., Hufford, G. L., Bauer, C., Pieri, D., & Servranckx, R. (2002). The February 2001 eruption of Mount Cleveland, Alaska: Case study of an aviation hazard [DOI: https://doi.org/10.1175/1520-0434(2002)017%3C0691:TFEOMC%3E2.0.CO;2]. *Weather and Forecasting*, *17*(4), 691–704.

Smith, K. R., Edwards, P. M., Evans, M. J., Lee, J. D., Shaw, M. D., Squires, F., Wilde, S., & Lewis, A. C. (2017). Clustering approaches to improve the performance of low cost air pollution sensors [DOI: https://doi.org/10.1039/C7FD00020K]. *Faraday discussions*, *200*, 621–637.

Sousan, S., Koehler, K., Hallett, L., & Peters, T. M. (2016). Evaluation of the Alphasense optical particle counter (OPC-N2) and the Grimm portable aerosol spectrometer (PAS-1.108) [DOI: https://doi.org/10.1080/02786826.2016.1232859]. *Aerosol Science and Technology*, *50*(12), 1352–1365.

Stein, A., Draxler, R. R., Rolph, G. D., Stunder, B. J., Cohen, M., & Ngan, F. (2015). NOAA's HYSPLIT atmospheric transport and dispersion modeling system [DOI: https://doi.org/10.1175/BAMS-D-14-00110.1]. *Bulletin of the American Meteorological Society*, *96*(12), 2059–2077.

Stewart, C., Damby, D. E., Horwell, C. J., Elias, T., Ilyinskaya, E., Tomašek, I., Longo, B. M., Schmidt, A., Carlsen, H. K., Mason, E. et al. (2022). Volcanic air pollution and human health: Recent advances and future directions [DOI: https://doi.org/10.1007/s00445-021-01513-9]. *Bulletin of Volcanology*, *84*(1), 1–25.

Stockwell, W. R., & Calvert, J. G. (1983). The mechanism of the ho^{-}so$_2$ reaction [DOI: https://doi.org/10.1016/0004-6981(83)90220-2]. *Atmospheric Environment (1967)*, *17*(11), 2231–2235.

Stoiber, R. E., & Jepsen, A. (1973). Sulfur dioxide contributions to the atmosphere by volcanoes [DOI: https://www.science.org/doi/10.1126/science.182.4112.577]. *Science*, *182*(4112), 577–578.

Stoiber, R. E., Williams, S. N., & Huebert, B. J. (1986). Sulfur and halogen gases at Masaya caldera complex, Nicaragua: Total flux and variations with time [DOI:

https://doi.org/10.1029/JB091iB12p12215]. *Journal of Geophysical Research: Solid Earth*, *91*(B12), 12215–12231.

Sturkell, E., Einarsson, P., Sigmundsson, F., Geirsson, H., Olafsson, H., Pedersen, R., de Zeeuw-van Dalfsen, E., Linde, A. T., Sacks, S. I., & Stefánsson, R. (2006). Volcano geodesy and magma dynamics in Iceland [DOI: https://doi.org/10.1016/j.jvolgeores.2005.07.010]. *Journal of Volcanology and Geothermal Research*, *150*(1-3), 14–34.

Sutton, A., Elias, T., Gerlach, T., & Stokes, J. (2001). Implications for eruptive processes as indicated by sulfur dioxide emissions from Kı¯lauea Volcano, Hawa 'i, 1979–1997 [DOI: https://doi.org/10.1016/S0377-0273(00)00291-2]. *Journal of Volcanology and Geothermal Research*, *108*(1-4), 283–302.

Swingedouw, D., Mignot, J., Ortega, P., Khodri, M., Menegoz, M., Cassou, C., & Hanquiez, V. (2017). Impact of explosive volcanic eruptions on the main climate variability modes [DOI: https://doi.org/10.1016/j.gloplacha.2017.01.006]. *Global and Planetary Change*, *150*, 24–45.

Tam, E., Miike, R., Labrenz, S., Sutton, A. J., Elias, T., Davis, J., Chen, Y.-L., Tantisira, K., Dockery, D., & Avol, E. (2016). Volcanic air pollution over the Island of Hawai'i: Emissions, dispersal, and composition. association with respiratory symptoms and lung function in Hawai'i Island school children [DOI: https://doi.org/10.1016/j.envint.2016.03.025]. *Environment international*, *92*, 543–552.

Tayanç, M., & Berçin, A. (2007). SO2 modeling in Izmit Gulf, Turkey during the winter of 1997: 3 cases [DOI: https://doi.org/10.1007/s10666-006-9056-4]. *Environmental Modeling & Assessment*, *12*(2), 119–129.

Thermo Fisher Scientific. (2010). Model 43i sulphur dioxide analyser - product specifications [Available at: https://www.thermofisher.com/order/catalog/product/43I#/43I].

Thermo Fisher Scientific. (2015). Model 43i Instruction Manual [Available at: https://www.thermofisher.com/document-connect/document-connect.html?url=https%3A%2F%2Fassets.thermofisher.com%2FTFS-Assets%2FLSG%2Fmanuals%2FEPM-manual-Model%2043i.pdf]. *Pulsed Fluorescence SO_2 Analyzer*.

Theys, N., Campion, R., Clarisse, L., Brenot, H., Gent, J. v., Dils, B., Corradini, S., Merucci, L., Coheur, P.-F., Roozendael, M. V. et al. (2013). Volcanic SO2 fluxes derived from satellite data: A survey using OMI, GOME-2, IASI and MODIS [DOI: https://doi.org/10.5194/acp-13-5945-2013]. *Atmospheric Chemistry and Physics*, *13*(12), 5945–5968.

Theys, N., De Smedt, I., Yu, H., Danckaert, T., van Gent, J., Hörmann, C., Wagner, T., Hedelt, P., Bauer, H., Romahn, F. et al. (2017). Sulfur dioxide retrievals from TROPOMI onboard Sentinel-5 Precursor: algorithm theoretical basis [DOI:

https://doi.org/10.5194/amt-10-119-2017]. *Atmospheric Measurement Techniques*, *10*(1), 119–153.

Thomason, L., & Peter, T. (Eds.). (2006). *SPARC Assessment of Stratospheric Aerosol Properties (ASAP)* (tech. rep.). SPARC. SPARC Office.

Thordarson, T., & Larsen, G. (2007). Volcanism in Iceland in historical time: Volcano types, eruption styles and eruptive history [DOI: https://doi.org/10.1016/j.jog.2006.09.005]. *Journal of Geodynamics*, *43*(1), 118–152.

Timmreck, C. (2012). Modeling the climatic effects of large explosive volcanic eruptions [DOI: https://wires.onlinelibrary.wiley.com/doi/pdf/10.1002/wcc.192]. *Wiley Interdisciplinary Reviews: Climate Change*, *3*(6), 545–564.

van Manen, S. M. (2014). Perception of a chronic volcanic hazard: Persistent degassing at Masaya volcano, Nicaragua [DOI: https://doi.org/10.1186/s13617-014-0009-3]. *Journal of Applied Volcanology*, *3*(1), 9.

von Glasow, R., Bobrowski, N., & Kern, C. (2009). The effects of volcanic eruptions on atmospheric chemistry [DOI: https://doi.org/10.1016/j.chemgeo.2008.08.020]. *Chemical Geology*, *263*(1-4), 131–142.

Wang, Y., Li, J., Jing, H., Zhang, Q., Jiang, J., & Biswas, P. (2015). Laboratory evaluation and calibration of three low-cost particle sensors for particulate matter measurement [DOI: https://doi.org/10.1080/02786826.2015.1100710]. *Aerosol Science and Technology*, *49*(11), 1063–1077.

Whitty, R. C. W., Ilyinskaya, E., Mason, E., Wieser, P. E., Liu, E. J., Schmidt, A., Roberts, T., Pfeffer, M. A., Brooks, B., Mather, T. A., Edmonds, M., Elias, T., Schneider, D. J., Oppenheimer, C., Dybwad, A., A, N. P., & Kern, C. (2020). Spatial and temporal variations in SO_2 and $PM_{2.5}$ levels around Kīlauea volcano, Hawai'i during 2007–2018 [DOI: https://doi.org/10.3389/feart.2020.00036]. *Frontiers in Earth Science*, *8*, 36.

Williams-Jones, G., & Rymer, H. (2015). Hazards of volcanic gases [DOI: https://doi.org/10.1016/B978-0-12-385938-9.00057-2]. *The Encyclopedia of Volcanoes*, *2*, 985–992.

Williams-Jones, G., Horton, K. A., Elias, T., Garbeil, H., Mouginis-Mark, P. J., Sutton, A. J., & Harris, A. J. (2006). Accurately measuring volcanic plume velocity with multiple UV spectrometers [DOI: https://doi.org/10.1007/s00445-005-0013-x]. *Bulletin of Volcanology*, *68*(4), 328–332.

Williams-Jones, G., Rymer, H., & Rothery, D. A. (2003). Gravity changes and passive SO2 degassing at the Masaya caldera complex, Nicaragua [DOI: https://doi.org/10.1016/S0377-0273(03)00033-7]. *Journal of Volcanology and Geothermal Research*, *123*(1-2), 137–160.

Wilson, D., Elias, T., Orr, T., Patrick, M., Sutton, J., & Swanson, D. (2008). Small explosion from new vent at Kı¯lauea's summit [DOI: https://doi.org/10.1029/

2008EO220003]. *Eos, Transactions American Geophysical Union*, *89*(22), 203–203.

Witt, M., Mather, T., Pyle, D., Aiuppa, A., Bagnato, E., & Tsanev, V. (2008). Mercury and halogen emissions from Masaya and Telica volcanoes, Nicaragua [DOI: https://doi.org/10.1029/2007JB005401]. *Journal of Geophysical Research: Solid Earth*, *113*(B6).

World Food Programme. (2022). Nicaragua [Available at: https://www.wfp.org/countries/nicaragua#:~:text=Nicaragua%20is%20a%20low%2Dincome,percent%20of%20the%20country's%20GDP.].

World Health Organization. (2005). WHO Air quality guidelines for particulate matter, ozone, nitrogen dioxide and sulfur dioxide [Available at: https://apps.who.int/iris/bitstream/handle/10665/69477/WHO_SDE_PHE_OEH_06.02_eng.pdf]. *Global update*.

World Health Organization. (2021). Ambient (outdoor) air pollution [Available at: https://www.who.int/news-room/fact-sheets/detail/ambient-(outdoor)-air-quality-and-health].

Yim, S. H., Fung, J. C., & Lau, A. K. (2010). Use of high-resolution MM5 / CALMET / CALPUFF system: SO2 apportionment to air quality in Hong Kong [DOI: https://doi.org/10.1016/j.atmosenv.2010.08.037]. *Atmospheric Environment*, *44*(38), 4850–4858.

Zheng, T., Bergin, M. H., Johnson, K. K., Tripathi, S. N., Shirodkar, S., Landis, M. S., Sutaria, R., & Carlson, D. E. (2018). Field evaluation of low-cost particulate matter sensors in high-and low-concentration environments [DOI: https://doi.org/10.5194/amt-11-4823-2018]. *Atmospheric Measurement Techniques*, *11*(8), 4823–4846.

Zhou, Y., Levy, J. I., Hammitt, J. K., & Evans, J. S. (2003). Estimating population exposure to power plant emissions using CALPUFF: a case study in Beijing, China [DOI: https://doi.org/10.1016/S1352-2310(02)00937-8]. *Atmospheric Environment*, *37*(6), 815–826.

Zikova, N., Hopke, P. K., & Ferro, A. R. (2017a). Evaluation of new low-cost particle monitors for $PM_{2.5}$ concentrations measurements [DOI: https://doi.org/10.1016/j.jaerosci.2016.11.010]. *Journal of Aerosol Science*, *105*, 24–34.

Zikova, N., Masiol, M., Chalupa, D. C., Rich, D. Q., Ferro, A. R., & Hopke, P. K. (2017b). Estimating hourly concentrations of $PM_{2.5}$ across a metropolitan area using low-cost particle monitors [DOI: https://doi.org/10.3390/s17081922]. *Sensors*, *17*(8), 1922.

Chapter 2

Spatial and Temporal Variations in SO_2 and $PM_{2.5}$ Levels from 2007 - 2018 Kīlauea Volcano, Hawai‘i

Abstract

Among the hazards posed by volcanoes are the emissions of gases and particles that can affect air quality and damage agriculture and infrastructure. A recent intense episode of volcanic degassing associated with severe impacts on air quality accompanied the 2018 lower East Rift Zone (LERZ) eruption of Kīlauea volcano, Hawai‘i. This resulted in a major increase in gas emission rates with respect to usual emission values for this volcano, along with a shift in the source of the dominant plume to a populated area in the lower flank of the volcano. This led to reduced air quality in downwind communities. We analyse open-access data from the permanent air quality monitoring networks operated by the Hawaii Department of Health (HDOH) and National Park Service (NPS), and report on measurements of atmospheric sulfur dioxide (SO_2) between 2007 - 2018 and $PM_{2.5}$ (aerosol particulate matter with diameter $<$2.5 µm) between 2010 - 2018. Additional air quality data were collected through a community-operated network of low-cost $PM_{2.5}$ sensors during the 2018 LERZ eruption. From 2007 - 2018 the two most significant escalations in Kīlauea's volcanic emissions were: the summit eruption that began in 2008 (Kīlauea emissions averaged 5 - 6 kt/day SO_2 from 2008 until summit activity decreased in May 2018) and the LERZ eruption in 2018 when SO_2 emission rates reached a monthly average of 200 kt/day during June. In this paper we focus on characterising the airborne pollutants arising from the 2018 LERZ eruption and

the spatial distribution and severity of volcanic air pollution events across the Island of Hawai‘i. The LERZ eruption caused the most frequent and severe exceedances of the Environmental Protection Agency (EPA) $PM_{2.5}$ air quality threshold ($35\,\mu g/m^3$ as a daily average) in Hawai‘i in the period 2010 - 2018. In Kona, for example, the maximum 24-hour-mean mass concentration of $PM_{2.5}$ was recorded as $59\,\mu g/m^3$ on the twenty-ninth of May 2018, which was one of eight recorded exceedances of the EPA air quality threshold during the 2018 LERZ eruption, where there had been no exceedances in the previous eight years as measured by the HDOH and NPS networks. SO_2 air pollution during the LERZ eruption was most severe in communities in the south and west of the island, as measured by selected HDOH and NPS stations in this study, with a maximum 24-hour-mean mass concentration of $728\,\mu g/m^3$ recorded in Ocean View (100 km west of the LERZ emission source) in May 2018. Data from the low-cost sensor network correlated well with data from the HDOH $PM_{2.5}$ instruments, confirming that these low-cost sensors provide a robust means to augment reference-grade instrument networks.

2.1 Introduction

Volcanic clouds are complex, evolving mixtures of volcanic and atmospheric gases, primary and secondary aerosol particles, ash and dust (Oppenheimer and McGonigle 2004; Pfeffer et al. 2006b; von Glasow et al. 2009; Oppenheimer et al. 2010; Langmann 2014). As well as the potential for global climatic consequences from explosive or large-scale volcanic emissions, low altitude volcanic clouds can have important impacts on air quality, human and animal health and the environment on the local to regional scale (Hansell and Oppenheimer 2004; Barsotti et al. 2010; Tam et al. 2016; Andronico and Del Carlo 2016; Schmidt et al. 2015; Mather 2015; Ilyinskaya et al. 2017).

Gaseous sulfur dioxide (SO_2) is usually highly concentrated in volcanic emissions compared to the background atmosphere and is often the focus of gas emission monitoring due to the relative ease of its measurement and its important environmental and air quality consequences (Cadle et al., 1971; Lambert et al., 1988; Loughlin et al., 2012; Schmidt et al., 2015). Population sub-groups including children, asthmatics and cardiac- or respiratory-compromised individuals are particularly vulnerable to exposure to SO_2 (ATSDR, 1998; CRI, 2004). For example, exposure to mass concentrations of $1310\,\mu g/m^3$ SO_2 for three minutes can induce respiratory attacks in asthmatic individuals (ATSDR, 1998; Balmes et al., 1987). In 2010 the U.S. Environmental Protection Agency (EPA) set the National Ambient Air Quality Standard (NAAQS) for SO_2 mass concentration exposure limits at $195\,\mu g/m^3$ as an hourly average (EPA, 2010). Persistent volcanic SO_2 emissions on the Island of Hawai‘i led the state of Hawai‘i being designated as unclassifiable for the EPA 2010 NAAQS, and as such Hawai‘i uses the pre-2010 EPA SO_2 exposure limit of $366\,\mu g/m^3$ as 24-hour average (EPA, 2013). The

European Commission (EC) air quality standards recommend a SO_2 mass concentration threshold of 350 µg/m^3 for a three-hour average, and 125 µg/m^3 as a daily average (EC, 2018).

Particulate matter (PM) in volcanic clouds is also significant in the context of environment and health. The chemical composition of volcanogenic $PM_{2.5}$ (PM with diameter <2.5 µm) is highly heterogeneous. Typical chemical species include sulfates (primary emissions or formed via oxidation of sulfur gases) (Allen et al., 2002; Cadle et al., 1971; Langmann, 2014; Mather et al., 2003; Stockwell and Calvert, 1983) and halides, with an array of metals and metalloids including environmentally-harmful species such as lead and cadmium (Langmann, 2014; Longo, 2013). $PM_{2.5}$ is a well-established indicator for air quality, since it commonly includes particulates derived from transport and industrial sources, fine wind-blown mineral dust, ambient matter and volcanic material (Butwin et al., 2019; Holgate, 2017; Lim et al., 2012; Tam et al., 2016). It has been estimated that the health burden due to exposure to ambient $PM_{2.5}$ globally amounts to more than three million premature deaths each year (Lim et al., 2012), and is especially linked to increases in death from cardiovascular and respiratory diseases in vulnerable individuals (Holgate, 2017). EPA NAAQS thresholds recommend a $PM_{2.5}$ mass concentration exposure limit of 35 µg/m^3 as a daily average (EPA, 2013). This is higher than the 24-hour mean exposure guideline of 25 µg/m^3 established by the World Health Organization (WHO, 2005).

2.2 Kīlauea eruptive activity, 2007 - 2018

Kīlauea volcano on the Island of Hawai‘i consists of a summit caldera at 1200 m a.s.l. and rift zones to the south-west and east. From 1983 until 2008, activity at Kīlauea was concentrated on the middle East Rift Zone (ERZ), primarily near the Pu‘u ‘Ō‘ō vent (Elias and Sutton, 2007; Poland et al., 2008) [Figure 2.1(A)]. Between 2002 and 2006, average SO_2 flux from the ERZ was 1.7 ± 0.7 kt/day, while emissions from the summit were low at 0.1 kt/day (Elias and Sutton, 2007). From November 2007 to March 2008, SO_2 emissions at the summit increased to levels 10 times the long-term background (Wooten et al., 2009) [Figure 2.2(A)]. On the twelfth of March 2008, a new vent opened within the Halema‘uma‘u summit crater, leading to sporadic explosive eruptions and increased degassing of SO_2.

Kīlauea's SO_2 emissions peaked in the summer of 2008, when a total emission rate of up to 20 kt/day was measured by satellite sensors (Beirle et al., 2014). At this time, emissions from both the ERZ and the summit were significant, with the two sources contributing variable amounts to the total degassing rate (Elias and Sutton, 2012). For the period 2009 - 2017, the dynamic activity at Kīlauea was reflected in variable emissions, with a long-term average of 5 - 6 kt/day based on satellite and ground-based

measurements (Carn et al., 2016; Eguchi et al., 2011; Elias et al., 2018; Elias and Sutton, 2012) [Figure 2.2(A)]. Lava was first observed in the Halema‘uma‘u summit crater in September 2008, with a permanent lava lake visible from February 2010 until May 2018 (Neal et al., 2019; Patrick et al., 2013).

The 2018 Kīlauea eruption in the lower East Rift Zone (LERZ) began following the collapse of the Pu‘u ‘Ō‘ō vent on the thirtieth of April (Neal et al. 2019; HVO, 2018). Twenty-four fissures opened over a distance of 6.8 km in the vicinity of Leilani Estates [Figure 2.1(A)]. During the first week of the LERZ eruption, spattering activity at individual fissures was typically short-lived (minutes to hours in duration) and lava was viscous with spatter deposition within tens of meters of individual fissures. On the eighteenth of May, the eruptive style evolved to less viscous lava and resulted in fast-moving lava flows which reached the ocean two days later (HVO, 2018). By the end of May 2018, activity had become focused at Fissure 8, and this remained the dominant fissure for the remainder of the LERZ eruption (Neal et al., 2019). Lava fountains from Fissure 8 reached heights of 80 m, and lava effusion rates ranged from 50 - 200 m^3/s (Neal et al., 2019). Lava from Fissure 8 flowed in a semi-stable channel to the ocean and eventually covered an area of land 35.5 km^2 (Neal et al. 2019; HVO, 2018). This eruption was the largest along Kīlauea's LERZ in the last two centuries and had far-reaching impacts around the Island of Hawai‘i. With the collapse of the Pu‘u ‘Ō‘ō vent and draining of Kīlauea's summit magma reservoir, the dominant source of volcanic SO_2 became the LERZ eruptive vents. SO_2 emissions reached an average of 200 kt/day in June 2018 (Kern et al. 2019), severely impacting island-wide air quality. The eruption declined rapidly at the end of July and lava effusion ceased on the fourth of August 2018 (Neal et al., 2019).

2.2.1 Downwind processes and impacts

Since initiation of intermittent fountaining activity at Kīlauea in 1983, SO_2 emissions have been a health concern among downwind communities on the Island of Hawai‘i. As emissions from Kīlauea are dispersed downwind, communities are exposed to volcanic smog, locally known as vog, predominantly composed of SO_2 and fine particles of sulfuric acid aerosol (Elias and Sutton, 2017; Halliday et al., 2015; Longo, 2009; Longo et al., 2010; Tam et al., 2016). Prevailing trade winds from the north-east, particularly during the period from April to October, carry Kīlauea's emissions over the communities to the south and west (Elias and Sutton, 2017; Longo et al., 2008; Longo et al., 2005; Michaud et al., 2007; Tam et al., 2016) [Figure 2.1(A)]. The Island of Hawai‘i has relatively low population density in the south [Figure 2.1(B)], with $\approx$ 4400 residents in Ocean View and $\approx$ 1300 residents in Pahala. Trade winds from the north-east are influenced by the high topography of Mauna Loa and Mauna Kea, generating more localised air movement in the lee of the island on the west coast (Michaud et al., 2007) [Figure 2.1(A)]. This

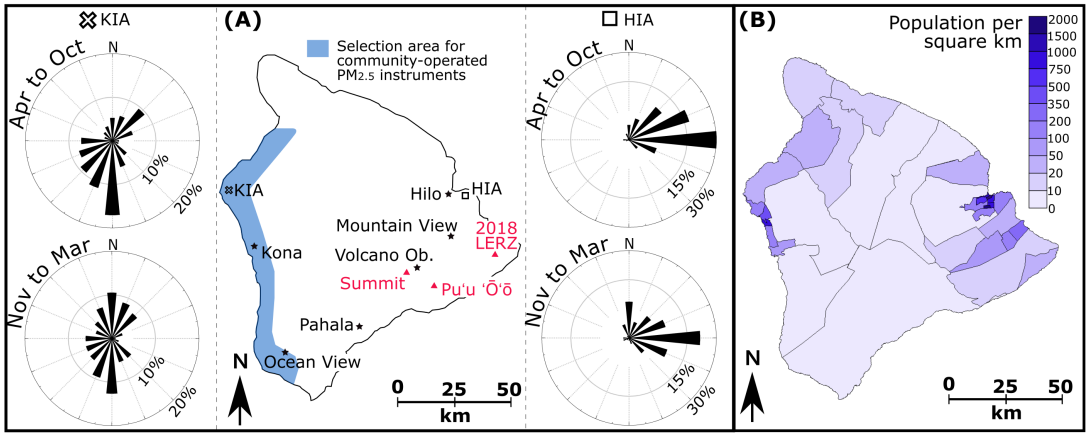

Figure 2.1: Island of Hawai'i. (A) Ground-based sampling networks; HDOH and NPS stations indicated with black stars. Kīlauea summit, Pu'u 'Ō'ō vent and 2018 lower East Rift Zone eruption site indicated with red triangles. Selection area of community-operated $PM_{2.5}$ instruments indicated with blue highlight. Wind directions at Kona International Airport (KIA, empty black cross) and Hilo International Airport (HIA, empty black square) displayed as seasonal wind roses for period 2007 - 2018 (NOAA, 2019). Note "Volcano Ob." stands for Volcano Observatory. (B) Population density per square kilometer on the Island of Hawai'i, based on 2010 Census data. Highest population density is located in the east-coast city of Hilo (population ≈ 45,700) and the west-coast city of Kailua-Kona (population ≈ 28,500) (Hawai'i Department of Business Economic Development and Tourism, 2011).

wind shadow allows a potentially longer residence time for air pollutants (volcanogenic or otherwise) along the densely-populated western coastline [Figure 2.1(B)]. During the winter months (November to March), the trade winds weaken and southerly and westerly winds may distribute vog towards the densely-populated eastern coastline of the island (Mannino et al., 1996; Michaud et al., 2004; Wyrtki and Meyers, 1976) [Figure 2.1(B)].

Numerous studies have investigated the impact of Kīlauea's SO_2 emissions on the health of island residents, even at the relatively low levels of degassing prior to the emergence of the lava lake in 2008. Mannino et al., 1996 reviewed the frequency of visits to emergency departments and hospitalisations for respiratory issues during periods of continuous and discontinuous SO_2 emissions throughout the 1980s. Communities on the western side of the island frequently exposed to vog were found to have higher rates of hospitalisations for chronic obstructive pulmonary disease than the east-coast city of Hilo, which is rarely exposed to vog. Periods of weakened north-easterly trade winds coincided with a 15 % increase in emergency department visits for asthma in Hilo (Mannino et al., 1996). In 2004, the health of Hawai'i residents in vog-exposed and -unexposed communities was surveyed (Longo et al., 2008; Longo, 2009). Those in exposed communities were found to have a significantly increased prevalence of cough, phlegm, sinus congestion, rhinorrhoea, wheezing, eye irritation and bronchitis than those in unexposed communities. Following the increase in SO_2 flux from Kīlauea's

summit in 2008, Longo, 2013 reassessed the vog-related health impacts on the residents of the Island of Hawai‘i. The magnitude of cardio-respiratory issues in vog-exposed communities was found to have increased as compared to 2004 (Longo et al., 2008), with the risk factor of acute cardiac events in persons aged >50 years increased by 12 % (Longo, 2013). A study by Tam et al., 2016 investigated the effects of vog on the respiratory health of school children across Hawai‘i, finding that chronic exposure to vog was associated with increased prevalence of cough and potential decrease in lung function, but not with the prevalence of asthma or bronchitis. The unprecedented emission rates of the 2018 LERZ eruption has presented a continued motivation to further characterise the severity and distribution of volcanic air pollution during elevated volcanic activity.

The 2018 Kīlauea LERZ eruption provided a unique opportunity to study the impacts arising from a large low-altitude cloud rich in SO_2 in a populated and well-instrumented part of the world. Here we used open-access data from a network of reference-grade instruments in populated areas around the Island of Hawai‘i to determine the severity of SO_2 and $PM_{2.5}$ impact on air quality from the LERZ eruption. We compare air quality during the LERZ eruption to that from a lower emission period, defined to be January 2007 to December 2017 for SO_2 and January 2010 to December 2017 for $PM_{2.5}$. We examine a network of community-operated $PM_{2.5}$ instruments and compare their measurements to those from reference-grade instruments. From these data, we demonstrate that SO_2 and $PM_{2.5}$ mass concentrations during the 2018 LERZ eruption in selected communities around the island were of a higher magnitude than during volcanic activity from Kīlauea during 2007 to 2017.

2.3 Data and Methods

2.3.1 Continuous SO_2 and $PM_{2.5}$ air quality monitoring

Hawaii Department of Health (HDOH) ambient air quality stations continuously monitor SO_2 and $PM_{2.5}$ mass concentrations around the Island of Hawai‘i [Figure 2.1(A)]. Automated SO_2 monitoring stations have been operational since 1997 in Hilo, 2005 in Kona, 2007 in Pahala and 2010 in Ocean View. A National Park Service (NPS) ambient air quality station monitors SO_2 inside of Hawai‘i Volcanoes National Park at the Volcano Observatory. $PM_{2.5}$ has been autonomously monitored since 2005 in Mountain View and Kona, 2008 in Hilo and Pahala and since 2010 in Ocean View.

SO_2 is measured by a pulsed fluorescence spectroscopy analyser (model 43i manufactured by Thermo Scientific) that is designated by the EPA for measurements in the range of 0 - 1000 ppb, with a lower detectable SO_2 limit of 0.5 ppb and a precision of 1 ppb (Thermo Fisher Scientific 2010; EPA, 2016). FEM-designated instruments

(Forum for Environmental Measurements), such as this SO_2 analyser, promote consistency in measurements and laboratory conditions ensuring that the instruments are of reference-grade quality (EPA, 2016). Following EPA regulations, the analysers undergo in-situ calibration checks weekly, with a multi-point calibration run every six months. $PM_{2.5}$ mass concentrations are measured by a Beta Attenuation Monitor (BAM) with a 60-minute sampling rate. The BAM instrument (model BAM-1020, manufactured by Met One Instruments) is FEM-designated for measurements of particles in the size range of 0 - 1000 µm (with $PM_{2.5}$ being a small subset of the measured particle size range), with a resolution of 1 µm particle diameter and a lower detection limit of 4 µg/m^3 (Met One Instruments Inc. 2008; EPA, 2016). The BAM instruments undergo calibration and auditing every six months. Permanent HDOH ambient air quality stations are kept in air-conditioned enclosures to maintain long-term stability. Data from the air quality stations are streamed in near-real time to the HDOH website, which is open-access and publicly-available (HDOH, 2019).

Data from the HDOH and NPS station networks used in this study have been categorised into regions for the purpose of data analysis. The western region includes Kona HDOH station on the west coast of the Island of Hawai‘i. The southern region includes Volcano Observatory NPS station and Pahala and Ocean View HDOH stations. The eastern region includes the Hilo and Mountain View HDOH stations. We compare the HDOH and NPS SO_2 timeseries data against the European Commission 24-hour air quality threshold (125 µg/m^3) and the Hawai‘i 24-hour ambient air quality standard (366 µg/m^3). The HDOH $PM_{2.5}$ timeseries data is compared to the World Health Organization 24-hour exposure limit (25 µg/m^3) and the Environmental Protection Agency NAAQS 24-hour limit (35 µg/m^3).

2.3.2 Community-operated $PM_{2.5}$ instruments

PurpleAir (Utah, USA) instruments are low-cost (approximately $250 per unit) particulate sensors that are purchased and operated by individuals and provide open access data online (PurpleAir, 2019). PurpleAir instruments contain Plantower PMS5003 nephelometer sensors, which use a small fan to draw air through a laser-induced light, and a photo-diode detector converts 90°-scattered light into a voltage pulse (Kelly et al., 2017). PMS5003 sensors have a 10 second response time and detect particles between 0.3 µm - 10 µm in diameter (Kelly et al., 2017; Sayahi et al., 2019). The maximum consistency error of the sensors is stated by the manufacturer to be ± 10 µg/m^3 between 0 - 100 µg/m^3 (Plantower, 2016). The instruments are factory calibrated prior to sale (PurpleAir, 2019). PM mass concentration measurements are calculated using an atmospheric calibration factor, details of which are not provided by the manufacturer (Kelly et al., 2017; Sayahi et al., 2019; Zheng et al., 2018). PurpleAir instruments con-

tain two Plantower PMS5003 sensors mounted in one housing, allowing self-consistency checks to alert when significant differences are reported between the internal sensors. An ESP8266 wireless chip is included in PurpleAir instruments to upload data via WiFi to an online cloud database, which is open-access (Sayahi et al., 2019).

Prior to the 2018 LERZ eruption, six community-operated PurpleAir instruments were located on the Island of Hawai‘i, three of which were in the Kona area in the western region. Installation dates ranged from August 2017 to February 2018. Following the onset of the LERZ eruption and island-wide increase in atmospheric pollutants, the number of PurpleAir instruments increased, with a further twenty instruments installed across the western region of the island over the course of May to July 2018. These instruments were purchased and installed by individuals and were not part of a coordinated community network.

We carried out fieldwork during the 2018 LERZ eruption and co-located PurpleAir instruments with HDOH ambient air quality stations at Kona and Ocean View [Figure 2.1(A)]. Two PurpleAir PA-II instruments were installed at the Kona station, one from the fifth of June to September 2018 and a second from the nineteenth of July to the third of August, and one PurpleAir PA-II instrument was installed at the Ocean View station from the nineteenth of July to the third of August 2018. The PurpleAir instruments were installed close to the inlet for the BAM instruments, on the roofs of the air quality shelters and away from obstructions. Other than the coordinates of the instrument, no spatial environmental information is provided in association with the PurpleAir instruments. The digital location of PurpleAir instruments is manually pin-pointed by the user during the installation process and we assume that the given measurement location matches reality. However we cannot determine whether the instrument location is optimised for PM measurements, i.e. away from potential contaminants or obstacles which would bias the PM measurements. For this reason, measurement uncertainty arising from factors such as installation in proximity to potential contamination sources in community-operated PurpleAir instruments should be considered significantly higher than those placed in optimal conditions near HDOH stations. Community-operated PurpleAir instruments were selected for analysis along the region highlighted in blue in Figure 2.1(A).

2.4 Results

2.4.1 SO_2 mass concentrations 2007 - 2018

2.4.1.1 Western region: Kona

During 2007 - 2017, the west-coast city of Kailua-Kona was commonly exposed to low mass concentrations of SO_2, with a maximum recorded 24-hour-mean mass concentra-

tion of 79 µg/m^3 recorded at the Kona HDOH station [Table 2.1]. SO_2 air pollution in Kona increased with the onset of summit activity in 2008 (2008 - 2017 average mass concentrations were 7.7 µg/m^3 compared to 3 µg/m^3 in 2007) [Figure 2.2(B)]. During 2007 - 2017 there were no 24-hour periods where SO_2 mean mass concentrations at the HDOH Kona station exceeded Hawai‘i or EC recommended thresholds [Figure 2.2(B)].

Kona experienced elevated SO_2 mass concentrations during the 2018 LERZ eruption, with a peak 24-hour-mean mass concentration of 136 µg/m^3 measured at the Kona station. During the 2018 LERZ eruption, SO_2 mass concentrations in Kona did not exceed the Hawai‘i SO_2 threshold of 366 µg/m^3 [Figure 2.2(B)], but did exceed the 125 µg/m^3 EC threshold on one occasion [Table 2.1].

2.4.1.2 Southern region: Volcano Observatory, Pahala and Ocean View

Following initiation of Kīlauea's summit activity in 2008, the HDOH-operated Pahala station and the NPS-operated Volcano Observatory station routinely recorded high concentrations of SO_2 [Figure 2.2(C)], with SO_2 mass concentrations exceeding the Hawai‘i 366 µg/m^3 24-hour-mean threshold 0.7 % of the time at both Volcano Observatory (twenty-eight exceedance events) and Pahala (thirty exceedance events) [Table 2.1]. The maximum 24-hour-mean mass concentration recorded by the NPS station at Volcano Observatory during 2007 - 2017 was 1068 µg/m^3, and by the HDOH station in Pahala was 776 µg/m^3. The Ocean View HDOH station is located farther to the south-west than Pahala and Volcano Observatory, at a greater distance from Kīlauea's summit and the ERZ [Figure 2.1(A)]. During the period 2010 - 2017, SO_2 mass concentrations recorded at Ocean View exceeded the Hawai‘i 24-hour-mean threshold 0.1 % of the time (three exceedance events). The maximum 24-hour-mean mass concentration recorded at Ocean View was 403 µg/m^3, significantly lower than measured at Volcano Observatory and Pahala [Table 2.1].

In comparison, during the 3-months of the 2018 LERZ eruption, SO_2 mass concentrations exceeded the Hawai‘i 366 µg/m^3 threshold 2.1 % of the time at Volcano Observatory (two exceedance events), 5.3 % of the time at Pahala (five exceedance events) and 4.2 % at Ocean View (four exceedance events). Maximum 24-hour-mean mass concentrations at Volcano Observatory and Pahala were lower than those measured during 2008 - 2017 (450 µg/m^3 and 555 µg/m^3, respectively), but the relative frequency of exceedance events increased [Table 2.1]. During the 2018 LERZ eruption, the Ocean View station recorded a peak 24-hour-mean mass concentration of 728 µg/m^3, almost double the previous peak measurement of 403 µg/m^3 recorded at that station in January 2016.

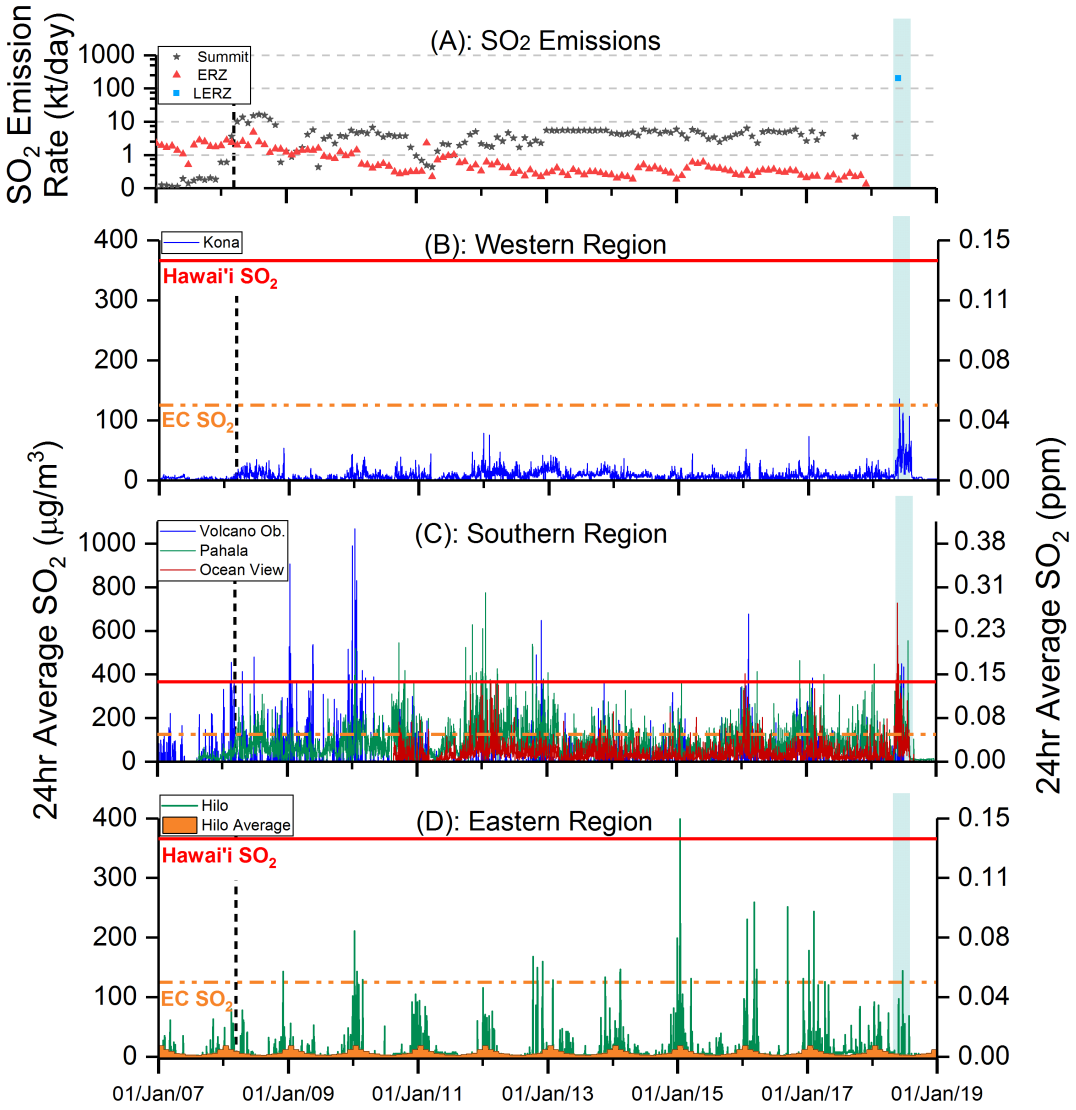

Figure 2.2: SO_2 mass concentrations relative to health guidelines in selected populated areas of Island of Hawai'i. (A): SO_2 emissions from Kīlauea summit indicated with black stars; from ERZ indicated with red triangles; from 2018 LERZ eruption indicated with blue square. Note logarithmic scale. (B,C,D): SO_2 air quality (24-hour mean) in communities from 2007 to the end of 2018. Solid red line: Hawai'i Standard air quality threshold (24-hr mean - 366 µg/m^3); dashed orange line: European Commission (EC) air quality threshold (24-hr mean - 125 µg/m^3). Dashed black line: 2008 initiation of summit activity; blue highlight: 2018 LERZ eruption duration. (A): SO_2 emissions data sourced from Beirle et al., 2014; Elias et al., 2018; Elias and Sutton, 2012; Elias et al., in preparation. Summit emissions for 2008 - 2012 are from Beirle et al., 2014. LERZ data-point represents the average SO_2 emission from the LERZ eruption for June 2018, taken from Kern et al., 2019. (B) note that "Volcano Ob." stands for Volcano Observatory; (D) seasonal average for Hilo between 2007 - 2017 indicated by orange bars.

2.4.1.3 Eastern region: Hilo

During the period 2007 - 2017, SO_2 mass concentrations in Hilo followed a distinct seasonality [Figure 2.2(D)]. Peak SO_2 mass concentrations were commonly observed in Hilo in November to March (average monthly concentration of 11 $\mu g/m^3$) with low mass concentrations in the intervening months of April to October (average monthly mass concentration of 3.6 $\mu g/m^3$, as calculated from 2007 - 2017) [Figure 2.2(D)]. Exceedances of the EC 24-hour-mean threshold (125 $\mu g/m^3$) rarely occurred outside this peak season. In the period 2007 - 2017 there were twenty-one exceedance events during November to March, compared with just three between April to October. The seasonal variations in SO_2 mass concentrations observed in Hilo can be explained by the strong prevalence of northeasterly trade winds during April to October (Wyrtki and Meyers, 1976) [Figure 2.1(A)]. During these months, emissions from Kīlauea's summit and the ERZ were dispersed predominantly to the south-west of the Island. The trade winds weaken between November to March, allowing SO_2 to be dispersed to the east of the island (Elias and Sutton, 2017; Mannino et al., 1996; Michaud et al., 2004).

During the third of May to fourth of August LERZ eruption, the HDOH station in Hilo recorded a maximum 24-hour-mean mass concentration of 144 $\mu g/m^3$, which was recorded on the twenty-first of June [Table 2.1], and was the only exceedance of the EC 24-hour-mean threshold during the three-month eruption. The SO_2 mass concentrations measured during the LERZ eruption were lower than the average measurements during the 2007 - 2017 period. SO_2 mass concentrations in Hilo are usually low during the months when the LERZ eruption occurred. Nevertheless, during the 2018 LERZ eruption, SO_2 mass concentrations in Hilo rose significantly above the average for the season (average 24-hour-mean SO_2 mass concentration during 2018 LERZ eruption was 6.9 $\mu g/m^3$, in comparison to the usual seasonal average of 3.6 $\mu g/m^3$).

Table 2.1: Impact of the 2018 LERZ eruption on concentrations of SO_2 and $PM_{2.5}$. All units in µg/m^3. Exceedances of air quality standards are indicated for 24 hour means, and calculated as percentage of total measurement duration. Distances between emission points and measurements sites are straight line distances; the emissions will not always follow the most direct route from near- to far-field. Note: no data available for $PM_{2.5}$ at Volcano Observatory, or Hilo for 2010 - 2017; no data available for SO_2 at Mountain View. * Low emission period for SO_2 from the first of January 2007 to the thirty-first of December 2017 and for $PM_{2.5}$ from the first of September 2010 to the thirty-first of December 2017; ** high emission 2018 LERZ period for SO_2 and $PM_{2.5}$ from the third of May 2018 to the sixth of August 2018. *** Exceptions due to data availability: Mountain View low emission for $PM_{2.5}$ from the first of December 2010 to the thirty-first of December 2017; Volcano Observatory high emission 2018 LERZ period for SO_2 from the third of May 2018 to the third of July 2018; Ocean View low emission for SO_2 from twenty-third of August 2010 to the thirty-first of December 2017.

Station Location	Measurement Period	Sulfur Dioxide (SO_2)				Particulates ($PM_{2.5}$)			
		(SO_2) (ug/m^3) 24-hour mean		Exceedance Hawai'i threshold (24-hour > 366 ug/m^3)	Exceedance EC threshold (24-hr > 125 ug/m^3)	($PM_{2.5}$) (ug/m^3) 24-hour mean		Exceedance EPA threshold (24-hour > 35 ug/m^3)	Exceedance WHO guideline (24-hr > 25 ug/m^3)
Hilo Elevation: 121 m asl 40 km NE of summit 35 km NW of Fissure 8	Low Emission *	Average	7	1 day 0%	24 days 0.6%	Average	-	[No Data]	[No Data]
		σ	19			σ	-		
		Max	403			Max	-		
	High Emission 2018 LERZ **	Average	6	0 days 0%	1 day 1.1%	Average	5	0 days 0%	0 days 0%
		σ	21			σ	2		
		Max	144			Max	15		
Mountain View Elevation: 426 m asl 26 km NE of summit 23 km NW of Fissure 8	Low Emission ***	Average	-	[No Data]	[No Data]	Average	4	1 day 0%	3 days 0.1%
		σ	-			σ	4		
		Max	-			Max	35		
	High Emission 2018 LERZ **	Average	-	[No Data]	[No Data]	Average	7	0 days 0%	0 days 0%
		σ	-			σ	6		
		Max	-			Max	18		
Volcano Observatory Elevation: 1161 m asl 2 km NW of summit 35 km W of Fissure 8	Low Emission *	Average	24	28 days 0.7%	204 days 5.1%	Average	-	[No Data]	[No Data]
		σ	67			σ	-		
		Max	1068			Max	-		
	High Emission 2018 LERZ ***	Average	56	2 days 2.1%	10 days 10.5%	Average		[No Data]	[No Data]
		σ	106			σ	-		
		Max	450			Max	-		

Table 2.2: Continuation of Table 2.1

Station Location	Measurement Period	Sulfur Dioxide (SO_2)				Particulates ($PM_{2.5}$)			
		(SO_2) (ug/m^3) 24-hour mean		Exceedance Hawai'i threshold (24-hour > 366 ug/m^3)	Exceedance EC threshold (24-hr > 125 ug/m^3)	($PM_{2.5}$) (ug/m^3) 24-hour mean		Exceedance EPA threshold (24-hour > 35 ug/m^3)	Exceedance WHO guideline (24-hr > 25 ug/m^3)
Pahala Elevation: 320 m asl 30 km SW of summit 66 km SW of Fissure 8	Low Emission *	Average	81	30 days 0.7%	729 days 18.1%	Average	6	2 days 0.1%	3 days 0.1%
		σ	72			σ	5		
		Max	776			Max	97		
	High Emission 2018 LERZ **	Average	129	5 days 5.3%	34 days 35.8%	Average	10	0 days 0%	0 days 0%
		σ	108			σ	5		
		Max	555			Max	24		
Ocean View Elevation: 862 m asl 61 km W of summit 100 km W of Fissure 8	Low Emission ***	Average	26	3 days 0.1%	93 days 3.5%	Average	12	4 days 0.1%	25 days 0.9%
		σ	39			σ	5		
		Max	403			Max	42		
	High Emission 2018 LERZ **	Average	117	4 days 4.2%	27 days 28.4%	Average	26	10 days 10.5%	44 days 46.3%
		σ	114			σ	8		
		Max	728			Max	56		
Kona Elevation: 517 m asl 67 km W of summit 106 km W of Fissure 8	Low Emission *	Average	7	0 days 0%	0 days 0%	Average	12	0 days 0%	33 days 1.2%
		σ	7			σ	5		
		Max	79			Max	33		
	High Emission 2018 LERZ **	Average	39	0 days 0%	1 days 1.1%	Average	24	8 days 8.4%	33 days 34.7%
		σ	25			σ	9		
		Max	136			Max	59		

2.4.2 $PM_{2.5}$ mass concentrations 2010 - 2018

2.4.2.1 Western region: Kona

In the period 2010 - 2017, $PM_{2.5}$ recorded by HDOH Kona station never exceeded the EPA 24-hour-mean threshold of 35 µg/m^3 [Figure 2.3(A)]. The WHO 24-hour-mean guideline of 25 µg/m^3 was exceeded 1.2 % of the time at the Kona site (thirty-three exceedance events). The maximum $PM_{2.5}$ 24-hour-mean mass concentrations was 33 µg/m^3, recorded in April 2016 [Table 2.1].

During the 2018 LERZ eruption, $PM_{2.5}$ exceeded the 24-hour-mean 35 µg/m^3 EPA threshold 8.4 % of the time at the Kona station (eight exceedance events). The lower guideline of 25 µg/m^3 established by the WHO was exceeded 34.7 % of the time at the Kona site (thirty-three exceedance events). The maximum $PM_{2.5}$ 24-hour-mean mass concentration at the site was recorded as 59 µg/m^3 on the twenty-ninth of May 2018.

2.4.2.2 Southern region: Pahala and Ocean View

During the period 2010 - 2017, the southern region of the Island of Hawai‘i experienced variable levels of $PM_{2.5}$ [Figure 2.3(B)]. The maximum $PM_{2.5}$ 24-hour-mean mass concentration recorded in Ocean View was 42 µg/m^3, recorded in March 2016. In Pahala the maximum recorded $PM_{2.5}$ 24-hour-mean mass concentration was 97 µg/m^3, recorded on the eighteenth of June 2012, and coincident with two brush fires in the vicinity of Pahala which burned approximately 5600 acres (Hawai‘i Emergency Management Agency, 2018). The EPA 35 µg/m^3 $PM_{2.5}$ threshold was exceeded 0.1 % of the time at both Ocean View and Pahala (four exceedance events and two exceedance events, respectively). The lower $PM_{2.5}$ guideline of 25 µg/m^3 established by the WHO was exceeded 0.9 % of the time at Ocean View (twenty-five exceedance events) and 0.1 % of the time at Pahala (three exceedance events).

Mean $PM_{2.5}$ mass concentrations in Pahala during the 2018 LERZ eruption were higher than the 2010 - 2017 average (10 µg/m^3 with respect to 6 µg/m^3) [Table 2.1], however there were no 24-hour periods which exceeded either the EPA or WHO 24-hour-mean thresholds. During the 2018 LERZ eruption, $PM_{2.5}$ recorded in Ocean View exceeded the 35 µg/m^3 EPA threshold 10.5 % of the time (ten exceedance events) and exceeded the WHO 24-hour-mean guideline 46.3 % of the time (forty-four exceedance events). In mid-June 2018, the Ocean View HDOH station recorded three consecutive days where 24-hour-mean mass concentrations exceeded 35 µg/m^3, unprecedented in the period 2010 - 2017. The maximum 24-hour-mean mass concentration recorded in Ocean View during the 2018 LERZ eruption was 56 µg/m^3, somewhat higher than the peak 24-hour-mean mass concentration recorded at Ocean View in 2016 (42 µg/m^3).

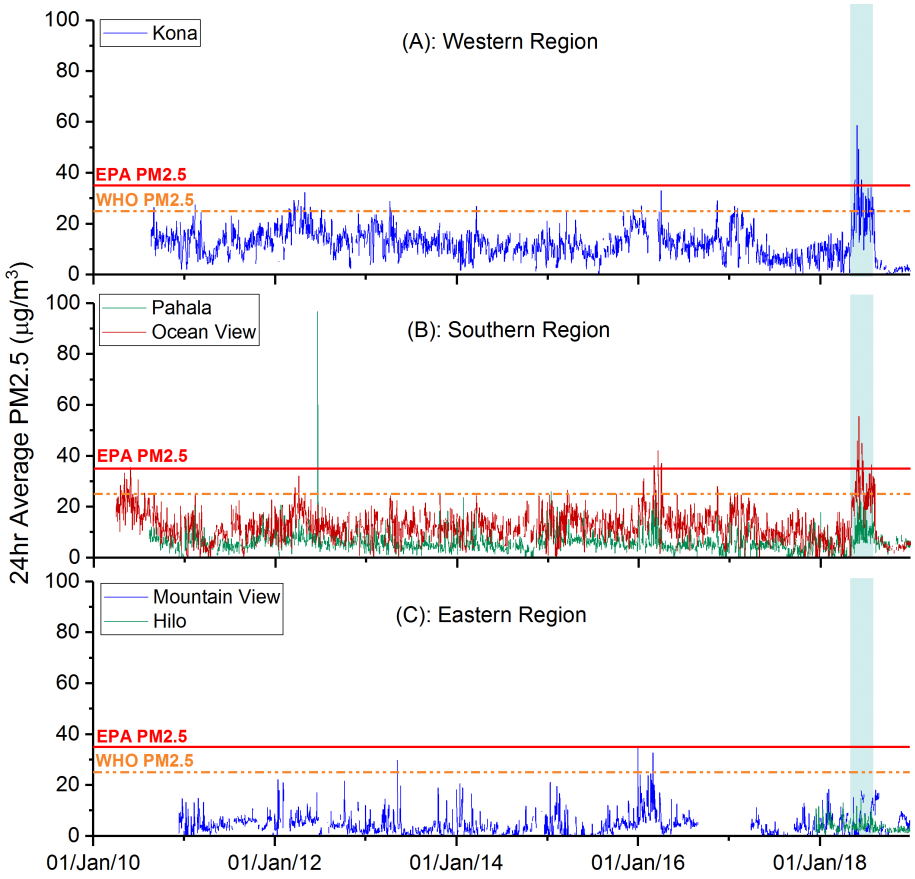

Figure 2.3: $PM_{2.5}$ mass concentrations relative to health guidelines in select populated areas of Island of Hawai'i. (A,B,C): concentrations of $PM_{2.5}$ (24-hour mean) in populated areas from 2010 to the end of 2018. Solid red line: EPA Federal Standard air quality threshold (24-hr mean - 35 µg/m^3); dashed orange line: World Health Organization (WHO) air quality guideline (24-hr mean - 25 µg/m^3); blue highlight: 2018 LERZ eruption duration.

2.4.2.3 Eastern region: Hilo and Mountain View

HDOH stations in the eastern region of the Island of Hawai'i recorded variable levels of $PM_{2.5}$ during 2010 - 2017 [Figure 2.3(C)]. The maximum $PM_{2.5}$ 24-hour-mean mass concentration in Mountain View was 35 µg/m^3, which was recorded in December 2015, and was the only exceedance of the 35 µg/m^3 24-hour-mean EPA threshold during the period 2010 - 2017 [Figure 2.3(C)]. The lower $PM_{2.5}$ 24-hour-mean guideline of 25 µg/m^3 established by the WHO was exceeded 0.1 % of the time at Mountain View (three exceedance events).

During the 2018 LERZ eruption, $PM_{2.5}$ mass concentrations in Mountain View were higher than the average mass concentrations for 2010 - 2017 (7 µg/m^3 and 4 µg/m^3, respectively) [Table 2.1]. However, during the 2018 LERZ eruption, $PM_{2.5}$ mass concentrations did not exceed either the EPA threshold of 35 µg/m^3 or the WHO guideline

of 25 µg/m^3.

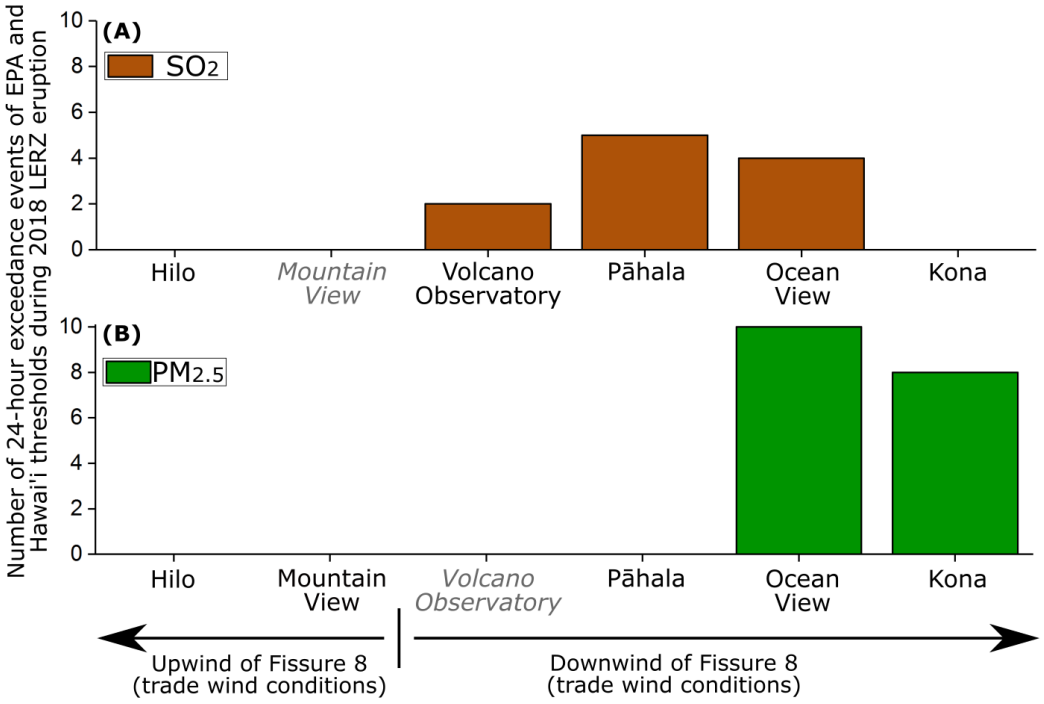

Figure 2.4: Exceedances of (A) 24-hour Hawai'i Standard for SO_2 during 2018 LERZ eruption and (B) EPA threshold for $PM_{2.5}$ during 2018 LERZ eruption. Note: data were unavailable for $PM_{2.5}$ at Volcano Observatory and SO_2 at Mountain View.

2.5 Discussion

2.5.1 Dispersal of volcanic emissions

Time series of SO_2 mass concentrations were analysed in five populated areas on the Island of Hawai'i; Hilo, Volcano Observatory, Pahala, Ocean View and Kona, for the period 2007 - 2018 [Figure 2.2]. Time series of $PM_{2.5}$ were analysed in Hilo, Mountain View, Pahala, Ocean View and Kona for the duration 2010 - 2018 [Figure 2.3]. Significant escalations in emissions from Kīlauea volcano can be identified [Figure 2.2(A)], which were registered by the air quality monitoring instruments around the Island of Hawai'i [Table 2.1, section 4.1 and 4.2].

High mass concentrations of SO_2 and $PM_{2.5}$ generally occurred in the southern and western parts of the Island of Hawai'i. Prevailing trade winds from the north-east dispersed SO_2 emissions from Kīlauea volcano towards communities in the south and west of the island, as reported in previous studies (Longo et al., 2008; Longo et al., 2005; Michaud et al., 2007; Tam et al., 2016). During the 2018 LERZ eruption, the EPA 24-hour-mean threshold for $PM_{2.5}$ (35 µg/m^3) and the Hawai'i threshold for SO_2 (366 µg/m^3) were exceeded in the south and west of the island [Figure 2.4]. HDOH

stations in the south of the island, 35 - 100 km away from Fissure 8, recorded 24-hour events where SO_2 exceeded Hawai'i thresholds (note that there were no HDOH or NPS permanent monitoring stations for SO_2 in proximal location to the 2018 LERZ eruption site), but $PM_{2.5}$ EPA exceedance events only occurred at HDOH stations 100 km or further away from Fissure 8 [Figure 2.4]. This spatial variance between distribution of $PM_{2.5}$ and SO_2 is well-documented and thought to reflect the timescale of oxidation of sulfur dioxide gas into sulfate aerosol during dispersion (Cadle et al., 1971; Ilyinskaya et al., 2017; Porter et al., 2002; Stockwell and Calvert, 1983).

Volcanic emissions at source commonly consist of a mixture of silicate ash particles, various gases and non-silicate aerosol (Langmann, 2014; Oppenheimer and McGonigle, 2004; von Glasow et al., 2009). The lifetime of SO_2 in the lower troposphere is generally considered to be on the order of one - three days to a week (Allen et al., 2002; Pattantyus et al., 2018; Pfeffer et al., 2006a; Rotstayn and Lohmann, 2002), the rate of conversion depending on relative humidity and temperature, the availability of oxidants, and interaction with cloud or fog (Oppenheimer et al., 1998; Saxena and Seigneur, 1987). However, the SO_2 oxidation pathways in a volcanic cloud are not necessarily the same as under background conditions (Galeazzo et al., 2018). Through a variety of reaction pathways (including oxidation with the hydroxyl radical, -OH, with hydrogen peroxide, H_2O_2, and with ozone, O_3), SO_2 in volcanic clouds is gradually converted to sulfate aerosol (Allen et al., 2002; Stockwell and Calvert, 1983), which is a dominant component of volcanic $PM_{2.5}$ (Pattantyus et al., 2018; Tam et al., 2016). The conversion rate of SO_2 to sulfate aerosol is important for estimating the potential hazard of volcanic $PM_{2.5}$ to human health and the downwind environments (Kroll et al., 2015).

HDOH stations measure the ambient air, which contains SO_2 and $PM_{2.5}$ derived from anthropogenic sources as well as natural non-volcanic and volcanic sources. In order to determine the influence of the volcanic eruption on the measured SO_2 and aerosol abundances, it is first necessary to calculate the volcanic component of the HDOH measurements. During the 2018 LERZ eruption, Fissure 8 was the dominant source of volcanic SO_2 emissions on the island, and following the decline of the eruption, the SO_2 and $PM_{2.5}$ mass concentrations decreased to below pre-LERZ eruption levels at all HDOH stations analysed in this study [Figure 2.2, 2.3]. The mass of pollutants recorded at HDOH stations during this post-LERZ eruption period (mid-August 2018 to the first of February 2019) are therefore used to define the background abundances arising from all other non-volcanic sources. During this time there was some SO_2 emitted from Kīlauea's summit but at the lowest rate measured in decades at 0.1 kt/year (Nadeau et al., 2019). The volcanic component of the HDOH measurements was calculated by subtracting the average $PM_{2.5}$ and SO_2 mass concentration following the end of the 2018 LERZ eruption for each station from the mass concentrations measured during the LERZ eruption, to estimate the volcanogenic component. The sulfate aerosol

component within the volcanic $PM_{2.5}$ mass concentration was then estimated to be in the range 77 % - 92 %, following the methods of Mather et al., 2012 and Kroll et al., 2015, of $PM_{2.5}$ composition from Kīlauea.

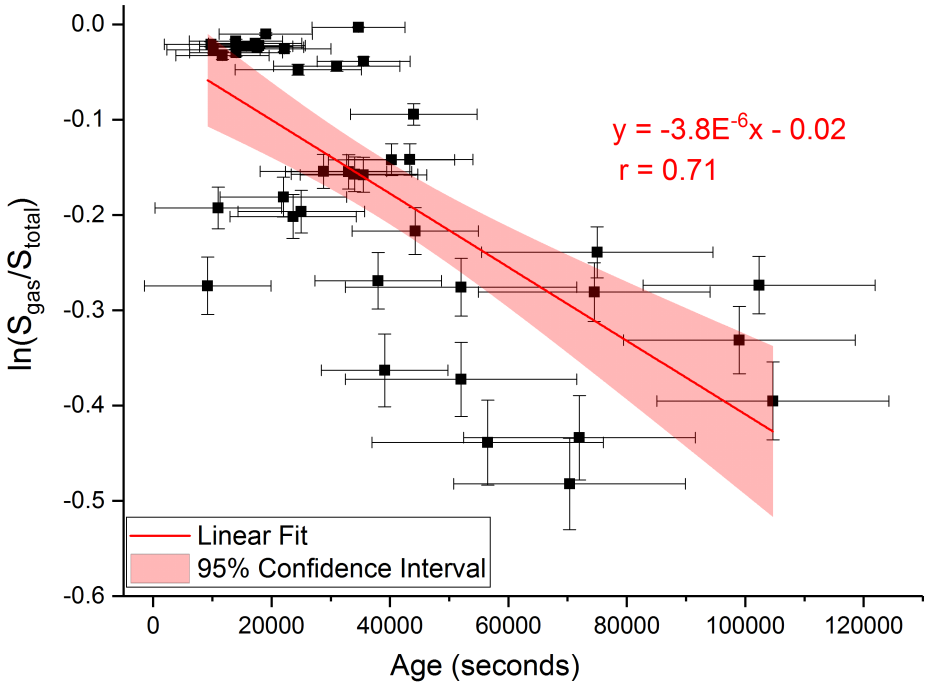

Figure 2.5: Relationship between the age of the volcanic cloud and the volcanic sulfur components measured at Pahala, Ocean View and Kona HDOH ambient air quality stations. S_{gas} is the sulfur component of the volcanic SO_2 mass concentration, S_{total} is the sum of sulfur components of the volcanic SO_4^{2-} and SO_2 mass concentrations. Age is derived from HYSPLIT back-trajectory simulations (Ilyinskaya et al., in preparation). Y axis error bars indicate range of SO_4^{2-} component in volcanic $PM_{2.5}$ composition from Kīlauea. X axis error bars indicate one standard deviation of HYSPLIT back-trajectory results specific to Kona, Ocean View and Pahala. Correlation trendline based on the data points, with a first-order decay constant of 3.8 x 10^{-6} s^{-1} with a 95 % confidence interval of ± 1.26 x 10^{-6} s^{-1}.

Estimating the conversion rate of SO_2 to sulfate from SO_2 and SO_4^{2-} datasets is not straightforward because several processes can occur simultaneously, including SO_2 oxidation to sulfate, dispersion-dilution and deposition of SO_2 and/or SO_4^{2-} to the surface.

Here, a first-order decay constant for SO_2 is estimated by the relationship between volcanic components of SO_2 and SO_4^{2-}, as follows;

$$\ln\left(\frac{S_{gas}}{S_{total}}\right) = -kt \tag{2.1}$$

where S_{gas} is the sulfur component of the volcanic SO_2 mass concentration (µg/m^3),

S_{total} is the sum of sulfur components of the volcanic SO_4^{2-} and SO_2 mass concentrations ($\mu g/m^3$), t is the age of the volcanic cloud (seconds) and $-k$ is a first-order decay constant.

The age of the volcanic cloud is here considered to be the time between emission of the cloud at the LERZ eruption source point and subsequent measurement at the HDOH station. From back-trajectory HYSPLIT simulations run between the HDOH ambient air quality stations and Fissure 8, the average age of the emissions and dispersal distance was calculated for dates between the eighteenth of July to the second of August 2018 (Ilyinskaya et al., in preparation). An estimate of the average first-order decay constant from our data-set is indicated in Figure 2.5. Although there is considerable scatter in the data, a broad trend of decreasing S fraction in the gas phase is apparent and a linear fit allows us to estimate a first-order rate constant of 3.8 x 10^{-6} s^{-1} with a 95 % confidence interval of ± 1.26 x 10^{-6} s^{-1}. This first-order decay constant for SO_2 relative to total sulfur can represent an estimate of the average rate of SO_2 oxidation to sulfate only if negligible sulfur deposition has occurred. Nevertheless, our value is similar to the SO_2 oxidation rate calculated by Kroll et al., 2015 from direct measurements of sulfur in gas and particle phase in Kīlauea's emission cloud from the summit to Pahala. Kroll et al., 2015 identified a diurnal cycle in measured sulfate as a fraction of total sulfur, from which they calculated a noontime instantaneous SO_2 oxidation rate of 2.4 x 10^{-6} s^{-1}.

2.5.2 Reliability assessment of community-operated $PM_{2.5}$ instruments

A subset of the community-operated PurpleAir instruments on the Island of Hawai'i were selected for intercomparison with the established institutional data-sets across the western region of the island. The low-cost and portable nature of the PurpleAir instruments facilitated installation of a monitoring network across the western region [Figure 2.6(A)], with a high spatial resolution of measurements in comparison to the locations of HDOH ambient air quality sites [Figure 2.6(A)]. This can be advantageous to capture the effects of local topographic and meteorological factors, which may influence dispersion of and deposition from volcanic plumes. Mass concentrations from PurpleAir instruments and HDOH $PM_{2.5}$ instruments during the course of the 2018 LERZ eruption are presented in Figure 2.6 (B - E).

Small differences were found between individual PurpleAir instruments in the same location. Two PurpleAir instruments [Figure 2.6(A), PurpleAir references 10 and 11] were co-located at the Kona HDOH station, and the PurpleAir instruments ran together for 16 days. During this time, the maximum absolute differences in 24-hour average measurements between the PurpleAir instruments was 2.3 $\mu g/m^3$; which was 6 % of the total measured concentration. Correlation between the two PurpleAir instruments was very strong (Pearson's r = 0.99). Similar results were found by Malings et al., 2019 with co-location of nine PurpleAir instruments at a site in Pennsylvania for a period of 66

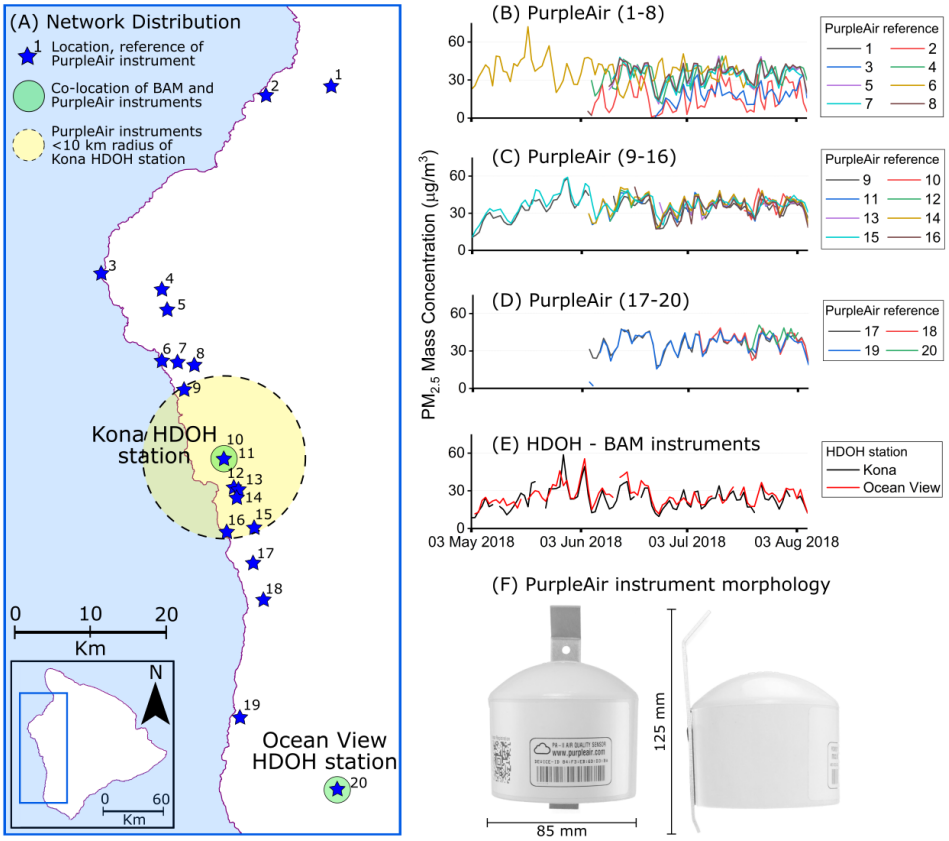

Figure 2.6: Hawaii Department of Health ambient air quality stations and community-operated PurpleAir instruments along the western region of the Island of Hawai'i selected for analysis in this study. [A]: distribution of publicly-owned PurpleAir instruments, indicated by blue stars with reference numbers, distribution of Kona and Ocean View HDOH stations indicated by green circles. PurpleAir instruments within 10 km radius of Kona HDOH station indicated by dashed yellow circle. [B,C,D]: 24-hour average mass concentration measurements from 20 PurpleAir instruments during the 2018 LERZ eruption; [E]: 24-hour average $PM_{2.5}$ from BAM instruments at Kona and Ocean View HDOH ambient air quality stations during the 2018 LERZ eruption. [F] Size and morphology of the PurpleAir instruments, seen from the front (left image) and side (right image). Photos by kind permission of PurpleAir LLC.

days (Pearson's r $>$ 0.9). The high correlation between co-located individual PurpleAir instruments indicates high standardisation. With this being the case, relative $PM_{2.5}$ mass concentrations measured by PurpleAir instruments over a wider geographical area should be comparably reliable.

Three PurpleAir instruments were co-located with HDOH $PM_{2.5}$ instruments (BAM) to determine the accuracy of PurpleAir instrument $PM_{2.5}$ measurements in relation to reference-grade instruments [Figure 2.6(A), PurpleAir references 10, 11 and 20]. The co-located PurpleAir measurements correlated well with the BAM measurements, with Pearson's r values of 0.99, 0.97 and 0.91 [Figure 2.7(A, B)]. However, PurpleAir instruments did record higher mass concentrations of $PM_{2.5}$ in comparison to the BAM analysers [Figure 2.7(A, B)]. PurpleAir reference 10 (co-located with Kona HDOH sta-

tion) [Figure 2.6(A)] recorded the greatest measurement off-set, with up to 40 % higher mass concentrations of $PM_{2.5}$ relative to the Kona BAM analyser measurements [Figure 2.7(A)]. This trend was also found when the community-operated PurpleAir instruments across the western region of the island were compared to the BAM at Kona HDOH station [Figure 2.7(C)], with strong correlation between PurpleAir instruments and BAM (Pearson's r = 0.92) but an average 30 % higher mass concentrations measured by PurpleAir instruments within 10 km of the Kona BAM instrument. Previous testing of PurpleAir instruments in Pennsylvania and California has yielded similar findings (AQ-SPEC, 2017; Malings et al., 2019), with over-estimation of $PM_{2.5}$ mass concentrations measured by PurpleAir instruments relative to BAM reference-grade analysers.

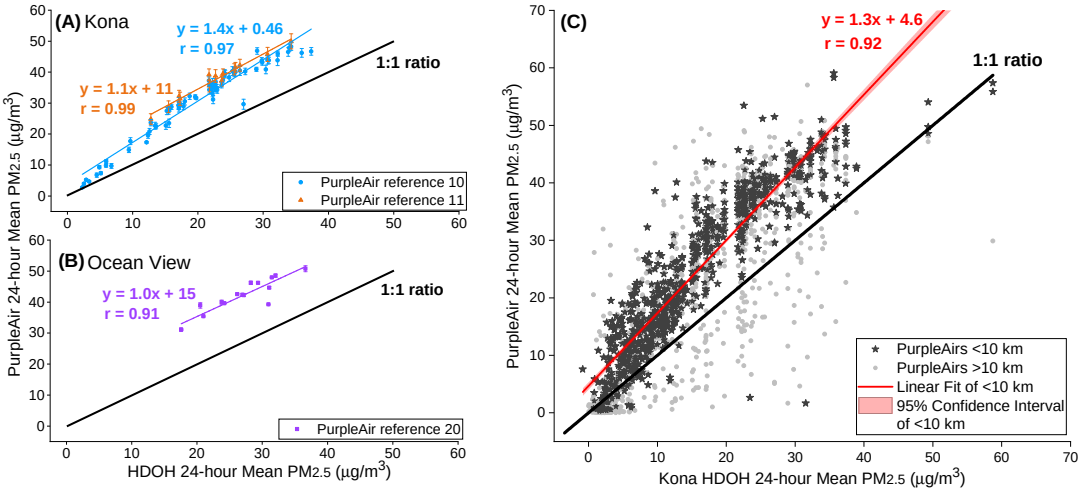

Figure 2.7: PurpleAir and HDOH $PM_{2.5}$ comparison. (A) two PurpleAir instruments co-located with Kona HDOH station; (B) one PurpleAir instrument co-located with Ocean View HDOH station. (C) comparison of all PurpleAir instruments along the western region of the Island of Hawai'i compared with Kona HDOH measurements. PurpleAir instruments within 10 km of Kona HDOH indicated by dark grey stars, PurpleAir instruments at greater distances are indicated by light grey circles. Linear regression and 95 % confidence interval fit to instruments $<$ 10 km from Kona HDOH ambient air quality station. Measurement periods vary with earliest PurpleAir data from August 2017 and most recent from January 2019. (A,B) PurpleAir error bars show measurement variations between the two sensors within a single PurpleAir instrument, and therefore indicate the minimum error.

As discussed above, the PM measurements from the community-operated PurpleAir instruments within 10 km of the Kona HDOH station correlated well to the Kona BAM analyser during the 2018 LERZ eruption, but overestimated the concentration of $PM_{2.5}$ by up to 30 % [Figure 2.7]. The PurpleAir measurements could be corrected to reduce the overestimation off-set, allowing a better accuracy determination of the low-cost instrument with respect to the reference-grade analyser. However, in this instance we chose not to correct the PM measurements from the PurpleAir instruments as the purpose of this analysis was to determine whether the measurements from the PurpleAir sensors were providing an accurate source of information to the public during the LERZ

eruption. During the 2018 LERZ eruption, the measurements from the PurpleAir instruments were automatically uploaded in near-real-time to the dedicated web browser and were used by members of the public as a source of additional information regarding the day-to-day volcanic PM air quality in their region. Our analysis here allows an assessment of whether the PurpleAir measurements which were available to the public were representative and accurate indicators of the concentration and spread of particulates. Future studies could investigate whether use of humidity correction factors, such as discussed in Crilley et al., 2018; Crilley et al., 2020 and used in Whitty et al., 2022, could be implemented on the 2018 LERZ eruption PurpleAir data to limit the overestimation.

Some discrepancy between PurpleAir and BAM measurements may be expected, as it is well-known that low-cost instruments measuring $PM_{2.5}$ with light scattering methods have not historically agreed with measurements obtained from reference grade instruments with different operating principles (Burkart et al., 2010; Chow et al., 2008; Watson et al., 1998; Wilson et al., 2002). In comparison with sensors of other operating principles, light-scattering optical particle sensors have been shown to suffer effects of relative humidity (Crilley et al., 2018; Wang et al., 2015), since the operating principle relies on indirect measurement of particle size based on scattered light, and an assumed particle shape and refractive index. Conversely, BAM instruments measure direct changes in aerosol mass concentrations based on the loss of electrons on a filter which the aerosol has been deposited on (Manikonda et al., 2016; Watson et al., 1998), and so are not influenced by the hygroscopic growth of individual particles. Zheng et al., 2018 analysed the performance of Plantower PMS3003 (an earlier version of the Plantower PMS5003 housed in PurpleAir instruments used in this study) against a reference grade scattered light spectrometer (with good correlation of $R^2 = 0.8$) and a BAM instrument (with lower correlation of $R^2 = 0.5$). They concluded that a likely explanation contributing to the discrepancy is the potential for hygroscopic growth of aerosol particles due to ambient humidity, which alters the light-scattering properties of the aerosol and therefore the measurement made by the optical sensor (Cabada et al., 2004; Jayaratne et al., 2018; Spinetti and Buongiorno, 2007; Watson et al., 1998). In this instance, Zheng et al., 2018 found that the low-cost light-scattering sensor correlated best with the reference-grade instrument of the same operating principle, finding a lower correlation against the reference-grade instrument operating on principles other than light-scattering. The PurpleAir instrument over-estimation of $PM_{2.5}$ relative to the BAM reference-grade instrument may therefore be due to influences of humidity acting on the light scattering (Zheng et al., 2018).

An additional consideration in explaining the overestimation of $PM_{2.5}$ by the PurpleAir instruments relative to the reference-grade BAM is the particle density of the measured particulates. The Plantower PMS5003 sensors contained within the Pur-

pleAir instruments provide mass concentration measurements which are calculated by an unreported atmospheric calibration factor (Zheng et al., 2018). We assume that this calibration factor uses an average particle density, likely similar to that for an urban environment, such as 1.65 g cm^{-3} (Crilley et al., 2018; Liu et al., 2015; Pitz et al., 2003). If the Plantower PMS5003 sensor measures ambient air with a particle density dissimilar to the average particle density used in the atmospheric calibration factor, the resulting sensor output would be biased. For example, introduction of volcanic aerosol, primarily sulfate with an average particle density of 1.77 g cm^{-3} (Sarangi et al., 2016), into the air measured by the sensor could result in sensor output bias as a result of dissimilarity between the real and assumed particle density.

Despite the $PM_{2.5}$ over-estimation, the strong correlation between the PurpleAir and BAM instruments indicates that the PurpleAir instruments provided qualitatively valuable measurements of the atmospheric conditions. The high degree of intra-instrument performance, similar to findings by Malings et al., 2019, indicates that the PurpleAir instruments are reliable for determining relative variations in $PM_{2.5}$. The dense network of instruments with a high spatial resolution along the western region of Hawai‘i during the 2018 LERZ eruption gives a good indication of the relative amounts of $PM_{2.5}$ across the region, at a finer spatial resolution than available from the sparsely-located BAM instruments [Figure 2.6(A)]. Low-cost community-operated networks, such as the PurpleAir instruments across the western region of Hawai‘i during the 2018 LERZ eruption, can therefore be invaluable in providing insights into smaller-scale heterogeneities in air quality across a regional area at a scale inaccessible by the usually more disperse reference-grade instruments [Figure 2.6(B - E)]. Additionally, as far as the authors are aware, this is the first validation of PurpleAir instruments in a volcanic environment. Their strong correlation to the BAM instruments along the west coast of the Island of Hawai‘i during the 2018 LERZ eruption indicates that they are suitable for augmenting reference-grade instrument networks in periods of volcanic unrest. Considering that these instruments also provide a source of open-access data to the public, they present an opportunity to improve community awareness and inclusion of the general public in hazard assessment of downwind volcanic $PM_{2.5}$ air pollution.

2.6 Conclusions

Kīlauea's 2018 eruption was the largest LERZ eruption in the last two centuries. SO_2 emissions reached a monthly average of 200 kt/day during June (Kern et al. 2019), significantly exceeding emissions from Kīlauea during 2008 - 2017, which averaged 5 - 6 kt/day (Beirle et al., 2014; Carn et al., 2016; Eguchi et al., 2011; Elias et al., 2018). During the 2018 LERZ eruption, SO_2 mass concentrations exceeding the Hawai‘i 24-hour-mean threshold (366 µg/m^3) primarily occurred in the south of the island, at Volcano Observatory and in Pahala and Ocean View (2.1 %, 5.3 % and 4.2 % of the time during

the three-month long eruption, respectively). SO_2 mass concentrations were elevated at the HDOH Kona station (average 24-hour-mean mass concentration of 39 µg/m^3 during the LERZ eruption, relative to 7 µg/m^3 during 2007 - 2017), but mass concentrations were highest in Ocean View, Pahala and at Volcano Observatory (average 24-hour-mean mass concentrations of 117 µg/m^3, 129 µg/m^3 and 56 µg/m^3, respectively). The Hawai‘i 24-hour-mean threshold was exceeded five times in Pahala and twice at Volcano Observatory, but peak mass concentrations did not exceed those from the period 2007 - 2017. In Ocean View, the Hawai‘i 24-hour-mean threshold was exceeded four times and 24-hour-mean mass concentrations peaked at 728 µg/m^3, almost double the previous peak measurement of 403 µg/m^3 recorded at that station in January 2016.

$PM_{2.5}$ mass concentrations recorded at HDOH stations around the island from 2010 - 2017 rarely exceeded the EPA 24-hour-mean threshold of 35 µg/m^3 (0.1 % of the time at both Ocean View and Pahala). The lower 24-hour-mean $PM_{2.5}$ limit (25 µg/m^3) set by the World Health Organization was exceeded with greater frequency, particularly in Kona and Ocean View (1.2 % and 0.9 % of the time, respectively). During the 2018 LERZ eruption, $PM_{2.5}$ air pollution was significantly higher than 2010 - 2017 levels in Kona and Ocean View, exceeding WHO guidelines 34.7 % and 46.3 % of the time, respectively. Peak 24-hour-mean mass concentrations in Ocean View were recorded at 56 µg/m^3, and three consecutive days in June were recorded with mean 24-hour mass concentrations exceeding 35 µg/m^3. The Kona HDOH stations recorded eight 24-hour periods which exceeded EPA thresholds, unprecedented in the 2010 - 2017 period.

Following the decline of the 2018 LERZ eruption, mass concentrations of both SO_2 and $PM_{2.5}$ measured at the HDOH stations decreased to below pre-LERZ eruption levels, indicating that a large proportion of the air quality anomalies measured during the eruption were volcanogenic. The post-LERZ HDOH measurements are here assumed to be representative of the background (non-volcanically-perturbed) atmosphere, and subtracting these abundances from those recorded during the LERZ eruption provides an estimate of the purely volcanogenic $PM_{2.5}$ and SO_2. The sulfate aerosol component within the volcanic $PM_{2.5}$ is calculated as between 77 - 92 %, following Mather et al., 2012. HYSPLIT back-trajectory simulations provide an estimate of emission age following dispersion from source to measurement point (Ilyinskaya et al., in preparation), and a first-order SO_2 decay constant is estimated at 3.8 x 10^{-6} s^{-1}.

Community-operated PurpleAir instruments provided a high spatial resolution network across the western region of the island, informing the public regarding $PM_{2.5}$ mass concentrations in their locality. Low measurement variability (Pearson's r = 0.99) was found between co-located individual PurpleAir instruments, indicating a high level of intra-instrument performance. Observations recorded by co-located PurpleAir and BAM instruments correlated well (Pearson's r = 0.99, 0.97 and 0.94), but PurpleAir instruments were found to overestimate the $PM_{2.5}$ mass concentration by up to 40 %,

relative to the BAM instrument. This likely reflects inherent differences in instrument operating principles and may be associated with changes in optical-properties of aerosol arising from hygroscopic growth in ambient humidity. Nevertheless, the PurpleAir instruments are suitable for providing a low-cost network to augment reference-grade instruments, and contribute an open-access source of readily-available information to the public leading to development of community awareness towards air quality.

This study has assessed the impacts to air quality in downwind communities around the Island of Hawai‘i from 2007 to 2018. Spatial variability of air quality around the island during the 2018 LERZ eruption was comparable to patterns identified over the previous decade, but $PM_{2.5}$ and SO_2 pollution levels resulting from the 2018 LERZ eruption were significantly higher in western and southern regions of the island. A study of the potential health burden of these significant impacts on air quality might further illuminate aspects of the dose-response to volcanogenic emissions in addition to the impacts of public health protection measures put in place during the eruption.

2.7 Conflict of Interest Statement

AD was employed by company PurpleAir LLC. The remaining authors declare that the research was conducted in the absence of any commercial or financial relationships that could be construed as a potential conflict of interest.

2.8 Author Contributions

RCWW performed the data analysis and wrote the original draft. EI, AS, TR, MAP, and TAM contributed to data interpretation. All co-authors contributed to draft review and editing.

2.9 Funding

RCWW is funded by the Leeds-York Natural Environment Research Council (NERC) Doctoral Training Partnership (DTP) NE/L002574/1, in CASE partnership with the Icelandic Meteorological Office. RCWW, EI, EM, PEW and EL were funded for campaign-fieldwork by the Centre for the Observation and Modelling of Earthquakes, Volcanoes and Tectonics (COMET) grant COME3001.

The authors also acknowledge support to EI from the NERC urgency grant NE/M021130/1 "Source and longevity of sulfur in Icelandic flood basalt eruption plumes" and GCRF NE/P015271/1 and NE/R009465/1 "Unseen but not unfelt: resilience to persistent volcanic emissions (UNRESP)". We acknowledge support from the NERC ESS DTP to PW, EPSRC CASE funding to EM, Alfred P Sloan Foundation through support of

the Deep Carbon Observatory to ME and EJL and Leverhulme Early Career Fellowship to EJL, and ANR Projet de Recherche Collaborative VOLC-HAL-CLIM ANR-18-CE01-0018 and Orléans Labex Voltaire ANR-10-LABX-100-0 to TR. CO acknowledges support from NERC grant NE/N009312/1, and EI, TAM, ME and CO further acknowledge support from NERC grant NE/S00436X/1: "Volcanic plume understanding and forecasting: Integrating remote-sensing, in-situ observations and models (V-PLUS)".

2.10 Acknowledgments

We thank James Ciszewski at the Hawaii Department of Health for assistance with fieldwork and data-gathering; Lacey Holland and Steven Businger at the University of Hawai‘i at Manoa for volcanic emissions trajectory and HYSPLIT discussions; and the National Park Service and Hawai‘i Volcanoes National Park for their contributions.

Any use of trade, firm, or product names is for descriptive purposes only and does not imply endorsement by the U.S. Government.

2.11 Data Availability Statement

The datasets analysed for this study can be found in the Hawaii Department of Health Ambient Air Quality Data repository [http://health.hawaii.gov/cab/hawaii-ambient-air-quality-data/], and in the PurpleAir sensor list repository [https://www.purpleair.com/sensorlist].

References

Allen, A., Oppenheimer, C., Ferm, M., Baxter, P., Horrocks, L., Galle, B., McGonigle, A., & Duffell, H. (2002). Primary sulfate aerosol and associated emissions from Masaya Volcano, Nicaragua [DOI: https://doi.org/10.1029/2002JD002120]. *Journal of Geophysical Research: Atmospheres*, *107*(D23), ACH–5.

Andronico, D., & Del Carlo, P. (2016). PM_{10} measurements in urban settlements after lava fountain episodes at Mt. Etna, Italy: pilot test to assess volcanic ash hazard to human health [DOI: https://doi.org/10.5194/nhess-16-29-2016]. *Natural Hazards and Earth System Sciences (NHESS)*.

AQ-SPEC. (2017). PurpleAir PA-I Sensor Evaluation Report [(Accessed 13/2/2019)]. *http://www.aqmd.gov/aq-spec/product/purpleair-pa-ii*.

ATSDR. (1998). Agency for Toxic Substances and Disease Registry; public health statement sulfur dioxide [Available at: https://www.atsdr.cdc.gov/ToxProfiles/tp116-c1-b.pdf]. *7446-09-5*.

Balmes, J., Fine, J., & Sheppard, D. (1987). Symptomatic bronchoconstriction after short-term inhalation of sulfur dioxide [DOI: https://doi.org/10.1164/ajrccm/136.5.1117]. *American Review of Respiratory Disease*, *136*(5).

Barsotti, S., Andronico, D., Neri, A., Del Carlo, P., Baxter, P., Aspinall, W., & Hincks, T. (2010). Quantitative assessment of volcanic ash hazards for health and infrastructure at Mt. Etna (Italy) by numerical simulation [DOI: https://doi.org/10.1016/j.jvolgeores.2010.02.011]. *Journal of Volcanology and Geothermal Research*, *192*(1-2), 85–96.

Beirle, S., Hörmann, C., Penning de Vries, M., Dörner, S., Kern, C., & Wagner, T. (2014). Estimating the volcanic emission rate and atmospheric lifetime of SO2 from space: A case study for Kı¯lauea volcano, Hawai'i [DOI: https://doi.org/10.5194/acp-14-8309-2014]. *Atmospheric Chemistry and Physics*, *14*(16), 8309–8322.

Burkart, J., Steiner, G., Reischl, G., Moshammer, H., Neuberger, M., & Hitzenberger, R. (2010). Characterizing the performance of two optical particle counters (Grimm OPC1. 108 and OPC1. 109) under urban aerosol conditions [DOI: https://doi.org/10.1016/j.jaerosci.2010.07.007]. *Journal of Aerosol Science*, *41*(10), 953–962.

Butwin, M. K., von Löwis, S., Pfeffer, M. A., & Thorsteinsson, T. (2019). The effects of volcanic eruptions on the frequency of particulate matter suspension events in Iceland [DOI: https://doi.org/10.1016/j.jaerosci.2018.12.004]. *Journal of Aerosol Science*, *128*, 99–113.

Cabada, J. C., Khlystov, A., Wittig, A. E., Pilinis, C., & Pandis, S. N. (2004). Light scattering by fine particles during the Pittsburgh Air Quality Study: Measure-

ments and modeling [DOI: https://doi.org/10.1029/2003JD004155]. *Journal of Geophysical Research: Atmospheres*, *109*(D16).

Cadle, R., Wartburg, A., & Grahek, P. (1971). The proportion of sulfate to sulfur dioxide in Kı¯lauea Volcano fume [DOI: https://doi.org/10.1016/0016-7037(71)90046-9]. *Geochimica et Cosmochimica Acta*, *35*(5), 503–507.

Carn, S., Clarisse, L., & Prata, A. J. (2016). Multi-decadal satellite measurements of global volcanic degassing [DOI: https://doi.org/10.1016/j.jvolgeores.2016.01.002]. *Journal of Volcanology and Geothermal Research*, *311*, 99–134.

Chow, J. C., Doraiswamy, P., Watson, J. G., Chen, L.-W. A., Ho, S. S. H., & Sodeman, D. A. (2008). Advances in integrated and continuous measurements for particle mass and chemical composition [DOI: https://doi.org/10.3155/1047-3289.58.2.141]. *Journal of the Air & Waste Management Association*, *58*(2), 141–163.

CRI. (2004). The Centre for Research Information, health effects of project shad chemical agent: Sulfur dioxide [cas 7446-09-5]. *National Academies*.

Crilley, L. R., Shaw, M., Pound, R., Kramer, L. J., Price, R., Young, S., Lewis, A. C., & Pope, F. D. (2018). Evaluation of a low-cost optical particle counter (Alphasense OPC-N2) for ambient air monitoring [DOI: https://doi.org/10.5194/amt-11-709-2018]. *Atmospheric Measurement Techniques*, 709–720.

Crilley, L. R., Singh, A., Kramer, L. J., Shaw, M. D., Alam, M. S., Apte, J. S., Bloss, W. J., Hildebrandt Ruiz, L., Fu, P., Fu, W. et al. (2020). Effect of aerosol composition on the performance of low-cost optical particle counter correction factors [DOI: https://doi.org/10.5194/amt-13-1181-2020]. *Atmospheric Measurement Techniques*, *13*(3), 1181–1193.

Eguchi, K., Uno, I., Yumimoto, K., Takemura, T., Nakajima, T. Y., Uematsu, M., & Liu, Z. (2011). Modulation of cloud droplets and radiation over the North Pacific by sulfate aerosol erupted from Mount Kı¯lauea [DOI: https://doi.org/10.2151/sola.2011-020]. *SOLA*, *7*, 77–80.

Elias, T., Kern, C., Horton, K., Sutton, A. J., & Garbeil, H. (2018). Measuring SO2 emission rates at Kı¯lauea Volcano, Hawai‘i USA, 2014-2017 [DOI: https://doi.org/10.3389/feart.2018.00214]. *Frontiers in Earth Science*, *6*, 214.

Elias, T., & Sutton, A. J. (2017). *Volcanic air pollution hazards in Hawai‘i* (tech. rep.) [Available at: https://pubs.usgs.gov/fs/2017/3017/fs20173017.pdf]. US Geological Survey.

Elias, T., & Sutton, A. J. (2007). *Sulfur dioxide emission rates from Kı¯lauea Volcano, Hawai‘i, an update: 2002-2006* [Available at: https://doi.org/10.3133/ofr20071114]. US Geological Survey.

Elias, T., & Sutton, A. J. (2012). *Sulfur dioxide emission rates from Kı¯lauea Volcano, Hawai‘i, 2007–2010* (tech. rep.) [Available at: https://pubs.usgs.gov/of/2012/1107/of2012-1107_text.pdf]. US Geological Survey.

Environmental Protection Agency. (2010). Primary National Ambient Air Quality Standard for Sulfur Dioxide; Final Rule [(Accessed 15/1/2019)]. *https://www.govinfo.gov/content/pkg/FR-2010-06-22/pdf/2010-13947.pdf*, *40 CFR Parts 50, 53, and 58*.

Environmental Protection Agency. (2013). Federal and State Ambient Air Quality Standards [(Accessed 15/1/2019)]. *http://health.hawaii.gov/cab/files/2013/05/naaqs_jan_2013.pdf*.

Environmental Protection Agency. (2016). List of designated reference and equivalent methods [Available at: https://www.epa.gov/sites/production/files/2019-08/documents/designated_reference_and-equivalent_methods.pdf]. *National Exposure Research Laboratory*.

European Commission. (2018). Environment Air Quality Standards [(Accessed 21/1/2019)]. *http://ec.europa.eu/environment/air/quality/standards.htm*.

Galeazzo, T., Bekki, S., Martin, E., Savarino, J., & Arnold, S. R. (2018). Photochemical box modelling of volcanic SO2 oxidation: Isotopic constraints [DOI: https://doi.org/10.5194/acp-18-17909-2018]. *Atmospheric Chemistry and Physics*, *18*(24), 17909–17931.

Halliday, T., Lynham, J., & de Paula Neto, A. (2015). *Vog: Using volcanic eruptions to estimate the health costs of particulates and SO2* [DOI: https://doi.org/10.1111/ecoj.12609]. College of Social Sciences, Department of Economics.

Hansell, A., & Oppenheimer, C. (2004). Health hazards from volcanic gases: A systematic literature review [DOI: https://doi.org/10.1080/00039890409602947]. *Archives of Environmental Health: An International Journal*, *59*(12), 628–639.

Hawai‘i Department of Business Economic Development and Tourism. (2011). Research and Economic Analysis Division. Statistics and Data Support Branch. Hawai‘i State Data Center. 2010 census tract names and their population, housing and land area for the State of Hawai‘i. Honolulu: 2011 [Available at: https://files.hawaii.gov/dbedt/census/Census_2010/PL94-171/hsdc_rep2010_2.pdf]. *Hawai‘i State Data Center Report Number 2010-2*.

Hawai‘i Emergency Management Agency. (2018). 2018 State of Hawai‘i Hazard Mitigation Plan. *Section 4.15; Wildfire https://dod.hawaii.gov/hiema/files/2018/06/Draft-Section-4.15-Wildfire-Placeholder.pdf*, *(Accessed 9/8/2019)*.

HDOH. (2019). Hawaii Department of Health Clean Air Branch, Hawai‘i Ambient Air Quality Data [(Accessed 13/8/2018)]. *http://health.hawaii.gov/cab/hawaii-ambient-air-quality-data/*.

Holgate, S. (2017). "Every breath we take: the lifelong impact of air pollution" - a call for action [DOI: https://doi.org/10.7861/clinmedicine.17-1-8]. *Clinical Medicine*, *17*(1), 8–12.

Ilyinskaya, E., Schmidt, A., Mather, T. A., Pope, F. D., Witham, C., Baxter, P., Jóhannsson, T., Pfeffer, M., Barsotti, S., Singh, A. et al. (2017). Understanding

the environmental impacts of large fissure eruptions: Aerosol and gas emissions from the 2014–2015 Holuhraun eruption (Iceland) [DOI: https://doi.org/10.1016/j.epsl.2017.05.025]. *Earth and Planetary Science Letters*, *472*, 309–322.

Jayaratne, R., Liu, X., Thai, P., Dunbabin, M., & Morawska, L. (2018). The influence of humidity on the performance of a low-cost air particle mass sensor and the effect of atmospheric fog [DOI: https://doi.org/10.5194/amt-11-4883-2018]. *Atmospheric Measurement Techniques*, *11*(8), 4883–4890.

Kelly, K., Whitaker, J., Petty, A., Widmer, C., Dybwad, A., Sleeth, D., Martin, R., & Butterfield, A. (2017). Ambient and laboratory evaluation of a low-cost particulate matter sensor [DOI: https://doi.org/10.1016/j.envpol.2016.12.039]. *Environmental Pollution*, *221*, 491–500.

Kern, C., Elias, T., Nadeau, P., Lerner, A., Werner, C., Cappos, M., Clor, L., Kelly, P., Realmuto, V., Theys, N., & Carn, S. (2019). Sulfur dioxide emissions associated with Kı¯lauea Volcano's 2018 fissure eruption; V43C-0209 [Available at: https://ui.adsabs.harvard.edu/abs/2019AGUFM.V43C0209L/abstract]. *American Geophysical Union Fall Meeting*.

Kroll, J. H., Cross, E. S., Hunter, J. F., Pai, S., XII, T., XI, T., Wallace, L. M., Croteau, P. L., Jayne, J. T., Worsnop, D. R. et al. (2015). Atmospheric evolution of sulfur emissions from Kılauea: real-time measurements of oxidation, dilution, and neutralization within a volcanic plume [Available at: https://pubs.acs.org/doi/pdf/10.1021/es506119x]. *Environmental science & technology*, *49*(7), 4129–4137.

Lambert, G., Le Cloarec, M., & Pennisi, M. (1988). Volcanic output of SO2 and trace metals: A new approach [DOI: https://doi.org/10.1016/0016-7037(88)90054-3]. *Geochimica et Cosmochimica Acta*, *52*(1), 39–42.

Langmann, B. (2014). On the role of climate forcing by volcanic sulphate and volcanic ash [DOI: https://doi.org/10.1155/2014/340123]. *Advances in Meteorology*, *2014*, 1–17.

Lim, S. S., Vos, T., Flaxman, A. D., Danaei, G., Shibuya, K., Adair-Rohani, H., Al-Mazroa, M. A., Amann, M., Anderson, H. R., Andrews, K. G. et al. (2012). A comparative risk assessment of burden of disease and injury attributable to 67 risk factors and risk factor clusters in 21 regions, 1990–2010: A systematic analysis for the Global Burden of Disease Study 2010 [DOI: https://doi.org/10.1016/S0140-6736(12)61766-8]. *The lancet*, *380*(9859), 2224–2260.

Liu, Z., Hu, B., Ji, D., Wang, Y., Wang, M., & Wang, Y. (2015). Diurnal and seasonal variation of the $pm_{2.5}$ apparent particle density in Beijing, China [DOI: https://doi.org/10.1016/j.atmosenv.2015.09.005]. *Atmospheric Environment*, *120*, 328–338.

Longo, B., Rossignol, A., & Green, J. (2008). Cardiorespiratory health effects associated with sulphurous volcanic air pollution [DOI: https://doi.org/10.1016/j.puhe.2007.09.017]. *Public Health*, *122*(8), 809–20.

Longo, B. M. (2009). The Kı¯lauea Volcano adult health study [Available at: https://journals.lww.com/nursingresearchonline/Fulltext/2009/01000/The_Kilauea_Volcano_Adult_Health_Study.4.aspx]. *Nursing research*, *58*(1), 23–31.

Longo, B. M. (2013). Adverse health effects associated with increased activity at Kı¯lauea Volcano: A repeated population-based survey [DOI: https://doi.org/10.1155/2013/475962]. *ISRN Public Health*, *2013*.

Longo, B. M., Grunder, A., Chuan, R., & Rossignol, A. (2005). SO2 and fine aerosol dispersion from the Kı¯lauea plume, Kau district, Hawai'i, USA [DOI: https://doi.org/10.1130/G21167.1]. *Geology*, *33*(3), 217–220.

Longo, B. M., Yang, W., Green, J. B., Crosby, F. L., & Crosby, V. L. (2010). Acute health effects associated with exposure to volcanic air pollution (vog) from increased activity at Kı¯lauea Volcano in 2008 [DOI: https://doi.org/10.1080/15287394.2010.497440]. *Journal of Toxicology and Environmental Health, Part A*, *73*(20), 1370–1381.

Loughlin, S., Aspinall, W., Vye-Brown, C., Baxter, P., Braban, C., Hort, M., Schmidt, A., Thordarson, T., & Witham, C. (2012). Large-magnitude fissure eruptions in Iceland: Source characterisation [DOI: https://eprints.whiterose.ac.uk/80209/]. *BGS Open File Report*, *OR/12/098*.

Malings, C., Tanzer, R., Hauryliuk, A., Saha, P. K., Robinson, A. L., Presto, A. A., & Subramanian, R. (2019). Fine particle mass monitoring with low-cost sensors: Corrections and long-term performance evaluation [DOI: https://doi.org/10.1080/02786826.2019.1623863]. *Aerosol Science and Technology*, 1–40.

Manikonda, A., Zıḱová, N., Hopke, P. K., & Ferro, A. R. (2016). Laboratory assessment of low-cost PM monitors [DOI: https://doi.org/10.1016/j.jaerosci.2016.08.010]. *Journal of Aerosol Science*, *102*, 29–40.

Mannino, D. M., Ruben, S., Holschuh, F. C., Holschuh, T. C., Wilson, M. D., & Holschuh, T. (1996). Emergency department visits and hospitalizations for respiratory disease on the Island of Hawai'i, 1981 to 1991 [DOI: http://hdl.handle.net/10524/54120]. *Hawai'i medical journal*, *55*(3).

Mather, T. A., Witt, M., Pyle, D., Quayle, B., Aiuppa, A., Bagnato, E., Martin, R., Sims, K., Edmonds, M., Sutton, A. et al. (2012). Halogens and trace metal emissions from the ongoing 2008 summit eruption of Kı¯lauea volcano, Hawai'i [DOI: https://doi.org/10.1016/j.gca.2011.11.029]. *Geochimica et Cosmochimica Acta*, *83*, 292–323.

Mather, T., Allen, A., Oppenheimer, C., Pyle, D., & McGonigle, A. (2003). Size-resolved characterisation of soluble ions in the particles in the tropospheric plume of Masaya volcano, Nicaragua: origins and plume processing [DOI: https://doi.

org/10.1023/A:1026327502060]. *Journal of Atmospheric Chemistry*, *46*(3), 207–237.

Mather, T. A. (2015). Volcanoes and the environment: Lessons for understanding Earth's past and future from studies of present-day volcanic emissions [DOI: https://doi.org/10.1016/j.jvolgeores.2015.08.016]. *Journal of Volcanology and Geothermal Research*, *304*, 160–179.

Met One Instruments Inc. (2008). BAM 1020 particulate monitor operation manual [Available at: https://www.arb.ca.gov/airwebmanual/instrument_manuals/Documents/BAM-1020-9800_Manual_Rev_H.pdf]. *[BAM-1020-9800 Rev H]*.

Michaud, J. D., Michaud, J.-P., & Krupitsky, D. (2007). Temporal variability in SO2 exposures at Hawai'i Volcanoes National Park, USA [DOI: 10.1007/S00254-006-0459-Y]. *Environmental geology*, *52*(1), 81–92.

Michaud, J.-P., Grove, J. S., & Krupitsky, D. (2004). Emergency department visits and 'vog'-related air quality in Hilo, Hawai'i [DOI: https://doi.org/10.1016/S0013-9351(03)00122-1]. *Environmental Research*, *95*(1), 11–19.

Nadeau, P., Elias, T., Kern, C., Lerner, A., C, W., L, C., M, C., P, K., & AJ, S. (2019). The 2018 Eruption and Beyond: a New Era of Degassing at Kı¯lauea Volcano. *IUGG19-1696*.

National Oceanic and Atmospheric Administration. (2019). Climate Data Online Data Tools [(Accessed 01/5/2019)].

Neal, C., Brantley, S., Antolik, L., Babb, J., Burgess, M., Calles, K., Cappos, M., Chang, J., Conway, S., Desmither, L. et al. (2019). The 2018 rift eruption and summit collapse of Kı¯lauea Volcano [DOI: https://www.science.org/doi/10.1126/science.aav7046]. *Science*, *363*(6425), 367–374.

Oppenheimer, C., & McGonigle, J. (2004). Exploiting ground-based optical sensing technologies for volcanic gas surveillance [DOI: https://doi.org/10.4401/ag-3353]. *Annals Geophysics*, *47*(4).

Oppenheimer, C., Francis, P., & Stix, J. (1998). Depletion rates of sulfur dioxide in tropospheric volcanic plumes [DOI: https://doi.org/10.1029/98GL01988]. *Geophysical Research Letters*, *25*(14), 2671–2674.

Oppenheimer, C., Kyle, P., Eisele, F., Crawford, J., Huey, G., Tanner, D., Kim, S., Mauldin, L., Blake, D., Beyersdorf, A. et al. (2010). Atmospheric chemistry of an Antarctic volcanic plume [DOI: https://doi.org/10.1029/2009JD011910]. *Journal of Geophysical Research: Atmospheres*, *115*(D4).

Patrick, M. R., Orr, T., Sutton, A. J., Tamar, E., & Swanson, D. (2013). The first five years of Kı¯lauea's Summit Eruption in Halema'uma'u Crater, 2008-2013 [U.S. Geological Survey Fact Sheet 2013–3116. Available at: https://pubs.er.usgs.gov/publication/fs20133116]. *US Department of the Interior, US Geological Survey*.

Pattantyus, A. K., Businger, S., & Howell, S. G. (2018). Review of sulfur dioxide to sulfate aerosol chemistry at Kı¯lauea Volcano, Hawai'i [DOI: https://doi.org/10.1016/j.atmosenv.2018.04.055]. *Atmospheric Environment*, *185*, 262–271.

Pfeffer, M., Langmann, B., & Graf, H.-F. (2006a). Atmospheric transport and deposition of Indonesian volcanic emissions [DOI: https://doi.org/10.5194/acp-6-2525-2006]. *Atmospheric Chemistry and Physics*, *6*(9), 2525–2537.

Pfeffer, M., Rietmeijer, F., Brearley, A., & Fischer, T. P. (2006b). Electron microbeam analyses of aerosol particles from the plume of Poás Volcano, Costa Rica and comparison with equilibrium plume chemistry modeling [DOI: https://doi.org/10.1016/j.jvolgeores.2005.10.009]. *Journal of volcanology and geothermal research*, *152*(1-2), 174–188.

Pitz, M., Cyrys, J., Karg, E., Wiedensohler, A., Wichmann, H.-E., & Heinrich, J. (2003). Variability of apparent particle density of an urban aerosol [DOI: https://doi.org/10.1021/es034322p]. *Environmental Science & Technology*, *37*(19), 4336–4342.

Plantower. (2016). Digital universal particle concentration sensor PMS5003 series data manual [(Accessed 13/11/2018)]. *http://www.aqmd.gov/docs/default-source/aq-spec/resources-page/plantower-pms5003-manual_v2-3.pdf*.

Poland, M., Miklius, A., Orr, T., Sutton, J., Thornber, C., & Wilson, D. (2008). New episodes of volcanism at Kı¯lauea Volcano, Hawai'i [DOI: https://doi.org/10.1029/2008EO050001]. *Eos, Transactions American Geophysical Union*, *89*(5), 37–38.

Porter, J. N., Horton, K. A., Mouginis-Mark, P. J., Lienert, B., Sharma, S. K., Lau, E., Sutton, A. J., Elias, T., & Oppenheimer, C. (2002). Sun photometer and lidar measurements of the plume from the Hawai'i Kı¯lauea Volcano, Hawai'i Volcano Pu'u 'Ō'ō vent: Aerosol flux and SO_2 lifetime [DOI: https://doi.org/10.1029/2002GL014744]. *Geophysical Research Letters*, *29*(16), 30–1.

PurpleAir. (2019). PurpleAir: Air Quality Monitoring [(Accessed 26/10/2018)]. *https://www.purpleair.com/*.

Rotstayn, L. D., & Lohmann, U. (2002). Simulation of the tropospheric sulfur cycle in a global model with a physically based cloud scheme [DOI: https://doi.org/10.1029/2002JD002128]. *Journal of Geophysical Research: Atmospheres*, *107*(D21).

Sarangi, B., Aggarwal, S. G., Sinha, D., & Gupta, P. K. (2016). Aerosol effective density measurement using scanning mobility particle sizer and quartz crystal microbalance with the estimation of involved uncertainty [DOI: https://doi.org/10.5194/amt-9-859-2016]. *Atmospheric Measurement Techniques*, *9*(3), 859–875.

Saxena, P., & Seigneur, C. (1987). On the oxidation of SO2 to sulfate in atmospheric aerosols [DOI: https://doi.org/10.1016/0004-6981(87)90077-1]. *Atmospheric Environment (1967)*, *21*(4), 807–812.

Sayahi, T., Butterfield, A., & Kelly, K. (2019). Long-term field evaluation of the Plantower PMS low-cost particulate matter sensors [DOI: https://doi.org/10.1016/j.envpol.2018.11.065]. *Environmental Pollution*, *245*, 932–940.

Schmidt, A., Leadbetter, S., Theys, N., Carboni, E., Witham, C., Stevenson, J., Birch, C., Thordarson, T., Turnock, S., Barsotti, S., Delaney, L., Feng, W., Grainger, R., Hort, M., Höskuldsson, Á., Ialongo, I., Ilyinskaya, E., Jóhannsson, T., Kenny, P., ... Shepherd, J. (2015). Satellite detection, long-range transport, and air quality impacts of volcanic sulfur dioxide from the 2014–2015 flood lava eruption at Bárðarbunga (Iceland) [DOI: https://doi.org/10.1002/2015JD023638]. *Journal of Geophysical Research: Atmospheres*, *120*(18), 9739–9757.

Spinetti, C., & Buongiorno, M. (2007). Volcanic aerosol optical characteristics of Mt. Etna tropospheric plume retrieved by means of airborne multispectral images [DOI: https://doi.org/10.1016/j.jastp.2007.03.014]. *Journal of atmospheric and solar-terrestrial physics*, *69*(9), 981–994.

Stockwell, W. R., & Calvert, J. G. (1983). The mechanism of the ho¯so$_2$ reaction [DOI: https://doi.org/10.1016/0004-6981(83)90220-2]. *Atmospheric Environment (1967)*, *17*(11), 2231–2235.

Tam, E., Miike, R., Labrenz, S., Sutton, A. J., Elias, T., Davis, J., Chen, Y.-L., Tantisira, K., Dockery, D., & Avol, E. (2016). Volcanic air pollution over the Island of Hawai'i: Emissions, dispersal, and composition. association with respiratory symptoms and lung function in Hawai'i Island school children [DOI: https://doi.org/10.1016/j.envint.2016.03.025]. *Environment international*, *92*, 543–552.

Thermo Fisher Scientific. (2010). Model 43i sulphur dioxide analyser - product specifications [Available at: https://www.thermofisher.com/order/catalog/product/43I#/43I].

US Geological Survey Hawai'ian Volcano Observatory. (2018). Cooperator report to Hawai'i County Civil Deference; preliminary analysis of the ongoing Lower East Rift Zone (LERZ) eruption of Kı¯lauea Volcano, Fissure 8 prognosis and ongoing hazards [(Accessed 27/2/2019)]. *https://volcanoes.usgs.gov/vsc/file_mngr/file-185/USGS%20Preliminary%20Analysis_LERZ_7-15-18_v1.1.pdf*.

von Glasow, R., Bobrowski, N., & Kern, C. (2009). The effects of volcanic eruptions on atmospheric chemistry [DOI: https://doi.org/10.1016/j.chemgeo.2008.08.020]. *Chemical Geology*, *263*(1-4), 131–142.

Wang, Y., Li, J., Jing, H., Zhang, Q., Jiang, J., & Biswas, P. (2015). Laboratory evaluation and calibration of three low-cost particle sensors for particulate matter measurement [DOI: https://doi.org/10.1080/02786826.2015.1100710]. *Aerosol Science and Technology*, *49*(11), 1063–1077.

Watson, J., Chow, J., Moosmüller, H., Green, M., Frank, N., & Pitchford, M. (1998). Guidance for using continuous monitors in $PM_{2.5}$ monitoring networks [Available

at: https://www3.epa.gov/ttnamti1/files/ambient/pm25/r-98-012.pdf]. *Environmental Protection Agency, Office of Air Quality, EPA-454/R-98-012.*

Whitty, R., Pfeffer, M., Ilyinskaya, E., Roberts, T., Schmidt, A., Barsotti, S., Strauch, W., Crilley, L., Pope, F., Bellanger, H., Mendoza, E., Mather, T., Liu, E., Peters, N., Taylor, I., Francis, H., Hernández Leiva, X., Lynch, D., Nobert, S., & Baxter, P. (2022). Effectiveness of low-cost air quality monitors for identifying volcanic SO_2 and PM downwind from Masaya volcano, Nicaragua [DOI: https://doi.org/10.30909/vol.05.01.3359]. *Volcanica*, *5*(1), 33–59.

Wilson, W., Chow, J. C., Claiborn, C., Fusheng, W., Engelbrecht, J., & Watson, J. G. (2002). Monitoring of particulate matter outdoors [DOI: https://doi.org/10.1016/S0045-6535(02)00270-9]. *Chemosphere*, *49*(9), 1009–1043.

Wooten, K. M., Thornber, C. R., Orr, T. R., Ellis, J. F., & Trusdell, F. A. (2009). Catalog of Tephra Samples from Kı¯lauea's Summit Eruption, March-December 2008 [Available at: https://pubs.usgs.gov/of/2009/1134/of2009-1134.pdf]. *U.S. Geological Survey Open-File Report 2009-1134, 26 p.*

World Health Organization. (2005). WHO Air quality guidelines for particulate matter, ozone, nitrogen dioxide and sulfur dioxide [Available at: https://apps.who.int/iris/bitstream/handle/10665/69477/WHO_SDE_PHE_OEH_06.02_eng.pdf]. *Global update.*

Wyrtki, K., & Meyers, G. (1976). The trade wind field over the Pacific Ocean [DOI: https://doi.org/10.1175/1520-0450(1976)015%3C0698:TTWFOT%3E2.0.CO;2]. *Journal of Applied Meteorology*, *15*(7), 698–704.

Zheng, T., Bergin, M. H., Johnson, K. K., Tripathi, S. N., Shirodkar, S., Landis, M. S., Sutaria, R., & Carlson, D. E. (2018). Field evaluation of low-cost particulate matter sensors in high-and low-concentration environments [DOI: https://doi.org/10.5194/amt-11-4823-2018]. *Atmospheric Measurement Techniques*, *11*(8), 4823–4846.

Chapter 3

Effectiveness of low-cost air quality monitors for identifying volcanic SO_2 and PM downwind from Masaya volcano, Nicaragua

Abstract

Gas and particulate matter (PM) emissions from Masaya volcano, Nicaragua, cause substantial regional volcanic air pollution (VAP). We evaluate the suitability of low-cost SO_2 and PM sensors for a continuous air-quality network. The network was deployed for six months in five populated areas (4 - 16 km from the crater). The SO_2 sensors failed and recorded erroneous values on multiple occasions, likely due to corrosion, requiring significant maintenance commitment. The PM sensors were found to be robust but data required correction for humidity. SO_2 measurements could not be used as stand-alone tools to detect occurrence of VAP episodes (VAPE), but a SO_2/PM correlation reliably achieved this at near-field stations, as confirmed by meteorological forecasts and satellite imagery. Above-background PM concentrations reliably identified VAPE at both near-field and far-field stations. We suggest that a continuous network can be built from a combination of low-cost PM and SO_2 sensors with a greater number of PM-only sensors.

3.1 Introduction

Masaya is an active basalt volcanic complex in Nicaragua, Central America. It has a near continuous history of pit crater formation, sporadic lava lake activity and degassing

as far back as, at least, the 1500s (Rymer et al., 1998). Santiago pit crater, initially formed around 1858-1859 (McBirney, 1956), is the location of current volcanic activity and has undergone five periods of lava lake development and multiple phases of gas crisis with intense degassing activity (McBirney, 1956; Stoiber et al., 1986). The latest and current outgassing crisis started in 1993 and has resulted in large fluxes of volcanic gas into the atmosphere (Burton et al., 2000; Mather et al., 2006b; Rymer et al., 1998; Williams-Jones et al., 2003) with sulphur dioxide (SO_2) flux ranging from 120 to 2680 metric tons/day [Figure 3.1].

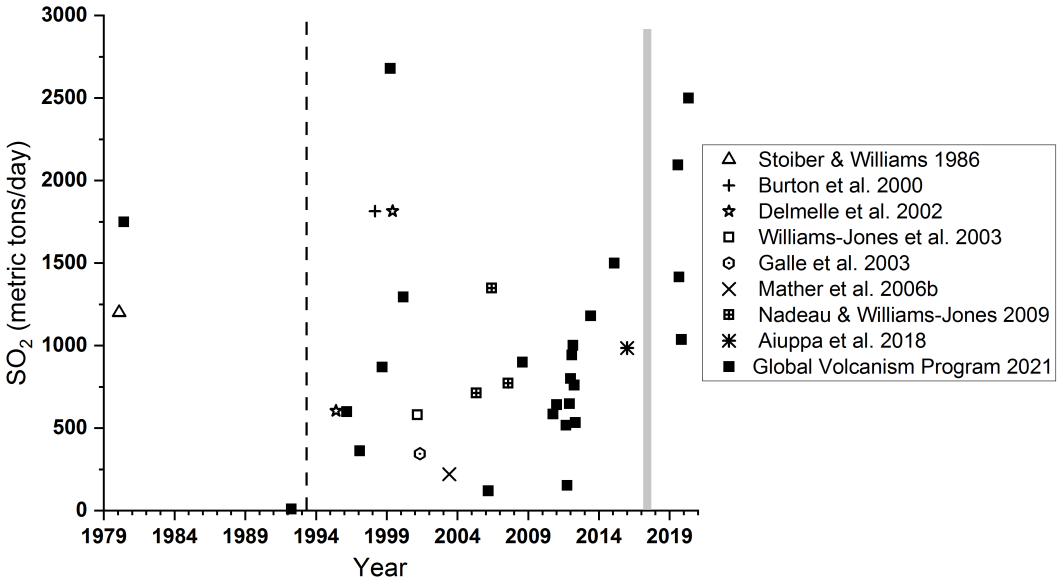

Figure 3.1: SO_2 emissions from Santiago crater, Masaya volcano, from 1979 to 2020. Black dashed line indicates initiation of gas crisis in May 1993. Grey shaded area indicates the AQMesh downwind measurement period (this study) from February to August 2017. SO_2 emissions data sourced from Aiuppa et al., 2018; Burton et al., 2000; Delmelle et al., 2002; Galle et al., 2003; Global Volcanism Program, 2021; Mather et al., 2006a; Nadeau and Williams-Jones, 2009; Stoiber et al., 1986; Williams-Jones et al., 2003.

Masaya volcano has a subdued topography, situated at 635 metres above sea level, and this often results in the volcanic plume remaining in the atmospheric boundary layer (Delmelle et al., 2002). The injection of the plume into the low atmosphere means that the plume can "ground", causing exposure of the land-surface to high concentrations of toxic gas and aerosols. Prevailing easterly winds mean the plume is commonly moved towards the Las Sierras highlands, an area higher (925 metres asl) than the crater summit, causing damage to vegetation (including cultivated crops), machinery and buildings over a large area downwind of the crater (Baxter et al., 1982; Delmelle et al., 1999; van Manen, 2014; Williams-Jones and Rymer, 2015). Volcanic plumes that remain in the lower atmosphere, such as that emitted from Masaya volcano, are commonly composed of a complex and chemically-evolving mixture of both volcanic and atmospheric gases as well as primary and secondary aerosol particles, dust and ash

(Langmann, 2014; Mason et al., 2021; Oppenheimer and McGonigle, 2004; Pfeffer et al., 2006b; von Glasow et al., 2009). Volcanic emissions released into the lower atmosphere can have a large impact on air quality, the environment, and human and animal health across local to regional areas (Carlsen et al., 2021a; Carlsen et al., 2021b; Ilyinskaya et al., 2021; Ilyinskaya et al., 2017; Mather, 2015; Schmidt et al., 2015; Tam et al., 2016; Whitty et al., 2020).

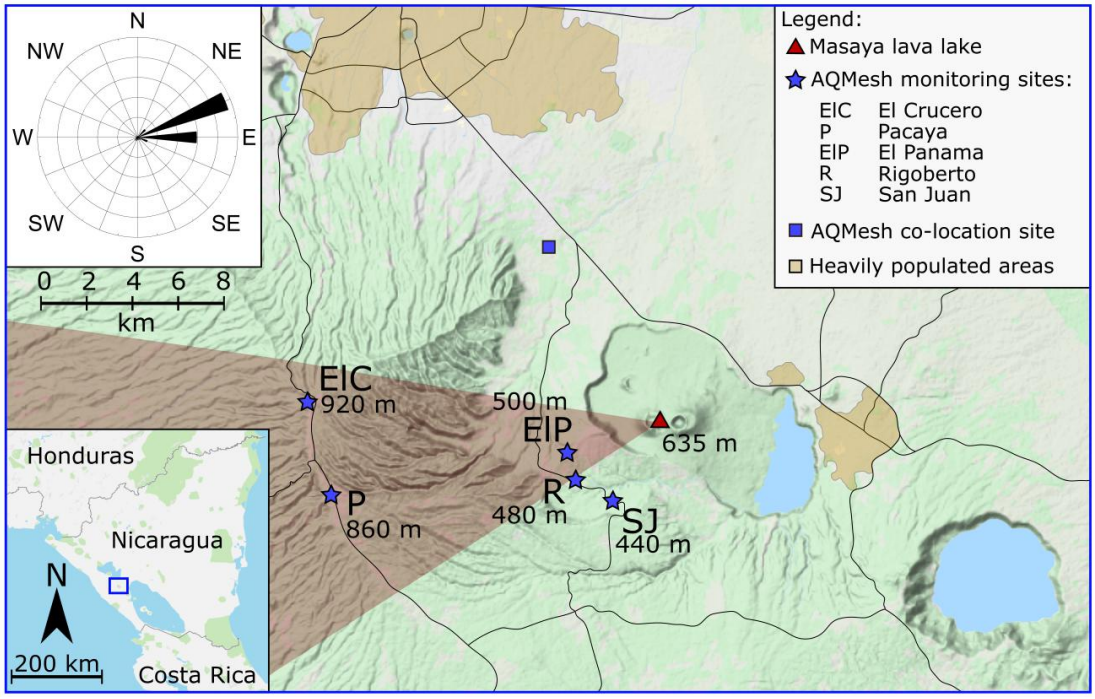

Figure 3.2: Topographic map of Masaya volcano and the AQMesh sampling stations with heights in metres above sea level (asl) for sampling stations and Masaya's Santiago Crater. Upper left inset indicates the wind rose referring to 948 metres asl for the period February to August 2017, data derived from ECMWF forecast meteorological data. The red shaded area indicates prevailing plume dispersion, graphically presented from the most frequent (76%) wind direction derived from ECMWF data at 948 metres asl. Lower left inset indicates geographical position of Masaya volcano. Base topographic map from Krogh, 2021.

SO_2 is often the focal point of gas emission monitoring at volcanoes due to its high concentration in volcanic plumes relative to the background ambient atmosphere, as well as its well-recognised environmental and air quality impacts (Cadle et al., 1971; Lambert et al., 1988; Loughlin et al., 2012; Schmidt et al., 2015). Methods to monitor volcanic SO_2 emissions include remote sensing approaches (that enable determination of gas flux) and in situ methods such as Multi-Gas instruments that contain electrochemical sensors for SO_2 detection. Studies using Multi-Gas have mostly focused on the near-source near-summit plume, detecting SO_2 at up to tens or even hundreds of parts per million volume (ppmv) (Aiuppa et al., 2018; Roberts et al., 2012; Shinohara et al., 2008). While the principle of SO_2 measurements is the same (electrochemical sensors), the concentration range in downwind areas is several orders of magnitude lower than near-

source and therefore presents different challenges for detection accuracy. Measurement of volcanic SO_2 at sub-ppmv levels has also been demonstrated using electrochemical sensors (Hagan et al., 2018; Roberts et al., 2018). In a recent study, networks of low-cost SO_2 and particle sensors have been used to monitor volcanic pollution from Kīlauea volcano (Crawford et al., 2021).

Exposure to SO_2 can result in irritation and inflammation of the eyes and the upper respiratory tract (Longo et al., 2008; Miller, 2004; Pohl, 1998). Population sub-groups including asthmatics, children, and respiratory- or cardiac-compromised individuals are particularly vulnerable to exposure to SO_2 (ATSDR, 1998; CRI, 2004).

Once in the atmosphere, SO_2 is affected by chemical and physical processes, including gas-phase reactions and reactions with liquid and solid suspended particles, leading to conversion of SO_2 to sulphate aerosols (Allen et al., 2002; Delmelle et al., 2002; Stockwell and Calvert, 1983). The lifetime of SO_2 in the troposphere is usually considered to be in the range of days to a week (Allen et al., 2002; Pattantyus et al., 2018; Pfeffer et al., 2006a; Rotstayn and Lohmann, 2002), with the rate of SO_2 conversion depending on the relative humidity, temperature, interactions with clouds and the availability of oxidants (Oppenheimer et al., 1998; Saxena and Seigneur, 1987). Through a number of reaction pathways (including oxidation with the hydroxyl radical, -OH, and with hydrogen peroxide, H_2O_2, and ozone, O_3), SO_2 is gradually converted to sulphate aerosol, H_2SO_4, (Allen et al., 2002; Stockwell and Calvert, 1983), which is a dominant component of volcanic particulate matter (PM) (Pattantyus et al., 2018; Tam et al., 2016).

Volcanic PM can be monitored in situ in real-time by deploying devices designed to measure atmospheric PM such as optical particle counters and other PM instruments (Allen et al., 2006; Ilyinskaya et al., 2010; Mather et al., 2003; Roberts et al., 2018; Whitty et al., 2020). PM is commonly sub-divided into size categories of PM_1, $PM_{2.5}$ and PM_{10} (PM with particle diameters $<$1 µm, $<$2.5 µm and $<$10 µm, respectively). This categorisation into cumulative size modes is important because particles of different sizes can have varying health impacts, with smaller particles having a larger relative surface area for the absorption of toxic chemicals as well as a greater efficiency at physical translocation from the respiratory tract to other areas of the body (Schlesinger et al., 2006). For example, exposure to fine particulates in the $PM_{2.5}$ size category has been found to cause 3% of global mortality from cardiopulmonary disease and 5% mortality from cancer of the bronchus, lung and trachea (Cohen et al., 2005). Recent studies have also investigated a link between exposure to PM and decline in short-term cognitive abilities (Gao et al., 2021; Shehab and Pope, 2019). The chemical composition of volcanic PM is heterogeneous, with common chemical species including sulphates (primary emissions or formed via oxidation of sulphur gases) (Allen et al., 2002; Cadle et al., 1971; Langmann, 2014; Mather et al., 2003; Stockwell and Calvert,

1983) and halides, with an array of metals and metalloids including environmentally-harmful species such as lead and cadmium (Ilyinskaya et al., 2021; Ilyinskaya et al., 2017; Langmann, 2014; Longo, 2013; Mason et al., 2021). Volcanic PM may also include particles mixed in from the background atmosphere derived from sources such as sea spray, industrial and transport sources, ambient matter, and fine wind-blown mineral dust (Butwin et al., 2019; Holgate, 2017; Lim et al., 2012; Tam et al., 2016). Exposure to H_2SO_4, a dominant component of volcanic PM (Ilyinskaya et al., 2017; Mason et al., 2021; Mather et al., 2006a), can result in irritation of the eyes and respiratory tract (Carlsen et al., 2021a; Schlesinger, 1985; Williams-Jones and Rymer, 2015).

The persistent SO_2 and PM-rich volcanic plume emitted from Masaya volcano has led to long-term contamination and fumigation of an area >1200 km^2 downwind of the volcano following the prevailing wind direction (Delmelle et al., 2002; Williams-Jones and Rymer, 2015). A study by Delmelle et al., 2002 using time-averaged samplers found background concentrations of SO_2 <2 ppbv (parts per billion by volume) to the east of Masaya volcano in upwind locations in 1998 and 1999. The highest SO_2 levels were measured in the fumigated area to the west in the area within 4 km of Masaya volcano, with concentrations of up to 230 ppbv coinciding with descriptions of the local vegetation as "devastated" (Delmelle et al., 2002). Average SO_2 concentrations in the Las Sierras highlands were $\approx$ 100 ppbv in 1999 (Delmelle et al., 2002). In 2010, the U.S. Environmental Protection Agency (EPA) set the National Ambient Air Quality Standard (NAAQS) for SO_2 mass concentration exposure limits at 75 ppbv as a 1-hour average (EPA, 2010). As well as impacting the local vegetation, Masaya's volcanic plume interacts strongly with metal structures, particularly the roofs of buildings, which consistently have to be replaced or painted every six months due to rapid corrosion (Baxter et al., 1982; Delmelle et al., 2002; van Manen, 2014).

Volcanic activity at Masaya volcano is monitored by Instituto Nicaragüense de Estudios Territoriales (INETER). During periods of extreme degassing the likely-affected population are informed about the specific hazard and, on the basis of recommendations from INETER, protective measures are recommended according to the established protocols of the National System for Disaster Prevention, Mitigation and Attention (SINAPRED). The national park which covers all the Masaya Caldera, or more frequently the viewing platforms near the active Santiago crater, are occasionally closed to the public and tourists during periods of strong degassing (Duffell et al., 2003). There is no routine monitoring of air quality downwind from the volcano.

The 2016 - 2019 "Unseen but not unfelt: resilience to persistent volcanic emissions" (UNRESP) Global Challenges Research Fund project investigated resilience to living with persistent volcanic emissions and the environmental pollution hazard they pose, with Masaya as the case study. Here we examine data collected by the UNRESP project using a relatively low-cost gas and particle sensor network of five stations installed in

communities near Masaya. This is the first time, to the authors' knowledge, that the performance of low-cost sensors over long-term deployment (six months over February to August 2017) in a volcanic environment is assessed, where the sensors are placed in downwind locations (4 - 16 km) to determine concentrations of volcanic SO_2 and particulates in distal locations. The robustness and reliability of the network is discussed, in particular, the ability of the network to recognise volcanic air pollution episodes (VAPE), defined here as a period when the ground surface is exposed to volcanic SO_2 and particulates above what would be expected under non-volcanic background conditions. We give recommendations for improved set-up and consider other monitoring network instrument options.

3.2 Methodology

3.2.1 AQMesh pods and network set up

AQMesh pods are air quality monitoring systems which cost around £7,000 (≈ US$9,600) per pod (quote from ACOEM Air Monitors, 2021), relatively low-cost in relation to standard reference-grade instrumentation. Their configuration can be specified by the purchaser allowing a range of possible monitoring options including a variety of gas species, PM, humidity and ambient noise and wind conditions. Gases are measured by electrochemical sensors (B4 series manufactured by Alphasense Ltd). The electrochemical gas sensors and the humidity sensor are mounted into a base plate which allows them to come into contact with the ambient air. Here the gas-measurement focus is on SO_2. PM is measured by an OPC-N2 optical particle counter (manufactured by Alphasense Ltd) which uses a laser beam to detect particles from 0.38 to 17 µm in diameter (Crilley et al., 2018). Particles are assigned into size fractions of PM_1, $PM_{2.5}$ and PM_{10} using an embedded algorithm developed by AQMesh, and the raw size-resolved data are not available to the user except upon request (AQMesh, 2021a). The AQMesh pods are fitted with a small pump to pass the ambient air through the OPC-N2 which is fitted internally at the top of the instrument. The system is housed in an ABS IP65 box with a mounting bracket for installation. The dimensions are 170 mm by 220 mm by 250 mm with an additional 180 mm height if an antenna is fitted (AQMesh, 2021b). The pods weigh between 2 and 2.7 kg depending on sensor and battery configuration. Power is supplied either by mains power at 9 - 24V or by an internal lithium metal battery pack at 3.6V with 273.6Wh (AQMesh, 2021b). The battery recharging frequency is dependent on the user settings, including the data upload frequency. Here, the pods were used with an internal battery due to unavailability of mains power, and in this study the battery recharge frequency was four weeks. The electrochemical gas sensors and optical particle counter are calibrated during the manufacturing process and have an expected lifespan of two years before replacement is necessary (AQMesh, 2021b).

AQMesh pods are manufactured primarily for the monitoring of urban and commercial environments. The measurements are uploaded automatically via mobile network to the AQMesh server which allows data to be downloaded and also to be viewed in tabular and graphical formats. There is an annual fee of £480 (≈ US$650) for use of the online web server (quote from ACOEM Air Monitors, 2021). The specifications of the sensors used in the AQMesh pods installed in Nicaragua by the UNRESP project are outlined in Table 3.1.

Five AQMesh pods were installed in settlements to the west of Masaya volcano, downwind of the volcano during prevalent wind conditions. AQMesh pods were installed 1 - 5 metres above the ground. The sites were deemed to have low likelihood of localised pollution sources, with the exception of Rigoberto, which was located on a roof of a home and relatively close to the outlet of domestic cooking fire smoke. The sites of AQMesh installation were restricted by the limited infrastructure in the region, under more ideal conditions none of the instruments would have been placed in areas with likely contamination from non-volcanic sources. The locations of the AQMesh measurement stations and the prevailing plume trajectory are indicated in Figure 3.2. Based on local knowledge and previous studies (Delmelle et al., 2002; Mather et al., 2003), four of the stations (El Panama, Rigoberto, El Crucero and Pacaya) are frequently impacted by VAP. San Juan is significantly less likely to be impacted and was therefore used as a background station. El Panama, Rigoberto and San Juan stations were installed at domestic household sites in low-income rural communities; El Crucero and Pacaya stations were installed in public buildings in more built-up areas. El Panama and Rigoberto are considered near-field stations (≈ 4 km from the crater), and El Crucero and Pacaya are considered far-field stations (≈ 16 km from the crater) [Figure 3.2].

The AQMesh pods were maintained by the UNRESP project and INETER. Technical specifications of the AQMesh pods state that the electrochemical sensors require replacing after 2 years (AQMesh, 2021b), however the electrochemical sensors needed replacing several times during the six month experiment period [Table 3.2]. For example, at El Crucero station, issues with the SO_2 sensor and corrosion of the battery connectors required replacement parts to be installed on four occasions within the six months of AQMesh pod deployment, resulting in corrupted data over 36% of the measurement time [Table 3.2, Figure 3.8]. In some instances the internal batteries could not be recharged promptly after four weeks, resulting in periods of missing data due to lack of power. Exposure of the AQMesh pods to a volcanic environment, even in reasonably dilute downwind conditions, likely led to mechanical issues with the pod operating systems (Li et al., 2018). A high level of fast-acting corrosion impacted the pods at all of the measurement stations, but especially those in closer proximity to the volcanic source point. Corrosion occurred both externally (e.g. to the mounting brackets, Figure 3.3A, B) and internally (e.g. to the metal parts of the sensors, computer

boards and battery charging connectors, Figure 3.3C, D), resulting in long periods of missing or erroneous data until replacement parts could be installed.

3.2.2 Sensor Precision and Accuracy

To test the precision of the AQMesh sensors, all pods were placed in proximity together in an urban location [Figure 3.2] with minimal anthropogenic pollution sources (e.g. away from busy roads), away from volcanic input for an eleven day test period in July 2017. During the co-location test period we simultaneously exposed the PM sensors to episodes of highly elevated particle concentrations from a diesel car exhaust. The pods were placed at the same height and orientation to reduce environmental bias.

To test the accuracy of the SO_2 measurements, two AQMesh pods were co-located with a pulsed fluorescence spectroscopy analyser (Thermo Scientific 43i) for two days in December 2017. The 43i SO_2 analyser is designated by the Environmental Protection Agency (EPA) for measurements in the range of 0 - 1000 ppbv, with a precision of 1 ppbv and a lower detectable SO_2 limit of 0.5 ppbv [Thermo Fisher Scientific 2010; EPA, 2016]. The FEM (Forum for Environmental Measurements) designation of instruments, such as this SO_2 analyser, aims to promote consistency in measurements between different environmental monitoring networks by ensuring that instruments are of reference-grade quality [EPA, 2016]. The SO_2 analyser was installed in an air-conditioned building at El Crucero [Figure 3.2] with an inlet tube feeding air in from outside. AQMesh pods 712150 and 735150 were installed within a few meters of the SO_2 analyser inlet. The SO_2 analyser was calibrated on return to the UK and found to have a baseline drift of 2 ppbv and an underestimation of 18% (Read, 2018). The SO_2 analyser was verified using a National Physical Laboratory certified Cylinder (Cylinder number: 176433, BOC Ltd) with the blender set-up within the AMOF COZI Laboratory, National Centre for Atmospheric Science (NCAS, https://amof.ac.uk/laboratory/carbon-monoxide-and-ozone-calibration-laboratory-cozi/).

Table 3.1: AQMesh pod sensor specifications for Nicaragua installation. Instrument specifications as stated by AQMesh, 2021b.

Sensor	Type	Units	Range	Precision	Accuracy	Lower limit
SO_2	Electrochemical	ppb	0 - 100,000 ppb	>0.7	20 ppb	<5 ppb
NO	Electrochemical	ppb	0 - 20,000 ppb	>0.9	1 ppb	<1 ppb
NO_2	Electrochemical	ppb	0 - 20,000 ppb	>0.85	4 ppb	<1 ppb
CO	Electrochemical	ppb	0 - 1,000,000 ppb	>0.8	20 ppb	<50 ppb
O_3	Electrochemical	ppb	0 - 20,000 ppb	>0.9	5 ppb	<1 ppb
PM	Optical particle counter	$\mu g/m^3$	0 - 250,000 $\mu g/m^3$	>0.85	5 $\mu g/m^3$	0 $\mu g/m^3$
Humidity	Solid sate	%	0 to 100 %	>0.9	5% RH	1% RH

Table 3.2: Frequency of AQMesh pods being offline due to sensor failure or corrosion of key components impacting ability to function.

AQMesh number	Installation date	Measurement station	Time in field (days)	Number of events	Days offline	Time offline
712150	01/03/17	El Crucero	183	4	66	36%
1733150	25/02/17	El Panama	187	5	41	22%
789150	27/02/17	Pacaya	184	3	56	30%
803150	27/02/17	Rigoberto	170	3	19	11%
735150	28/02/17	San Juan	157	1	8	5%

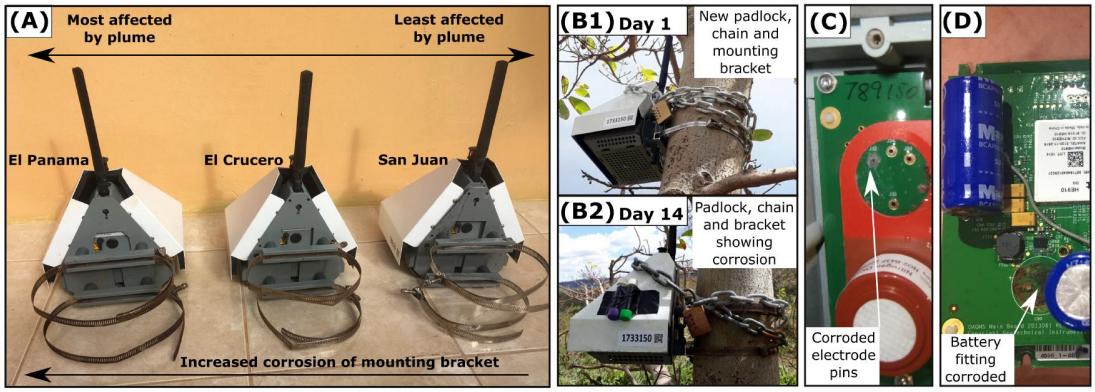

Figure 3.3: Issues with AQMesh pod corrosion and maintenance. (A) corrosion of metal installation mounting bracket is more advanced in measurement stations more frequently impacted by the volcanic plume; (B) corrosion as a result of the volcanic plume is fast-acting. AQMesh pod 1733150 installed at El Panama with new metal fittings, padlock and chain (B1) shows obvious signs of corrosion after 14 days (B2); (C) mounting board for the electrochemical sensors with signs of corrosion on the electrode pins for one of the sensors; (D) an AQMesh internal computer board which controls the sensors showing signs of corrosion with one of the board battery units disconnected.

3.2.3 Electrochemical Sensor Cross-Sensitivities

Electrochemical sensors operate by diffusion of the target gas through a porous membrane, following which changes in the chemical potential are measured by a sensing electrode (Austin et al., 2006; Mead et al., 2013). However, other substances may interfere with the chemical potential of the electrochemical sensor, causing a positive or negative interference to the sensor output, resulting in a biased measurement (Austin et al., 2006; Lewis et al., 2016). These interfering substances can include a number of compounds, only some of which are reported by the manufacturer. Studies such as Mead et al., 2013 have shown that electrochemical sensors are suitable for monitoring gas levels in low ppbv concentrations, but it must also be recognised that cross-sensitivities of the sensors may have a substantial impact on the sensor output.

The cross-sensitivities of the SO_2-B4 sensor used in this study can be found in the instrument data sheet (https://www.alphasense.com/WEB1213/wp-content/uploads/2019/09/SO2-B4.pdf). Of these, cross-sensitivities to NO_2 and O_3 are the most likely to impact the accuracy of the SO_2 measurement (Alphasense, 2021). Changes in temperature and humidity can also impact electrochemical sensor performance (Lewis et al., 2016; Mead et al., 2013). However, in this study we are not investigating quantitative concentrations of SO_2 but the AQMesh pods' efficiency at determining the simultaneous enhancement of SO_2 and PM and hence the equipment's ability to recognise the presence or absence of volcanic plume, and as such it is sufficient to measure relative changes even when the absolute concentrations of SO_2 are unreliable.

3.2.4 PM sensor humidity correction factor

The optical particle counter (OPC) used in the AQMesh pods is a small, low-cost sensor making it suitable for deployment in compact instrument systems. Such sensors are becoming widely used in the air quality aerosol-monitoring community as they offer an alternative to more expensive reference-grade instrumentation which often require high power input and surrounding infrastructure (Kelly et al., 2017; Lewis et al., 2016; Sousan et al., 2016a; Sousan et al., 2016b). However, the trade-off of using these low-cost compact OPCs is that they do not currently provide such precise, accurate or sensitive measurements as their reference-grade counterparts (Crilley et al., 2018; Crilley et al., 2020; Sousan et al., 2016a).

Part of the issue lies with the methodology for acquiring the number and size of the particles. Many low-cost OPCs measure the number of particles and the particle diameters by examining the light-scattering as each particle passes through a laser beam. These measurements are then converted to particle mass concentrations by assuming that the particles are spherical and of a uniform density. However, most low-cost OPCs do not dry the sampled air prior to measurement, as this would require additional hardware and power costs. Atmospheric particles are typically hygroscopic in that they absorb moisture from the air, and at high humidities it is often water which is the dominant component of atmospheric particles (Gysel et al., 2007). The ability of particles to absorb water depends on the particle composition, with the variability of hygroscopicity determined by the inorganic mass fraction, with sulphate in particular being a very hygroscopic particle composition (Crilley et al., 2020; Gysel et al., 2007; McFiggans et al., 2005). When the sampled air is not dried prior to measurement by OPCs, the particle hygroscopicity can lead to significant bias in the determination of particle size and shape, especially under high humidity conditions (Crilley et al., 2018; Crilley et al., 2020; Jayaratne et al., 2018). As a consequence of this, the reported particle mass concentrations from OPCs without a heated inlet need to be converted from wet particle mass concentrations to dry particle mass concentrations in order to be more accurate and comparable to reference-grade instruments and measurements made at different humidity levels.

Here we follow the methodology described in Crilley et al., 2018 and Crilley et al., 2020 to apply a correction factor to the reported results for PM_1, $PM_{2.5}$ and PM_{10} from the AQMesh network in Nicaragua. The correction factor (C) is applied in the following manner as described in Equation 3.1:

$$C = 1 + \frac{\frac{\kappa}{\rho_{\mathrm{p}}}}{-1 + \frac{1}{a_{\mathrm{w}}}} \tag{3.1}$$

where ρ_{p} is the density of the dry particles (here we use 1.65 g cm^{-3} which is the

ambient particle density assumed by the OPC-N2); a_w is the water activity (RH/100) and the value for κ can be found by a non-linear curve fitting of a humidogram (a_w vs m/m_0 where m and m_0 are the wet and dry (RH=0%) aerosol mass, respectively). For PM_1 and $PM_{2.5}$ measurements we used a κ value of 0.53 relating to ammonium sulphate (Petters and Kreidenweis, 2007) and for PM_{10} measurements we use a κ value of 0.33 relating to dust particles as these have a lower hygroscopicity and would normally be found in the PM_{10} size fraction (Pringle et al., 2010). For the correction factor calculations we use the relative humidity as measured by the humidity sensor installed in the base plate of the AQMesh pods.

The raw particle mass concentrations reported by the AQMesh pods can then be corrected according to Equation 3.2:

$$PM_{\text{Corr}} = \frac{PM_{\text{Raw}}}{C} \tag{3.2}$$

The manufacturer states that the OPC-N2 instruments are factory calibrated prior to sale. The application of the correction factor as described above should remove the impact of high humidity conditions from the measurements (Crilley et al., 2018; Crilley et al., 2020).

3.2.5 Detecting volcanic air pollution episodes

By definition, VAP elevates concentrations of SO_2 and PM at ground level for a period of time. However, the SO_2 sensors periodically recorded seemingly unrealistic peaks and troughs in concentration [Figure 3.8]. Therefore, we attempted to evaluate how reliable the AQMesh pods are in identifying VAPE by using different data analyses approaches and independent sources of data. We analysed the AQMesh data for correlations between SO_2 and PM and for variability in PM concentrations and size fractions. Forecast meteorological data (ECMWF) and high-resolution satellite images of the volcanic plume were used as independent proxies for the likely presence of VAPE.

3.2.5.1 Concurrent SO_2 and PM

We expect a strong correlation between SO_2 and PM during VAPE as both species are abundant in volcanic plumes. SO_2 has no strong non-volcanic local sources (some amounts are emitted from cooking fires and fuel combustion) and would therefore only become elevated at ground level during VAPE. PM is released in high concentrations both from volcanic and non-volcanic origins (likely local sources include cooking fires, traffic, household waste burning and agricultural fires) and would become elevated during both types of pollution events. SO_2 alone, or the simultaneous presence of both SO_2 and PM, will distinguish episodes of volcanic pollution from non-volcanic pollution.

The data obtained from the AQMesh instruments were processed into hourly averages. Periods of erroneous or missing data [Table 3.2] were not included in the analysis. The remaining data were analysed using RatioCalc 3.2 software following Tamburello, 2015. RatioCalc software was used to determine periods of time when there were strong correlations (r^2 greater than 0.5) between SO_2 and the humidity-corrected measurements of PM_1, $PM_{2.5}$ and PM_{10} (henceforth termed simultaneous enhancement of SO_2 and PM) indicating VAPE. A minimum threshold of four consecutive days of good correlation was set to ensure that the concurrent SO_2 and PM signal was real and not a result of instrumental error or drift. Data were excluded from further analysis when SO_2 had a correlation to the relative humidity greater than an r^2 value of 0.25, as a dependence on humidity indicates the SO_2 response is not representative of the actual atmospheric SO_2 concentrations but an instrumental artefact (Roberts et al., 2012). Correlation periods were only included where SO_2 concentration peaks reached at least 20 ppbv, as concentrations lower than this are beneath the unambiguous detection limit of the electrochemical SO_2 sensor. At Rigoberto station, the AQMesh pod recorded some instances where SO_2 concentrations peaked at 300 ppbv for short (< 3 hour) durations. Such peaks in SO_2 were not found elsewhere during the analysis and have been interpreted to be anthropogenic pollution, most likely from the local cooking fires. These cooking-fire related detections were removed from the analysis.

3.2.5.2 PM concentration and size fractions

We analysed the concentration and change in size fractions of PM_1, $PM_{2.5}$ and PM_{10} from each of the measurement stations. Using the VAPE identification from ECMWF and satellite imagery (respective methods in 3.2.5.3 and 3.2.5.4), the PM data were divided into categories of VAPE-likely and VAPE-unlikely conditions and analysed to investigate any significant differences in the number and range of PM under the different conditions. A two-sample t-test, used to test whether the means of two datasets are equal, was applied to determine the significance level of any differences between the VAPE-likely and VAPE-unlikely conditions for each of the size fraction categories. Using the VAPE-unlikely data-set, a monthly average background concentration was calculated for each PM size category at each measurement station. The VAPE-likely and VAPE-unlikely data-sets were then compared to the monthly background average to determine significant outliers indicating PM pollution events.

3.2.5.3 ECMWF Forecast Data

We used meteorological data to determine the likely volcanic plume transport direction, as an indication for how likely VAPEs were during a particular period. Observations from meteorological stations could not be obtained within the scope of this project. Instead we used forecast meteorological data from the European Centre for Medium-Range

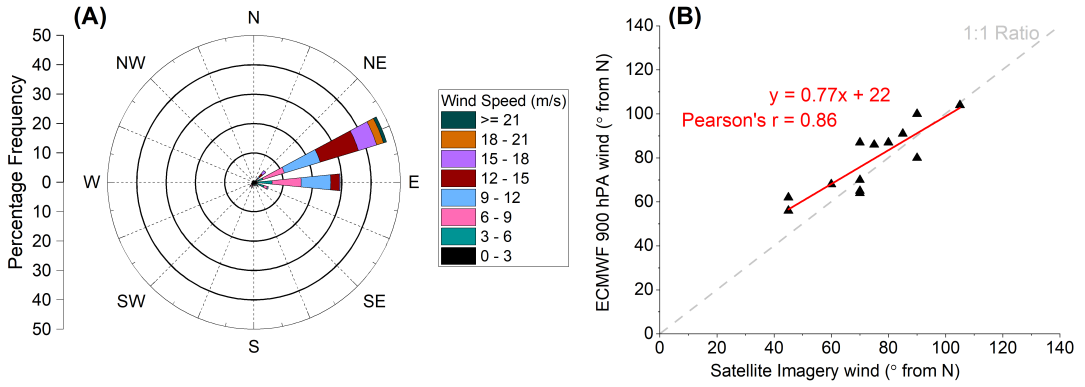

Figure 3.4: Forecast meteorological data for Masaya volcano. (A) Wind rose for the period February to August 2017 at 900 hPa, with an average geopotential height of 948 m ± 113 m. Wind direction is predominantly from the ENE and E. Data are derived from ECMWF forecast and are displayed as the direction the wind is blowing from. (B) Comparison between the ECMWF 900 hPA wind direction data and the wind directions derived from the satellite imagery over Masaya volcano.

Weather Forecasts (ECMWF) to determine when volcanic plume was likely to have been present at the measurement stations. ECMWF uses ensemble forecasting to predict the evolution of atmospheric conditions through time (Buizza et al., 2005; Molteni et al., 1996). Forecast data were extracted from the ECMWF model at 12.0000 N 273.8750 E, which is the closest grid point to Masaya volcano, located approximately 1 km to the north and 3 km to the west from the active volcanic vent. The ECMWF forecast resolution was 0.125 degrees (≈ 12 km at the equator).

ECWMF forecasts were obtained for the period 27th February to 28th August 2017. Data were retrieved in a three-hour cycle, with each output producing forecast results at twenty-five pressure levels through the atmosphere, from 1000 hPa (average geopotential height of 104 m asl) to 1 hPa (average geopotential height of 46,197 m asl). Model estimates of temperature (K), wind direction (° from north), wind speed (m/s), geopotential height (m), vertical velocity (m/s) and humidity (% RH) were extracted for each pressure level. The wind speed and direction were examined graphically in wind roses to determine changes in the wind direction through a vertical profile of the atmosphere from near ground-level to 3000 m asl. The predominant wind direction was found to be from an East or East-North-East direction for the lower 3000 m of the atmospheric column during the period of interest.

The wind direction at each pressure level, derived from the ECMWF forecasts, was compared to the wind direction derived visually from visible plume extension seen in satellite imagery [Section 3.2.5.4] to determine best correlation and likely height of the plume. The time of satellite imagery acquisition was obtained from the image metadata, and the comparison to ECMWF forecasts was calculated at the closest model output time to reduce discrepancies from changes in wind direction before and after satellite

imagery acquisition. The ECMWF forecast at 900 hPa (948 m ± 112 m asl) had the highest correlation with plume extension orientation seen in satellite imagery during the thirteen days of overlapping data, with a Pearson's r value of 0.86 [Figure 3.4]. As a result we interpret that the plume is most commonly being dispersed away from Masaya volcano at a geopotential height of 948 m asl. This is consistent with the volcano summit height (635 m asl) plus some thermal plume rise above the crater. However, we recognise that this interpreted plume height may have some bias resulting from only using visible plume extension from satellite imagery on days with clear skies if we consider that overcast days may have a different air pressure causing the plume to travel at a different height in the atmosphere. The ECMWF forecasts at 900 hPa were used throughout the study to determine which AQMesh station was likely exposed to volcanic plume throughout the period of interest. We recognise that using ECMWF forecast data at an average height in the atmosphere of 948 m asl to interpret the dispersion direction of Masaya's volcanic plume may introduce errors in the prediction of which AQMesh station was exposed to volcanic pollutants as there is no guarantee that the plume will "ground" at the AQMesh station to allow ground-based measurement of the pollutants. ECMWF forecast data were used in 24-hour averages to give a good representation of the overall meteorological conditions. The likely presence of plume at each AQMesh measurement station was evaluated and compared to the AQMesh measurements to quantify the effectiveness of the AQMesh pods at recognising the presence of volcanic plume.

3.2.5.4 Satellite Imagery

Visual satellite imagery of the volcanic plume from Masaya was used as another indication for a greater likelihood of a VAPE. The USGS Landlook Viewer (https://landlook.usgs.gov/) displays high-resolution satellite images from Sentinel 2, Landsat 7, and Landsat 8. The satellite imagery obtained was non-continuous over 2017. Twenty-seven satellite images were obtained of the region around Masaya volcano between 5th March and 28th August 2017. Of these, twelve could not be effectively examined to determine plume direction due to the extent of opaque cloud cover, and two occurred during periods of unavailable ECMWF data. The remaining thirteen satellite images were compared to the ECMWF forecast wind directions. Visual inspection of the plume trajectory was also used to determine which AQMesh station was likely exposed to volcanic plume on a given day.

Visual analysis of the satellite imagery suggested sources of potential errors in the identification of likely plume presence at an AQMesh station using the ECMWF forecasts. Some satellite imagery indicated non-linear movement of Masaya's volcanic plume. A non-linear plume trajectory [Figure 3.5A] may result in bias in the assignment of which AQMesh station was likely exposed to volcanic plume, as the wind direction does not remain constant following plume dispersal away from the source point. As

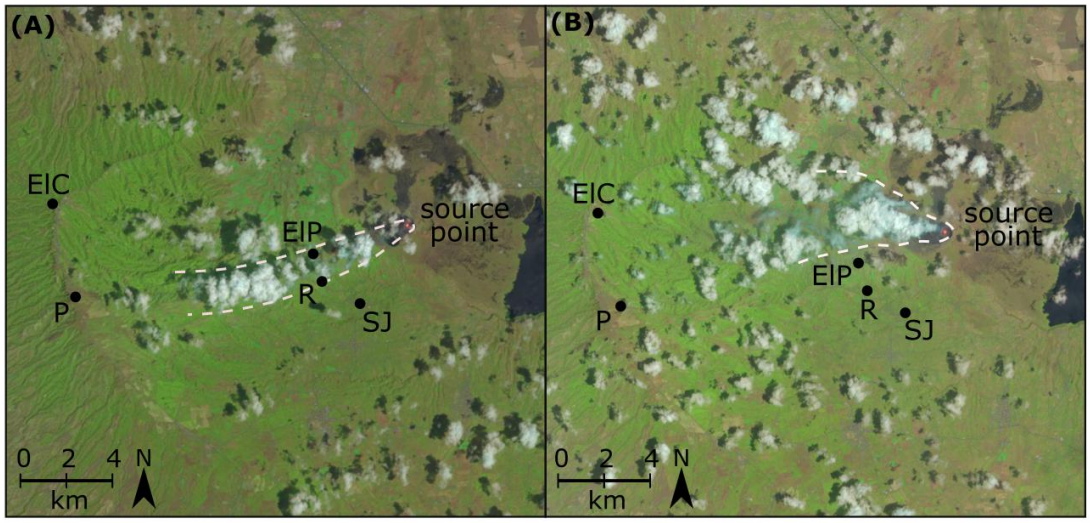

Figure 3.5: Satellite imagery obtained from the USGS Landlook viewer, annotated with plume trajectories indicated by white dashed lines. The source point (Masaya volcano's Santiago crater) is visible with the lava lake. AQMesh measurement stations are indicated with black circles and labelled as follows: ElC - El Crucero; P - Pacaya; ElP - El Panama; R - Rigoberto; SJ - San Juan. Plume is visible by semi-linear feature of white condensing clouds initiating from the source point, often interspersed with blue-tinged haze which is likely due to the particulate component. (A) 13^{th} March 2017 where the plume moves initially towards the south-west before the trajectory alters towards the west. Plume width is approximately 1.5 km. (B) 30^{th} March 2017 where the plume moves west with a wide lateral spread of approximately 3 km within the first 4 km from the source point.

there is limited availability of satellite imagery for use in comparison to the ECMWF data, it is not possible to determine the frequency of occurrences of non-linear plume trajectory. Another potential source of error is the width of the plume. Figure 3.5A and B indicate the variability in lateral plume width (by a factor of ≈ 2), which is not determinable from the ECMWF forecast wind direction and may cause errors when characterising stations as being likely exposed to VAP on a specific day. Satellite imagery also suffers from the same "grounding" uncertainty where it isn't certain that a visible plume is reaching the Earth's surface.

3.3 Results

3.3.1 Precision of AQMesh Pods PM Measurements

During the co-location testing period [section 3.2.2] the SO_2 concentrations were low and within the noise limit for the electrochemical sensors. As such, only the PM measurements from this co-location period were considered, the results of which for PM_1 and $PM_{2.5}$ are shown in Figure 3.6. During the testing period, the PM_1 concentrations were less than $15\,\mu g/m^3$ and the $PM_{2.5}$ were less than $30\,\mu g/m^3$.

The PM measurements of each of the five AQMesh pods were analysed and as-

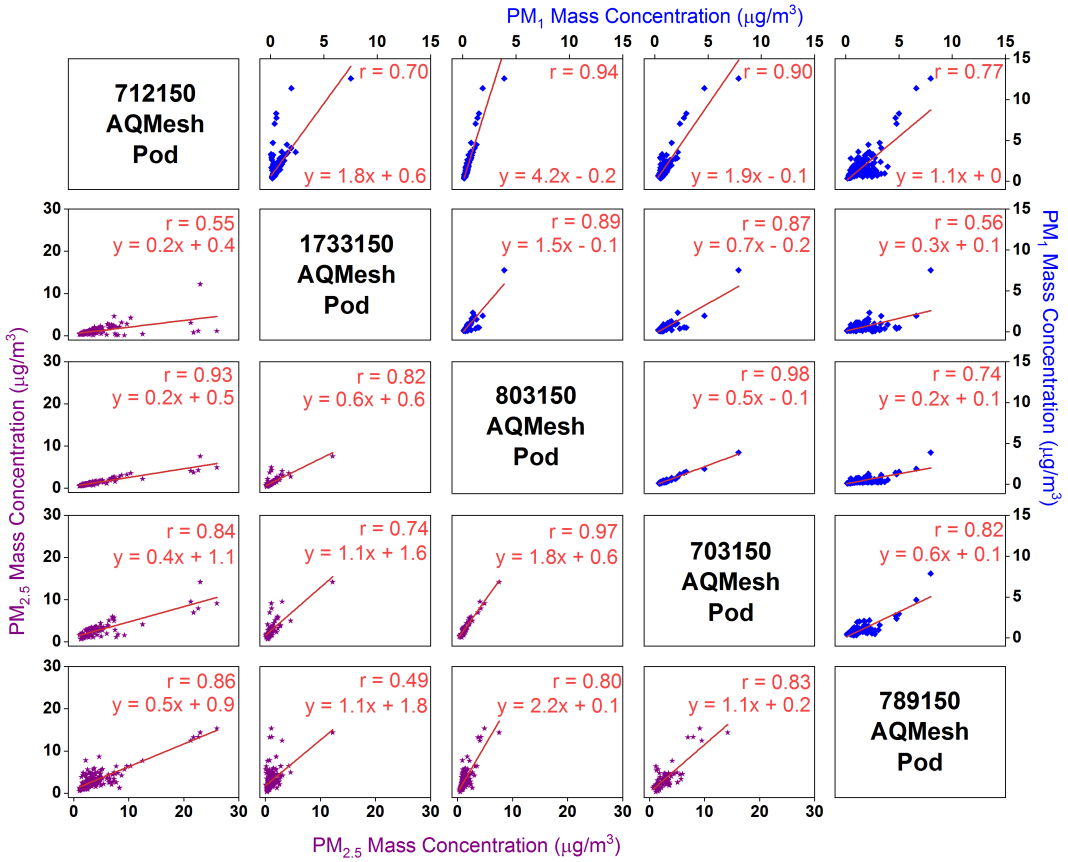

Figure 3.6: Scatter plot matrix of PM_1 and $PM_{2.5}$ results from co-location of AQMesh pods for eleven days in July 2017, all data are in hourly averages. PM_1 results are displayed in the ten plots in the upper triangle with data plotted in blue. $PM_{2.5}$ results are displayed in the ten plots in the lower triangle with data plotted in purple. All data presented have been processed with the correction factor outlined in section 3.2.4.

sessed for correlation during the co-location period. For PM_1 measurements, Pearson's r values were high between instruments, with 30% of the r values above 0.9 and 60% above 0.8. However there was significant variability in the magnitude of PM recorded, with AQMesh pods 712150 and 789150 consistently measuring higher values than pods 803150, 1733150 and 703150. For $PM_{2.5}$ measurements, similar Pearson's r values were found, with 20% above 0.9 and 70% above 0.8. Measurement variability was reduced in $PM_{2.5}$ measurements, though pod 712150 consistently reported lower values with respect to the other instruments [Figure 3.6].

The co-location indicated that there was some significant variability among the OPC-N2 instruments within the AQMesh pods at low concentrations. However, despite the variability in absolute measurements, all the instruments recorded high concentrations simultaneously, suggesting that the AQMesh pods are suitable for monitoring increases in PM above background concentrations, even if there is variability in the absolute concentration of PM recorded.

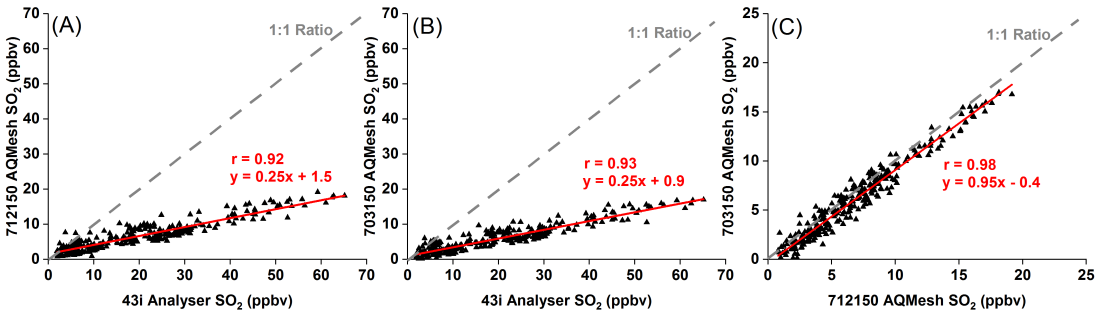

Figure 3.7: Co-location of 43i SO_2 analyser and two AQMesh pods at El Crucero measurement station. Comparisons of SO_2 measurements between (A) 43i analyser and the SO_2 electrochemical sensor in the 712150 AQMesh pod; (B) 43i analyser and the SO_2 electrochemical sensor in the 703150 AQMesh pod; (C) SO_2 electrochemical sensor in the 712150 AQMesh pod and the SO_2 electrochemical sensor in the 703150 AQMesh pod. Comparisons and data presented here are the peaks in data, near-baseline measurements were removed as they were within the baseline noise fluctuations of the AQMesh sensors. Measurements from the 43i analyser have been corrected to remove baseline drift and to account for 18% underestimation as indicated by post-fieldtrip calibration.

3.3.2 Accuracy of AQMesh Pod SO_2 Measurements

During the testing period of AQMesh and the pulsed fluorescence spectroscopy SO_2 analyser [Section 3.2.2], both co-located AQMesh pods underestimated the concentrations measured by the SO_2 analyser by up to 75% [Figure 3.7]. The correlation between the electrochemical sensors and the SO_2 analyser was very good, with Pearson's r values of 0.92 and 0.93 respectively across both AQMesh pods. The two AQMesh pods correlated very well with each other, with a Pearson's r value of 0.98 and 5% variance in the measurement trend [Figure 3.7C]. The Alphasense B4 sensors may not be suitable for reporting absolute values of SO_2 at low concentrations (see discussion below), but are reliable for detecting when SO_2 in the atmosphere is increased to above background concentrations. We therefore suggest that they are suitable for a low-cost sensor network where the instruments are used to determine the presence or absence of volcanic plume and where identifying changes is the greatest priority.

Although AQMesh indicates that the SO_2 sensors were calibrated in the factory prior to sale, it is likely that each electrochemical sensor will have a slightly different level of accuracy and measurement precision with the potential for some baseline drift (Alphasense, 2021). The impact of the corrosive volcanic environment was the likely cause of the SO_2 electrochemical sensors frequently failing and requiring replacement. This means that there will be temporal inconsistencies as sensors are replaced, adding an additional source of uncertainty to the data. One of the symptoms of the SO_2 sensor failures was extreme peaks and troughs in the recorded SO_2 [Figure 3.8]. These peaks and troughs were not recorded at the background measurement station at San Juan,

or at the Rigoberto measurement station which was located closer to the edge of the prevailing plume dispersion region [Figure 3.8A, B]. The near-field site at El Panama and the far-field sites at El Crucero and Pacaya recorded extreme peaks and troughs in SO_2 [Figure 3.8C, D, E], likely due to volcanic pollutant-induced corrosion. SO_2 measurements at some AQMesh stations recorded a diurnal signal which is likely due to the humidity and/or temperature impacting the sensor baseline [Figure 3.8F, I]. These diurnal signals are difficult to remove as each SO_2 sensor can have sensor-specific responses and several sensors had to be replaced during the six-month experiment period. Due to the frequent SO_2 sensor failure and extreme erroneous measurements, the SO_2 data is here concluded to be unreliable as a stand-alone measurement, at least for long-term deployment with minimal maintenance commitment. This further motivates our methodology choice to use simultaneous enhancement of SO_2 and PM (i.e. correlation with $r^2 > 0.5$, see Section 3.2.5.1) as an indicator of the presence of volcanic plume [Figure 3.9].

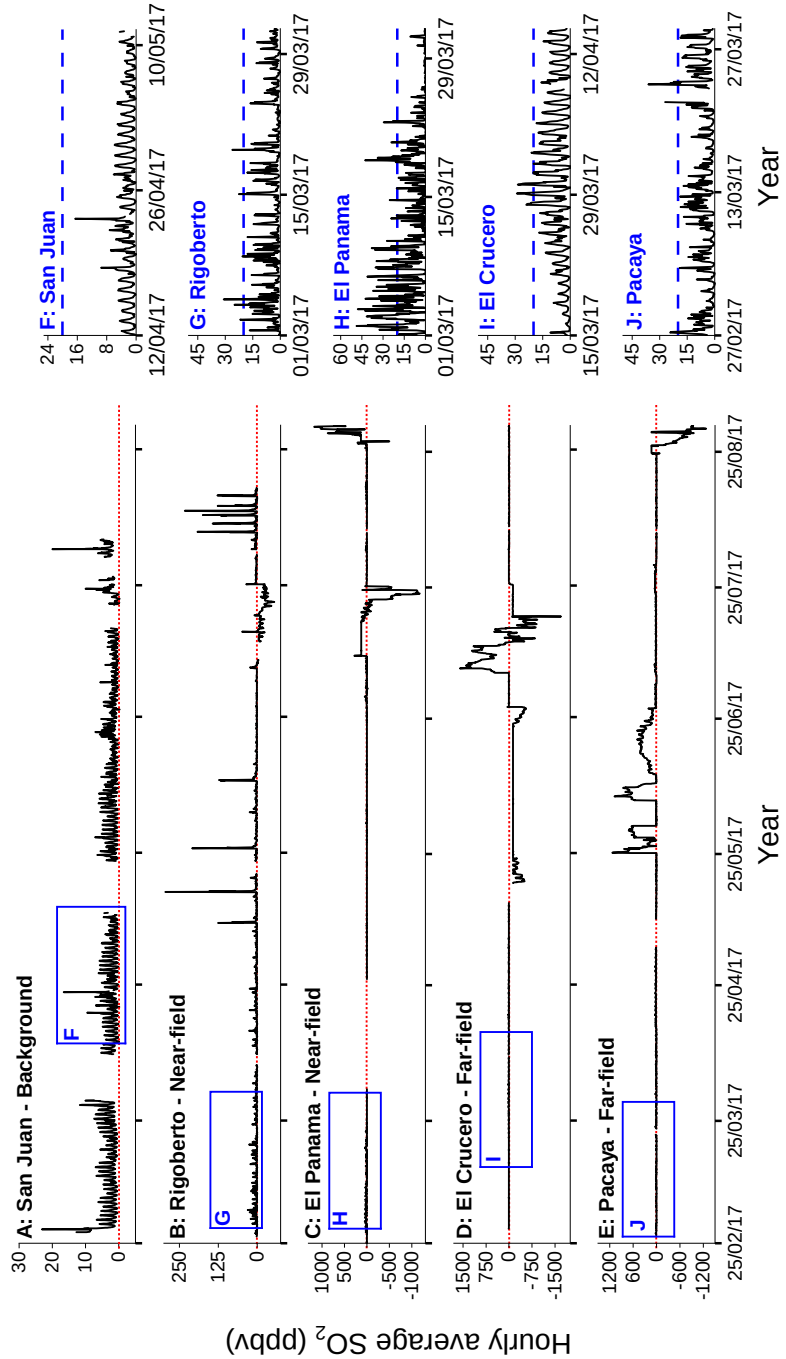

Figure 3.8: Electrochemical SO_2 measurements from the five AQMesh stations. (A-E): timeseries of hourly-average electrochemical SO_2 measurements over the six-month experiment period. Periods of missing data result from lack of power due to corroded battery connectors or batteries remaining uncharged after four weeks. Corrupted data resulting from failure of the SO_2 electrochemical sensors caused extreme SO_2 peaks and troughs as seen in C, D and E. Red dashed line indicates 0 ppb line. Blue outlines indicate time-periods for F-J. (F-J): 1-month excerpts from the SO_2 timeseries at each AQMesh station, indicating periods of data with no extreme peaks and troughs. Blue dashed line indicates 20 ppb, the lower limit used for identifying periods of simultaneously enhanced SO_2 to PM.

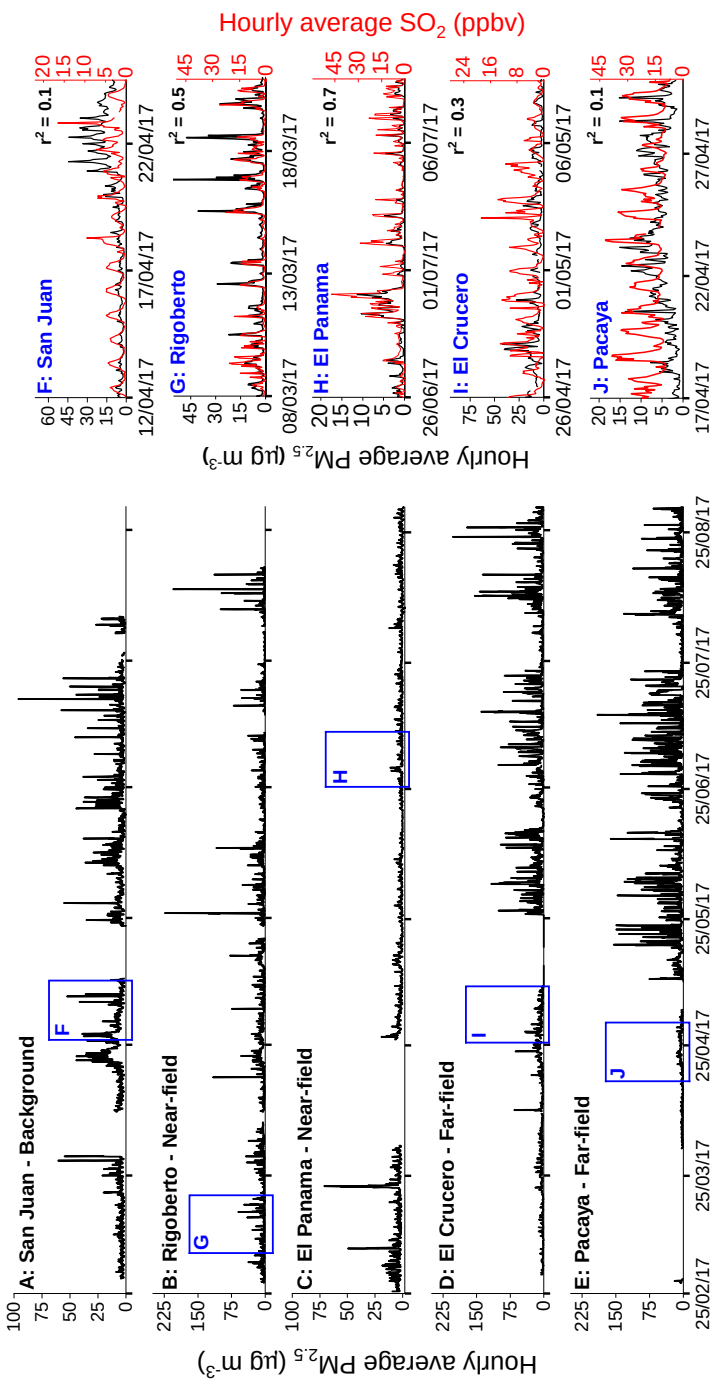

Figure 3.9: $PM_{2.5}$ measurements from the five AQMesh stations. (A-E): timeseries of hourly-average $PM_{2.5}$ measurements over the six-month experiment period, with all results corrected for humidity using the method outlined in Section 3.2.4. Periods of missing data result from lack of power due to corroded battery connectors or batteries remaining uncharged after four weeks. Blue outlines indicate time-periods for F-J. (F-J): 14-day excerpts from the $PM_{2.5}$ timeseries at each AQMesh station. SO_2 measurements for the same time-period indicated by the red data-line, with corresponding scale on the right-hand y-axis. Correlation between $PM_{2.5}$ and SO_2 for the excerpt period is indicated in the top-right corner of each plot. Time-periods for the 14-day excerpts were chosen where $PM_{2.5}$ and SO_2 data were both available (with no extreme SO_2 peaks or troughs), and where there were simultaneous elevations of SO_2 and PM, if available.

3.3.3 Efficiency of AQMesh pods at recognising volcanic plume

3.3.3.1 Simultaneous enhancement of SO_2 and PM indicates VAP

Wind directions from the ECMWF 900 hPa forecast and the satellite imagery were analysed to determine when VAPE was likely to be present at an AQMesh measurement station. The VAPE-likely days were cross-referenced with the AQMesh data periods of simultaneously elevated SO_2 and PM to determine the ability of the instruments to detect VAPE. This approach will miss identification of VAPE by the instruments when the sensors recorded simultaneously elevated SO_2 and PM for less time than our defined minimum threshold of four consecutive days. The results are presented in Figure 3.10.

A control analysis was implemented to identify agreement-positives (where ECMWF or satellite imagery indicated VAPE-likely at the same time as the AQMesh instruments also detected a simultaneous enhancement of SO_2 and PM) and disagreement-positives (where ECMWF or satellite imagery indicated VAPE-unlikely but the AQMesh instruments reported a simultaneous enhancement of SO_2 and PM). It should be noted that the determination of VAPE from the ECMWF data and satellite imagery may have substantial bias (see Sections 3.2.5.3 and 3.2.5.4). The meteorological data is a forecast rather than an observation, and therefore there may be instances of the plume being present at a measurement station without the forecast successfully predicting its presence. The forecast may also not successfully predict whether the plume is at ground level. The potential bias of the satellite imagery is caused by the fact that the images are a snapshot in time and do not capture conditions where the plume direction is dynamic. The results of the control analysis are presented in Figure 3.11.

At the background San Juan station [Figure 3.2], the AQMesh pod detected no simultaneous enhancement of elevated SO_2 and PM. ECMWF data and satellite imagery indicated no intervals of VAPE-likely, in agreement with the AQMesh.

At the near-field sites (Rigoberto and El Panama), the AQMesh pods detected the presence of the plume in reasonably good agreement with the ECMWF and satellite imagery given the potential sources of bias detailed above. At El Panama the AQMesh pod detected the plume with elevated SO_2 and $PM_{2.5}$ for 65% of the time that ECMWF indicated VAPE-likely, and 42% of the time that satellite imagery indicated VAPE-likely [Figure 3.10]. The AQMesh at Rigoberto identified the presence of the plume with elevated levels of SO_2 and $PM_{2.5}$ for 42% of the time that ECMWF indicated VAPE-likely and 30% of the time that satellite imagery indicated VAPE-likely [Figure 3.10]. The results were very similar for SO_2/PM_1 and $SO_2/PM_{2.5}$ correlations. For SO_2/PM_{10} correlation the plume was less often identified at El Panama and never at Rigoberto. Null hypothesis tests were then performed on the data sets with VAPE-likely or VAPE-unlikely defined according to combined ECMWF and satellite imagery methods [Figure 3.11]. The null-hypothesis test at the near-field sites indicated a much

higher level of agreement-positive than disagreement-positive results for both AQMesh stations. At El Panama station the AQMesh pod recorded agreement-positive identifications of VAPE 59% of the time for SO_2 and PM_1, 61% of the time for SO_2 and $PM_{2.5}$, and 46% of the time for SO_2 and PM_{10} [Figure 3.11]. There were significantly lower numbers of disagreement-positive plume identifications at El Panama, at 18% for PM_1 and PM_{10} and 23% for $PM_{2.5}$ [Figure 3.11]. Rigoberto AQMesh pod likewise had a higher percentage of agreement-positive instances than disagreement-positives for simultaneously elevated SO_2 and PM_1 (41% agreement-positive and 22% disagreement-positive) and $PM_{2.5}$ (41% agreement-positive and 15% disagreement-positive), with no occasions of correlations in SO_2 and PM_{10} at $r^2 > 0.5$. However, the absolute number of disagreement-positive identifications was higher at Rigoberto for SO_2 to PM_1, with 16 agreement-positive events and 21 disagreement-positive events. Rigoberto station was located closer to the edge of the prevailing plume dispersion region [Figure 3.2] and also relatively close to domestic cooking fires and the occurrences of disagreement-positives at this measurement site may be due to pollution events not related to Masaya volcano.

The far-field sites situated on the Las Sierras highlands (El Crucero and Pacaya) were not able to effectively recognise the presence of volcanic plume via means of simultaneously elevated SO_2 and PM. The El Crucero AQMesh pod recognised a volcanic signature 5% of the time that ECMWF indicated VAPE-likely at the station, and 0% of the time that satellite imagery indicated VAPE-likely [Figure 3.10]. The AQMesh at Pacaya never detected VAPE as defined by simultaneous enhancement of SO_2 and PM. Likewise the null-hypothesis test at the far-field sites indicated that the far-field AQMesh pods were not able to effectively recognise the presence or absence of the volcanic plume. El Crucero AQMesh station had an equal percentage of agreement-positive and disagreement-positive events for SO_2 to PM_1, and no periods of simultaneously elevated SO_2 and $PM_{2.5}$ or PM_{10}. The likely reasons for this are discussed in Section 3.4.1.2.

The agreement in VAPE identification was higher between AQMesh and ECMWF than between AQMesh and satellite imagery for El Panama, Rigoberto and El Crucero stations [Figure 3.10]. This is potentially due to satellite images providing only a snapshot of the meteorological conditions, whereas the ECMWF data were analysed as daily averages to provide an overview of conditions and reducing the impact of outlying wind directions.

3.3.3.2 Enhancement in fine PM associated with the presence of volcanic plume

PM data were analysed to determine whether there were significant differences in the mass concentrations of different size fractions (PM_1, $PM_{2.5}$ and PM_{10}) under VAPE-likely and VAPE-unlikely conditions. A two-sample t-test indicated significant differ-

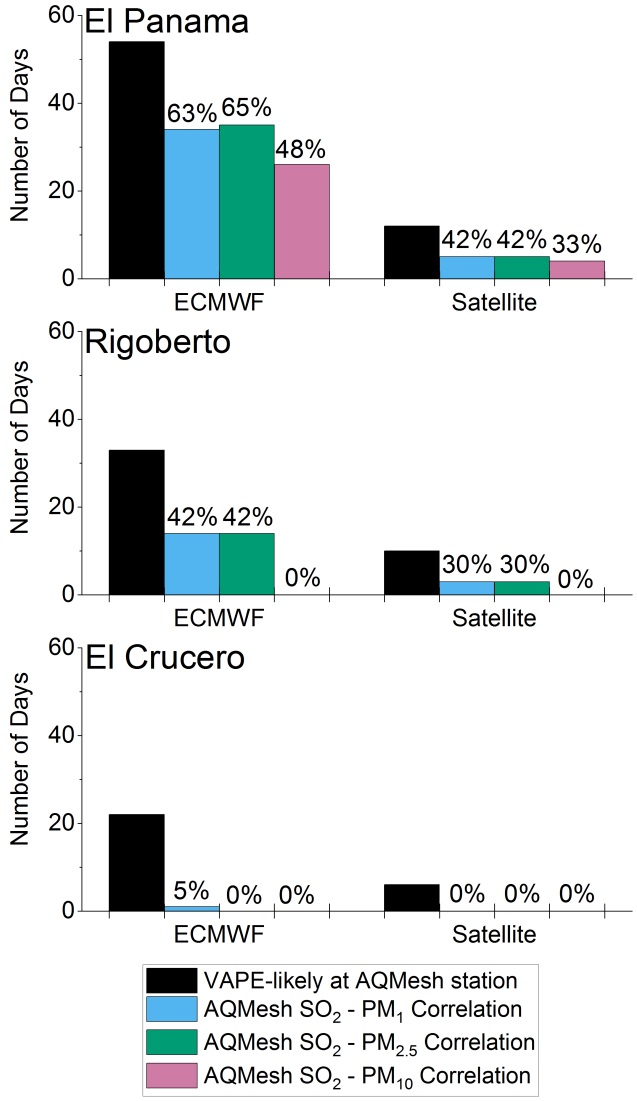

Figure 3.10: Efficiency of AQMesh pods at recognising VAPE derived from satellite and ECMWF data at three measurement stations. The frequency of VAPE-likely periods at the measurement station is indicated by the black bar, and frequency of simultaneous enhancement of SO_2 and PM AQMesh measurements are indicated by the blue, green and pink bars. Only periods where the AQMesh instrument was functional are considered here. Results are split into VAPE-likely periods derived from ECMWF forecasts and from satellite imagery. Percentages noted on each coloured bar indicate the proportion of how often that the AQMesh pods recognised VAPE derived from the relevant meteorological data. San Juan and Pacaya AQMesh stations are not displayed as no simultaneous enhancement of SO_2 and PM were found at these stations.

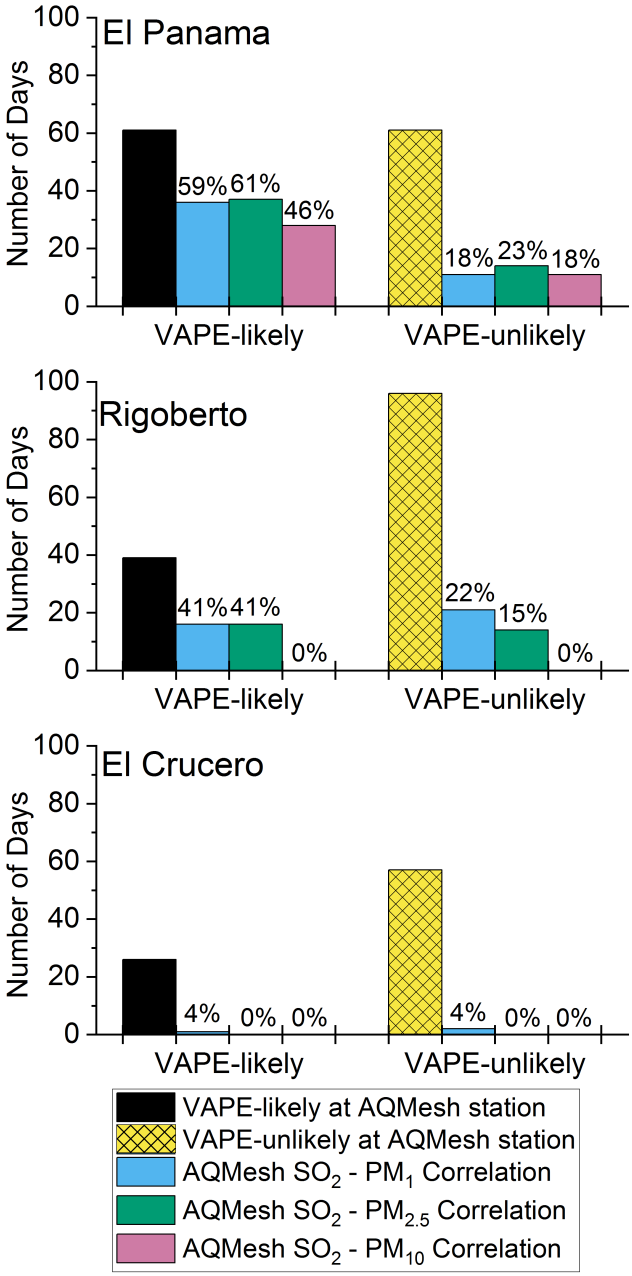

Figure 3.11: Efficiency of AQMesh pods at recognising VAPE at three measurement stations. Black bars indicate frequency of VAPE-likely conditions at the measurement station, as derived from both ECMWF and satellite data, during periods when the AQMesh pod was fully-functional. Yellow hatched bars indicate frequency of VAPE-unlikely conditions at the measurement station, as derived from both ECMWF and satellite data, during periods when the AQMesh pod was fully-functional. Percentages noted on each coloured bar under VAPE-likely conditions indicate the proportion of how often that the AQMesh pods recognised VAPE by means of simultaneous enhancement of SO_2 and PM. Percentages noted on each coloured bar under VAPE-unlikely conditions indicate the proportion of how often that the AQMesh pods gave a disagreement-positive result and falsely indicated VAPE. San Juan and Pacaya AQMesh stations are not displayed as no simultaneous enhancement of SO_2 and PM were found at these stations.

ences in the mean PM under VAPE-likely and VAPE-unlikely conditions at El Crucero and El Panama with all probabilities well below the significance level of 0.05. The two-sample t-test at Pacaya also showed significant difference between VAPE-likely and VAPE-unlikely conditions, although with probabilities closer to the significance level of 0.05. Rigoberto data proved to have an insignificant difference between the VAPE-likely and VAPE-unlikely conditions for all size fractions. A two-sample t-test could not be calculated for San Juan AQMesh station as ECMWF and satellite imagery did not indicate any periods where the plume was likely to have been present there, consistent with it being a background site. At El Panama and El Crucero, the two-sample t-test indicated a larger significance in the difference between VAPE-likely and VAPE-unlikely conditions for PM_1 than for the larger size fractions, while at Pacaya the highest significance was for $PM_{2.5}$ followed by PM_1. This indicates that the majority of the volcanic PM are very fine (typically <1 µm diameter), which follows the findings of previous studies where volcanic PM are often found to be in the smallest size fraction (Ilyinskaya et al., 2021; Ilyinskaya et al., 2017; Martin et al., 2011; Mason et al., 2021).

Peaks in PM concentrations for each size fraction do not appear to be linked to the presence or absence of the plume, with equally high maximum hourly concentrations recorded under both VAPE-likely and VAPE-unlikely conditions [Figure 3.12]. However, at El Panama and El Crucero, the average PM concentration across the six-month measurement period for all size fractions is higher during VAPE-likely conditions than VAPE-unlikely conditions [Figure 3.12], as was shown by the t-tests above. This is in agreement with observations of a PM-rich volcanic plume in Iceland (Ilyinskaya et al., 2017). From this we infer that at these stations there is a background level of PM that persists under both VAPE-unlikely and VAPE-likely conditions, whilst in VAPE-likely conditions there is an additional contribution from volcanically-sourced PM.

We calculated the frequency of episodes when PM size-dependent concentrations are above-background [Table 3.3]. We identified events where the average daily concentration exceeded one standard deviation above the long-term background average, indicating a PM pollution event (hereafter termed as such). At El Panama there was a much higher frequency of PM pollution events during VAPE-likely periods (41% for PM_1, 40% for $PM_{2.5}$ and 44% for PM_{10}) than during VAPE-unlikely periods (17% for PM_1, and 21% for both $PM_{2.5}$ and PM_{10}) [Table 3.3]. The El Crucero measurement station had a higher frequency of PM pollution events during VAPE-likely conditions (48% for both PM_1 and $PM_{2.5}$ and 25% for PM_{10}) than during VAPE-unlikely conditions (8.6% for PM_1, 5.5% for $PM_{2.5}$ and 13% for PM_{10}). Enhanced frequency of PM pollution events during VAPE-likely periods is also seen at the Pacaya and Rigoberto stations but it is much smaller than at the other stations [Table 3.3]. At the background San Juan station, the frequency of PM pollution events was comparable to VAPE-unlikely periods at the other stations [Table 3.3]. This supports the interpre-

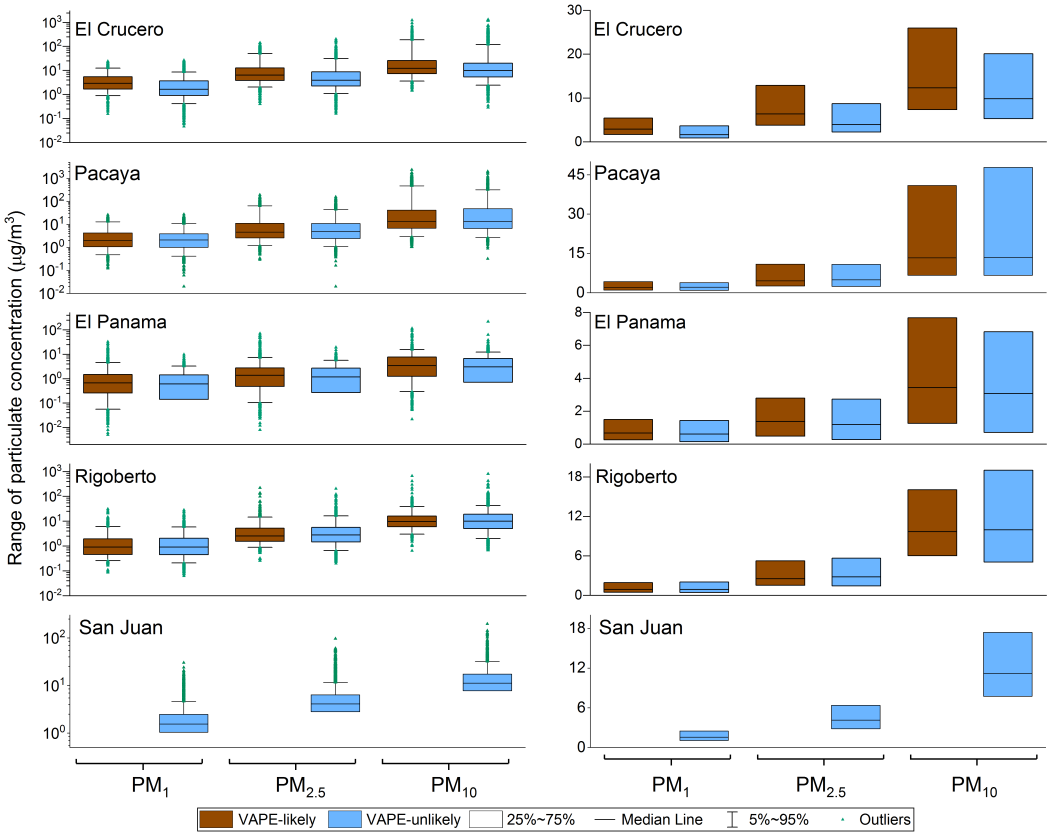

Figure 3.12: Range of PM concentrations at El Crucero, Pacaya, El Panama, Rigoberto and San Juan measurement stations under VAPE-likely (brown box-plots) and VAPE-unlikely (blue box-plots) conditions. Note the logarithmic y-axis scale on the left-hand graphs and linear y-axis scale on the right-hand graphs. VAPE-likely or VAPE-unlikely conditions are as identified by ECWMF forecasts and satellite imagery. Data plotted are hourly averages across the entire measurement period.

tation that AQMesh pods are reliably identifying PM pollution events of volcanic vs non-volcanic origin.

3.4 Discussion

3.4.1 Detection of VAP from Masaya volcano by AQMesh network

3.4.1.1 Near-source locations impacted by the plume

The AQMesh pods at both El Panama and Rigoberto were reasonably effective at recognising the presence of volcanic plume as defined by simultaneous enhancement of SO_2 and PM during periods when meteorological data suggested the plume was likely at the measurement station. Both stations also had a number of plume identifications during intervals when the meteorological data suggested VAPE-unlikely conditions, though the percentage of disagreement-positives was smaller than the percentage of agreement-

Table 3.3: PM pollution events defined as a period of 24-hours exceeding 1 standard deviation (SD) above the monthly background 24-hour PM average. VAPE-likely and VAPE-unlikely conditions are determined from ECMWF data and satellite imagery, and the monthly background average concentration is calculated from the VAPE-unlikely period data. The percentage of time exceeding the background average is calculated from the total time under VAPE-likely or VAPE-unlikely conditions.

Station Location	PM Size Group	Events exceeding 1∼SD above background average		Percentage time exceeding 1∼SD above background average	
		VAPE-likely Conditions	VAPE-unlikely Conditions	VAPE-likely Conditions	VAPE-unlikely Conditions
El Crucero	PM_1	19	11	48%	8.6%
	$PM_{2.5}$	19	7	48%	5.5%
	PM_{10}	10	16	25%	13%
Pacaya	PM_1	16	13	22%	18%
	$PM_{2.5}$	18	15	25%	20%
	PM_{10}	13	14	18%	19%
El Panama	PM_1	33	14	41%	17%
	$PM_{2.5}$	32	18	40%	21%
	PM_{10}	36	18	44%	21%
Rigoberto	PM_1	9	20	21%	16%
	$PM_{2.5}$	6	20	14%	16%
	PM_{10}	6	18	14%	15%
San Juan	PM_1	0	19	0%	14%
	$PM_{2.5}$	0	20	0%	15%
	PM_{10}	0	19	0%	14%

positives [Figure 3.11]. These findings support that simultaneous enhancement of SO_2 and PM measured by the AQMesh in near-field measurement stations around Masaya volcano are a suitable indicator for recognising the presence of the volcanic plume.

The PM distribution analysis indicated that the El Panama AQMesh pod recorded significantly higher frequencies of PM pollution events (for definition of PM pollution event see Section 3.3.3.2) during VAPE-likely conditions than VAPE-unlikely conditions [Table 3.3]. We infer that the PM pollution events during intervals when the plume was likely to be absent were caused by non-volcanic sources such as cooking fires, agricultural fires, or wildfire events. Satellite-derived information is available regarding wildfire events in Nicaragua (NASA, 2021), however smaller-scale events such as cooking fires, burning of household waste, and smaller-scale agricultural fires are not readily traceable. The PM pollution events during VAPE-unlikely conditions may also be caused by unsuccessful identification of plume presence by ECMWF data or satellite imagery (given the uncertainties as mentioned in Sections 3.2.5.3 and 3.2.5.4).

The AQMesh pod at the Rigoberto measurement station had an insignificant difference between VAPE-likely and VAPE-unlikely conditions for all PM size fractions in the two-sample t-test. There was also a low variability in the frequency of PM pollution events between VAPE-likely and VAPE-unlikely conditions [Table 3.3]. This is likely due to a coincidence of two factors. Rigoberto is located on the edge of the prevailing plume direction [Figure 3.2] and therefore is likely to receive a more dilute VAP with lower frequency of volcanic PM pollution events. The close proximity of the pod to

domestic cooking fires was likely the more important source of the local PM pollution events, overriding the signal of VAP. These results highlight the importance of considering different air pollution sources together and not placing volcanic-pollution detection instruments in places likely to be impacted by non-volcanic pollution.

3.4.1.2 Far-field locations impacted by the plume

The AQMesh pods at the El Crucero and Pacaya measurement stations were the least efficient at recognising the presence of the volcanic plume using simultaneously elevated concentrations of SO_2 and PM, with only minimal volcanic signatures recorded at El Crucero and none at the Pacaya station. The inefficiency of this method may be related to the greater distance between the volcanic source and the measurement sites (16 km from the crater, as opposed to 4 km for the near-field stations). Firstly, the greater distance may result in higher uncertainty in identifying the plume dispersal direction through meteorological forecasts. The ECMWF data were extracted for the grid point local to Santiago Crater and may not be representative of wind conditions over the full distance between the volcanic source and the Las Sierras highlands. The downwind variability in wind direction was observed on several occasions in satellite imagery with non-linear dispersion of the volcanic plume [Figure 3.5A]. Additionally, although meteorological data may correctly suggest the plume is being dispersed towards a measurement station on a given day, these parameters do not guarantee that the plume will "ground" and be measurable at ground-level. It is noted that the assumed plume height of 948 m ± 112 m asl could yield plume altitude below the Las Sierras ridge at 925 m, potentially acting to block the plume, although plume has been detected on the ridge previously (Delmelle et al., 2002; Mather et al., 2003). Secondly, over the 16 km distance between the volcanic source and the Las Sierras highlands, the plume may have become diluted into the atmosphere to the extent that the concentration was below the reliable range of the sensors. Thirdly, if in-plume conversion of SO_2 to PM was very extensive, this could eventually lower the correlation between SO_2 and PM. As such, the apparent inefficiency of the El Crucero and Pacaya AQMesh pods may be because the plume was not physically present at the stations at times when the ECMWF data and satellite imagery suggests it would be. Were the experiment to be repeated, it would be invaluable to set up a reference-grade measurement station for long-term monitoring alongside at least one of the far-field AQMesh stations. This would allow verification of the presence or absence of elevated SO_2 and PM at ground level and testing of the response of the AQMesh pod relative to the reference-grade instrument. This would allow verification of whether the AQMesh pods were correct in their positive or negative identification of the plume's presence. It would also be valuable to better constrain the plume height and extent in the vertical, potentially using drone or meteorological balloon measurements.

The PM distribution analysis at the El Crucero station indicated significantly higher frequencies of PM pollution events during VAPE-likely conditions than VAPE-unlikely conditions [Table 3.3], similar to that found at El Panama. At Pacaya AQMesh station the enhancement in VAPE-likely PM pollution events was lower than at El Crucero, in spite of the proximity of the two stations [Figure 3.2]. The cause for the smaller difference between VAPE-likely and VAPE-unlikely conditions at Pacaya is uncertain, but may be a result of localised anthropogenic pollution sources. The Pacaya station was located on the roof of a clinic, possibly resulting in more traffic-related pollution during the day. This potentially demonstrates the small-scale variability in pollution levels.

3.4.1.3 PM pollution events

Based on the SO_2 flux from 2016 [Figure 3.1] and visual observations of the plume during our fieldwork in 2017, the emissions from Masaya volcano were relatively low during the measurement period of this study. The frequency and concentration of the pollution events reported here should therefore be taken as a possible lower-limit at Masaya. Due to the high uncertainty in the quantitative measurements of SO_2 we refrain from discussing related air quality impacts, and focus on the PM data in this context. While the long-term average PM concentration is relatively low at all stations [Figure 3.9], the pollution events (both volcanic and non-volcanic) reach potentially unhealthy values (24-hour average: $PM_{2.5} > 35\,\mu g/m^3$ (EPA, 2013)) and support the need for an operational air quality network. At both near- and far-field stations impacted by the plume, the VAP-related pollution events enhance the concentration of PM_1 and $PM_{2.5}$ to a greater extent that PM_{10}, consistent with the fine size of volcanic particulates (Ilyinskaya et al., 2021; Ilyinskaya et al., 2017; Martin et al., 2011; Mason et al., 2021) [Table 3.3]. This is important for the potential impacts of VAP as fine PM is associated with more detrimental effects on human health, morbidity and mortality (Holgate, 2017).

3.4.2 Alternative air quality monitoring tools

The AQMesh pods are a relatively low-cost monitoring option. A network of five AQMesh pods for permanent installation would have an initial cost of £35,000 (≈ US$48,000), as quoted from ACOEM Air Monitors in 2021, followed by yearly server and maintenance costs. They are easy to install and do not require a large amount of infrastructure to operate. However, they suffered from frequent instrument failure in this case study, presumably to be due to the high level of fast-acting corrosion from the volcanic plume [Figure 3.3]. In such instances they require continual maintenance and purchase of replacement parts. Although having the advantage of being low-cost and relatively compact, the AQMesh instruments have the drawback of being less precise and accurate than larger reference-grade instruments, as indicated in Figure 3.7. The data from

the instruments also requires substantial processing and analysis, meaning that the current set-up is not useful for plume monitoring in real time until automatic algorithms can be implemented.

In comparison, if a network of reference-grade monitoring instruments were installed, the cost of installation and construction of the required infrastructure would be significantly higher. A single pulsed fluorescence spectroscopy SO_2 analyser costs in the range of £8,000 to £12,000 (≈ US$10,900 to US$16,300) depending on the configuration (quote from Thermo Fisher Scientific, 2021). A BAM-1020 (manufactured by Met One Instruments) which is a reference-grade FEM instrument for measuring PM would cost in the range of £17,000 (≈ US$23,200) (quote from Enviro Technology Services Ltd, 2021). The instrumentation cost of one reference-grade monitoring station would therefore be in the range of £25,000 to £29,000 (≈ US$34,000 to US$39,500), and a network of five would be approximately £135,000 (≈ US$184,000) for instrument purchase alone. Permanent ambient air quality stations such as these must be kept in air-conditioned enclosures to maintain long-term stability, adding considerable additional cost and time considerations related to construction of buildings with access to mains power. Although such a network of reference-grade monitoring instruments would provide accurate and reliable measurements of volcanic plume in downwind locations, the feasibility of installing such a high-expense monitoring network is restricted where resources are more limited.

An alternative option for an even cheaper low-cost instrument network would be PurpleAir sensors. PurpleAir (Utah, USA) instruments cost approximately US$250 (≈ £180) per unit (quote from PurpleAir, 2019) and can be purchased and operated by members of the community with all data available online in an open-access, user-friendly format (PurpleAir, 2019). PurpleAir instruments only have the capability of measuring PM, which they measure using Plantower PMS5003 sensors (Kelly et al., 2017; Sayahi et al., 2019). Each PurpleAir contains two Plantower PMS5003 sensors mounted in one housing, allowing self-consistency checks to alert when significant differences are reported between the internal sensors. The instruments are easy to install, though do require mains power and stable WiFi access. The data are uploaded automatically to the PurpleAir web server, removing the need for custom-made data infrastructure. The real-time map view allows the air quality to be interpreted by non-specialists with ease. During the 2018 eruption of Kīlauea's lower East Rift Zone on the Island of Hawai'i, PurpleAir instruments were installed across the island and provided an open-access source of air quality information with a high level of accuracy (Pearson's r value of 0.92) as compared to reference-grade PM sensors, though it should be noted that they overestimated the concentrations of PM by up to 30 % (Whitty et al., 2020).

A recent study by Crawford et al., 2021 deployed a network of low-cost sensors similar to the ones described here across the Island of Hawai'i to monitor Kīlauea's

lower East Rift Zone in 2018. They used a combination of OPC-N2 sensors, as found in AQMesh pods, and Plantower PMS5003 sensors, as found in PurpleAir instruments, to measure PM variability across a large spatial area. Additionally, SO_2 was measured using Alphasense B4-series electrochemical sensors, as used in the AQMesh pods. The network consisted of 33 sensor nodes, deployed for a total of 17 days during July to August 2018. The PM measurements were corrected for the effect of high humidity. Similar to this six-month study, in several of the network nodes Crawford et al., 2021 found SO_2 sensors to experience technical difficulties over the 17-day deployment period. The results from this combined-sensor low-cost network were successful, with similar PM and SO_2 measurements recorded as the regulatory reference-grade network and at a much higher spatial resolution (Crawford et al., 2021). Crawford et al., 2021 do not report on the performance of the network over long-term deployment so it is not possible to make a direct comparison with that of the AQMesh network at Masaya.

In a downwind volcanic setting, such as that surrounding Masaya volcano, conditions can be challenging for air quality monitoring networks, especially with the added complications of a warm and humid meteorological climate. In such settings it is necessary to consider the balance between a monitoring network's ability to generate accurate and reliable measurements against its financial cost, both for the initial installation of the network, and the on-going burden of instrument maintenance. In Global South countries such as Nicaragua, limited resources and infrastructure may determine that the financial burden of installing a full-scale reference-grade monitoring network is too high. In such instances, governmental bodies and researchers must weigh up the benefits and disadvantages of alternative monitoring networks at lower costs while attempting to develop a monitoring system which achieves the primary goal of effectively monitoring air quality and disseminating the information to local exposed communities. For the area impacted by Masaya volcano (and comparable areas elsewhere), we conclude that a combined monitoring approach is the one most likely to achieve this primary goal. The resources required would be for the installation and maintenance of one reference-grade monitoring station (consisting of FEM-approved instrumentation for monitoring of SO_2 and PM) and a network of lower-cost instruments to provide a higher spatial resolution. The continuous highly-accurate measurements from the reference-grade station would provide a reliable point-location determination of the daily concentration of SO_2 and PM, allowing residents to determine the potential likely health-impacts from the volcanic-induced air quality. The reference-grade monitoring station would also be used for regular calibrations of the lower-cost instruments under local atmospheric (ambient temperature, relative humidity, etc.) and environmental conditions (concentration and type of pollutants), including following maintenance and sensor replacements for the lower-cost instruments. The location of the reference-grade station would be strategically selected depending on a) how likely it is to be impacted by the volcanic plume

on a regular basis, b) how representative it is for local population exposure and c) how accessible it is for network maintenance, including the regular calibrations of the lower-cost instruments. We suggest that downwind of Masaya volcano, a reference-grade monitoring station installed in El Panama would fulfil these requirements. The type of lower-cost instruments that are to be selected for the network have to be carefully considered because, as shown in this work, they can be subject to frequent component failures which may result in significant total costs. Based on our results, we suggest that AQMesh pods (or comparable gas-sensing instruments from other manufacturers) would require some modifications and subsequent testing in a volcanic environment if they are to be used for permanent monitoring in order to reduce downtime due to component failures. The necessary modifications would include better insulation of the internal electronics [Section 3.4.3], which we found to corrode quickly in areas that are more exposed to the volcanic plume. PurpleAir PM-only sensors have been shown to be suitable for long-term deployment (three month duration) in the far-field volcanic environment on the Island of Hawai'i (Whitty et al., 2020), and we suggest that they may be a suitable instrument type for the far-field areas downwind of Masaya, which receive relatively low concentrations of SO_2 (considering the current SO_2 flux) but higher PM concentrations. The proposed combined network, at a medium cost level, would provide good spatial coverage across the exposed area and allow real-time information dissemination to exposed communities. The data accuracy would vary between the reference-grade and the lower-cost instruments but the ability to locally calibrate the lower-grade instruments would reduce uncertainty.

3.4.3 Recommendations for future use of low-cost sensor systems around Masaya volcano

Were the AQMesh pods to be installed as permanent monitoring stations in a volcanic environment similar to the region downwind of Masaya volcano, there are several practical measures that could be implemented to increase the effectiveness of the instruments to detect the plume and yield more quantitative data on air quality and plume exposure. The main issue faced during this deployment was the fast-acting high level of corrosion resulting from the volcanic environment. Where feasible this could be at least partially mitigated by shielding of exposed metal components within the AQMesh pods and circuit boards using protective coatings such as epoxy, aerosol spray, and solder masks to coat vulnerable components and minimise exposure to corrosion (González-Garcıá et al., 2007; Liu et al., 2009). This could improve the time-coverage and quantitative nature of the network measurements, by reducing the need to replace sensors, and thereby enabling a more detailed sensor characterisation and cross-calibration of sensors from the network pods to reference-grade SO_2 and PM instruments. Further to this, if infrastructure were implemented to allow the AQMesh pods to be connected to mains power,

this would remove the need for battery re-charging every four weeks, therefore reducing both the maintenance time and costs as well as reducing instances of the instruments being offline when recharging was delayed.

On-site measurements of humidity are crucial to allow effective correction of the PM counts (Crilley et al., 2018; Crilley et al., 2020). Humidity measurements are also important to allow filtering of the SO_2 measurements by the electrochemical sensors: this study focused on measurement intervals where sensors reported $SO_2 > 20$ ppbv because at low SO_2 abundances a diurnal signal with high correlation between recorded SO_2 and humidity might indicate a sensor response due to environmental conditions and not true SO_2 concentrations. Where funds and infrastructure allow, installation of a meteorological station at a suitable site close to the volcanic source (perhaps upwind to minimise corrosion) would also be invaluable to allow identification of local wind conditions and direction of plume dispersal on a real-time basis, as would methods to better constrain the plume height.

3.4.4 Volcanic air pollution exposure mitigation

Exposure to volcanic SO_2 and PM can cause long-term health impacts and result in significant issues, particularly for children and vulnerable individuals including people with asthma (ATSDR, 1998; CRI, 2004). In the communities downwind of persistently degassing volcanoes, like Masaya, exposure can be ongoing over years. Depending on the rate of volcanic degassing, the meteorological conditions and the characteristics of the plume, exposure to volcanic SO_2 and PM in any one location fluctuates, as shown in this study and by previous reports. If there is adequate monitoring of volcanic SO_2 and/or PM concentrations in downwind communities, the residents can react to the fluctuating presence of the plume. During periods of extreme degassing from Kīlauea volcano in Hawaii in 2018, official government advice included remaining indoors, closing doors and windows and recirculating air within buildings (Hawaii Emergency Management Agency, 2018). In low-latitude Global South countries such as Nicaragua, buildings are not commonly airtight and so mitigation strategies would focus more on avoiding excessive physical activity during especially high levels of exposure [Pohl 1998; Williams-Jones and Rymer 2015; IVHHN, 2020]. Highly vulnerable individuals may be advised to leave the affected area during extreme VAPE. These mitigation strategies work best when there is clear communication to the public regarding the concentration of volcanic SO_2 and PM that they are being exposed to in real-time. This most effectively works either with a well-maintained ground-based monitoring network with readily-accessible real-time data, or with a model forecast capable of accurately predicting the movement of the volcanic plume and allowing communication to community members of their level of volcanic exposure on any given day. Although the AQMesh network temporarily installed by the UNRESP project in Nicaragua was not able to provide a real-time

warning system, it demonstrated that it would be highly beneficial to the communities surrounding the volcano for an operational monitoring and/or forecasting system to be implemented.

3.5 Conclusions

A network of five AQMesh pods was installed in Nicaragua by the UNRESP project between February and August 2017. The network data were analysed to assess the pods' effectiveness at recognising the presence of volcanic plume at the measurement stations. Intervals where volcanic plume was likely to have been present at measurement stations were assessed from ECMWF meteorological forecasts and from visual inspection of visible plume extension seen in high-resolution satellite imagery. The data from the AQMesh pods were analysed to identify volcanic signatures by simultaneous enhancement of SO_2 and PM_1, $PM_{2.5}$ and PM_{10}, respectively. The PM data were also analysed separately to determine differences in the size distribution and concentration of particles under VAPE-likely and VAPE-unlikely conditions.

The near-field stations of El Panama and Rigoberto were reasonably effective at positively identifying the presence of the volcanic plume using simultaneous enhancement of SO_2 and PM during periods when meteorological data indicated plume dispersal towards the measurement station. Both these AQMesh sites measured plume more often during VAPE-likely periods (61% of the time for SO_2 and $PM_{2.5}$ at El Panama and 41% of the time for SO_2 and $PM_{2.5}$ at Rigoberto) than during VAPE-unlikely periods (23% of the time for SO_2 and $PM_{2.5}$ at El Panama and 15% of the time for SO_2 and $PM_{2.5}$ at Rigoberto). The far-field stations of El Crucero and Pacaya were least effective at identifying the plume's presence via means of simultaneous enhancement of SO_2 and PM. No SO_2 to PM enhancement were identified from data collected at the Pacaya station, and El Crucero's AQMesh pod positively identified the presence of the plume only 4% of the time during VAPE-likely intervals, with an equal occurrence of plume when it was indicated to be absent. The inefficiency of the El Crucero and Pacaya stations may be a result of the larger distance from the volcanic source, providing a greater potential for bias in the determination of VAPE-likely periods from meteorological conditions.

Analysis of the PM data indicated that both near-field and far-field stations can be suitable for identifying an increase in daily average PM during VAPE-likely conditions. The El Panama station recorded exceedance events above the background norm 40% of the measurement time for $PM_{2.5}$ under VAPE-likely conditions, as opposed to 21% of the time for VAPE-unlikely conditions. El Crucero similarly had a higher frequency of exceeding the background norm under VAPE-likely conditions (48% for $PM_{2.5}$) as opposed to VAPE-unlikely conditions (5.5% for $PM_{2.5}$). However, both the Pacaya and Rigoberto measurement stations showed small variations in the exceedances above

background norms (25% for VAPE-likely $PM_{2.5}$ periods and 20% for VAPE-unlikely $PM_{2.5}$ periods at Pacaya, and 14% for VAPE-likely $PM_{2.5}$ periods and 16% for VAPE-unlikely $PM_{2.5}$ periods at Rigoberto). At Rigoberto the small variations in exceedances above background PM concentrations is suggested to be caused by the reasonably close proximity to domestic cooking fires, and that it is located at the edge of the zone most impacted by the prevailing plume dispersion. With PM analysis it appears very important to have a strong understanding of the other pollution sources. As such, the AQMesh pods are suitable for monitoring the presence of volcanic plume if it is possible to carefully site them to avoid other sources of contamination and if they are able to be frequently maintained to replace failed sensors.

The AQMesh pods that were installed in Nicaragua were originally designed for monitoring air quality in urban and commercial environments, and were severely affected by the volcanic environment in this study. All AQMesh pods required replacement parts to be installed, likely due to instrument failure or corrosion of key components, and there was a high frequency of AQMesh pods going offline. The AQMesh pods provide a relatively low-cost opportunity for monitoring volcanic gas and PM downwind from Masaya volcano, in comparison to reference-grade instrument networks. However, we propose a combined monitoring network approach that utilises a strategically-placed reference-grade monitoring station, supplemented by a wider network of low-cost instrument nodes. Countries with persistently outgassing volcanoes could greatly benefit from installation of permanent monitoring networks to track volcanic plume presence in downwind communities in real-time, together with the relevant information flow to communicate this information to vulnerable communities.

Acknowledgements

The authors would like to thank the communities of El Panama, Rigoberto, San Juan de La Concepción, Pacaya and El Crucero in Nicaragua where the AQMesh pods were installed. The UNRESP team dedicates this work to the memory of Dr. Caroline Williams, University of Bristol.

Author contributions

RCWW performed the data analysis and wrote the original draft. MAP, EI, TJR, TAM contributed to data interpretation and manuscript drafting. EI was the principal investigator of UNRESP and developed the project idea with SN, XHL, PB, SB, WS, DL, HF, TAM and AS. WS advised on and, together with EI, coordinated the work in Nicaragua. EI, HB, EM, NP, IAT, PB, EJL, TAM and RCWW collected the field data through network set-up and maintenance. LRC and FDP contributed to PM humidity correction. SB and AS contributed to ECMWF forecast data. All co-authors

contributed to draft review and editing.

Funding

RCWW is funded by the Leeds-York Natural Environment Research Council (NERC) Doctoral Training Partnership (DTP) NE/L002574/1, in CASE partnership with the Icelandic Meteorological Office. TJR acknowledges ANR Projet de Recherche Collaborative VOLC-HAL-CLIM (Volcanic Halogens: from Deep Earth to Atmospheric Impacts), ANR-18-CE01-11. IAT acknowledges the support of the Centre for Observation and Modelling of Earthquakes, Volcanoes and Tectonics (COMET) and NERC funding through the Oxford Environmental Research DTP (NE/L002612/1). The "Unseen but not unfelt: resilience to persistent volcanic emissions (UNRESP)" project was funded by GCRF NE/P015271/1 and NE/R009465/1.

Data availability

The datasets analysed for this study can be found on figshare at 10.6084/m9.figshare.14916543

References

Aiuppa, A., de Moor, J. M., Arellano, S., Coppola, D., Francofonte, V., Galle, B., Giudice, G., Liuzzo, M., Mendoza, E., Saballos, A. et al. (2018). Tracking formation of a lava lake from ground and space: Masaya volcano (Nicaragua), 2014–2017 [DOI: https://agupubs.onlinelibrary.wiley.com/doi/full/10.1002/2017GC007227]. *Geochemistry, Geophysics, Geosystems*, *19*(2), 496–515.

Allen, A., Mather, T., McGonigle, A., Aiuppa, A., Delmelle, P., Davison, B., Bobrowski, N., Oppenheimer, C., Pyle, D., & Inguaggiato, S. (2006). Sources, size distribution, and downwind grounding of aerosols from Mount Etna [DOI: https://doi.org/10.1029/2005JD006015]. *Journal of Geophysical Research: Atmospheres*, *111*(D10).

Allen, A., Oppenheimer, C., Ferm, M., Baxter, P., Horrocks, L., Galle, B., McGonigle, A., & Duffell, H. (2002). Primary sulfate aerosol and associated emissions from Masaya Volcano, Nicaragua [DOI: https://doi.org/10.1029/2002JD002120]. *Journal of Geophysical Research: Atmospheres*, *107*(D23), ACH–5.

Alphasense. (2021). SO2-B4 Sulfur Dioxide Sensor Data Sheet [(Accessed 05/02/2021)]. *https://www.alphasense.com/wp-content/uploads/2019/09/SO2-B4.pdf*.

AQMesh. (2021a). Data Access [(Accessed 27/02/2021)]. *https://www.aqmesh.com/products/data-access/*.

AQMesh. (2021b). Technical Specifications [(Accessed 27/02/2021)]. *https://www.aqmesh.com/products/technical-specification/*.

ATSDR. (1998). Agency for Toxic Substances and Disease Registry; public health statement sulfur dioxide [Available at: https://www.atsdr.cdc.gov/ToxProfiles/tp116-c1-b.pdf]. *7446-09-5*.

Austin, C. C., Roberge, B., & Goyer, N. (2006). Cross-sensitivities of electrochemical detectors used to monitor worker exposures to airborne contaminants: False positive responses in the absence of target analytes [DOI: https://doi.org/10.1039/B510084D]. *Journal of Environmental Monitoring*, *8*(1), 161–166.

Baxter, P., Stoiber, R., & Williams, S. (1982). Volcanic gases and health: Masaya volcano, Nicaragua [DOI: https://doi.org/10.1016/S0140-6736(82)91109-6]. *The Lancet*.

Buizza, R., Houtekamer, P., Pellerin, G., Toth, Z., Zhu, Y., & Wei, M. (2005). A comparison of the ECMWF, MSC, and NCEP global ensemble prediction systems [DOI: https://doi.org/10.1175/MWR2905.1]. *Monthly Weather Review*, *133*(5), 1076–1097.

Burton, M., Oppenheimer, C., Horrocks, L., & Francis, P. (2000). Remote sensing of CO2 and H2O emission rates from Masaya volcano, Nicaragua [DOI: https://doi.org/Doi10.1130/0091-7613(2000)28<915:Rsocah>2.0.Co;2]. *Geology*, *28*(10), 915–918.

Butwin, M. K., von Löwis, S., Pfeffer, M. A., & Thorsteinsson, T. (2019). The effects of volcanic eruptions on the frequency of particulate matter suspension events in Iceland [DOI: https://doi.org/10.1016/j.jaerosci.2018.12.004]. *Journal of Aerosol Science*, *128*, 99–113.

Cadle, R., Wartburg, A., & Grahek, P. (1971). The proportion of sulfate to sulfur dioxide in Kı¯lauea Volcano fume [DOI: https://doi.org/10.1016/0016-7037(71)90046-9]. *Geochimica et Cosmochimica Acta*, *35*(5), 503–507.

Carlsen, H. K., Ilyinskaya, E., Baxter, P., Schmidt, A., Thorsteinsson, T., Pfeffer, M., Barsotti, S., Dominici, F., Finnbjornsdottir, R. G., Jóhannsson, T., Aspelund, T., Gislason, T., Valdimarsdóttir, U., Briem, H., & Gudnason, T. (2021a). Increased respiratory morbidity associated with exposure to a mature volcanic plume from a large Icelandic fissure eruption [DOI: https://doi.org/10.1038/s41467-021-22432-5]. *Nature Communications*, *12*.

Carlsen, H. K., Valdimarsdóttir, U., Briem, H., Dominici, F., Finnbjornsdottir, R. G., Jóhannsson, T., Aspelund, T., Gislason, T., & Gudnason, T. (2021b). Severe volcanic SO2 exposure and respiratory morbidity in the Icelandic population–a register study [DOI: https://doi.org/10.1186/s12940-021-00698-y]. *Environmental Health*, *20*(1), 1–12.

Cohen, A. J., Ross Anderson, H., Ostro, B., Pandey, K. D., Krzyzanowski, M., Künzli, N., Gutschmidt, K., Pope, A., Romieu, I., Samet, J. M. et al. (2005). The global burden of disease due to outdoor air pollution [DOI: https://doi.org/10.1080/15287390590936166]. *Journal of Toxicology and Environmental Health, Part A*, *68*(13-14), 1301–1307.

Crawford, B., Hagan, D. H., Grossman, I., Cole, E., Holland, L., Heald, C. L., & Kroll, J. H. (2021). Mapping pollution exposure and chemistry during an extreme air quality event (the 2018 Kı¯lauea eruption) using a low-cost sensor network [DOI: https://doi.org/10.1073/pnas.2025540118]. *Proceedings of the National Academy of Sciences*, *118*(27).

CRI. (2004). The Centre for Research Information, health effects of project shad chemical agent: Sulfur dioxide [cas 7446-09-5]. *National Academies*.

Crilley, L. R., Shaw, M., Pound, R., Kramer, L. J., Price, R., Young, S., Lewis, A. C., & Pope, F. D. (2018). Evaluation of a low-cost optical particle counter (Alphasense OPC-N2) for ambient air monitoring [DOI: https://doi.org/10.5194/amt-11-709-2018]. *Atmospheric Measurement Techniques*, 709–720.

Crilley, L. R., Singh, A., Kramer, L. J., Shaw, M. D., Alam, M. S., Apte, J. S., Bloss, W. J., Hildebrandt Ruiz, L., Fu, P., Fu, W. et al. (2020). Effect of aerosol composition on the performance of low-cost optical particle counter correction factors [DOI: https://doi.org/10.5194/amt-13-1181-2020]. *Atmospheric Measurement Techniques*, *13*(3), 1181–1193.

Delmelle, P., Baxter, P., Beaulieu, A., Burton, M., Francis, P., Garcia-Alvarez, J., Horrocks, L., Navarro, M., Oppenheimer, C., Rothery, D. et al. (1999). Origin, effects of Masaya volcano's continued unrest probed in Nicaragua [DOI: https://doi.org/10.1029/EO080i048p00575]. *Eos, Transactions American Geophysical Union*, *80*(48), 575–581.

Delmelle, P., Stix, J., Baxter, P., Garcia-Alvarez, J., & Barquero, J. (2002). Atmospheric dispersion, environmental effects and potential health hazard associated with the low-altitude gas plume of Masaya volcano, Nicaragua [DOI: https://doi.org/10.1007/s00445-002-0221-6]. *Bulletin of Volcanology*, *64*(6), 423–434.

Duffell, H. J., Oppenheimer, C., Pyle, D. M., Galle, B., McGonigle, A. J., & Burton, M. R. (2003). Changes in gas composition prior to a minor explosive eruption at Masaya volcano, Nicaragua [DOI: https://doi.org/10.1016/S0377-0273(03)00156-2]. *Journal of Volcanology and Geothermal Research*, *126*(3-4), 327–339.

Environmental Protection Agency. (2010). Primary National Ambient Air Quality Standard for Sulfur Dioxide; Final Rule [(Accessed 15/1/2019)]. *https://www.govinfo.gov/content/pkg/FR-2010-06-22/pdf/2010-13947.pdf*, *40 CFR Parts 50, 53, and 58*.

Environmental Protection Agency. (2013). Federal and State Ambient Air Quality Standards [(Accessed 15/1/2019)]. *http://health.hawaii.gov/cab/files/2013/05/naaqs_jan_2013.pdf*.

Environmental Protection Agency. (2016). List of designated reference and equivalent methods [Available at: https://www.epa.gov/sites/production/files/2019-08/documents/designated_reference_and-equivalent_methods.pdf]. *National Exposure Research Laboratory*.

Galle, B., Oppenheimer, C., Geyer, A., McGonigle, A. J., Edmonds, M., & Horrocks, L. (2003). A miniaturised ultraviolet spectrometer for remote sensing of SO2 fluxes: A new tool for volcano surveillance [DOI: https://doi.org/10.1016/S0377-0273(02)00356-6]. *Journal of Volcanology and Geothermal Research*, *119*(1-4), 241–254.

Gao, X., Coull, B., Lin, X., Vokonas, P., Spiro, A., Hou, L., Schwartz, J., & Baccarelli, A. A. (2021). Short-term air pollution, cognitive performance and nonsteroidal anti-inflammatory drug use in the veterans affairs normative aging study [DOI: https://doi.org/10.1038/s43587-021-00060-4]. *Nature Aging*, *1*(5), 430–437.

Global Volcanism Program. (2021). Report on Masaya (Nicaragua) Bulletin of the Global Volcanism Network [(Accessed 03/03/2021)]. *https://volcano.si.edu/volcano.cfm?vn=344100*.

González-Garcıá, Y., González, S., & Souto, R. (2007). Electrochemical and structural properties of a polyurethane coating on steel substrates for corrosion protection [DOI: https://doi.org/10.1016/j.corsci.2007.03.018]. *Corrosion Science*, *49*(9), 3514–3526.

Gysel, M., Crosier, J., Topping, D., Whitehead, J., Bower, K., Cubison, M., Williams, P., Flynn, M., McFiggans, G., & Coe, H. (2007). Closure study between chemical composition and hygroscopic growth of aerosol particles during TORCH2 [DOI: https://doi.org/10.5194/acp-7-6131-2007]. *Atmospheric Chemistry and Physics*, *7*(24), 6131–6144.

Hagan, D. H., Isaacman-VanWertz, G., Franklin, J. P., Wallace, L. M., Kocar, B. D., Heald, C. L., & Kroll, J. H. (2018). Calibration and assessment of electrochemical air quality sensors by co-location with regulatory-grade instruments [DOI: https://doi.org/10.5194/amt-11-315-2018]. *Atmospheric Measurement Techniques*, *11*(1), 315–328.

Hawaii Emergency Management Agency. (2018). How to cope with hazardous volcanic gas emissions [(Accessed 15/4/2021)]. *http://dod.hawaii.gov/hiema/how-to-cope-with-hazardous-volcanic-gas-emissions/*.

Holgate, S. (2017). "Every breath we take: the lifelong impact of air pollution" - a call for action [DOI: https://doi.org/10.7861/clinmedicine.17-1-8]. *Clinical Medicine*, *17*(1), 8–12.

Ilyinskaya, E., Mason, E., Wieser, P., Holland, L., Liu, E., Mather, T., Edmonds, M., Whitty, R., Elias, T., Nadeau, P., Schneider, D., McQuaid, J., Allen, S., Harvey, J., Oppenheimer, C., Kern, C., & Damby, D. (2021). Rapid metal pollutant deposition from the volcanic plume of Kı¯lauea, Hawai'i [DOI: https://doi.org/10.1038/s43247-021-00146-2]. *Communications Earth and Environment*.

Ilyinskaya, E., Oppenheimer, C., Mather, T., Martin, R., & Kyle, P. (2010). Size-resolved chemical composition of aerosol emitted by Erebus volcano, Antarctica [DOI: https://doi.org/10.1029/2009GC002855]. *Geochemistry, Geophysics, Geosystems*, *11*(3).

Ilyinskaya, E., Schmidt, A., Mather, T. A., Pope, F. D., Witham, C., Baxter, P., Jóhannsson, T., Pfeffer, M., Barsotti, S., Singh, A. et al. (2017). Understanding the environmental impacts of large fissure eruptions: Aerosol and gas emissions from the 2014–2015 Holuhraun eruption (Iceland) [DOI: https://doi.org/10.1016/j.epsl.2017.05.025]. *Earth and Planetary Science Letters*, *472*, 309–322.

International Volcanic Health Hazard Network. (2020). The health hazards of volcanic and geothermal gases: A guide for the public [(Accessed 12/4/2021)]. *https://www.ivhhn.org/information/health-impacts-volcanic-gases#Howtolivewithvolcanicemissions*.

Jayaratne, R., Liu, X., Thai, P., Dunbabin, M., & Morawska, L. (2018). The influence of humidity on the performance of a low-cost air particle mass sensor and the effect of atmospheric fog [DOI: https://doi.org/10.5194/amt-11-4883-2018]. *Atmospheric Measurement Techniques*, *11*(8), 4883–4890.

Kelly, K., Whitaker, J., Petty, A., Widmer, C., Dybwad, A., Sleeth, D., Martin, R., & Butterfield, A. (2017). Ambient and laboratory evaluation of a low-cost par-

ticulate matter sensor [DOI: https://doi.org/10.1016/j.envpol.2016.12.039]. *Environmental Pollution*, *221*, 491–500.

Krogh, A. (2021). Snazzy maps [(Accessed 20/01/2021)]. *https://snazzymaps.com/*.

Lambert, G., Le Cloarec, M., & Pennisi, M. (1988). Volcanic output of SO2 and trace metals: A new approach [DOI: https://doi.org/10.1016/0016-7037(88)90054-3]. *Geochimica et Cosmochimica Acta*, *52*(1), 39–42.

Langmann, B. (2014). On the role of climate forcing by volcanic sulphate and volcanic ash [DOI: https://doi.org/10.1155/2014/340123]. *Advances in Meteorology*, *2014*, 1–17.

Lewis, A. C., Lee, J. D., Edwards, P. M., Shaw, M. D., Evans, M. J., Moller, S. J., Smith, K. R., Buckley, J. W., Ellis, M., Gillot, S. R. et al. (2016). Evaluating the performance of low cost chemical sensors for air pollution research [Available at: https://pubs.rsc.org/en/content/articlelanding/2016/FD/C5FD00201J]. *Faraday discussions*, *189*, 85–103.

Li, Z., Marston, N., & Stokes, K. (2018). Materials within geothermal environments [Available at: https://d39d3mj7qio96p.cloudfront.net/media/documents/SR393_Materials_within_geothermal_environments.pdf]. *BRANZ study report SR393*.

Lim, S. S., Vos, T., Flaxman, A. D., Danaei, G., Shibuya, K., Adair-Rohani, H., Al-Mazroa, M. A., Amann, M., Anderson, H. R., Andrews, K. G. et al. (2012). A comparative risk assessment of burden of disease and injury attributable to 67 risk factors and risk factor clusters in 21 regions, 1990–2010: A systematic analysis for the Global Burden of Disease Study 2010 [DOI: https://doi.org/10.1016/S0140-6736(12)61766-8]. *The lancet*, *380*(9859), 2224–2260.

Liu, X., Xiong, J., Lv, Y., & Zuo, Y. (2009). Study on corrosion electrochemical behavior of several different coating systems by EIS [DOI: https://doi.org/10.1016/j.porgcoat.2008.08.012]. *Progress in Organic Coatings*, *64*(4), 497–503.

Longo, B., Rossignol, A., & Green, J. (2008). Cardiorespiratory health effects associated with sulphurous volcanic air pollution [DOI: https://doi.org/10.1016/j.puhe.2007.09.017]. *Public Health*, *122*(8), 809–20.

Longo, B. M. (2013). Adverse health effects associated with increased activity at Kı¯lauea Volcano: A repeated population-based survey [DOI: https://doi.org/10.1155/2013/475962]. *ISRN Public Health*, *2013*.

Loughlin, S., Aspinall, W., Vye-Brown, C., Baxter, P., Braban, C., Hort, M., Schmidt, A., Thordarson, T., & Witham, C. (2012). Large-magnitude fissure eruptions in Iceland: Source characterisation [DOI: https://eprints.whiterose.ac.uk/80209/]. *BGS Open File Report*, *OR/12/098*.

Martin, R. S., Ilyinskaya, E., Sawyer, G. M., Tsanev, V. I., & Oppenheimer, C. (2011). A re-assessment of aerosol size distributions from Masaya volcano (Nicaragua)

[DOI: https://doi.org/10.1016/j.atmosenv.2010.10.049]. *Atmospheric Environment*, *45*(3), 547–560.

Mason, E., Wieser, P., Liu, E., Edmonds, M., Ilyinskaya, E., Whitty, R., Mather, T., Elias, T., Nadeau, P., Wilkes, T. et al. (2021). Volatile metal emissions from volcanic degassing and lava-seawater interactions at Kı¯lauea Volcano, Hawai'i [DOI: https://doi.org/10.1038/s43247-021-00145-3]. *Communications Earth and Environment*.

Mather, T. A., McCabe, J. R., Rai, V. K., Thiemens, M. H., Pyle, D. M., Heaton, T. H. E., Sloane, H. J., & Fern, G. R. (2006a). Oxygen and sulfur isotopic composition of volcanic sulfate aerosol at the point of emission [DOI: https://doi.org/10.1029/2005JD006584]. *Journal of Geophysical Research*, *111*.

Mather, T. A., Pyle, D., Tsanev, V., McGonigle, A., Oppenheimer, C., & Allen, A. (2006b). A reassessment of current volcanic emissions from the Central American arc with specific examples from Nicaragua [DOI: https://doi.org/10.1016/j.jvolgeores.2005.07.021]. *Journal of volcanology and geothermal Research*, *149*(3-4), 297–311.

Mather, T., Allen, A., Oppenheimer, C., Pyle, D., & McGonigle, A. (2003). Size-resolved characterisation of soluble ions in the particles in the tropospheric plume of Masaya volcano, Nicaragua: origins and plume processing [DOI: https://doi.org/10.1023/A:1026327502060]. *Journal of Atmospheric Chemistry*, *46*(3), 207–237.

Mather, T. A. (2015). Volcanoes and the environment: Lessons for understanding Earth's past and future from studies of present-day volcanic emissions [DOI: https://doi.org/10.1016/j.jvolgeores.2015.08.016]. *Journal of Volcanology and Geothermal Research*, *304*, 160–179.

McBirney, A. R. (1956). The Nicaraguan volcano Masaya and its caldera [DOI: https://doi.org/10.1029/TR037i001p00083]. *Eos, Transactions American Geophysical Union*, *37*(1), 83–96.

McFiggans, G., Alfarra, M. R., Allan, J., Bower, K., Coe, H., Cubison, M., Topping, D., Williams, P., Decesari, S., Facchini, C. et al. (2005). Simplification of the representation of the organic component of atmospheric particulates [DOI: https://doi.org/10.1039/B419435G]. *Faraday Discussions*, *130*, 341–362.

Mead, M., Popoola, O., Stewart, G., Landshoff, P., Calleja, M., Hayes, M., Baldovi, J., McLeod, M., Hodgson, T., Dicks, J. et al. (2013). The use of electrochemical sensors for monitoring urban air quality in low-cost, high-density networks [DOI: https://doi.org/10.1016/j.atmosenv.2012.11.060]. *Atmospheric Environment*, *70*, 186–203.

Miller, V. (2004). Health Effects of Project SHAD Chemical Agent: Sulfur Dioxide, Prepared for the National Academies by The Center for Research Information

[Available at: https://paperzz.com/doc/8956749/health-effects-of-project-shad-chemical-agent]. *Contract No. IOM-2794-04-001*, 1–58.

Molteni, F., Buizza, R., Palmer, T. N., & Petroliagis, T. (1996). The ECMWF ensemble prediction system: Methodology and validation [DOI: https://doi.org/10.1002/qj.49712252905]. *Quarterly journal of the royal meteorological society*, *122*(529), 73–119.

Nadeau, P. A., & Williams-Jones, G. (2009). Apparent downwind depletion of volcanic SO2 flux — lessons from Masaya Volcano, Nicaragua [DOI: https://doi.org/10.1007/s00445-008-0251-9]. *Bulletin of Volcanology*, *71*(4), 389–400.

NASA. (2021). Fire Information for Resource Management System [(Accessed 02/06/2021)]. *https://firms.modaps.eosdis.nasa.gov/map/#t:adv;d:2021-05-18..2021-05-19;@-85.7,11.9,10z*.

Oppenheimer, C., & McGonigle, J. (2004). Exploiting ground-based optical sensing technologies for volcanic gas surveillance [DOI: https://doi.org/10.4401/ag-3353]. *Annals Geophysics*, *47*(4).

Oppenheimer, C., Francis, P., & Stix, J. (1998). Depletion rates of sulfur dioxide in tropospheric volcanic plumes [DOI: https://doi.org/10.1029/98GL01988]. *Geophysical Research Letters*, *25*(14), 2671–2674.

Pattantyus, A. K., Businger, S., & Howell, S. G. (2018). Review of sulfur dioxide to sulfate aerosol chemistry at Kı¯lauea Volcano, Hawai'i [DOI: https://doi.org/10.1016/j.atmosenv.2018.04.055]. *Atmospheric Environment*, *185*, 262–271.

Petters, M., & Kreidenweis, S. (2007). A single parameter representation of hygroscopic growth and cloud condensation nucleus activity [DOI: https://doi.org/10.5194/acp-7-1961-2007]. *Atmospheric Chemistry and Physics*, *7*(8), 1961–1971.

Pfeffer, M., Langmann, B., & Graf, H.-F. (2006a). Atmospheric transport and deposition of Indonesian volcanic emissions [DOI: https://doi.org/10.5194/acp-6-2525-2006]. *Atmospheric Chemistry and Physics*, *6*(9), 2525–2537.

Pfeffer, M., Rietmeijer, F., Brearley, A., & Fischer, T. P. (2006b). Electron microbeam analyses of aerosol particles from the plume of Poás Volcano, Costa Rica and comparison with equilibrium plume chemistry modeling [DOI: https://doi.org/10.1016/j.jvolgeores.2005.10.009]. *Journal of volcanology and geothermal research*, *152*(1-2), 174–188.

Pohl, H. R. (1998). Toxicological profile for sulfur dioxide [Available at: https://www.atsdr.cdc.gov/toxprofiles/tp116.pdf]. *U.S. Department for Health and Human Services*.

Pringle, K., Tost, H., Pozzer, A., Pöschl, U., & Lelieveld, J. (2010). Global distribution of the effective aerosol hygroscopicity parameter for ccn activation [DOI: https://doi.org/10.5194/acp-10-5241-2010]. *Atmospheric Chemistry and Physics*, *10*(12), 5241–5255.

PurpleAir. (2019). PurpleAir: Air Quality Monitoring [(Accessed 26/10/2018)]. *https://www.purpleair.com/*.

Read, K. (2018). Report of Calibration Work. *https://github.com/ncasuk/ncas-cozi-lab-additionaldata/blob/main/20180117_Certificate_SO2_43I_TRACE.pdf*.

Roberts, T., Braban, C., Oppenheimer, C., Martin, R., Freshwater, R., Dawson, D., Griffiths, P., Cox, R., Saffell, J., & Jones, R. (2012). Electrochemical sensing of volcanic gases [DOI: https://doi.org/10.1016/j.chemgeo.2012.08.027]. *Chemical Geology*, *332*, 74–91.

Roberts, T. J., Vignelles, D., Liuzzo, M., Giudice, G., Aiuppa, A., Coltelli, M., Salerno, G., Chartier, M., Couté, B., Berthet, G. et al. (2018). The primary volcanic aerosol emission from Mt Etna: Size-resolved particles with SO2 and role in plume reactive halogen chemistry [DOI: https://doi.org/10.1016/j.gca.2017.09.040]. *Geochimica et Cosmochimica Acta*, *222*, 74–93.

Rotstayn, L. D., & Lohmann, U. (2002). Simulation of the tropospheric sulfur cycle in a global model with a physically based cloud scheme [DOI: https://doi.org/10.1029/2002JD002128]. *Journal of Geophysical Research: Atmospheres*, *107*(D21).

Rymer, H., de Vries, B. v. W., Stix, J., & Williams-Jones, G. (1998). Pit crater structure and processes governing persistent activity at Masaya Volcano, Nicaragua [DOI: https://doi.org/10.1007/s004450050196]. *Bulletin of Volcanology*, *59*(5), 345–355.

Saxena, P., & Seigneur, C. (1987). On the oxidation of SO2 to sulfate in atmospheric aerosols [DOI: https://doi.org/10.1016/0004-6981(87)90077-1]. *Atmospheric Environment (1967)*, *21*(4), 807–812.

Sayahi, T., Butterfield, A., & Kelly, K. (2019). Long-term field evaluation of the Plantower PMS low-cost particulate matter sensors [DOI: https://doi.org/10.1016/j.envpol.2018.11.065]. *Environmental Pollution*, *245*, 932–940.

Schlesinger, R., Kunzli, N., Hidy, G., Gotschi, T., & Jerrett, M. (2006). The health relevance of ambient particulate matter characteristics: Coherence of toxicological and epidemiological inferences [DOI: https://doi.org/10.1080/08958370500306016]. *Inhalation toxicology*, *18*(2), 95–125.

Schlesinger, R. B. (1985). Effects of inhaled acids on respiratory tract defense mechanisms [DOI: https://doi.org/10.1289/ehp.856325]. *Environmental health perspectives*, *63*, 25–38.

Schmidt, A., Leadbetter, S., Theys, N., Carboni, E., Witham, C., Stevenson, J., Birch, C., Thordarson, T., Turnock, S., Barsotti, S., Delaney, L., Feng, W., Grainger, R., Hort, M., Höskuldsson, Á., Ialongo, I., Ilyinskaya, E., Jóhannsson, T., Kenny, P., ... Shepherd, J. (2015). Satellite detection, long-range transport, and air quality impacts of volcanic sulfur dioxide from the 2014–2015 flood lava eruption at Bárðarbunga (Iceland) [DOI: https://doi.org/10.1002/2015JD023638]. *Journal of Geophysical Research: Atmospheres*, *120*(18), 9739–9757.

Shehab, M., & Pope, F. (2019). Effects of short-term exposure to particulate matter air pollution on cognitive performance [DOI: https://doi.org/10.1038/s41598-019-44561-0]. *Scientific reports*, *9*(1), 1–10.

Shinohara, H., Aiuppa, A., Giudice, G., Gurrieri, S., & Liuzzo, M. (2008). Variation of H2O/CO2 and CO2/SO2 ratios of volcanic gases discharged by continuous degassing of Mount Etna volcano, Italy [DOI: https://doi.org/10.1029/2007JB005185]. *Journal of Geophysical Research: Solid Earth*, *113*(B9).

Sousan, S., Koehler, K., Hallett, L., & Peters, T. M. (2016a). Evaluation of the Alphasense optical particle counter (OPC-N2) and the Grimm portable aerosol spectrometer (PAS-1.108) [DOI: https://doi.org/10.1080/02786826.2016.1232859]. *Aerosol Science and Technology*, *50*(12), 1352–1365.

Sousan, S., Koehler, K., Thomas, G., Park, J. H., Hillman, M., Halterman, A., & Peters, T. M. (2016b). Inter-comparison of low-cost sensors for measuring the mass concentration of occupational aerosols [DOI: https://doi.org/10.1080/02786826.2016.1162901]. *Aerosol Science and Technology*, *50*(5), 462–473.

Stockwell, W. R., & Calvert, J. G. (1983). The mechanism of the ho¯so_2 reaction [DOI: https://doi.org/10.1016/0004-6981(83)90220-2]. *Atmospheric Environment (1967)*, *17*(11), 2231–2235.

Stoiber, R. E., Williams, S. N., & Huebert, B. J. (1986). Sulfur and halogen gases at Masaya caldera complex, Nicaragua: Total flux and variations with time [DOI: https://doi.org/10.1029/JB091iB12p12215]. *Journal of Geophysical Research: Solid Earth*, *91*(B12), 12215–12231.

Tam, E., Miike, R., Labrenz, S., Sutton, A. J., Elias, T., Davis, J., Chen, Y.-L., Tantisira, K., Dockery, D., & Avol, E. (2016). Volcanic air pollution over the Island of Hawai'i: Emissions, dispersal, and composition. association with respiratory symptoms and lung function in Hawai'i Island school children [DOI: https://doi.org/10.1016/j.envint.2016.03.025]. *Environment international*, *92*, 543–552.

Tamburello, G. (2015). Ratiocalc: Software for processing data from multicomponent volcanic gas analyzers [DOI: https://doi.org/10.1016/j.cageo.2015.05.004]. *Computers & Geosciences*, *82*, 63–67.

Thermo Fisher Scientific. (2010). Model 43i sulphur dioxide analyser - product specifications [Available at: https://www.thermofisher.com/order/catalog/product/43I#/43I].

van Manen, S. M. (2014). Perception of a chronic volcanic hazard: Persistent degassing at Masaya volcano, Nicaragua [DOI: https://doi.org/10.1186/s13617-014-0009-3]. *Journal of Applied Volcanology*, *3*(1), 9.

von Glasow, R., Bobrowski, N., & Kern, C. (2009). The effects of volcanic eruptions on atmospheric chemistry [DOI: https://doi.org/10.1016/j.chemgeo.2008.08.020]. *Chemical Geology*, *263*(1-4), 131–142.

Whitty, R. C. W., Ilyinskaya, E., Mason, E., Wieser, P. E., Liu, E. J., Schmidt, A., Roberts, T., Pfeffer, M. A., Brooks, B., Mather, T. A., Edmonds, M., Elias, T., Schneider, D. J., Oppenheimer, C., Dybwad, A., A, N. P., & Kern, C. (2020). Spatial and temporal variations in SO_2 and $PM_{2.5}$ levels around Kīlauea volcano, Hawai'i during 2007–2018 [DOI: https://doi.org/10.3389/feart.2020.00036]. *Frontiers in Earth Science*, *8*, 36.

Williams-Jones, G., & Rymer, H. (2015). Hazards of volcanic gases [DOI: https://doi.org/10.1016/B978-0-12-385938-9.00057-2]. *The Encyclopedia of Volcanoes*, *2*, 985–992.

Williams-Jones, G., Rymer, H., & Rothery, D. A. (2003). Gravity changes and passive SO2 degassing at the Masaya caldera complex, Nicaragua [DOI: https://doi.org/10.1016/S0377-0273(03)00033-7]. *Journal of Volcanology and Geothermal Research*, *123*(1-2), 137–160.

Chapter 4

SO_2 and PM air quality and Icelandic population exposure during the 2021 Fagradalsfjall eruption

Abstract

The 2021 Fagradalsfjall eruption was the first modern eruption to occur in proximity ($<$ 30 km) to the densely populated capital area of Reykjavík in Iceland. The eruption lasted for six months and released between 0.3 to 0.9 Mt sulfur dioxide (SO_2) into the atmosphere. Here we analyse data from 32 air quality monitoring stations, some reference-grade and some not, around Iceland during the eruption and over a background non-volcanic period to determine the impact of the volcanic emissions on concentrations of SO_2 and particulate matter (PM). This is the first known analysis of such a dense network for a volcanic eruption, providing a unique opportunity to investigate fine spatial and temporal variations in air quality during the eruption. Airborne concentrations of SO_2 above the Icelandic Directive (ID) health threshold (350 µg/m^3 as an hourly average) were predominantly located within a 20 km radius of the eruption. The monitoring station closest to the emission source (0.6 km distance) recorded 1,372 hourly events where SO_2 concentrations exceeded this value. The maximum SO_2 concentration recorded by this air quality station was 17,820 µg/m^3 as an hourly average. During the course of the eruption there were $\approx$ 300,000 visitors to the eruption site who may have been temporarily exposed to such exceptionally high SO_2 concentrations. Air quality stations further afield recorded lower concentrations of SO_2, though SO_2 health thresholds were still exceeded on multiple occasions. Air quality stations in Reykjavík

housed the closest available particulate instrumentation and found $PM_{2.5}$ concentrations exceeded the World Health Organization (WHO) health threshold (15 µg/m^3 as a daily-mean) on 51 days and PM_{10} concentrations exceeded the ID threshold (50 µg/m^3 as a daily-mean) on 13 days. The CALPUFF dispersion model with an Icelandic population map was used to estimate the number of residents who may have been exposed to concentrations of SO_2 above the ID hourly threshold. Analysis indicated that ≈ 47,000 Icelandic residents (≈ 13% of the population) were exposed to SO_2 concentrations exceeding the ID health threshold on more than 24 instances during the eruption (the maximum annual allowable instances according to the ID). Within the population exposed to > 24 events where SO_2 exceeded hourly threshold levels, we determined that ≈ 8,500 people were more vulnerable due to their age (≤ 4 and ≥ 65 years of age). We undertook a point-verification of plume presence from the CALPUFF dispersion model compared to an air quality station on the outskirts of Reykjavík. We found that the CALPUFF model correctly predicted the presence of the plume 79% of the time and the absence of the plume 80% of the time (with false positives and negatives of 21% and 20%), indicating a high-level of confidence in the CALPUFF temporal and spatial gas presence forecasts. Point-analysis of satellite imagery indicates that the plume was grounding across 36% of instances where SO_2 was observed in the atmospheric column. This point-analysis of satellite imagery has useful implications for future studies where SO_2 in the atmospheric column is used as a proxy for exposure of the population at ground level. The 2021 Fagradalsfjall eruption is expected to be followed by more volcanic unrest on the Reykjanes Peninsula in the coming years, making this study useful for risk reduction efforts for following eruptions in the area.

4.1 Introduction

Among the hazards posed by volcanic eruptions are emissions of sulfur dioxide (SO_2) gas and aerosol particulate matter (PM) which can affect air quality up to thousands of kilometers from the source (Carlsen et al., 2021a; Ilyinskaya et al., 2017; Schmidt et al., 2015; Schmidt et al., 2011). SO_2 is a highly hazardous air pollutant, which has well-defined hourly, daily and annual limits (Icelandic Directive, 2016). Asthma suffers and those with pre-existing respiratory or cardiac conditions are particularly sensitive to low levels of SO_2 (< 200 ppbv) (ATSDR, 1998; Carlsen et al., 2021b; CRI, 2004). Acute and chronic exposure to PM from natural and anthropogenic sources has a well-recognised link with a number of negative health outcomes. Size-resolved PM concentration is an important factor impacting on health, with fine PM being associated with more detrimental effects (Cohen et al., 2005). For air quality and health impact assessments, PM size distribution is commonly sub-divided into categories of PM_1, $PM_{2.5}$ and PM_{10} (PM with particle diameters of <1 µm, <2.5 µm and <10 µm, respectively). Evidence-based air quality thresholds have been defined for $PM_{2.5}$ and PM_{10} but not for PM_1

(WHO, 2021).

Throughout this work, we will refer to "volcanic emissions", and unless otherwise stated, our intended meaning is SO_2 gas and PM emissions, collectively. Emissions from basaltic fissure eruptions can be a very significant source of air pollution, on local and regional scales. Due to the low explosivity, the emissions are released into the troposphere, elevating concentrations of gases (including SO_2) and PM at ground level. This can affect air quality and human health, as well as damaging infrastructure and agriculture (Carlsen et al., 2021b; Delmelle et al., 2002; Hansell and Oppenheimer, 2004; Ilyinskaya et al., 2017; Schmidt et al., 2015; Stewart et al., 2022). Fissure eruption plumes are typically ash-poor. The PM in the plume is predominantly formed through gas-to-particle conversion and is typically very fine, falling within the PM_1 or $PM_{2.5}$ size fractions (Ilyinskaya et al., 2021; Ilyinskaya et al., 2017; Martin et al., 2011; Mason et al., 2021). In such volcanic plumes the PM is a complex chemical mixture of sulfate and an array of other species, including potentially toxic metals and metalloids (e.g. lead, cadmium) (Ilyinskaya et al., 2021; Langmann, 2014; Mason et al., 2021). Exposure to sulfate aerosol in volcanic plumes has been associated with exacerbation of various health problems, particularly those related to the respiratory tract (Stewart et al., 2022). After emission, volcanic plumes in the troposphere are advected by the prevailing wind, and mature compositionally through dynamic physico-chemical processes (Ilyinskaya et al., 2021; Ilyinskaya et al., 2017). One of the key processes is the transformation of SO_2 gas into sulfate PM (SO_4) at a rate that depends on multiple parameters including ambient humidity and temperature, solar flux, the availability of oxidants, and interactions with other PM (Green et al., 2019; Pattantyus et al., 2018). PM derived from other sources, such as sea spray, anthropogenic activities (e.g. traffic), and wind-blown mineral dust, will also be incorporated into the volcanic plume by mixing with the background atmosphere (Butwin et al., 2019; Holgate, 2017; Lim et al., 2012; Tam et al., 2016).

Emissions from past Icelandic fissure eruptions have had significant societal consequences in Iceland and, in larger events, across the northern hemisphere (Schmidt et al., 2015; Schmidt et al., 2011). They are included in national risk assessments in Iceland and in the UK (HM Government, 2020). Notable examples of large Icelandic fissure eruptions in the past are the Laki eruption of 1783 - 1784 (which erupted 14 km^3 of lava and 120 Mt of SO_2 over 8 months) and the Holuhraun eruption of 2014 - 2015 (which erupted 1.6 km^3 of lava and 9.6 Mt of SO_2 over 6 months) (Gıślason et al., 2015; Ilyinskaya et al., 2017; Schmidt et al., 2015; Schmidt et al., 2011). During the Holuhraun eruption it was discovered that volcanic emissions could circle back to the same location, as a chemically mature plume, long after the initial public health advisory had been lifted, exposing the population unexpectedly to volcanic pollutants (Carlsen et al., 2021a; Ilyinskaya et al., 2017). Population exposure to the Holuhraun

emissions in Iceland's capital area was found to be associated with an increase in register-measured health care utilisation for respiratory disease (Carlsen et al., 2021a; Carlsen et al., 2021b). Absence of public advisories about the presence of the chemically mature plume was associated with further increases in visits to primary care medical doctors and to hospital emergency departments (Carlsen et al., 2021a).

The 2021 Fagradalsfjall eruption, the first Icelandic fissure eruption since Holuhraun, presented a unique opportunity to advance our understanding of the intensity and spread of volcanic air pollution in populated areas (in Iceland, and potentially elsewhere) for the four main reasons listed below. In addition, based on the eruption history of the Reyjkanes Peninsula where Fagradalsfjall is located, the 2021 eruption could be heralding the start of a decades-to-centuries long eruptive period. Therefore, all investigations into this eruption may prove useful for risk reduction efforts for years, and generations, to come.

- This was the first eruption since the 12^{th} and 13^{th} centuries to occur in the most densely-populated area of Iceland (Pedersen et al., 2021). While the Holuhraun eruption was 90 - 100 km from the nearest towns and 250 km from the Reykjavík capital area; the Fagradalsfjall eruption was $\approx$ 9 km from the township of Grindavík and approximately $\approx$ 30 km from Reykjavík. In addition, the proximity of the Fagradalsfjall eruption to Reykjavík, and the relatively easy site access, meant that it received a high number of visitors, totaling $\approx$ 300,000 individuals (equivalent to $\approx$ 80 % of Iceland's total population, although many visitors were international tourists and not Icelandic residents). The combination of these factors meant that the volcanic emissions posed a significant public health hazard despite the relatively small size of the eruption.

- The eruption was monitored by the densest reference-grade air quality monitoring network of any in the world (to our knowledge), with 27 stations across Iceland and 14 stations within 0 - 40 km distance from the eruption site. This allowed investigation into very fine-scale changes in spatial and temporal air quality impacts with respect to SO_2, and fine PM (PM_1, $PM_{2.5}$, PM_{10}). This is the first time (to our knowledge) that volcanic emissions have been monitored for PM_1 levels using a reference-grade network.

- During the Holuhraun eruption, 72-hour forecasts of plume dispersion and the likelihood of ground level SO_2 concentrations exceeding air quality thresholds were produced by the Icelandic Meteorological Office (IMO) using the CALPUFF dispersion model (Barsotti, 2020). These forecasts enabled public advisories to be issued and became an important mitigation tool for reducing the impact of volcanic air pollution (Barsotti, 2020; Carlsen et al., 2021a). The 2021 Fagradalsfjall eruption presented a new challenge for forecasting the plume dispersion, and the

associated ground level air pollution. This was due to a combination of several factors: a) the unstable local meteorological conditions with frequent changes in wind direction and speed; b) the relatively small size of the eruption (with 4.82 km^2 of lava and 0.3 to 0.9 Mt of SO_2 erupted over 6 months [Pfeffer et al., in prep]), and c) the close proximity to populated areas, where even a small change in plume advection conditions resulted in an impact to different parts of the population.

- The availability of an air quality monitoring network with a high spatial resolution allowed for a novel comparison with plume detection by satellite imagery. Satellite imagery is an invaluable tool for plume detection in the absence of ground-based measurements and/or dispersion modelling. The comparison of ground-based and satellite observations is an important area to be advanced.

We make use of this research opportunity by analysing the following data sets:

(a) High-resolution time-series of SO_2 and PM measured by the Icelandic air quality (AQ) network (27 reference-grade stations and 5 eruption-response stations). We compare the time-series during the eruption to a background non-eruptive period to determine the frequency with which air quality thresholds were exceeded due to advection of volcanic emissions.

(b) Outputs from the CALPUFF plume dispersion model that was used for operational forecasting of volcanic pollution during the eruption. Ground-level SO_2 concentrations predicted by the CALPUFF model are compared to those measured by the AQ network to examine the effectiveness of the model given the challenging conditions listed above.

(c) Satellite imagery of SO_2 from TROPOMI on the Sentinel-5 Precursor satellite. We use the satellite imagery as an independent method for detecting the volcanic plume. In particular, we analyse the frequency with which volcanic plume was present at ground level when SO_2 was detected by satellite in the same location as an AQ station.

(d) Population count, distribution and demographics to analyse the potential exposure to volcanic SO_2. We combine the plume dispersion calculated by the CALPUFF model, the air quality measurements, and population data to investigate the number of people likely exposed to concentrations of SO_2 above the Icelandic Directive (ID) hourly threshold of 350 $\mu g/m^3$. The number of people within more vulnerable age groups (≤ 4 and ≥ 65 years of age) are identified, as well as the exposure of main hospital locations. In a separate analysis, we examine the potential exposure of visitors to the eruption site.

4.1.1 Fagradalsfjall eruption

The Fagradalsfjall fissure eruption began on the 19th March 2021 on the Reykjanes Peninsula in southwest Iceland [Figure 4.2]. The fissure was initially small at approximately 200 m long, with a lava extrusion rate of 9.5 $\pm$ 0.2 m^3/s (Pedersen et al., 2021). In early April five new fissures opened $\approx$ 1 km to the North-East of the original site (IMO, 2021c). A total of eight fissures opened in the Fagradalsfjall area but only the fissure which opened fifth in the sequence remained active over the remainder of the duration of the eruption period (IMO, 2021e) [Figure 4.1A, B]. From early May, the eruption began a pulsating activity with lava-fountaining up to 200 m above the ground during active pulses, and periods of intermittent activity with pauses in the eruption lasting from several hours to days (Barsotti et al., in prep). On the 17th September 2021 the lava field was estimated to be 4.82 km^2 (Pedersen et al., 2021) [Figure 4.1C]. The SO_2 flux from the Fagradalsfjall eruption varied significantly between 2 to 3 kt/day (IMO, 2021c), with higher flux rates concurrent with more active volcanic pulses, and the total SO_2 emission estimated at 0.3 to 0.9 Mt (Pfeffer et al., in prep). No fresh extrusion of lava was detected from Fagradalsfjall from the 18th September onwards, with SO_2 out-gassing continuing in very low amounts (IMO, 2021f). Three months after the last activity this phase of the eruption was officially declared over, while new intrusions and eruptions are anticipated to potentially occur for the next century. The lava flows caused no damage to homes or infrastructure because the eruption occurred in an unpopulated area and the lava flows were confined within a series of valleys. Above-background peaks of SO_2 and PM air pollutants were detected at air quality stations throughout the eruption.

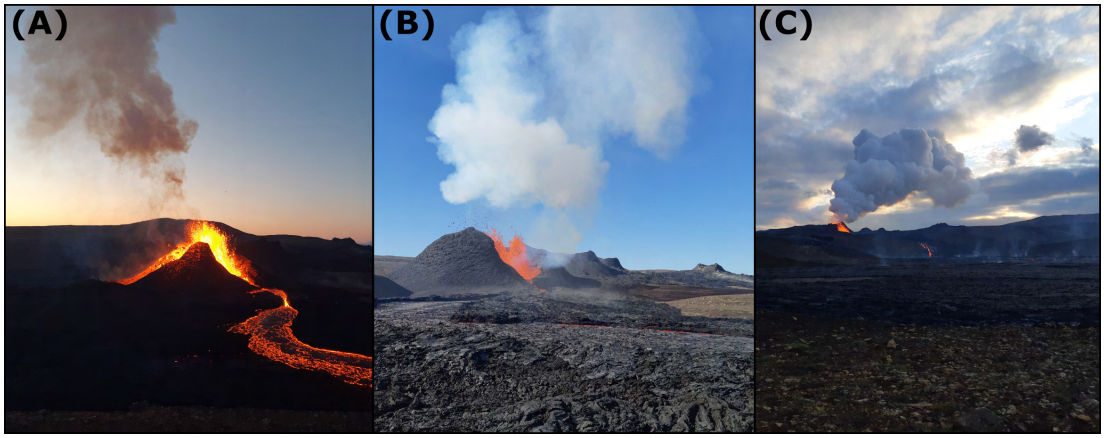

Figure 4.1: The Fagradalsfjall eruption, Iceland. (A) View of an eruptive vent with lava fountaining into an active lava channel. Photo taken on 2nd May 2021. (B) Lava fountaining at active vent with view of previous vents, inactive at the time of photo capture, in the background. Photo taken on 5th May 2021. (C) View of the eruption across the fresh lava field (in the foreground). The volcanic plume is clearly visible from the erupting vent. Photo taken on 10th July 2021. All photos taken by Melissa Pfeffer, IMO.

4.1.2 Population and background air quality of Iceland

Iceland has a population of ≈ 369,000 people, with the majority of the population living in the southwest part of the country, in the capital city of Reykjavík and the surrounding municipalities. There are ≈ 263,000 residents, 71% of the population, living within 50 km of the Fagradalsfjall eruption site. Of the total population, 6% and 15% of the population are in the potentially more vulnerable age groups of ≤ 4 and ≥ 65 years of age, respectively. Iceland is a Global North country and has low-to-moderate levels of air pollution with urban traffic and natural dust storms being the two main pollution sources (Carlsen and Thorsteinsson, 2021). Background concentrations of SO_2 during non-eruptive periods in Iceland are generally low (a few $\mu g/m^3$, Ilyinskaya et al., 2017), with some rare escalations to higher levels of tens or hundreds of $\mu g/m^3$ in the vicinity of aluminium smelters or geothermal power plants. The PM concentrations have high seasonal variabilities and can reach high levels in both urban and rural areas. In rural areas, the main source of PM is re-suspended natural dust sourced from highland deserts, with higher levels in the drier summer seasons (Butwin et al., 2019). In urban areas, the PM pollution peaks are typically higher in the winter with the main source being tarmac erosion by studded tyres (Carlsen and Thorsteinsson, 2021).

4.2 Methodology

4.2.1 Time-series of SO_2 and PM from air quality instrument network

Air quality (AQ) in municipal areas around Iceland is continuously monitored by reference-grade instruments managed by the Environmental Agency of Iceland. Most of the monitoring stations measure SO_2 and several also monitor concentrations of PM_1, $PM_{2.5}$, and PM_{10}. Specifications of the municipal air quality measurement systems are indicated in Table 4.1. All the instruments in the municipal air quality network are calibrated every six months.

Data from the municipal air quality network were obtained from www.airquality.is. SO_2 measurements were downloaded from 25 measurement stations. SO_2 data were downloaded from January 2020 until the 30th September 2021, however some instruments were installed within the time period so the time-series is truncated. PM_{10} data were obtained from thirteen measurement stations around Iceland, $PM_{2.5}$ from seven stations and PM_1 were obtained from three stations. PM data were downloaded from October 2018, where available, to 30th September 2021. The PM pre-eruptive background time is longer than for SO_2 as PM is frequently elevated due to a variety of natural and man-made sources and is highly variable (Butwin et al., 2019). Background non-eruptive periods were selected in the data during the same annual dates that the

2021 Fagradalsfjall eruption occurred to reduce seasonal impacts on the PM concentration. These periods are referred to as BG1 (19^{th} March 2019 to 18^{th} September 2019) and BG2 (19^{th} March 2020 to 18^{th} September 2020). Routine calibration peaks were removed from the data, as were dates when fireworks contributed a significant component to atmospheric PM (29^{th} December to 1^{st} January each year, following Ilyinskaya et al., 2017).

Around the eruption site, the Icelandic Meteorological Office (IMO) installed a network of five eruption-response SO_2-monitoring instruments between April to July 2021 to monitor air quality in the near-field (0.6 to 3 km from the eruption) [Table 4.1]. These instruments were installed after the start of the eruption and do not provide pre-eruption background air quality measurements. This does not affect our interpretation as SO_2 is negligible in Icelandic atmosphere free from volcanic emissions (Ilyinskaya et al., 2017). Table 4.1 states the manufacturer detection limits of the eruption-response SO_2-monitoring instruments. A recent study has found that low-cost sensors may be subject to interferences restricting their capability to monitor SO_2 in low ppbv concentrations (Whitty et al., 2022), but this does not affect our interpretation of measurements recorded at the eruption site where SO_2 concentrations were significantly above detection limits.

SO_2 data from the municipal air quality network and the eruption site stations were processed into hourly averages and the PM_1, $PM_{2.5}$, and PM_{10} data were processed into daily-means. Where data was available for both the pre-eruptive and eruptive periods, two-sample t-tests were applied to test whether the means of the two datasets were equal to determine if the two periods were significantly different.

We sorted the AQ stations around Iceland into geographic clusters to investigate regional air quality. The defined groups are the eruption site (G1), the Reykjanes Peninsula (G2), the capital area of Reykjavík (G3), Southwest Iceland (G4), Hvalfjörður (G5), East Iceland (G6) and North Iceland (G7) [Figure 4.2]. Within these groups, data were examined for exceedances of air quality thresholds. For SO_2, we used the Icelandic Directive (ID) hourly threshold of $350\,\mu g/m^3$ (Icelandic Directive, 2016). For PM_{10} we used the ID daily-mean threshold of $50\,\mu g/m^3$ (Icelandic Directive, 2016), and for $PM_{2.5}$ we used the World Health Organization (WHO) daily-mean guideline of $15\,\mu g/m^3$ (WHO, 2021). There were no health thresholds applied for PM_1. For SO_2, $PM_{2.5}$, and PM_{10}, the number of exceedances of health thresholds in the background periods and during the eruption period were counted. For SO_2 measurements in G1 (eruption site) and G2 (Reykjanes Peninsula), the regional clustering approach did not work due to high variability in SO_2 concentrations recorded across the stations in these regional groups. The AQ stations within G1 and G2 were therefore treated individually.

Three measurement stations within G3 (Reykjavík area) recorded PM_1, $PM_{2.5}$ and

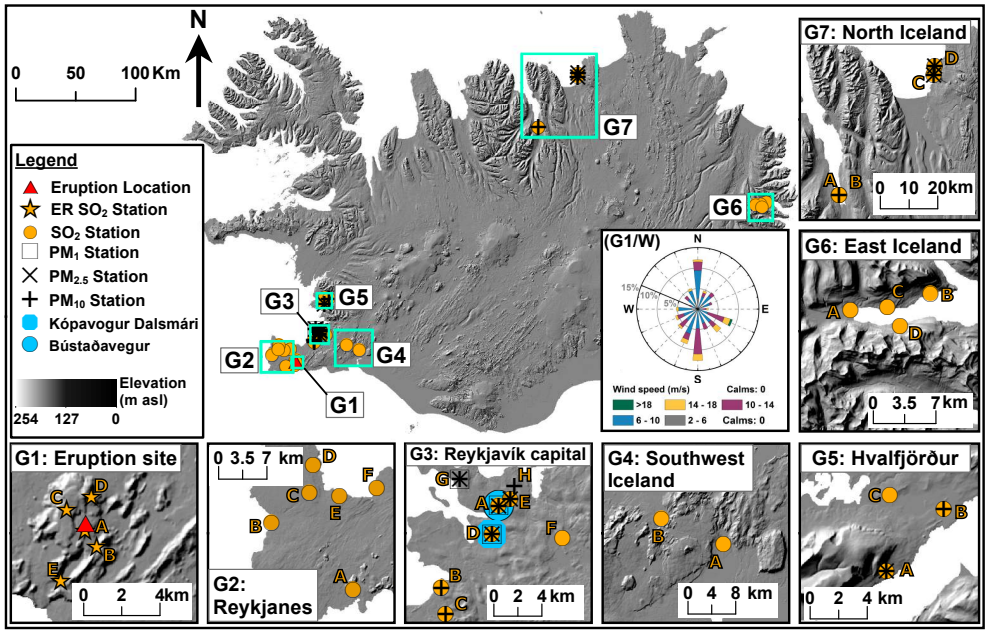

Figure 4.2: Distribution of AQ monitoring stations around Iceland. The location of the Fagradalsfjall eruption is indicated by the red triangle [G1 inset] and eruption-response (ER) SO_2 stations are indicated by yellow stars. Reference-grade AQ monitoring stations have the following symbols: yellow circles indicate monitoring of SO_2, black cross indicates monitoring of PM_{10}, black X indicates monitoring of $PM_{2.5}$, black square outline indicates monitoring of PM_1. Monitoring stations are lettered, and time-series of measurements at each station are available in the Appendix. Kópavogur Dalsmári AQ station, used for point-analysis of the CALPUFF dispersion model and for determining the frequency of plume grounding from satellite imagery, is shown by the filled blue octagon. Bústaðavegur AQ station, used for determining contributions of particle sizes, is shown by the filled blue circle. The basemap shows the topography of Iceland, sourced from Landmælingar Íslands, the National Land Survey of Iceland. AQ stations are separated into groups [G1 to G7] defined by their region, with enlarged views of the individual air quality groups shown in the inset maps. Inset G1/W shows a rose of wind conditions between 23rd March to 19th September 2021 at the eruption site. Wind directions are shown as the direction of provenance. Data retrieved from a meteorological station installed close to the Fagradalsfjall eruption site, providing wind conditions at 4.5 m above ground level.

PM_{10} size fractions. This provided an opportunity to determine if there were changes in the relative concentrations of PM of different size fractions in the eruptive period compared to the pre-eruptive period. PM_1 measurements at the three stations were not available during the BG1 period and were only available during the BG2 period at the Bústaðavegur AQ station [Figure 4.2]. At Bústaðavegur, the average concentration of PM_1, $PM_{2.5}$ and PM_{10} was calculated for the BG2 period and for the eruptive period. Since PM size modes are cumulative, in that PM_{10} contains all particles with diameters below $\leq$10 µm, the size modes were subtracted from one another to determine the relative concentrations of particles in the following categories: particles $\leq$1 µm in diameter, between 1 - 2.5 µm in diameter and those particles between 2.5 - 10 µm in diameter. The contributions of these particle size categories to the PM at Bústaðavegur were determined under the pre-eruptive and eruptive conditions.

Table 4.1: Specifications for instruments installed at AQ stations around Iceland. Specifications as detailed in Airpointer, 2021; Alphasense, 2021; Crowcon, 2021; Met One Instruments Inc., 2020; Palas, 2021; Teledyne, 2019; Thermo Scientific, 2017; Thermo Scientific, 2021. The near-field eruption-response instruments are those in G1. The municipal reference-grade AQ network instruments are those in Groups 2 to 7.

Measurement Group	Measurement Type	Instrument	Lower detection limit	Resolution
G1	SO_2	Crowcon Xgard	1 ppbv	1 ppbv
		Alphasense SO2-B4	5 ppbv	5 ppbv
G2	SO_2	Thermo 450i	1 ppbv	0.5 ppbv
G3	SO_2	Thermo 450i	1 ppbv	0.5 ppbv
		Recordum Airpointer	0.5 ppbv	0.25 ppbv
	PM_1, $PM_{2.5}$, PM_{10}	PALAS Fidas 200 S	0 µg/m3	0.1 µg/m3
	$PM_{2.5}$, PM_{10}	Thermo 5030 Sharp	4 µg/m3	0.1 µg/m3
G4	SO_2	Thermo 450i	1 ppbv	0.5 ppbv
G5	SO_2	Thermo 450i	1 ppbv	0.5 ppbv
	$PM_{2.5}$, PM_{10}	Thermo 5030 Sharp	4 µg/m3	0.1 µg/m3
G6	SO_2	Thermo 450i	1 ppbv	0.5 ppbv
G7	SO_2	Recordum Airpointer	0.5 ppbv	0.25 ppbv
		Teledyne T100	4 ppbv	0.2 ppbv

4.2.2 Comparison between different methods of plume identification

The reference-grade SO_2 instruments in the municipal AQ network can detect SO_2 concentrations with high accuracy even at low levels and therefore provided a reliable determination of plume-presence at ground level [Table 4.1]. We compared the detected SO_2 concentrations to results from the CALPUFF plume dispersion model and satellite Sentinel-5p imagery. We did this for one representative location, the Kópavogur Dalsmári AQ station in the southern part of the Reykjavík capital area [Figure 4.2], which was a station intermittently exposed to volcanic SO_2 during the eruption providing a useful comparison site for determining plume presence via means of multiple independent proxies. The comparison was run over the period 1st April to 31st May 2021.

4.2.2.1 AQ station SO_2 measurements

A subset of SO_2 time-series measurements from Kópavogur Dalsmári AQ station was used for this analysis. We selected a five hour sampling window (from 09:30 to 14:30) each day throughout April and May 2021 [selection of time window explained further in Section 4.2.2.3]. For a yes/no identification of plume presence we used a cut-off threshold of 8 µg/m^3 as an hourly mean. The background SO_2 concentration at Kópavogur Dalsmári from January 2020 to 18th March 2021 was 2 µg/m^3 ± 1 µg/m^3. We applied a threshold of 8 µg/m^3 in our analysis, several μg/m^3 higher than the average background concentration in order to ensure volcanic SO_2 was being detected and additionally to avoid interference from accidental instrumental noise because not all of the 2021 data had been quality controlled by the operating agency. Where the SO_2 concentration at any point within the five-hour window was > 8 µg/m^3, it was determined that volcanic plume was present at ground level at Kópavogur Dalsmári AQ station.

4.2.2.2 Plume presence determination by the CALPUFF model

The CALPUFF model was used to simulate the dispersal of the volcanic plume from the Fagradalsfjall eruption. CALPUFF is an atmospheric dispersion model which predicts the movement of gas emissions within a 3D computational domain (Barsotti, 2020; Gıślason et al., 2015; Scire et al., 2000). For the Fagradalsfjall eruption, CALPUFF was run on a 350 x 250 grid of 87,500 nodes, with a spatial resolution of 2 km. Simulations were run by the IMO to produce hourly forecasts of SO_2 and SO_4 concentrations at ground-level. The emission rate of SO_2 input to the model was regularly reviewed and changed throughout the eruption when DOAS measurements indicated significant changes in SO_2 flux from the eruption. Meteorological forecast data for use in the CALPUFF model were obtained from the European Centre for Medium-Range Weather Forecasts (ECMWF) with a resolution of 0.125 degrees ($\approx$ 12 km at the equator). The model output used for this analysis was the same as was used for operational forecasting

during the eruption.

The five nodes within 2 km of the Kópavogur Dalsmári AQ station were extracted from the CALPUFF computational results for a point-analysis with measurements from the Kópavogur Dalsmári AQ station. We assessed whether the model accurately determined the presence of volcanic SO_2 at ground level. A comparison of the observed SO_2 concentrations to the predicted SO_2 concentrations was done in a separate part of the analysis [Section 4.2.3]. We used a critical threshold of $0.5\,\mu g/m^3$ to determine if the model indicated the presence of volcanic SO_2 at Kópavogur Dalsmári, selected to be above the uncertainty of the model calculations. The CALPUFF model assumes that there is no SO_2 in the atmosphere which does not come from the volcanic source point, which is why the lower value of $0.5\,\mu g/m^3$ was used as the critical threshold. When the SO_2 concentration at any point within the five-hour window from the five closest nodes to Kópavogur Dalsmári was $>0.5\,\mu g/m^3$ SO_2, volcanic plume was considered to be present as forecast by the CALPUFF dispersion model at the comparison site. The CALPUFF model results were further used as the basis for a population exposure analysis [Section 4.2.3].

4.2.2.3 Plume presence indicated by satellite imagery

Satellite SO_2 imagery from TROPOMI on the Sentinel-5 Precursor satellite, hereafter termed Sentinel-5p, identifies the total atmospheric column amount of SO_2 in Dobson units. It is able to identify the spatial location of the volcanic plume but does not determine the altitude of the plume, i.e. it does not identify if the plume is at ground level. Here we assessed the frequency at which the volcanic plume identified by the satellite imagery was at ground level and therefore measurable by the AQ monitoring station. For each day during our April-May analysis period the satellite images were visually inspected and used to determine whether the volcanic plume was in the area around Kópavogur Dalsmári. Days where the satellite imagery showed plume visibly moving towards Kópavogur Dalsmári [Figure 4.3] were compared to the SO_2 measurements from the AQ station [Section 4.2.2.1]. The overpass of the Sentinel-5p satellite was around noon each day. A five hour window (from 09:30 to 14:30) each day during the April-May analysis period was used throughout the comparisons between different methods of plume identification (including the AQ station SO_2 measurements [Section 4.2.2.1] and the outputs from the CALPUFF dispersion model, [Section 4.2.2.2]) to allow comparison to the yes/no identification of plume from the satellite imagery.

The satellite detection of SO_2 was sensitive to the injection height of the volcanic plume, and was more effective at identifying the presence of SO_2 when the plume was not beneath meteorological clouds. Images where there was no visible SO_2 may have been due to volcanic plume being obscured by meteorological clouds. Another potential source of uncertainty was that the satellite images were assessed by visual inspection.

Nevertheless, this method is representative of the day-to-day efforts to use satellite imagery to guide community hazard assessment during an eruption such as Fagradalsfjall.

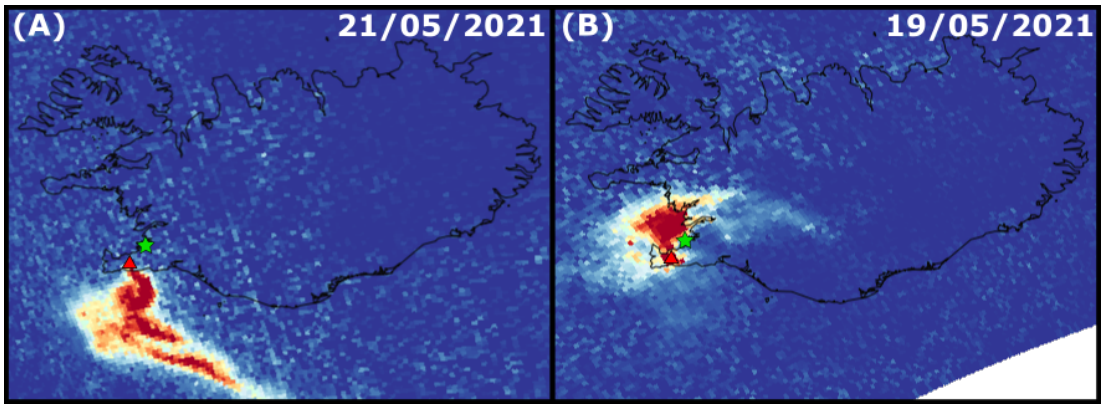

Figure 4.3: Examples of Sentinel-5p satellite imagery. The red triangle indicates the location of the Fagradalsfjall eruption, the green star indicates the location of Kópavogur Dalsmári AQ station. The colour scale indicates the relative column amount of SO_2 in Dobson units, with red colours indicating a high column amount of SO_2 (0.01 mol m^{-2}) and blue colours indicating a low column amount of SO_2. (A) Image capture on the 21st May 2021 where the SO_2 in the atmospheric column is being dispersed to the south from the eruption site and is likely not at Kópavogur Dalsmári AQ station. (B) Image capture on the 19th May 2021 where the SO_2 in the atmospheric column is being dispersed to the north from the eruption site and is likely at Kópavogur Dalsmári AQ station.

4.2.3 Population exposure analysis

4.2.3.1 Populated areas

The CALPUFF probabilistic model was used to determine which areas of Iceland were likely to have been exposed to SO_2 concentrations above 350 µg/m^3, which is the Icelandic Directive hourly threshold. The CALPUFF model output between the start of the eruption (19thMarch) and the 23rd March was not used in this analysis as the resolution was set at 4 km; following the 23rd March the resolution was raised to 2 km. The CALPUFF model results for the number of times on an hourly basis that the forecast concentration exceeded 350 µg/m^3 from 23rd March until 18th September 2021 at each model grid point were counted. Over the same time-period, the number of events when SO_2 exceeded 350 µg/m^3 at air quality stations within 70 km of the eruption site were counted. Only those AQ stations within 70 km of the eruption site were used for the comparison between the predicted and observed number of exceedance events as the CALPUFF model forecast the exceedances above threshold levels would predominantly occur within this region. Those AQ stations within 70 km of the eruption site which were not in operation for more than 20% of the time between 23rd March and 18th September 2021 were removed from the comparison with the CALPUFF model. The CALPUFF model was found to overestimate by 7 times the frequency at which the AQ stations were observing exceedance events where SO_2 concentrations were above

350 µg/m^3. An analysis was made to determine how to scale the CALPUFF model results so that they fit the measurements from the AQ stations better. It was found that the CALPUFF model forecasts for 700 µg/m^3 and 800 µg/m^3 compared best to station measurements of the number of exceedances above 350 µg/m^3 [Figure 4.4]. Here we use the CALPUFF probability output with an 800 µg/m^3 threshold to determine the predicted number of exceedances above 350 µg/m^3 hourly concentrations of SO_2 across Iceland.

We calculated potential population exposure to SO_2 from the eruption by GIS analysis of the population distribution, overlain by the CALPUFF 800 µg/m^3 exceedance frequency map. Data on the Icelandic population in the year 2020 were obtained from Statistics Iceland and were considered representative for 2021. Population data were obtained for each municipality of Iceland, both the total municipality population as well as population by age demographics. Within ArcGIS ArcMap 10.6, a GIS shapefile was uploaded with the Icelandic municipality population statistics and used to create a spatial determination of population distribution across the nation. For the purposes of the population exposure analysis, the very large municipalities of Reykjavík and Hafnarfjörður, which are extremely heterogeneous in terms of population distribution, were each split into two distinct re-designated zones. This was to account for densely populated areas of the Reykjavík and Hafnarfjörður municipalities which were exposed to significantly lower predicted SO_2 concentrations than other sparsely populated zones. The municipality of Reykjavík was re-designated as North Reykjavík and South Reykjavík, and the relative populations of each were determined using population data from WorldPop at a 100 m resolution for the year 2020 (WorldPop, 2021). The municipality of Hafnarfjörður was likewise re-designated as North Hafnarfjörður and South Hafnarfjörður, and the relative populations were determined in the same manner.

In ArcMap 10.6 the municipality population shapefile was overlain by the CALPUFF 800 µg/m^3 exceedance frequency grid. The intersect tool was used to determine which CALPUFF nodes where located within each municipality of Iceland. The CALPUFF nodes within each municipality were collated using the summarise tool and the attributes were extracted, allowing analysis of the number of exceedance events that the CALPUFF model predicted for each municipality. This then provided an estimate of the numbers of people across the Icelandic municipalities who may have been exposed to concentrations of SO_2 exceeding the ID 350 µg/m^3 hourly threshold.

Demographics within the population of each municipality were used to determine the numbers of people of different ages who were predicted to be exposed to SO_2 concentrations exceeding the ID hourly threshold. Those people aged ≤ 4 years and those aged ≥ 65 years were considered to be in the potentially more vulnerable categories and their exposure to above-threshold levels of SO_2 was also investigated. Across Iceland the locations of main hospitals were identified to allow investigation of additional

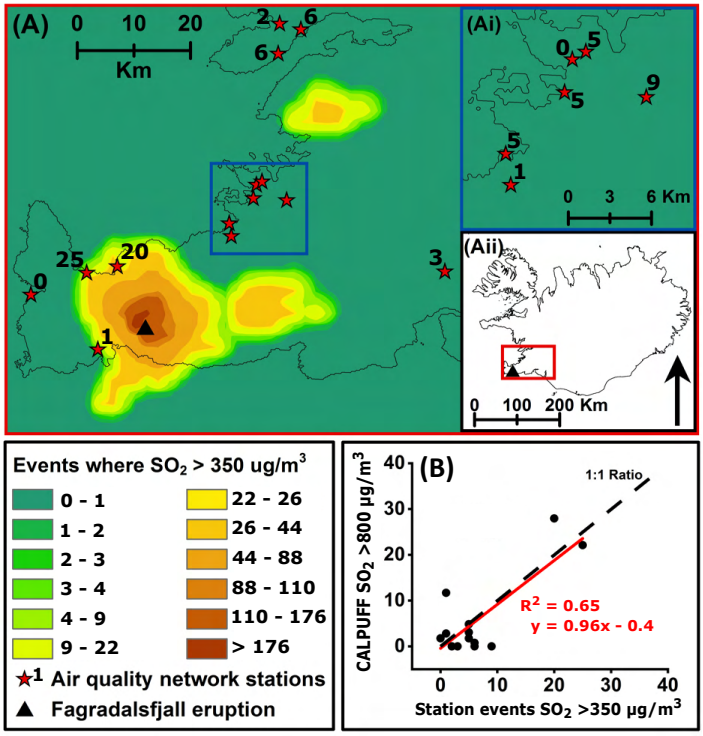

Figure 4.4: Re-scaling of the CALPUFF frequency model. (A) Map of instances that SO_2 exceeds an 800 µg/m^3 threshold in the CALPUFF model, which is scaled to translate to exceeding the ID 350 µg/m^3 threshold in measurements at AQ stations. Colour scale indicates the number of times that the scaled CALPUFF results predict SO_2 will exceed 350 µg/m^3. The eruption location is marked by the black triangle and AQ stations used in the re-scaling process are marked by red stars, with the number of observed exceedances above 350 µg/m^3 at each AQ station noted. (Ai) Enlarged view of the G3 stations in the Reykjavík area. (Aii) Location of the CALPUFF rescaling analysis area. (B) Comparison between the number of exceedances above 800 µg/m^3 in the CALPUFF model results (y axis) and the number of exceedances above 350 µg/m^3 as observed at the AQ stations (x axis). The trend is indicated by the solid red line, the black dashed line indicates a 1:1 ratio line. (A;B) The CALPUFF model results and the air quality network observations both cover the eruption period of 23rd March to 18th September 2021.

potentially vulnerable individuals (due to pre-existing illnesses).

The population exposure analysis was done at the municipality level. This is spatially coarse with potential for both under and over estimation. For each area demarcated as a municipality (with two areas each for Reykjavík and Hafnarfjörður) we calculate from the CALPUFF model the number of times that SO_2 exceeded the ID hourly threshold of 350 µg/m^3 (using the model results for 800 µg/m^3 as described above) over the course of the eruption. This gives an indication of the number of times that people living in the municipality may have been exposed to hourly SO_2 concentrations above 350 µg/m^3 but does not precisely determine this. This method does not account for variations in population exposure related to movement of the population outside their area of residence, nor does it account for any other sort of exposure reduction measures

that individuals may have taken. With respect to the more vulnerable age categories, potential exposure in the > 65 age group may have been limited by vulnerable individuals remaining indoors. Conversely, in Iceland it is common practice for young infants to be left outdoors to sleep during the day, and so the vulnerable category < 4 years of age may have had a higher potential exposure.

4.2.3.2 Visitors to the eruption site

The number of people visiting the eruption site peaked at $\approx$ 6,000 per day and totalled $\approx$ 300,000 individuals. A considerable effort was made by the national and local authorities to minimise the risk from volcanic and general outdoor hazards. Visitors were recommended to remain upwind of the eruptive vents, as SO_2 concentrations at the eruption site frequently exceeded the ID threshold (IMO, 2021d). A network of three footpaths was developed, starting at designated parking areas approximately 6 km from the town of Grindavík on the southern coastline of the Reykjanes Peninsula and leading towards the eruption and lava flows. The eruption site footpaths were installed over the course of the eruption period as the lava field expanded and new areas providing views of the volcanic activity were opened up. On the 24^{th} March, the Icelandic Tourist Board installed three automatic footpath counters, one on each footpath leading to the eruption site and viewpoints. The automatic counters were PYRO-Box (Eco-Counter, Canada) with an accuracy of 95% and a sensing capacity of 4 m in both directions (Eco Counter, 2021). Although the vast majority of visitors used the footpath network to reach the eruption site and viewpoints, some walked outside the bounds of the Eco-Counter instrument range and so were not counted. There were also a number of people who landed at the eruption site on helicopter sightseeing tours and would not have been counted. Children who were carried along paths and those travelling by vehicle, including scientists and rescue teams, were also not counted. The visitor numbers used here are therefore a minimum estimate. The numbers of visitors to the site does not include details of the age demographics and, as such, no identification of exposure of more-vulnerable age categories could be determined.

The analysis of potential population exposure to hourly SO_2 above $350\,\mu g/m^3$ at the eruption site was done by combining analysis of measurements of SO_2 from the five eruption-response monitoring stations installed by IMO, and site visitor data. The CALPUFF dispersion model was not used for this purpose as the model resolution is too low to adequately determine variability in SO_2 concentrations within the area in proximity (< 3 km) to the eruption location.

4.3 Results

4.3.1 Volcanic impact on SO_2 concentrations

Three out of four regional groups of AQ stations where pre-eruptive background data were available recorded statistically significant differences in concentrations of SO_2 between the eruptive and pre-eruptive periods. These include G3 (Reykjavík), G5 (Hvalfjörður) and G6 (East Iceland). The G7 measurement group (North Iceland) showed an insignificant difference between the average SO_2 concentrations during the pre-eruptive and eruptive periods but did have a higher maximum hourly value during the eruption, as detailed below [Figure 4.7]. The Icelandic Directive SO_2 air quality threshold of 350 µg/m^3 as an hourly mean was exceeded at the eruption site, and in different populated areas on multiple occasions, as detailed below. The ID specifies that the hourly SO_2 threshold of 350 µg/m^3 should not be exceeded more than 24 times per year; this guideline was also exceeded at several locations. Below we discuss the SO_2 levels in the different regions (G1 to G7), starting with the eruption site and moving progressively further away.

The area in the immediate vicinity of the eruption site (Group 1, between 0.6 and 3 km from the active craters) was subjected to the most frequent and the highest escalations of SO_2 [Figure 4.2]. Across the G1 stations there were a total of 1,445 exceedance events recorded, with Station A (the closest to the eruption site) individually recording 1,372 threshold exceedance events [Figure 4.5]. Station A also recorded the maximum concentration of hourly SO_2 over the eruption period, at 17,820 µg/m^3 [Figure 4.7A]. Following Station A, the next highest frequency of threshold exceedances were at Stations C and D, which were located 0.9 km to the north-west and 1.5 km to the north of the eruptive vents, respectively [Figure 4.5]. The hazard posed by these high concentrations was to the site visitors as there are no settlements within these distances.

In the populated areas across Iceland further away from the eruption site (G2 - G7, [Figure 4.2]), the SO_2 concentrations were highly variable both spatially and temporally. The Reykjanes Peninsula (G2, with a population of 29,000 residents across the municipalities in the region) recorded the highest frequency of threshold exceedances from the municipal AQ stations, with a total of 52 instances of SO_2 hourly concentrations exceeding the ID threshold [Figure 4.7A]. The maximum number of threshold exceedances was recorded at G2 Station E (25 instances), and there was an average of 9 instances of threshold exceedance across the six G2 stations [Figure 4.6]. The maximum hourly SO_2 concentration recorded in G2 was 1,070 µg/m^3, recorded at Station E. The towns to the northwest of the eruption site, particularly G2 Stations E and F at 12 -14 km distance from the eruption [Figure 4.6], were subjected to more frequent and more intense SO_2 pollution than the towns to the west and southwest (G2 Stations A and B, Figure 4.6).

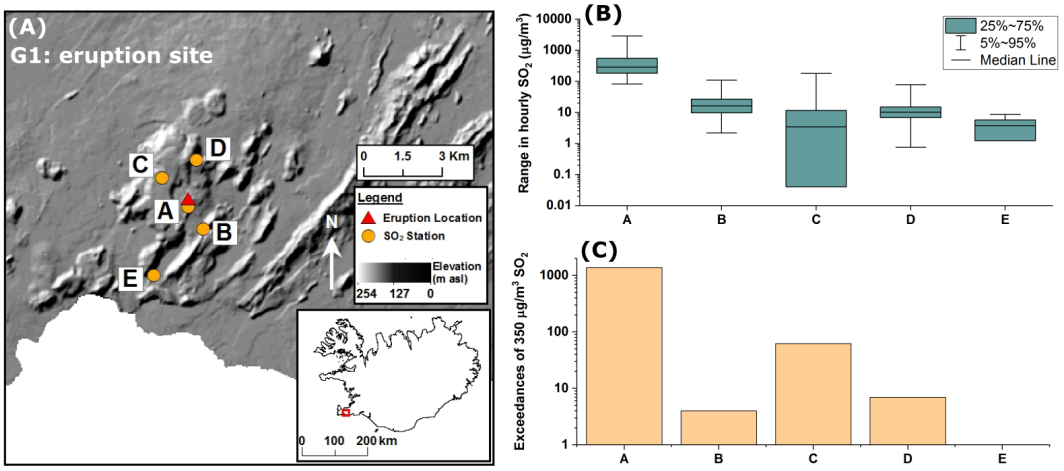

Figure 4.5: Individual station results from the eruption-response AQ network in G1. (A) Map of the G1 eruption-response SO_2 stations where station locations are indicated by the orange circles, with the red triangle indicating the eruption location. The basemap shows the topography of the area. (B) The range in hourly SO_2 measurements at each AQ station within G1. (C) The frequency of each station in G1 recording SO_2 hourly concentrations exceeding the ID hourly threshold of 350 µg/m^3. The installation dates of the G1 eruption-response stations are as follows: A) 07/04/2021; B) 17/05/2021; C) 21/06/2021; D) 21/06/2021; E) 29/06/2021. Note the logarithmic y axis scale in (B) and (C). Note that for some stations the maximum hourly-mean SO_2 concentrations greatly exceeded the statistical distribution shown here, this is shown on Figure 4.7.

For instance, G2 Station E (14 km from the eruption) recorded 25 instances of threshold exceedances [Figure 4.6] and a maximum hourly-average of 1,070 µg/m^3 [Figure 4.7A], while station G2-A (9 km from the eruption) recorded 1 instance of threshold exceedance [Figure 4.6] and a maximum hourly-average of 440 µg/m^3, despite being closer to the eruption.

The Reykjavík capital area (G3, 20 to 35 km from the eruption site, Figure 4.2) recorded the second highest impact on SO_2 levels out of the populated areas. The Reykjavík capital area had a total of 25 instances of threshold exceedances [Figure 4.7B], with the highest hourly-mean SO_2 concentration of 750 µg/m^3 (compared to a maximum hourly concentration of 60 µg/m^3 and no threshold exceedances in the background period) [Figure 4.7A]. During the eruption period there were a maximum of 9 threshold exceedance events recorded by an individual SO_2 AQ station, with an average of 4 threshold exceedance events across the six G3 AQ stations.

The air quality network of two stations in G4 (Southwest Iceland, 45 to 55 km from the eruption) and three stations in G5 (Hvalfjörður, 55 to 60 km from the eruption) recorded AQ threshold exceedances events 21 and 14 times, respectively [Figure 4.7B]. In the pre-eruptive period the G5 AQ stations recorded 1 event where SO_2 concentrations exceeded the ID threshold. Maximum hourly SO_2 concentrations in G4 and G5 during the eruption period (2,380 µg/m^3 and 860 µg/m^3, respectively) exceeded those in the

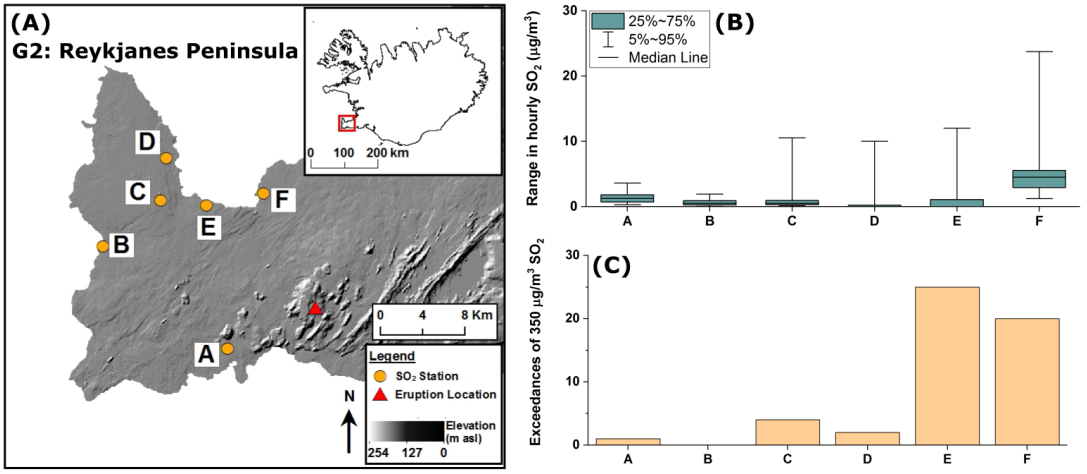

Figure 4.6: Individual station results from the AQ network in G2. (A) Map of the G2 AQ SO_2 stations where station locations are indicated by the orange circles, with the red triangle indicating the eruption location. The basemap shows the topography of the area. (B) The range in hourly SO_2 measurements at each AQ station within G2. (C) The frequency of each station in G2 recording SO_2 hourly concentrations exceeding the ID hourly threshold of 350 µg/m^3. Note that for some stations the maximum hourly-mean SO_2 concentrations greatly exceeded the statistical distribution shown here, this is shown on Figure 4.7.

pre-eruptive period (10 µg/m^3 and 440 µg/m^3, respectively).

G6 in the far East of Iceland (> 400 km from the eruption site, Figure 4.2) recorded 1 event where SO_2 concentrations exceeded the AQ threshold, with a maximum hourly SO_2 concentration of 440 µg/m^3 during the eruption, compared to 360 µg/m^3 in the pre-eruptive period.

G7 in the North of Iceland (between 280 to 340 km from the eruption site, Figure 4.2) recorded no exceedance events of SO_2 above the AQ threshold in either the pre-eruptive period or during the eruption [Figure 4.7A, B], and the difference in average concentration was statistically insignificant compared to the background. However, the maximum hourly-mean during the eruption (150 µg/m^3) was much higher than in the pre-eruptive period (50 µg/m^3).

4.3.2 Volcanic impact on PM concentrations

$PM_{2.5}$ and PM_{10} concentrations were analysed in three regions across Iceland, including in the capital area of Reykjavík (G3), Hvalfjörður (G5) and North Iceland (G7) [Figures 4.9 and 4.10, respectively]. PM_1 concentrations were analysed across the capital area of Reykjavík (G3), which was the only area where such measurements were made [Figure 4.8].

In Reykjavík (G3, seven AQ stations measuring PM, Figure 4.2), PM_1 and PM_{10} concentrations were significantly higher during the eruption compared to the pre-eruptive

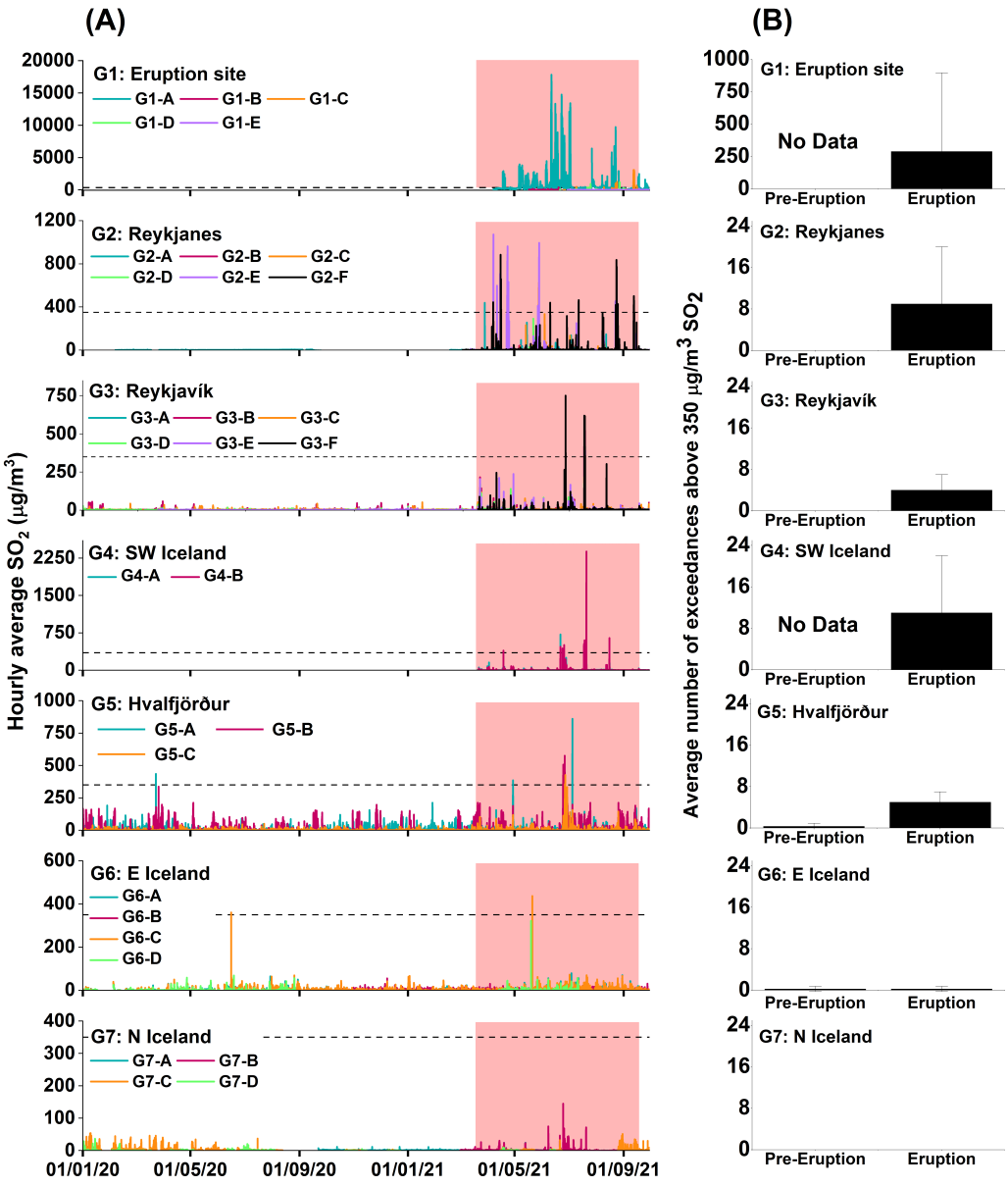

Figure 4.7: SO_2 measurements from the air quality network in Iceland. AQ stations are divided into regional groups as described in Section 4.2.1 and shown in Figure 4.2. (A) Time-series of SO_2 in regional areas around Iceland. The horizontal black dashed line indicates the ID SO_2 hourly threshold of 350 µg/m^3 and the red highlight indicates the 2021 Fagradalsfjall eruption period. Data presented are hourly averages. Note the changes in y axis. Graphs of individual station SO_2 measurements are available in the Appendix. (B) Exceedances of the ID SO_2 hourly threshold of 350 µg/m^3 during the pre-eruptive period and during the eruption. Bars represent the average number of exceedance events across the measurement group, with the error bars indicating one standard deviation from the average. Note that no pre-eruptive SO_2 data was available for G1 or G4 stations, and G2 had limited pre-eruptive SO_2 data with only one of six AQ stations in operation prior to the eruption. Note that the G1 y axis is 2 orders of magnitude greater than the y axis for Groups 2-7.

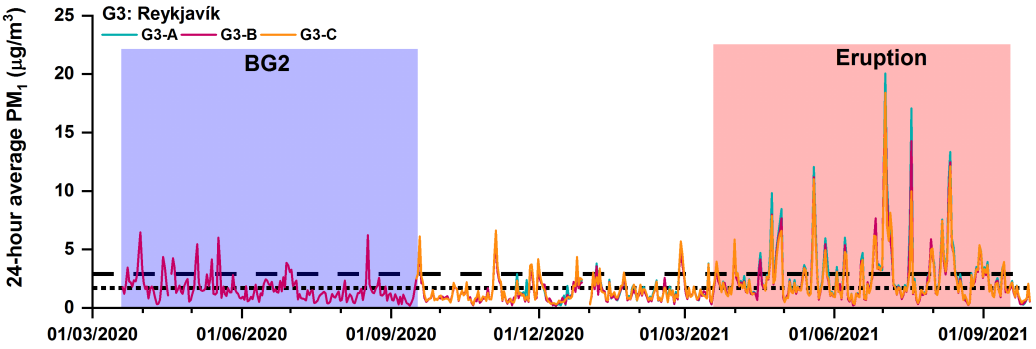

Figure 4.8: Timeseries of PM_1 measurements from the G3 air quality network in Iceland [Section 4.2.1 and Figure 4.2]. The blue highlight indicates the background period (BG2), the red highlight indicates the 2021 Fagradalsfjall eruption period. The horizontal black dotted line indicates the daily average PM_1 concentration during BG2, and the horizontal black dashed line indicates the daily average PM_1 concentration during the eruption. Data presented are daily-means. Graphs of individual station PM measurements are available in the Appendix.

periods (see Section 4.2.1 for definition of background periods). The maximum daily-mean PM_1 concentration was 20 µg/m^3 during the eruption compared to 7 µg/m^3 in the BG2 pre-eruptive period [Figure 4.8]. The average PM_1 concentration during the eruption was 3 µg/m^3 ± 3 µg/m^3 compared to 2 µg/m^3 ± 1 µg/m^3 during the BG2 per-eruptive period. The maximum PM_{10} daily-mean concentration during the eruption was 140 µg/m^3, which is higher than the maximum daily-mean recorded during the BG1 and BG2 periods (100 µg/m^3) [Figure 4.10]. PM_{10} exceeded the ID threshold (50 µg/m^3 as a daily-mean) 13 times during the eruption compared to 9.5 threshold exceedances as an average across the BG1 and BG2 periods [Figure 4.10]. $PM_{2.5}$ in the Reykjavík area did not show an overall increase in maximum recorded concentrations during the eruption (maximum daily-mean of 60 µg/m^3 during the eruption relative to a maximum of 130 µg/m^3 recorded across the BG1 and BG2 periods). The average concentration of $PM_{2.5}$ during the eruption (6 µg/m^3 ± 6 µg/m^3) also did not exceed that in the BG1 and BG2 periods (8 µg/m^3 ± 10 µg/m^3). During the eruption period the exceedances above the WHO $PM_{2.5}$ threshold (15 µg/m^3 as a daily-mean) were also lower than during the pre-eruptive periods, with the maximum number of 65 exceedance events recorded at a single station during the BG1 period, 21 during the BG2 period and 32 during the eruption [Figure 4.9].

In the Hvalfjörður region (G5, Figure 4.2), neither the $PM_{2.5}$ nor PM_{10} maximum daily-mean concentrations during the eruption (30 µg/m^3 and 60 µg/m^3, respectively) exceeded those in the pre-eruptive period (40 µg/m^3 and 60 µg/m^3, respectively) [Figures 4.9A and 4.10A]. The average concentrations of $PM_{2.5}$ (5 µg/m^3 ± 4 µg/m^3) and PM_{10} (7 µg/m^3 ± 6 µg/m^3) during the eruption period were the same as the averages during the BG1 and BG2 periods. However, $PM_{2.5}$ exceeded the WHO threshold 9 times during the eruption, relative to an average of 3.5 exceedance events across the

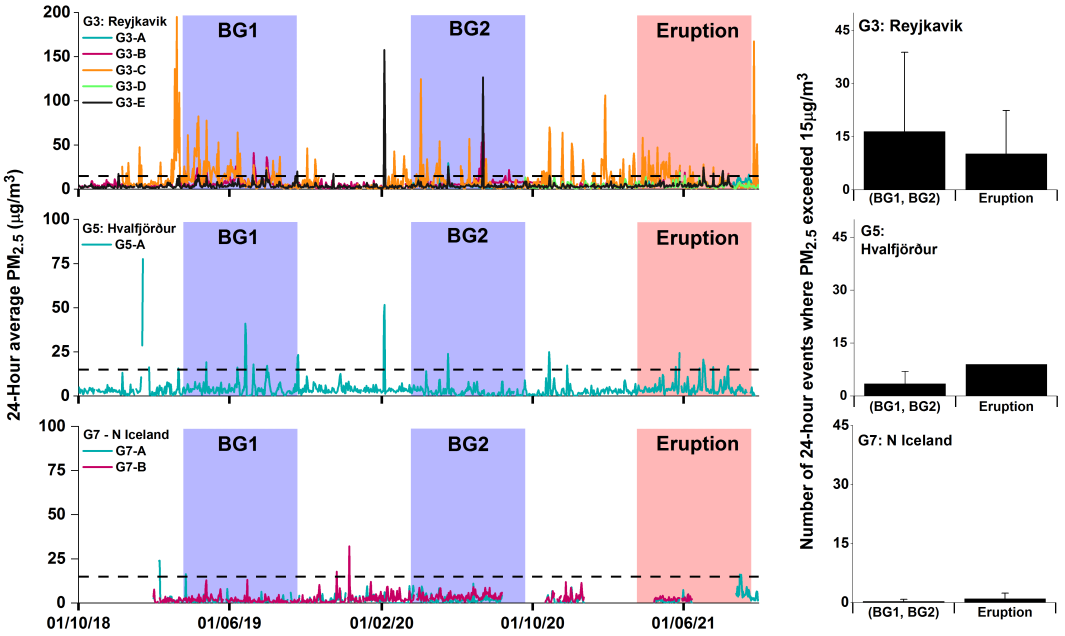

Figure 4.9: $PM_{2.5}$ measurements from the air quality network in Iceland. AQ stations are divided into regional groups as described in Section 4.2.1 and shown in Figure 4.2. (A) Time-series of $PM_{2.5}$ in regional areas around Iceland. The horizontal black dashed line indicates the WHO $PM_{2.5}$ daily-mean threshold of 15 µg/m^3. The blue highlights indicate the background periods (BG1 and BG2), the red highlight indicates the 2021 Fagradalsfjall eruption period. Data presented are daily-means. Note the changes in y axis. Graphs of individual station PM measurements are available in the Appendix. (B) Exceedances of the WHO $PM_{2.5}$ daily-mean threshold of 15 µg/m^3. Bars represent the average number of exceedance events across the measurement group, with the error bars indicating one standard deviation from the average. The average number of events during BG1 and B2 are compared to the total number of events during the eruption.

BG1 and BG2 periods [Figure 4.9B]. PM_{10} exceeded the ID threshold on 2 instances during the eruption, compared to 1 exceedance event across both the BG1 and BG2 periods in this region.

The maximum daily-mean concentration of $PM_{2.5}$ recorded in the North of Iceland [G7, Figure 4.2] during the eruptive period was 20 µg/m^3, equal to that recorded in the BG1 and BG2 periods. The maximum recorded daily-mean PM_{10} in this region during the eruption (80 µg/m^3) did not exceed that recorded in the BG1 and BG2 periods (90 µg/m^3) [Figure 4.10].The average $PM_{2.5}$ and PM_{10} concentrations in North Iceland during the eruption (3 µg/m^3 ± 3 µg/m^3 and 11 µg/m^3 ± 12 µg/m^3, respectively) equaled those in the pre-eruptive BG1 and BG2 periods. However, the number of exceedances above the WHO thresholds for $PM_{2.5}$ and above the ID threshold for PM_{10} during the eruptive period (2 and 9, respectively) exceeded the average exceedance count during the BG1 and BG2 pre-eruptive periods (1 and 8, respectively) [Figure 4.9B and Figure 4.10B].

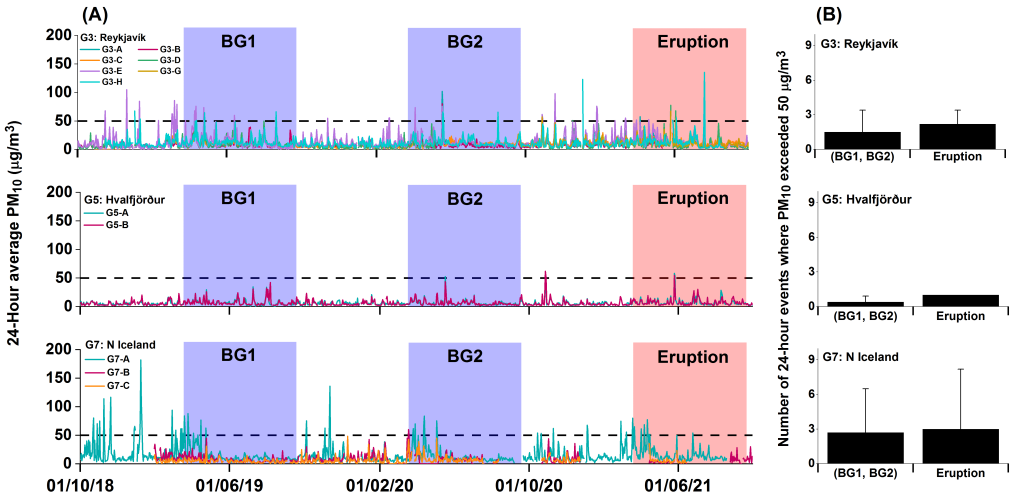

Figure 4.10: PM_{10} measurements from the air quality network in Iceland. AQ stations are divided into regional groups as described in Section 4.2.1 and shown in Figure 4.2. (A) Timeseries of PM_{10} in regional areas around Iceland. The horizontal black dashed line indicates the ID PM_{10} daily-mean threshold of $50\,\mu g/m^3$. The blue highlights indicate the background periods (BG1 and BG2), the red highlight indicates the 2021 Fagradalsfjall eruption period. Graphs of individual station PM measurements are available in the Appendix. (B) Exceedances of the ID PM_{10} daily-mean threshold of $50\,\mu g/m^3$. Bars represent the average number of exceedance events across the measurement group, with the error bars indicating one standard deviation from the average. The average number of events during BG1 and B2 are compared to the total number of events during the eruption.

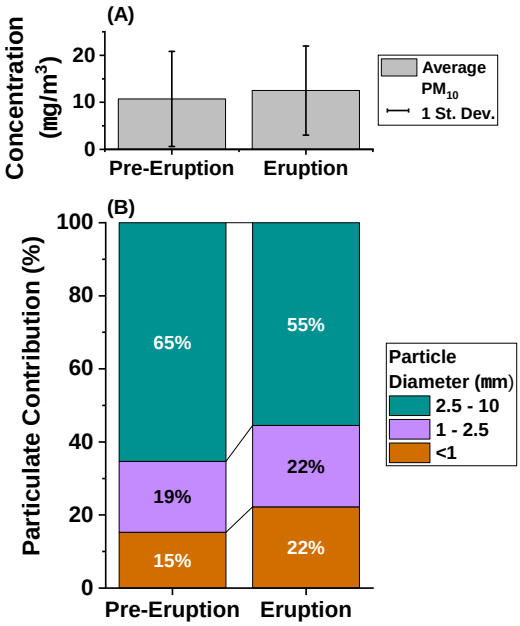

Figure 4.11: Particle size differences between the pre-eruptive period (BG2) and the eruptive period at Bústaðavegur station in G3. (A): the average PM_{10} concentration across BG2 and the eruption, with error bars showing 1 standard deviation. (B): Particle size contribution (%) for particles ≤ 1 µm in diameter, between 1 - 2.5 µm in diameter and those particles between 2.5 - 10 µm in diameter during BG2 and the eruption at Bústaðavegur station.

4.3.2.1 Impact on particle size distributions

The results of the particle size analysis at the G3 Bústaðavegur station are displayed in Figure 4.11. During both the eruptive and BG2 periods, the particulate matter was mostly comprised of particles sized between 2.5 - 10 µm in diameter [Figure 4.11]. The concentration of particles ≤ 1 µm in diameter during the eruption and the BG2 periods were statistically significantly different. The contribution of these particles increased from 15% in the BG2 period to 22% during the eruption [Figure 4.11]. The percentage contributions indicated in Figure 4.11 are contributions by mass. It is important to recognise that larger particles have a higher mass, and that a contribution increase of smaller particles from 15 to 22 % relates to a significant increase in the number of these particles. Since PM size groups are cumulative, an increase in particles <1 µm in diameter during the eruption would lead to increases in the concentrations of $PM_{2.5}$ and PM_{10}, as seen in Figures 4.9 and 4.10.

4.3.3 Detection of plume by different methods

4.3.3.1 Capability of CALPUFF dispersion model

Measurements of SO_2 at Kópavogur Dalsmári AQ station [Figure 4.2] were compared to the output of the CALPUFF dispersion model for the same location to assess the model's capability to forecast the presence of volcanic SO_2 at ground level (comparison period of 1st April to 31st May 2021). The plume was considered to be forecast when the SO_2 concentrations exceeded $0.5\,\mu g/m^3$ in the model output. The model output had a very high rate of true positives and true negatives [Figure 4.12A]. False positives (where the plume was not measured at the Kópavogur Dalsmári AQ station but plume presence was forecast by the CALPUFF model) and false negatives (where the plume was measured at the Kópavogur Dalsmári AQ station but plume presence was not forecast by the CALPUFF model) were only 20% and 21%, respectively [Figure 4.12A].

4.3.3.2 SO_2 measurements compared to satellite imagery

Visual analysis of satellite imagery of the SO_2 column were compared to SO_2 measurements at the Kópavogur Dalsmári AQ station to assess how frequently the volcanic plume was grounding on days when it was present in the atmospheric column at this location. From satellite imagery we identified 11 days (between 1st April to 31st May 2021) when the volcanic SO_2 was in the atmospheric column near the AQ station. Out of the 11 days, the plume was grounding for 36% of the time [Figure 4.12B] as identified by SO_2 concentrations $\geq 8\,\mu g/m^3$ measured by the AQ station. The remaining 64% of the time, the plume did not ground and the SO_2 very likely remained higher in the atmospheric column [Figure 4.12B].

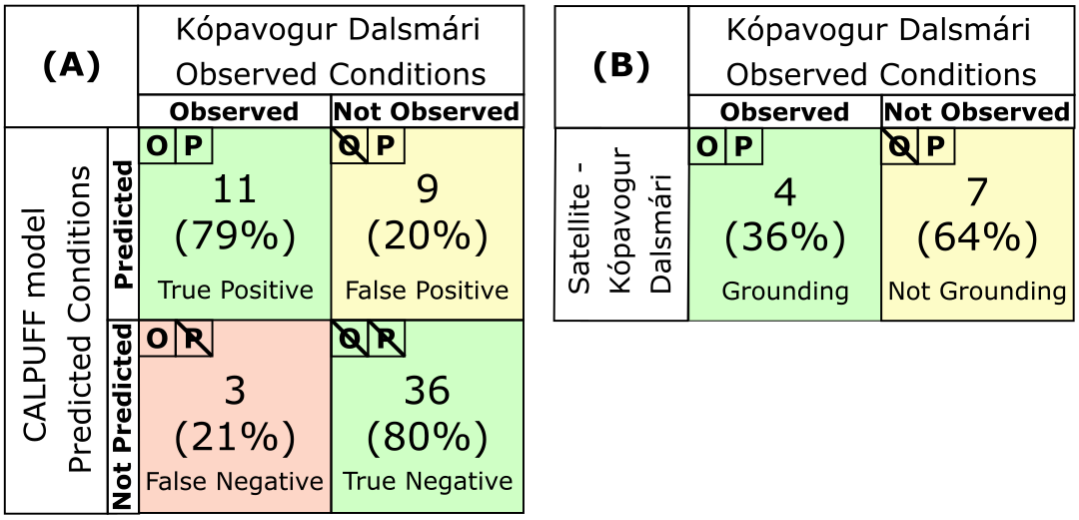

Figure 4.12: (A) Comparison between AQ station SO_2 measurements and CALPUFF predicted SO_2 data for Kópavogur Dalsmári. AQ measurements are split into "Observed" and "Not Observed" categories, and CALPUFF data are split into "Predicted" and "Not Predicted" categories. Percentages are calculated according to the AQ observations. (B) Comparison between AQ station SO_2 measurements and satellite SO_2 imagery. Data were used to indicate whether the SO_2 observed in the satellite imagery grounded to be measurable at Kópavogur Dalsmári.

4.3.4 Exposure of the general population

4.3.4.1 Accuracy of the CALPUFF model for predicting number of SO_2 threshold exceedances

The CALPUFF model was used to calculate the number of events when ground-level SO_2 concentrations exceeded the ID hourly threshold of 350 µg/m^3 over the course of the eruption across Iceland [Figure 4.13C]. The model result was compared to the number of exceedances observed by AQ stations within 70 km of the eruption site in order to verify and rescale the model output [Section 4.2.3]. The CALPUFF model was found to generally overestimate the ground-level SO_2 concentrations, resulting in a higher number of predicted threshold-exceedance events compared to the observed events (by a factor of 7). The best agreement was found between the number of observed events > 350 µg/m^3 and the number of model-forecast events > 800 µg/m^3 ($R^2 = 0.65$). The model output for the number of events > 800 µg/m^3 was therefore used in the rest of this analysis as the best estimate for the number of events > 350 µg/m^3 (hereafter termed as "rescaled model output"). The rescaled model output was found to predict concentrations of SO_2 more accurately for proximal sites ($\leq$ 15 km from the eruption) than for more distal sites ($>$ 15 km from the eruption) [Figure 4.4].

4.3.4.2 Population exposure to SO_2 above the ID air quality threshold

Municipality level population data [Figure 4.13A] was combined with the CALPUFF rescaled model output to determine numbers of individuals likely exposed to above-threshold SO_2 concentrations ($> 350\,\mu g/m^3$) for the total population [Figure 4.13D] and for more vulnerable subgroups [Figure 4.13E]. While the CALPUFF rescaled model output was used as the main method for calculating and displaying the population exposure [Figure 4.13], we highlight any significant differences between the rescaled model output and AQ observations where this was likely to affect the population exposure.

The CALPUFF model forecast that population exposure to above-threshold concentrations of SO_2 would predominantly occur within a 20 km radius of the volcanic eruption site [Figure 4.13C]. The population exposure analysis showed that 47,000 Icelandic residents ($\approx$ 13% of the total population) were potentially exposed to concentrations of SO_2 exceeding the hourly ID threshold for more than 24-times during the eruption [Figure 4.13D], thereby exceeding the recommendation for the number of annual exceedances (Icelandic Directive, 2016). Of those, $\approx$ 8,500 residents ($\approx$ 2.2 of the total population) were in the more vulnerable age categories of ≤ 4 years and ≥ 65 years of age [Figure 4.13E]. Within the population exposed to above-threshold SO_2 concentrations ≥ 24 times, the CALPUFF model indicated that $\approx$ 5,500 residents (1.5% of the population) may have been exposed to > 44 events were SO_2 concentrations exceeded the ID threshold [Figure 4.13C]. Of those exposed to more than 44 above-threshold events, $\approx$ 1,000 (0.2% of the total population) were in the more vulnerable age categories [Figure 4.13E].

The CALPUFF rescaled model output predicted a region of likely exposure in the North Reykjavík municipality, approximately 50 km from the eruption site [Figure 4.13C]. We interpret that the increased likelihood of exposure in this region is due to its higher elevation (800 m a.s.l.) which can intercept a lofted eruption cloud. However, there are no AQ stations within this region to confirm whether SO_2 concentrations frequently exceeded the ID threshold. With the exception of the forecast increased exposure in the North Reykjavík municipality, at distances ≥ 20 km from the eruption site the CALPUFF model largely forecast 1 or fewer events where SO_2 concentrations would exceed the ID threshold [Figure 4.13C]. In the Reykjavík capital area (G3, 20 to 35 km from the eruption, with a population of $\approx$ 210,000), the rescaled model output was not sufficiently accurate at predicting the number of SO_2 exceedance events. Using the AQ observations instead of the model, the residents of the densely-populated capital area were exposed to between 0 and 9 threshold exceedance events. The capital area has a high density of individuals in the more-vulnerable age groups [Figure 4.13B], and these individuals were potentially exposed to up to 9 events where SO_2 concentrations exceeded threshold levels as observed by the AQ stations in G3.

Of the 18 main hospitals identified in our analysis across Iceland, the hospital closest to the eruption site (20 km away) was located in a municipality which was exposed to above-threshold SO_2 concentrations on more than 24 occasions, as observed by AQ stations and predicted by the rescaled CALPUFF model output. However, the location of the hospital itself was in an area of the municipality where the rescaled model output predicted that exposure to above-threshold SO_2 concentrations would occur only once during the eruption. The nearest AQ station to this hospital ($\approx$ 1 km distance) recorded 2 instances where SO_2 concentrations exceeded the ID threshold during the eruption. The remainder of the main Icelandic hospitals were located in regions predicted to experience only one event where SO_2 concentrations exceeded threshold values. As discussed previously, AQ stations within the capital area of Reykjavík observed a maximum of 9 threshold-exceedance events, which may have impacted those vulnerable individuals in the three hospitals located within the Reykjavík area [Figure 4.13B].

4.3.4.3 Exposure of the visitors to the eruption site

Potential exposure levels of the visitors to the eruption site were assessed using the SO_2 measurements from the eruption-response AQ stations in G1 [Section 4.2.3.2]. During the footpath monitoring period (24th March to 18th September 2021), the site was visited by $\approx$ 300,000 people, averaging 1,600 visitors per day. The highest numbers were recorded in March, with a daily average of 3,300 visitors, and a peak of 6,000 visitors on the 28th March 2021 [Figure 4.14(iv)].

Figure 4.14 shows the location of eruption-response SO_2-monitors and footpaths at the eruption site. Stations A, B and E were in close proximity to the footpath network, while stations C and D were further afield to the north and northwest of the eruption site. The five G1 stations recorded variable levels of SO_2 [Figure 4.14(ii)] (maximum hourly SO_2 recorded by G1 Station A was 17,820 µg/m^3 compared to a maximum of 188 µg/m^3 recorded by G1 Station E). Exceedances above the ID threshold of 350 µg/m^3 likewise varied with a maximum exceedance count of 1,372 by G1 Station A but an average of 289 exceedances across the five stations [Figure 4.14(iii)]. Station A, located 0.6 km from the eruption and 0.5 km from the designated footpath, recorded an average SO_2 concentration across the eruption period of 780 µg/m^3, twice the concentration that the ID recommends to be the maximum exposure level. Station A was only accessible to foot-traffic until it was surrounded by lava on the 4th June 2021, after which time it was only accessible by helicopter.

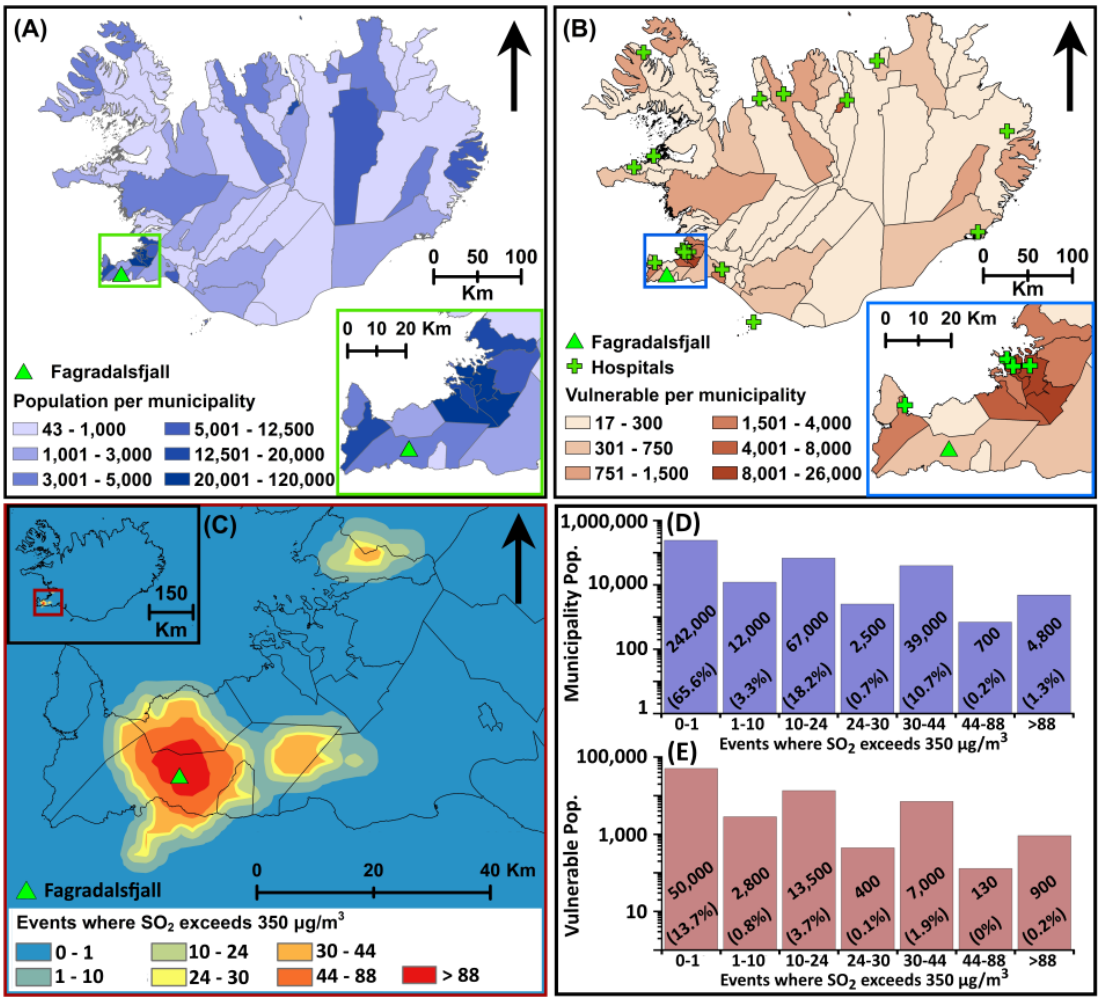

Figure 4.13: **(A):** Total populations across Iceland at the municipality level. The green triangle shows the Fagradalsfjall eruption site. Lower right inset shows enlarged view of the densely populated southwestern part of Iceland, including the Reykjavík capital. Population data for 2020 from Statistics Iceland. **(B):** Vulnerable sub-populations ($\leq$ 4 years and $\geq$ 65 years of age) in each municipality. Green crosses indicate the major hospitals and the green triangle shows the Fagradalsfjall eruption site. Lower right inset shows enlarged view of the densely populated southwestern part of Iceland, including the Reykjavík capital. Population data for 2020 from Statistics Iceland. **(C):** CALPUFF rescaled output [see Section 4.2.3 for details] of the number of events when SO_2 concentrations exceeded 350 $\mu g/m^3$ between the 23rd March and the 18th September 2021. The Fagradalsfjall eruption site is shown by the green triangle. **(D):** Number of people, based on municipality-level population data, who the CALPUFF rescaled output forecast would be exposed to above-threshold SO_2 exceedance events (shown as people count and as % of Iceland's total population). Where the number of exceedance events varied within one municipality, the maximum number was used. Note the logarithmic y axis scale. **(E):** The number of vulnerable people ($\leq$ 4 years and $\geq$ 65), based on municipality-level population data, who the CALPUFF rescaled output forecast would be exposed to above-threshold SO_2 exceedance events (shown as people count and as % of Iceland's total population). Where the number of exceedance events varied within one municipality, the maximum number was used. Note the logarithmic y axis scale.

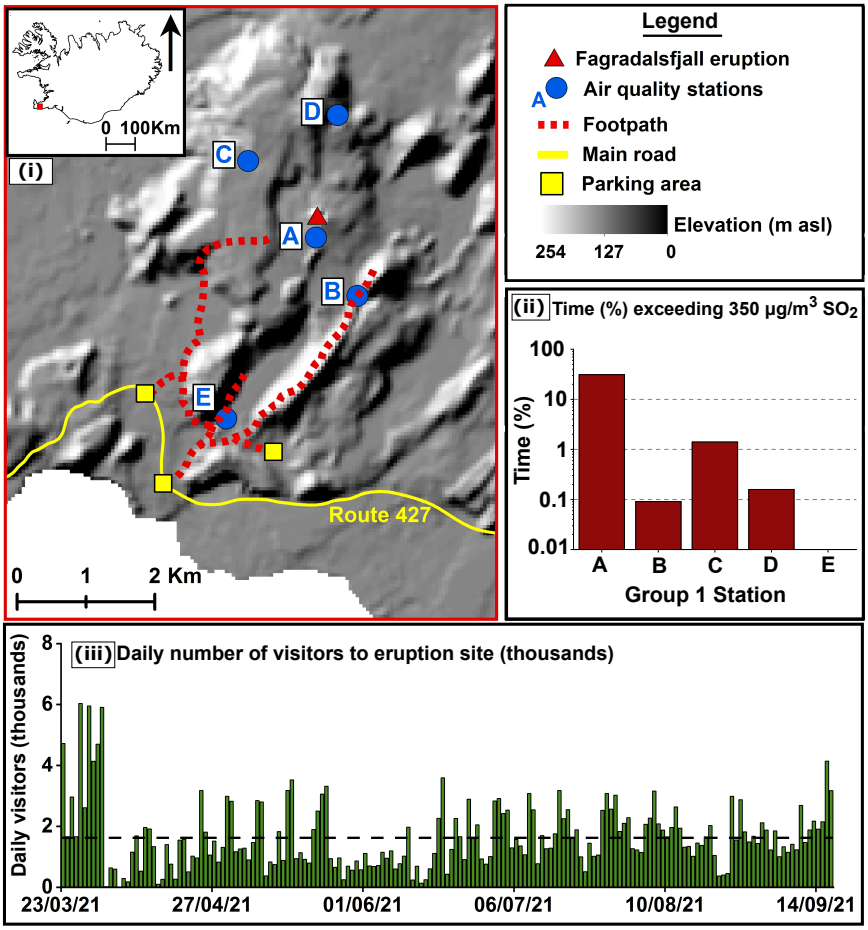

Figure 4.14: (i) Fagradalsfjall eruption site with public footpath network indicated by red hatched lines. Blue circles indicate location of eruption-response AQ stations in G1 [Figures 4.2 and 4.5]. (ii) Percentage of measurement time that the G1 AQ stations recorded SO_2 concentrations exceeding the ID hourly threshold of 350 µg/m^3, note the logarithmic y scale. (iii) Daily number of visitors to the eruption site, as counted by the Eco-Counter automatic counters installed on the footpath network [Section 4.2.3.2]. The black hatched line indicates the daily average visitor count of 1,600. Note that the y scale is in thousands.

4.4 Discussion

The 2021 Fagradalsfjall eruption was the first eruption in ≈ 800 years to occur close to the most densely-populated area of Iceland, with 71% of the population living within 50 km of the eruption site. It is well known from previous studies that emissions from basaltic fissure eruptions are rich in PM and SO_2 pollutants (Carlsen et al., 2021a; Gıślason et al., 2015; Ilyinskaya et al., 2017). The 2021 Fagradalsfjall eruption provided an opportunity for us to track the atmospheric dispersion of these pollutants with an unprecedented spatial and temporal resolution. We discuss and compare the air quality impacts of this eruption relative to previous eruptions [Section 4.4.1]. The availability of the dense AQ network also allowed us to assess the performance of the

CALPUFF dispersion model for operational forecasting of volcanic SO_2 [Section 4.4.2]; and to compare the ground-based observations with satellite imagery, a tool with huge potential for monitoring of remote eruptions [Section 4.4.3]. We also present the first assessment of population exposure to above-threshold concentrations of volcanic SO_2 in Iceland [Section 4.4.4].

4.4.1 Impacts of volcanic fissure eruptions on air quality

Fagradalsfjall was a relatively small fissure eruption when compared to some of the recent volcanic events in Iceland and elsewhere (e.g. the 2014 - 2015 Holuhraun eruption in Iceland; the 2018 Kīlauea lower East Rift Zone eruption in Hawai'i). However, its SO_2 emission volume (0.3 - 0.9 Mt) is significant when compared to anthropogenic emissions, for example, the daily SO_2 flux from the Fagradalsfjall eruption equates to $\approx$ 20 - 50 % of UK total anthropogenic SO_2 emissions in 2011 (OECD, 2011). Unlike country-scale anthropogenic emissions, volcanic pollutants come from a point-source and therefore have the potential to raise air pollutant levels in downwind areas to higher concentrations, causing potentially different hazards to human health. In Iceland, SO_2 emissions from non-volcanic sources are very small (Ilyinskaya et al., 2017), which makes the signal of the volcanic contribution even more apparent during periods of volcanic unrest.

The Fagradalsfjall eruption caused a nationwide impact on air quality around Iceland with respect to SO_2 and fine PM pollutants. The near-field (G1, $\leq$ 3 km distance, Figure 4.5) and far-field (G2-5, $\leq$ 60 km distance, Figures 4.6 and 4.7) recorded multiple events where SO_2 hourly concentrations exceeded the ID threshold (350 µg/m^3 as an hourly mean). In some locations, the number of events where SO_2 concentrations exceeded threshold levels was greater than the ID annual limit (24 events as an annual total). Even the very far-field (G6 and G7, $>$ 250 km distance, Figure 4.7) recorded a lower but measurable impact to air quality. The dense network of reference-grade AQ SO_2 stations allowed us to document very fine-scale variations in the ground-level dispersion of the volcanic plume and consequent impacts to air quality. The most common direction of volcanic plume advection was towards the north or north-west from the eruption site, as shown by Figure 4.2 (G1/W inset), and recorded by the highest and most-frequent above-threshold concentrations of SO_2 at AQ stations situated in these downwind locations [Figures 4.5, 4.6, 4.7]. However, the frequency and intensity of the SO_2 peaks at ground-level varied significantly, even within the predominant north-northwest direction. A good example of this is the difference between the AQ station measurements across the Reykjanes Peninsula (G2, Figure 4.6). Stations B-F are all located to the north and northwest of the eruption site with a maximum of 16 km distance between the furthest apart stations, but there are large differences in the number of SO_2 air quality threshold exceedances between the stations. Stations E

and F recorded 25 and 20 exceedance events, respectively, while Stations B, C and D recorded between 0 - 4 exceedance events. This highlights the variability in potential health burden from volcanic air pollution even from a relatively small eruption, and in particular when it occurs in close proximity to populated areas.

The eruption also caused a rise in concentrations of fine PM (PM_1, $PM_{2.5}$ and PM_{10}) compared to the pre-eruption background. Analysis of the impact of the eruption on PM concentrations is more challenging than for SO_2 concentrations due to the high variability in PM sources, both natural and anthropogenic, and the sparser AQ measurement network for PM. In particular, none of the stations within 20 km of the eruption site included instrumentation to monitor PM concentrations. In the light of the high variability of SO_2 pollution between AQ stations in this area, it is likely that PM concentrations were also variable, but this was not captured. Due to data availability, the background PM concentrations were based on data from two years preceding the eruption. Considering the high variability in PM across this period, the confidence in our conclusions could be improved in future studies with a longer background time-series that ideally includes 5 - 10 years of non-eruptive PM data. Nevertheless, some conclusions can be made with reasonable confidence. The average concentration of PM_1 in the Reykjavík area increased during the eruption period [Figure 4.8], and the number of exceedances of ID and WHO thresholds for PM_{10} and $PM_{2.5}$ increased across Iceland during the eruption with respect to the pre-eruptive periods (with the exception of $PM_{2.5}$ in the Reykjavík area) [Figures 4.9 and 4.10]. This national impact on PM concentrations is remarkable considering the relatively small size of the eruption. There was also a measurable change in the relative contributions of PM size fractions during the eruption period in the Reykjavík area, with an increase in the PM_1 size fraction relative to particles > 1 µm in diameter [Figure 4.11]. Air quality thresholds (ID and WHO) do not yet exist for PM_1, but studies unequivocally demonstrate a correlation between increased concentrations of PM_1 and negative health outcomes, though, as yet, research into the physical impacts of volcanic aerosol are extremely limited (Chen et al., 2017; Wang et al., 2021; Yang et al., 2018). When sampled at source, volcanic plumes from fissure eruptions contain a large amount of PM_1, but also a substantial proportion of supramicron PM (Ilyinskaya et al., 2017; Martin et al., 2011; Mason et al., 2021). The composition of the two size modes is typically very different, with the finer fraction formed via the conversion of SO_2 gas into sulfate particles and the larger supramicron particles composed of silicate material (i.e. ash, which is found in some small concentrations even in typically ash-poor fissure eruptions). The conversion of SO_2 gas to sulfate particles continues for hours and days after emission from the volcanic vents (Green et al., 2019; Pattantyus et al., 2018), forming new quantities of fine particles and likely resulting in the elevated concentrations of particles in the PM_1 size fraction observed downwind of the eruption site. The smaller impact of the eruption on the

concentrations of $PM_{2.5}$ and PM_{10} compared to the background levels is likely due to the relatively high levels of particles in these size fractions sourced from traffic and dust storms (Butwin et al., 2019; Carlsen and Thorsteinsson, 2021).

It is appropriate to compare the air quality impacts from the 2021 Fagradalsfjall eruption to the 2014 - 2015 Holuhraun eruption, which was the previous most recent volcanic eruption in Iceland and the first Icelandic large fissure eruption since the 18^{th} Century eruption of Laki. The Holuhraun eruption occurred in a very remote, uninhabited location, 250 km from the capital area of Reykjavík, and 90 - 100 km from the nearest town and AQ station. The Holuhraun eruption released a 10 times larger volume of SO_2 than the Fagradalsfjall eruption (9.6 Mt as opposed to 0.3 - 0.9 Mt) (Pfeffer et al., 2018). This provides an interesting comparison regarding the impacts of volcanic emissions on air quality when concerned with a relatively small eruption that is in proximity to population centres, relative to a larger eruption located far away from settlements. A comparison of the exceedances of the ID hourly SO_2 threshold during the Holuhraun and Fagradalsfjall eruptions at measurement stations around Iceland is shown in Table 4.2. During the Fagradalsfjall eruption, the ID hourly threshold of $350\,\mu g/m^3$ was exceeded regularly in proximal locations ($\leq$ 3 km distance), with an average of 289 threshold-exceedance events across the five eruption-response stations (G1). Further afield, exceedances of the ID threshold were greatly reduced, with individual stations recording a maximum of 25 exceedance events at 14 km from the eruption site [G2, Table 4.2], 9 exceedance events at 35 km from the eruption site [G3, Table 4.2] and 18 exceedance events at 45 km from the eruption site [G4, Table 4.2]. The impact of the Holuhraun eruption on SO_2 concentrations was more far-reaching, predominately as a result of its significantly higher emission rate. At 100 km from the eruption site, the monitoring station at Höfn recorded exceedances of SO_2 above the ID threshold on 124 instances [Table 4.2]. SO_2 concentrations exceeded the ID threshold on 59 instances in the capital area of Reykjavík, at 250 km away from the eruption source [Table 4.2]. As such, although the Holuhraun eruption was located in a rural area, the enormous scale of the eruption resulted in far-reaching air quality impacts. Although on a smaller scale, the relative proximity of the Fagradalsfjall eruption meant that SO_2 emissions could more readily reach inhabited areas, where the dense population resulted in high numbers of population exposure [Table 4.2]. The proximity and relative ease of access to the Fagradalsfjall eruption also meant that the eruption site was visited by a huge number of people who likely exposed themselves to unhealthy concentrations of SO_2, as shown in this study. Note that access to the Holuhraun eruption site was only available to scientists, journalists and other key staff, which reduced the number of people potentially impacted.

For the Holuhraun eruption, the number of reference-grade AQ stations was significantly smaller than those available to monitor the Fagradalsfjall eruption, in particular

with respect to SO_2 monitors. As shown by our results, significant fluctuations in volcanic SO_2 can occur on finer spatial scales than could have been resolved by such a sparse network, particularly for those areas within 20 km distance of the eruption. Arguably, the Holuhraun eruption did not require a dense reference-grade network at proximal distances from the eruption site as the closest towns were located relatively far away ($\approx$ 90 - 100 km). However, it is possible that significant pollutant fluctuations occurred in the far-field that were not captured by the network available at the time. Our results are in good agreement with Crawford et al., 2021 who augmented the reference-grade network on the Island of Hawai'i during the 2018 LERZ eruption with low-cost sensors and found a significant improvement in the ability to assess the population exposure on smaller spatial scales. The instrument cost for reference-grade stations is very high ($\approx$ £135,000 for one reference-grade station including SO_2 and PM instrumentation, (Whitty et al., 2022)), and they require significant infrastructure, maintenance and running costs. Use of low-cost sensors to augment a sparse reference-grade network, such as done by Crawford et al., 2021 and as discussed in Whitty et al., 2020, can improve the spatial and temporal resolution of AQ measurements and allow a developed understanding of how the volcanic pollutants are distributed across smaller localised areas than is often manageable solely by the use of reference-grade stations. However, as discussed by Whitty et al., 2022, low-cost sensors must be deployed with due consideration for their limitations and with strategies in place to maximise their potential and reduce errors in the collected data.

Table 4.2: Comparison of the frequency of volcanic pollutants (SO_2 and $PM_{2.5}$) exceeding health thresholds during the 2014 - 2015 Holuhraun eruption and the 2021 Fagradalsfjall eruption. Health thresholds used are the ID hourly limit of 350 µg/m^3 for SO_2 and the WHO daily-mean limit of 15 µg/m^3 for $PM_{2.5}$. Exceedance data for the Holuhraun eruption sourced from Gíslason et al., 2015, and SO_2 total emission estimate from Pfeffer et al., 2018. Exposed population in Iceland is shown for the municipality or municipalities in the area of the measurement station, 2020 data from Statistics Iceland.

2021 Fagradalsfjall Eruption, Iceland (Total SO_2 emission of 0.3 - 0.9 Mt over 6 months)				
Monitoring group	Distance from eruption (km)	No. events where hourly $SO_2 > 350$ µg/m^3 (Mean and [range])	No. events where 24-hr $PM_{2.5} > 15$ µg/m^3 (Mean and [range])	Approx. population in area (2020 data)
G1 - eruption	0.6 to 3	289 [0 to 1372]	-	3,500
G2 - Reykjanes P.	9 to 22	9 [0 to 25]	-	25,000
G3 - Reykjavík	22 to 36	4 [0 to 9]	10 [3 - 32]	210,000
G4 - SW Iceland	45 to 50	11 [3 to 18]	-	2,500
G5 - Hvalfjörður	60	5 [2 to 6]	9 [9]	1,000
G6 - E Iceland	400	0.5 [0 to 1]	-	6,000
G7 - N Iceland	280 to 340	0 [0]	1 [0 -2]	19,000
2014 - 2015 Holuhraun Eruption, Iceland (Total SO_2 emission of 9.6 Mt over 6 months)				
Monitoring station	Distance from eruption (km)	No. events where hourly $SO_2 > 350$ µg/m^3	No. events where 24-hr $PM_{2.5} > 15$ µg/m^3	Approx. population in area (2020 data)
Mývatn	90	86	-	8,000
Höfn	100	124	-	2,500
Reyðafjörður (G6)	125	58	-	6,000
Reykjavík (G3)	250	59	-	210,000

4.4.2 Performance of operational forecasting for dispersion of volcanic pollutants

We analysed the capability of the CALPUFF model in forecasting a) the presence or absence of volcanic SO_2 at ground level, and b) the concentration of SO_2 at ground level and the resulting exceedances of the ID SO_2 AQ threshold ($350\,\mu g/m^3$ as an hourly-mean). The CALPUFF model output we analysed was the same as was used for operational forecasting and release of public advisories during the Fagradalsfjall eruption. In summary, the CALPUFF model was found to effectively determine when volcanic SO_2 was present at ground level, but the predicted concentrations and threshold exceedances were much less accurate.

For the determination of plume presence there was a 79% rate of true-positives, where the CALPUFF model forecast the presence of volcanic SO_2 at ground-level within the set time window (5 hours) of the AQ station at Kópavogur Dalsmári detecting volcanic SO_2 [Figure 4.12A]. Similarly the CALPUFF model was successful at forecasting when volcanic SO_2 would be absent at the AQ station, with a rate of 80% true-negatives [Figure 4.12A]. False positives (where SO_2 was forecast but not measured at the AQ station) and false negatives (where the plume was not forecast but was measured by the AQ station) were only 21% and 20%, respectively [Figure 4.12A].

There were higher levels of uncertainty and error in the CALPUFF model when it was used to determine the ground-level concentrations of SO_2 within 70 km of the eruption location. Re-scaling of the CALPUFF model to forecast exceedances above $800\,\mu g/m^3$ correlated better to the AQ network observations of SO_2 exceeding $350\,\mu g/m^3$ [Figure 4.4]. The accuracy of the rescaled model output varied with distance from the eruption site. It was more accurate in the near-field ($\leq$ 15 km from the eruption), and less accurate at distances $>$ 15 km, which included the densely-populated capital area of Reykjavík (20 - 35 km from the eruption). In the Reykjavík area, the number of SO_2 threshold exceedances forecast by the rescaled model output were lower than the number which were observed at the AQ stations (1 or fewer events forecast, with a maximum of 9 events observed) [Figure 4.4].

Our results highlight the challenge in achieving accurate simulations of volcanic plume dispersion, as well as the importance for ongoing research and development in this area. While the CALPUFF model output in this study was $\approx$ 80% accurate at forecasting the absolute presence or absence of volcanic SO_2, as determined from a point-analysis, its performance remains to be improved with respect to forecasting the exact concentrations of volcanic SO_2. Advancing this capability of volcanic dispersion models is important, not only for its use with respect to forecasting air quality and health implications, but also for studies investigating the impact of volcanic emissions on weather and climate.

4.4.3 Comparison of ground-based observations with satellite imagery

This analysis is a small but important contribution to the understanding of volcanic plume detection by satellite imagery and the plume's vertical position in the atmospheric column. At volcanoes where there are no ground-based observations readily available, satellite imagery can be the only tool to monitor volcanic eruptions, as was shown most recently by the 2022 volcanic eruption at Hunga Tonga Hunga Ha'apai. As such, all comparisons between ground-based and satellite data, as presented here, provide valuable data points towards understanding the use of satellite imagery for monitoring of volcanic plumes.

Our analysis of the Sentinel-5p SO_2 satellite imagery (using Kópavogur Dalsmári as our case study location) showed that SO_2 in the volcanic plume grounded 36% of the measurement time [Figure 4.12B]. For the rest of the time the SO_2 plume remained lofted. This result is not directly applicable to other eruptions due to factors including differences in volcanic activity, SO_2 flux and its injection height, as well as the meteorological conditions and local topography. What our results do indicate is that caution should be implemented when using satellite data to identify the presence of volcanic SO_2 at ground level and the resulting impacts on air quality and health impacts.

4.4.4 Population exposure to above-threshold volcanic SO_2 levels

The general population exposure to potentially unhealthy levels of SO_2 occurred predominantly within a 20 km radius of the volcanic eruption site [Figure 4.13C], in the municipalities on the Reykjanes Peninsula. In this region, $\approx$ 47,000 residents ($\approx$ 8,500 of which were in more-vulnerable age categories) were forecast to be potentially exposed to SO_2 concentrations exceeding health thresholds more than 24 times, which also exceeds the ID recommended annual level (24 exceedances). It remains to be investigated whether this high level of exposure to SO_2 during the Fagradalsfjall eruption is translated into measurable health impacts.

The Reykjavík capital area (20 to 35 km from the eruption) experienced up to 9 SO_2 threshold exceedances, as recorded by the air quality network. As discussed in previous sections, the performance of the CALPUFF dispersion model for the number of exceedances of the ID threshold was sub-optimal in this area. With respect to the likely public health impacts, it was fortunate that the volcanic pollutants were predominantly transported to the north and northwest of the eruption site, reducing the number of SO_2 pollution episodes in the densely-populated capital area. The Reykjavík capital area not only contains most of Iceland's population ($\approx$ 210,000 residents, 60% of the total population), but also contains a large number of the major and minor hospitals hosting some of the most vulnerable individuals due to pre-existing health conditions.

The very high spatial and temporal variability in the SO_2 pollution dispersion was

a confounding factor to our population exposure analysis. We used a municipality-level population dataset, but as shown by our results the pollutant levels varied significantly on a much finer scale. The high variability likely results in further uncertainties in the population analysis. People who spend their working hours at some distance from their place of residence will likely have been exposed to different levels of volcanic pollution than is predicted from our analysis. For example, G2 Station A in the township of Grindavík recorded one event where SO_2 concentrations exceeded the ID threshold [Figure 4.6], but many of the residents of Grindavík work at Keflavik airport which recorded higher levels of SO_2 pollution [Figure 4.6, G2 Station D]. The reverse may apply for residents of Vogar (Figure 4.6, G2 Station F], many of whom work in the Reykjavík capital area, which was exposed to fewer events where SO_2 concentrations exceeded the ID threshold. The estimated exposure of children was likely more accurate than for adults because children tend to go to schools within walking distance or minimal commuting distance from their homes.

An interesting aspect of the eruption was that even though it took place in an uninhabited location, the site quickly became akin to a populated area due to the extremely high number of visitors ($\approx$ 300,000 people over the six months of the eruption, peaking at 6,000 visitors a day). There was a considerable effort by the national and local authorities and agencies to reduce the risk posed both by volcanic hazards and also those from the general outdoor environment. This included the installation of the five eruption-response AQ stations used in this analysis [G1]. The reason for the installation of a relatively dense near-field AQ network was that the agencies quickly recognised the highly variable dispersal pattern of volcanic SO_2 in the near-field, as was confirmed quantitatively by our results [Figure 4.5]. The high variability is a combination of the volcanic activity as well as local meteorological conditions and the local topography. Volcanic plumes can, on occasion, collapse and spread laterally as a result of thermal inversion, causing extremely high concentrations of SO_2 even at locations upwind of the volcanic vent. Our results show that the visitors to the eruption site had a much higher likelihood of being exposed to above-threshold concentrations of SO_2 than the general population across Iceland as a whole. We note that our estimate of the number of above-threshold events is likely a worst-case scenario because of the precautionary measures taken by the agencies. The visitors were clearly advised to remain upwind of the active craters and the lava field, and the site was staffed by rescue team members equipped with hand-held gas monitors. Staff members evacuated parts of the eruption site when SO_2 concentrations exceeded threshold levels. Nevertheless, it is likely that at least some visitors did experience potentially unhealthy levels of SO_2. This is supported by anecdotal reports in the Icelandic media regarding individuals accessing health care providers after visiting the eruption site, reportedly feeling unwell from the emissions. The footpath network leading to the eruption viewpoints included an elevation ascent

of ≈ 200 m, making it likely that visitors were undergoing physical exertion during periods of time that they were within 3 km of the eruption. High levels of physical exertion during exposure to air pollution can increase the exposure of the respiratory system which may result in more significant health impacts (International Volcanic Health Hazard Network, 2020; Pohl, 1998; Williams-Jones and Rymer, 2015).

4.5 Conclusions

The 2021 Fagradalsfjall eruption in Iceland provided an excellent opportunity to investigate the impact of a small-scale volcanic eruption on air quality around Iceland and with respect to nearby densely-populated areas. The Fagradalsfjall eruption was the first eruption in modern history to occur nearby to the capital area of Reykjavík. The dense network of reference-grade air quality stations allowed investigation into the spatial and temporal variations in dispersion of the volcanic pollutants. Air quality with respect to SO_2 concentrations was found to be most severely affected within a 20 km radius of the volcanic eruption site, with a recorded 45 instances (across two stations) where SO_2 concentrations in the northwest of the Reykjanes Peninsula exceeded the Icelandic Directive hourly threshold of $350\,\mu g/m^3$. The six AQ stations across the capital area of Reykjavík recorded 25 instances of SO_2 concentrations exceeding the ID hourly threshold. In the distal measurement stations in East (400 km distance) and North Iceland ($>$ 280 km distance), air quality impacts were lower but measurable. PM concentrations likewise increased around Iceland during the eruption. Across the measurement stations in the Reykjavík area, maximum concentrations of PM_1 and PM_{10} increased with respect to the background pre-eruptive measurement periods. Deployment of five eruption-response SO_2 monitors within 3 km of the eruption site allowed analysis of emissions at source, and the potential air quality hazard level for the ≈ 300,000 visitors to the eruption site.

A population exposure analysis with the CALPUFF dispersion model indicated that 47,000 Icelandic residents (≈ 13% of the population) were potentially exposed to concentrations of SO_2 exceeding the ID hourly threshold on more than 24 occurrences, which exceeds the ID recommended annual limit. Of those 47,000 residents, 8,500 (≈ 2.2% of the population) were identified as being in potentially more vulnerable age categories. Exposure to volcanic SO_2 in the capital area of Reykjavík was underestimated by the CALPUFF model, but AQ stations in the area indicated that there were up to nine events where SO_2 concentrations exceeded the threshold. Such exposure to volcanic pollutants is likely to have health impacts in those individuals frequently subjected to above-threshold concentrations of SO_2 or PM.

In comparison to the 2014 - 2015 Holuhraun eruption in Iceland, the 2021 Fagradalsfjall eruption was on a much smaller scale, releasing significantly lower total emissions

of SO_2. However, the eruption's proximity to densely-populated centres means that there were high numbers of population exposure to volcanic pollutants. The exposure was mitigated by the prevailing wind directions during the eruption period, which predominantly dispersed the volcanic emissions away from the capital area of Reykjavík. The dense network of reference-grade AQ stations around Iceland, particularly in the area < 70 km from the eruption site, provided fine-detail information regarding the high variability in the spatial and temporal air quality during the eruption period.

Acknowledgments

The authors would like to thank Kristín Björg Ólafsdóttir from the Icelandic Meteorological Office for compiling wind data from the Fagradalsfjall eruption site.

Author contributions

RCWW performed the data analysis and wrote the original draft. EI, SB, MAP, TR and AS contributed to data interpretation and manuscript drafting. SB ran the CALPUFF model and contributed to CALPUFF re-scaling for population analysis. TH, GMG and MAP designed, built and maintained IMO's measurement and data systems. ÞJ contributed access to and information on the municipality AQ network. DF and RHÞ assisted with ArcGIS ArcMap analysis methodology. GGS supplied the data from footpath counters. EMS facilitated use of satellite imagery. All coauthors contributed to draft review and editing.

Funding

RCWW is funded by the Leeds-York Natural Environment Research Council (NERC) Doctoral Training Partnership (DTP) NE/L002574/1, in CASE partnership with the Icelandic Meteorological Office. TJR is funded by the ANR Projet de Recherche Collaborative VOLC-HAL-CLIM (Volcanic Halogens: from Deep Earth to Atmospheric Impacts) ANR-18-CE01-0018, and Labex Orléans Labex VOLTAIRE (VOLatils-Terre Atmosphère Interactions–Ressources et Environnement, ANR-10-LABX-100-0).

References

Airpointer. (2021). Number 1 compact air quality monitoring system [(Accessed 15/11/2021)]. *https://www.airpointer.com/#sc-tabs-163697338033*.

Alphasense. (2021). SO2-B4 Sulfur Dioxide Sensor Data Sheet [(Accessed 05/02/2021)]. *https://www.alphasense.com/wp-content/uploads/2019/09/SO2-B4.pdf*.

ATSDR. (1998). Agency for Toxic Substances and Disease Registry; public health statement sulfur dioxide [Available at: https://www.atsdr.cdc.gov/ToxProfiles/tp116-c1-b.pdf]. *7446-09-5*.

Barsotti, S. (2020). Probabilistic hazard maps for operational use: The case of SO2 air pollution during the Holuhraun eruption (Bárðarbunga, Iceland) in 2014–2015 [DOI: https://doi.org/10.1007/s00445-020-01395-3]. *Bulletin of Volcanology*, *82*(7), 1–15.

Butwin, M. K., von Löwis, S., Pfeffer, M. A., & Thorsteinsson, T. (2019). The effects of volcanic eruptions on the frequency of particulate matter suspension events in Iceland [DOI: https://doi.org/10.1016/j.jaerosci.2018.12.004]. *Journal of Aerosol Science*, *128*, 99–113.

Carlsen, H. K., Ilyinskaya, E., Baxter, P., Schmidt, A., Thorsteinsson, T., Pfeffer, M., Barsotti, S., Dominici, F., Finnbjornsdottir, R. G., Jóhannsson, T., Aspelund, T., Gislason, T., Valdimarsdóttir, U., Briem, H., & Gudnason, T. (2021a). Increased respiratory morbidity associated with exposure to a mature volcanic plume from a large Icelandic fissure eruption [DOI: https://doi.org/10.1038/s41467-021-22432-5]. *Nature Communications*, *12*.

Carlsen, H. K., & Thorsteinsson, T. (2021). Associations between PM_{10} from traffic, resuspension, sand storms and volcanic sources and asthma drugs dispensing [Preprint, DOI: https://doi.org/10.21203/rs.3.rs-1017409/v1].

Carlsen, H. K., Valdimarsdóttir, U., Briem, H., Dominici, F., Finnbjornsdottir, R. G., Jóhannsson, T., Aspelund, T., Gislason, T., & Gudnason, T. (2021b). Severe volcanic SO2 exposure and respiratory morbidity in the Icelandic population–a register study [DOI: https://doi.org/10.1186/s12940-021-00698-y]. *Environmental Health*, *20*(1), 1–12.

Chen, G., Li, S., Zhang, Y., Zhang, W., Li, D., Wei, X., He, Y., Bell, M. L., Williams, G., Marks, G. B. et al. (2017). Effects of ambient PM_1 air pollution on daily emergency hospital visits in China: An epidemiological study [DOI: https://doi.org/10.1016/S2542-5196(17)30100-6]. *The Lancet Planetary Health*, *1*(6), e221–e229.

Cohen, A. J., Ross Anderson, H., Ostro, B., Pandey, K. D., Krzyzanowski, M., Künzli, N., Gutschmidt, K., Pope, A., Romieu, I., Samet, J. M. et al. (2005). The global burden of disease due to outdoor air pollution [DOI: https://doi.org/10.1080/15287390590936166]. *Journal of Toxicology and Environmental Health, Part A*, *68*(13-14), 1301–1307.

Crawford, B., Hagan, D. H., Grossman, I., Cole, E., Holland, L., Heald, C. L., & Kroll, J. H. (2021). Mapping pollution exposure and chemistry during an extreme air quality event (the 2018 Kı¯lauea eruption) using a low-cost sensor network [DOI: https://doi.org/10.1073/pnas.2025540118]. *Proceedings of the National Academy of Sciences*, *118*(27).

CRI. (2004). The Centre for Research Information, health effects of project shad chemical agent: Sulfur dioxide [cas 7446-09-5]. *National Academies*.

Crowcon. (2021). Xgard Fixed Gas Detector [(Accessed 15/11/2021)]. *https://www.crowcon.com/wp-content/uploads/2020/07/Xgard-Data-Sheet-Interactive.pdf*.

Delmelle, P., Stix, J., Baxter, P., Garcia-Alvarez, J., & Barquero, J. (2002). Atmospheric dispersion, environmental effects and potential health hazard associated with the low-altitude gas plume of Masaya volcano, Nicaragua [DOI: https://doi.org/10.1007/s00445-002-0221-6]. *Bulletin of Volcanology*, *64*(6), 423–434.

Eco Counter. (2021). PYRO-Box [(Accessed 09/11/2021)]. *https://www.eco-counter.com/produits/pyro-range/pyro-box/*.

Gıślason, S. R., Stefansdottir, G., Pfeffer, M., Barsotti, S., Jóhannsson, T., Galeczka, I. M., Bali, E., Sigmarsson, O., Stefánsson, A., Keller, N. S. et al. (2015). Environmental pressure from the 2014–15 eruption of Bárðarbunga volcano, Iceland [DOI: https://hdl.handle.net/20.500.11815/447].

Green, J. R., Fiddler, M. N., Holloway, J. S., Fibiger, D. L., McDuffie, E. E., Campuzano-Jost, P., Schroder, J. C., Jimenez, J. L., Weinheimer, A. J., Aquino, J. et al. (2019). Rates of wintertime atmospheric SO2 oxidation based on aircraft observations during clear-sky conditions over the eastern United States [DOI: https://doi.org/10.1029/2018JD030086]. *Journal of Geophysical Research: Atmospheres*, *124*(12), 6630–6649.

Hansell, A., & Oppenheimer, C. (2004). Health hazards from volcanic gases: A systematic literature review [DOI: https://doi.org/10.1080/00039890409602947]. *Archives of Environmental Health: An International Journal*, *59*(12), 628–639.

HM Government. (2020). National Risk Register 2020 edition [Available at: https://assets.publishing.service.gov.uk/government/uploads/system/uploads/attachment_data/file/952959/6.6920_CO_CCS_s_National_Risk_Register_2020_11-1-21-FINAL.pdf].

Holgate, S. (2017). "Every breath we take: the lifelong impact of air pollution" - a call for action [DOI: https://doi.org/10.7861/clinmedicine.17-1-8]. *Clinical Medicine*, *17*(1), 8–12.

Icelandic Directive. (2016). Reglugerð um brennisteinsdíoxíð, köfnunarefnisdíoxíð og köfnunarefnisoxíð, bensen, kolsýring, svifryk og blý í andrúmsloftinu [Available at: https://www.reglugerd.is/reglugerdir/eftir-raduneytum/umhverfisraduneyti/nr/20277]. *B-deild*, *Nr.920*.

Icelandic Meteorological Office. (2021a). "The small eruption" in Fagradalsfjall celebrates six months [(Accessed 27/10/2021)]. *https://en.vedur.is/about-imo/news/the-small-eruption-in-fagradalsfjall-celebrates-six-months*.

Icelandic Meteorological Office. (2021b). Re-evaluation needed of the size of the hazard area [(Accessed 08/09/2021)]. *https://en.vedur.is/about-imo/news/new-fissure-near-the-eruption-site-in-geldingadalir*.

Icelandic Meteorological Office. (2021c). The Civil protection crisis level lowered from alert to uncertainty phase [(Accessed 27/10/2021)]. *https://en.vedur.is/about-imo/news/the-civil-protection-crisis-level-lowered-from-orange-to-yellow-for-the-volcano-in-fagrdalsfjall*.

Icelandic Meteorological Office. (2021d). Volcanic gases [(Accessed 08/09/2021)]. *https://en.vedur.is/volcanoes/fagradalsfjall-eruption/volcanic-gases*.

Ilyinskaya, E., Mason, E., Wieser, P., Holland, L., Liu, E., Mather, T., Edmonds, M., Whitty, R., Elias, T., Nadeau, P., Schneider, D., McQuaid, J., Allen, S., Harvey, J., Oppenheimer, C., Kern, C., & Damby, D. (2021). Rapid metal pollutant deposition from the volcanic plume of Kı¯lauea, Hawai'i [DOI: https://doi.org/10.1038/s43247-021-00146-2]. *Communications Earth and Environment*.

Ilyinskaya, E., Schmidt, A., Mather, T. A., Pope, F. D., Witham, C., Baxter, P., Jóhannsson, T., Pfeffer, M., Barsotti, S., Singh, A. et al. (2017). Understanding the environmental impacts of large fissure eruptions: Aerosol and gas emissions from the 2014–2015 Holuhraun eruption (Iceland) [DOI: https://doi.org/10.1016/j.epsl.2017.05.025]. *Earth and Planetary Science Letters*, *472*, 309–322.

International Volcanic Health Hazard Network. (2020). The health hazards of volcanic and geothermal gases: A guide for the public [(Accessed 12/4/2021)]. *https://www.ivhhn.org/information/health-impacts-volcanic-gases#Howtolivewithvolcanicemissions*.

Langmann, B. (2014). On the role of climate forcing by volcanic sulphate and volcanic ash [DOI: https://doi.org/10.1155/2014/340123]. *Advances in Meteorology*, *2014*, 1–17.

Lim, S. S., Vos, T., Flaxman, A. D., Danaei, G., Shibuya, K., Adair-Rohani, H., Al-Mazroa, M. A., Amann, M., Anderson, H. R., Andrews, K. G. et al. (2012). A comparative risk assessment of burden of disease and injury attributable to 67 risk factors and risk factor clusters in 21 regions, 1990–2010: A systematic analysis for the Global Burden of Disease Study 2010 [DOI: https://doi.org/10.1016/S0140-6736(12)61766-8]. *The lancet*, *380*(9859), 2224–2260.

Martin, R. S., Ilyinskaya, E., Sawyer, G. M., Tsanev, V. I., & Oppenheimer, C. (2011). A re-assessment of aerosol size distributions from Masaya volcano (Nicaragua) [DOI: https://doi.org/10.1016/j.atmosenv.2010.10.049]. *Atmospheric Environment*, *45*(3), 547–560.

Mason, E., Wieser, P., Liu, E., Edmonds, M., Ilyinskaya, E., Whitty, R., Mather, T., Elias, T., Nadeau, P., Wilkes, T. et al. (2021). Volatile metal emissions from volcanic degassing and lava-seawater interactions at Kı¯lauea Volcano, Hawai'i [DOI: https://doi.org/10.1038/s43247-021-00145-3]. *Communications Earth and Environment*.

Met One Instruments Inc. (2020). BAM 1020 Beta Attenuation Mass Monitor [(Accessed 15/11/2021)]. *https://metone.com/wp-content/uploads/2020/10/BAM-1020-N.pdf*.

Organisation for Economic Cooperation and Development. (2022). Emissions of air pollutants [Available at: https://stats.oecd.org/Index.aspx?DataSetCode=AIR_EMISSIONS]. *OECD.Stat*.

Palas. (2021). Fine dust measurement device Fidas 200 S [(Accessed 15/11/2021)]. *https://www.palas.de/en/product/download/fidas200s/datasheet/pdf*.

Pattantyus, A. K., Businger, S., & Howell, S. G. (2018). Review of sulfur dioxide to sulfate aerosol chemistry at Kı¯lauea Volcano, Hawai'i [DOI: https://doi.org/10.1016/j.atmosenv.2018.04.055]. *Atmospheric Environment*, *185*, 262–271.

Pedersen, G. B. M., Belart, J. M. C., Óskarsson, B. V., Gudmundsson, M. T., Gies, N. B., Högnadóttir, T., Hjartardóttir, Á. R., Pinel, V., Berthier, E., Dürig, T., & et al. (2021). Volume, effusion rate, and lava transport during the 2021 Fagradalsfjall eruption: Results from near real-time photogrammetric monitoring [DOI: https://doi.org/10.1002/essoar.10509177.1]. *Earth and Space Science Open Archive*, 20.

Pfeffer, M. A., Bergsson, B., Barsotti, S., Stefánsdóttir, G., Galle, B., Arellano, S., Conde, V., Donovan, A., Ilyinskaya, E., Burton, M., Aiuppa, A., Whitty, R. C. W., Simmons, I. C., Arason, T., Jónasdóttir, E., Keller, N., Yeo, R. F., Arngrímsson, H., Jóhannsson, T., ... Mereu, L. (2018). Ground-based measurements of the 2014–2015 Holuhraun volcanic cloud (Iceland) [DOI: https://doi.org/10.3390/geosciences8010029]. *Geosciences*, *8*(1), 29.

Pohl, H. R. (1998). Toxicological profile for sulfur dioxide [Available at: https://www.atsdr.cdc.gov/toxprofiles/tp116.pdf]. *U.S. Department for Health and Human Services*.

Schmidt, A., Leadbetter, S., Theys, N., Carboni, E., Witham, C., Stevenson, J., Birch, C., Thordarson, T., Turnock, S., Barsotti, S., Delaney, L., Feng, W., Grainger, R., Hort, M., Höskuldsson, Á., Ialongo, I., Ilyinskaya, E., Jóhannsson, T., Kenny, P., ... Shepherd, J. (2015). Satellite detection, long-range transport, and air quality impacts of volcanic sulfur dioxide from the 2014–2015 flood lava eruption at Bárðarbunga (Iceland) [DOI: https://doi.org/10.1002/2015JD023638]. *Journal of Geophysical Research: Atmospheres*, *120*(18), 9739–9757.

Schmidt, A., Ostro, B., Carslaw, K. S., Wilson, M., Thordarson, T., Mann, G. W., & Simmons, A. J. (2011). Excess mortality in Europe following a future Laki-style Icelandic eruption [DOI: https://doi.org/10.1073/pnas.1108569108]. *Proceedings of the National Academy of Sciences*, *108*(38), 15710–15715.

Scire, J. S., Strimaitis, D. G., Yamartino, R. J. et al. (2000). A user's guide for the CALPUFF dispersion model [Available at: http://www.src.com/CALPUFF/download/CALPUFF_UsersGuide.pdf]. *Earth Tech, Inc*, *521*, 1–521.

Stewart, C., Damby, D. E., Horwell, C. J., Elias, T., Ilyinskaya, E., Tomašek, I., Longo, B. M., Schmidt, A., Carlsen, H. K., Mason, E. et al. (2022). Volcanic air pollution and human health: Recent advances and future directions [DOI: https://doi.org/10.1007/s00445-021-01513-9]. *Bulletin of Volcanology*, *84*(1), 1–25.

Tam, E., Miike, R., Labrenz, S., Sutton, A. J., Elias, T., Davis, J., Chen, Y.-L., Tantisira, K., Dockery, D., & Avol, E. (2016). Volcanic air pollution over the Island of Hawai'i: Emissions, dispersal, and composition. association with respiratory symptoms and lung function in Hawai'i Island school children [DOI: https://doi.org/10.1016/j.envint.2016.03.025]. *Environment international*, *92*, 543–552.

Teledyne. (2019). The Model T100 UV Fluorescence SO_2 Analyzer [(Accessed 15/11/2021)]. *https://www.teledyne-api.com/prod/Downloads/SAL000039H%20-%20T100.pdf*.

Thermo Scientific. (2017). Model 450i hydrogen sulfide and sulfur dioxide analyzer [(Accessed 15/11/2021)]. *https://www.thermofisher.com/document-connect/document-connect.html?url=https://assets.thermofisher.com/TFS-Assets%2FLSG%2FSpecification-Sheets%2FEPM-450i-Datasheet.pdf*.

Thermo Scientific. (2021). 5030i SHARP Synchronized Hybrid Ambient Real-time Particulate Monitor [(Accessed 15/11/2021)]. *https://www.thermofisher.com/document-connect/document-connect.html?url=https://assets.thermofisher.com/TFS-Assets%2FCAD%2FSpecification-Sheets%2FD01460.pdf*.

Wang, H., Lu, F., Guo, M., Fan, W., Ji, W., & Dong, Z. (2021). Associations between PM_1 exposure and daily emergency department visits in 19 hospitals, Beijing [DOI: https://doi.org/10.1016/j.scitotenv.2020.142507]. *Science of The Total Environment*, *755*, 142507.

Whitty, R., Pfeffer, M., Ilyinskaya, E., Roberts, T., Schmidt, A., Barsotti, S., Strauch, W., Crilley, L., Pope, F., Bellanger, H., Mendoza, E., Mather, T., Liu, E., Peters, N., Taylor, I., Francis, H., Hernández Leiva, X., Lynch, D., Nobert, S., & Baxter, P. (2022). Effectiveness of low-cost air quality monitors for identifying volcanic SO_2 and PM downwind from Masaya volcano, Nicaragua [DOI: https://doi.org/10.30909/vol.05.01.3359]. *Volcanica*, *5*(1), 33–59.

Whitty, R. C. W., Ilyinskaya, E., Mason, E., Wieser, P. E., Liu, E. J., Schmidt, A., Roberts, T., Pfeffer, M. A., Brooks, B., Mather, T. A., Edmonds, M., Elias, T., Schneider, D. J., Oppenheimer, C., Dybwad, A., A, N. P., & Kern, C. (2020). Spatial and temporal variations in SO_2 and $PM_{2.5}$ levels around Kīlauea volcano, Hawai'i during 2007–2018 [DOI: https://doi.org/10.3389/feart.2020.00036]. *Frontiers in Earth Science*, *8*, 36.

Williams-Jones, G., & Rymer, H. (2015). Hazards of volcanic gases [DOI: https://doi.org/10.1016/B978-0-12-385938-9.00057-2]. *The Encyclopedia of Volcanoes*, *2*, 985–992.

World Health Organization. (2021). Ambient (outdoor) air pollution [Available at: https://www.who.int/news-room/fact-sheets/detail/ambient-(outdoor)-air-quality-and-health].

WorldPop. (2021). The spatial distribution of population in 2020, Iceland [Available at: https://www.worldpop.org/geodata/summary?id=6379]. *Population Counts*.

Yang, M., Chu, C., Bloom, M. S., Li, S., Chen, G., Heinrich, J., Markevych, I., Knibbs, L. D., Bowatte, G., Dharmage, S. C. et al. (2018). Is smaller worse? new insights about associations of PM_1 and respiratory health in children and adolescents [DOI: https://doi.org/10.1016/j.envint.2018.08.027]. *Environment international*, *120*, 516–524.

Chapter 5

Discussion and Conclusions

This thesis examined the SO_2 and particulate air pollution which comes from volcanoes and is dispersed to downwind areas. These pollutants were measured using a number of different instruments, techniques and methods. In this Chapter, I critically examine the methods and outcomes of the previous chapters to discuss future ways of working and methods by which volcanic air quality monitoring networks can be improved. I discuss how monitoring networks must maintain a careful balance between the quantity of the instruments and the quality of data which may be obtained [Section 5.1]. I discuss the use of low-cost instruments for monitoring of downwind volcanic atmospheric pollutants and provide recommendations for how these instruments could be more successfully implemented for this purpose [Section 5.2]. I discuss how low-cost instrument technology may develop in the future [Section 5.3] and how the accessibility of such instrumentation to the public must be balanced by careful validation [Section 5.4]. I examine the use of the CALPUFF plume dispersal model and discuss options to improve the model output with respect to ground-based observations [Section 5.5]. I discuss how the communities living in the areas downwind of the volcanoes in this thesis have adapted to living with volcanic air pollution, and how research can benefit from including local knowledge and community participation [Section 5.6]. Finally, I indicate directions for future work [Section 5.7] and conclude [Section 5.8].

5.1 Optimising air quality monitoring networks

The monitoring networks used through Chapters 2, 3 and 4 of this thesis (Kīlauea volcano, Masaya volcano and Fagradalsfjall volcano, respectively) were composed of various combinations of reference-grade and low-cost instruments. In a scientific idealised case, all regions affected by volcanic air pollutants would have a dense network of reference-grade instrumentation to accurately and precisely determine the concentrations of volcanic SO_2 and particulates that communities may be exposed to. However,

the reality of the situation is less ideal and many regions downwind of degassing volcanoes may have extremely limited air quality monitoring networks, if any at all. In some cases the lack of reference-grade instrumentation may be a result of limited finances or infrastructure, making it difficult to determine ways to improve and progress volcanic pollutant monitoring approaches. In this section, I discuss how we may come to a compromise between the idealised and realistic monitoring options to maximise the potential of the instruments available.

When considering reference-grade air quality monitoring networks, Chapters 2 and 4 could be considered representative end-member examples with regard to the quantity of instruments available in a monitoring network. In Chapter 2, the air quality network across the Island of Hawai'i had a total of six reference-grade stations, while in Chapter 4, twenty-five reference-grade stations were available across Iceland during the 2021 Fagradalsfjall eruption. While Iceland has a considerably larger spatial area compared to the Island of Hawai'i (103,000 km^2 compared to 10,400 km^2), the number of reference-grade instruments was particularly dense across the most populated region, with sixteen reference-grade stations within the 3,000 km^2 area closest to the Fagradalsfjall eruption site [Figure 4.2]. The dense network of reference-grade instruments in this area of Iceland allowed for a more detailed study of the spatial variations in volcanic air quality across local scales than has ever, to my knowledge, been achieved for downwind volcanic monitoring. This level of spatial analysis was not possible in Chapter 2, especially in the near-field areas as no instruments were available within 20 km of the 2018 LERZ eruption emission source.

In an idealised scenario, the Island of Hawai'i would have a similar spatial resolution of reference-grade instruments to that in Iceland. This would provide higher-resolution monitoring, allowing for analysis of small-scale spatial variabilities in pollutant concentrations and a better determination of the altering ratio of gas to aerosol components. A network of limited reference-grade stations, such as that in Hawai'i, may be augmented and improved by installation of a more dense network of low-cost instruments. In Chapter 2, the community-operated network of PurpleAir instruments worked effectively to dramatically increase the spatial resolution of measurement points (Whitty et al., 2020). A similar technique was successfully implemented by Crawford et al., 2021, also during the 2018 LERZ eruption of Kīlauea volcano. As such, high-quality but limited-quantity reference-grade instruments can be balanced by lower-quality instruments in higher numbers to produce a hybrid monitoring approach that balances financial cost while delivering an impactful monitoring network.

Even in scenarios where reference-grade stations are more numerous, such as in Iceland, it can be invaluable to install low-cost instruments to create a finer spatial resolution network than could otherwise be achieved. For example, major hospitals in the most densely-populated areas of Iceland were frequently between 1 - 2 km from

the nearest reference-grade station, which restricted the analysis of pollutant exposure for the most-vulnerable individuals [Section 4.3.4.2]. During the 2021 Fagradalsfjall eruption, instruments located within 16 km of each other recorded an order of magnitude difference in the numbers of events where SO_2 exceeded health thresholds [Figure 4.6], indicating that the volcanic pollution fluctuated on small spatial scales. Installation of low-cost instruments at public buildings such as hospitals, schools and community centres across Iceland would allow a much finer analysis of pollutant dispersal and the potential exposure level of residents in their local areas. Low-cost instruments can therefore be an extremely valuable addition to air quality networks. However, in order to maximise their potential it is necessary to recognise their limitations and to install them with consideration of best-practice methods, as outlined in Section 5.2.

When considering air quality monitoring networks for volcanic areas, the availability of measurement type is as critical as the spatial resolution of the instruments. Wherever possible, measurements of the concentrations of SO_2, PM_1, $PM_{2.5}$ and PM_{10} should be recorded in order to allow investigation into the changing ratios between these pollutant types. In Iceland, there were six reference-grade stations monitoring SO_2 within 20 km of the volcanic eruption, but the nearest reference-grade station for particulate monitoring was 22 km away [Figure 4.2]. Similarly in Hawai‘i, SO_2 data was not available at the Mountain View reference-grade station (20 km from the eruption), nor were $PM_{2.5}$ measurements available at the Volcano Observatory station (35 km away from the eruption) [Table 2.1]. Measurement stations which are restricted to recording only one or two pollutant types limit the analysis that can be achieved, especially in terms of quantifying the changing gas-aerosol ratio as dispersion from the volcanic emission progresses with time.

The work in Chapter 4, as far as I am aware, is the first time that fine volcanic particulates in the PM_1 size mode have been monitored by reference-grade instruments in downwind environments. Volcanic particulate emissions are still relatively poorly understood in comparison to the emissions of gas species. Volcanic aerosol in ash-poor eruptions, such as investigated in this thesis, contain a large mass of very fine PM ($<$1 µm diameter) when sampled at source (Ilyinskaya et al., 2021; Mason et al., 2021), but there is currently a limited understanding of whether the ratio of PM size fractions in volcanic emissions varies as the volcanic plume ages with time and distance from the volcanic vent. It is also unknown whether volcanic particulates have the same ratio of PM size fractions to anthropogenic pollution in built-up urban areas, and from factory and vehicle emissions.

In studies of anthropogenic particulate pollution, fine particulates in the PM_1 size range are particularly of interest as research has demonstrated a correlation between increased concentrations of PM_1 and negative health outcomes (Chen et al., 2017; Wang et al., 2021; Yang et al., 2018). Research is still required to determine if similar correla-

tions occur between exposure to volcanic fine particulates and negative health impacts. PM_1 measurements have only recently started being incorporated into reference-grade air quality networks (the first reference-grade measurements of PM_1 in Iceland started in 2020), but they can provide huge insight into volcanic aerosol emissions and allow investigation into the scientific knowledge gaps indicated above. Currently, the reference-grade air quality network on the Island of Hawai'i does not monitor PM_1 concentrations. During the 2021 Fagradalsfjall eruption, three stations in the Icelandic network included instrumentation to monitor PM_1, though this has now increased to seven stations. Reference-grade instrument networks could be upgraded in future to include measurements across the range of pollutants, allowing analysis of particulates across the size fractions, increasing our knowledge and furthering our scientific understanding of these questions. However, in instances were the financial cost of improving reference-grade networks is a prohibitive factor, low-cost instruments could provide a potential alternative to augment the reference-grade network, provided that they are installed and used in line with the recommendations outlined in Section 5.2.

5.2 Recommendations for low-cost air quality instruments

Throughout this thesis, low-cost instruments were used to monitor volcanic air quality, with varying successes and challenges. It is clear that low-cost air quality instruments need to be used with careful consideration of their limitations. In particular, they should be installed and used in ways that reduce any potential sources of error and uncertainty in their measurements, as well as optimising the advantages of using such low-cost instruments. In this section, I will discuss practical strategies, methods and supporting infrastructure that could be used in future studies to improve the robustness of the low-cost systems for more effective monitoring, with particular focus on monitoring air quality in downwind volcanic environments.

My first recommendation, and one of the key considerations when using low-cost air quality instrumentation, is to ensure that the measurement location is away from potential sources of contaminants. If the purpose of the instrumentation is to measure volcanic air quality, then it is necessary to install the instrument away from direct sources of anthropogenic or natural non-volcanic air pollution. Although it is anticipated that the instrument will measure contaminants beyond the target volcanic pollutants, if the instrument is placed near to a non-volcanic contaminant source, it is likely that this will become the dominant signature that the instrument measures (Lewis et al., 2016; Whitty et al., 2022). In such cases it can become very challenging to identify and analyse the target pollution from the volcanic source, as it may be masked by the nearby non-volcanic contaminants. The low-cost AQMesh pod placed at Rigoberto in the environment downwind from Masaya volcano in Chapter 3 was installed in a location near to a domestic cook-fire chimney, and this likely resulted in the difficulties with

identifying particulate volcanic air pollution at this location [Table 3.3]. In contrast, the PurpleAir instruments installed on the roof of the reference-grade air quality stations in the environment downwind of Kīlauea volcano [Section 2.3.2] were in optimised locations away from pollution sources and the resulting data correlated well to reference-grade monitors (Whitty et al., 2020). When installing a low-cost instrument it is therefore critically important to ensure that the installation site is carefully chosen to minimise sources of nearby non-target pollution.

Secondly, to ensure that the data from the low-cost instruments is trustworthy and at a reasonable level of accuracy, I recommend regular in-field calibration checks against a reference-grade monitor. Most low-cost instruments are calibrated during their manufacturing process (Alphasense, 2015a; Alphasense, 2015b; Alphasense, 2021; Plantower, 2016a). However, for calibration to to be most effective and to accurately indicate the level of instrument bias, the calibration should be completed under the same environmental conditions as the location of instrument installation (AQ-SPEC, 2022a; Bulot et al., 2019; Clements et al., 2017; Malings et al., 2019). In order for the measurements from the low-cost instruments to be quantified and trusted it is necessary that they be periodically calibrated and compared to reference-grade instrumentation in the measuring environment (Bulot et al., 2019; Cross et al., 2017). Regular calibration checks with reference-grade instrumentation will also identify whether the low-cost instrumentation is undergoing measurement drift over time (Roberts et al., 2012; Roberts et al., 2014). If the level of error on the measurements from the low-cost instruments can be established by regular in-field calibration checks then the error can be corrected for and the measurements adjusted to more accurately reflect pollutant concentrations. This is especially necessary following maintenance of the low-cost stations where sensors are replaced and re-calibration is important to determine potential inconsistencies in measurements between individual sensors (Clements et al., 2017; Whitty et al., 2022). The most effective way to establish these calibration checks is to have one or more permanent reference-grade stations under the same volcanic and environmental conditions as the low-cost instruments [Section 3.4.2]. If the monitoring network is established in the manner described in Section 5.1 using a combination of low-cost and reference-grade instrumentation, calibration should be readily accessible via means of periodic co-location of instrument types across the network. The environmental conditions in the measurement location should also be monitored by installation of a meteorological station, periodically reporting accurate measurements of temperature and humidity, allowing for determination of any diurnal drift in measurements from low-cost sensors, and providing humidity measurements for hygroscopic particle correction [Section 1.5.2] (Crilley et al., 2020).

In the case of the low-cost instrument network downwind of Masaya volcano, Nicaragua, there were several challenges which restricted the reliability of the instruments for sus-

tained measurements over long-term installations. The following recommendations are towards improving the life-expectancy and durability of low-cost air quality instruments installed in downwind volcanic environments:

- Instruments can be subject to fast-acting corrosion in downwind volcanic environments which can damage internal circuit boards, sensors and battery units (Li et al., 2018). This was found in the environment downwind of Masaya volcano, where AQMesh pods more frequently exposed to the volcanic plume were found to have a faster corrosion rate of the metal components (Whitty et al., 2022). This could potentially be mitigated by shielding critical internal and external metal components with protective coatings such as epoxy, solder masks or aerosol sprays to reduce the effect of the corrosive environment and lengthen the life-expectancy of individual sensor nodes and hardware (González-Garcıá et al., 2007; Liu et al., 2009).

- If infrastructure is available, use of mains electricity to power low-cost instruments is highly beneficial as it reduces the potential for down-time resulting from delays in charging battery packs (Whitty et al., 2022). In instances were mains power is not a feasible option, provision of solar panels or a small wind turbine to recharge batteries may be a possibility.

- In instances where the maintenance requirements of a low-cost network is high, it is key to have a dedicated team available for the up-keep and maintenance of the network instruments and system. This necessitates training the staff with the skills required to repair or replace sensor nodes.

- In the case of the low-cost AQMesh network installed downwind of Masaya volcano, replacement sensors and parts required international shipping, delaying the up-keep of instruments and extending the offline duration of sensor nodes. These delays could be significantly reduced if a stockpile of the required materials and equipment to resolve technical issues and replace broken components was kept in a location convenient to the network.

My final comment, drawing on the above recommendations, is to caution future researchers with regards to the use of low-cost air quality networks in downwind volcanic environments. Although the compact size and weight of these instruments is appealing for deployment in remote or challenging locations, and the low cost of the instruments is favourable towards constructing a network with a limited financial burden, it is necessary to remember that low-cost sensors may have significant pitfalls with regards to the accuracy, precision and reliability of their measurements (Clements et al., 2017). Installing a network of low-cost sensors across a region, or strategic placement of one sensor in a specific location of interest, is the easy stage of the process. The subsequent and potentially lengthy duration of data analysis to untangle the data-set, establish the

level of trust in the reported data and attempt to determine a meaningful conclusion is a process that must also be recognised and considered. As such, I recommend that low-cost instruments should not be used as the sole means of air quality measurement. They are much more suited to supplement a network of reference-grade monitors [Section 5.1]. Under these conditions, the relationship between the reference-grade monitors and the low-cost instruments can be considered to be symbiotic: the low-cost instruments improve the spatial resolution of the reference-grade network, and the reference-grade monitors act to validate and confirm the concentrations of pollutants measured by the low-cost instruments. In such a way, low-cost instruments can be used effectively to augment a network's spatial resolution, targeting areas of interest and increasing the resolution of pollutant measurements over a local to regional area (Crawford et al., 2021; Whitty et al., 2020). This is particularly beneficial if the measurements from the low-cost sensors are uploaded in real-time, allowing information dissemination to exposed communities during periods of volcanic unrest [Section 5.4]. Future research using low-cost sensors for downwind volcanic monitoring should therefore proceed with due caution, taking into full consideration the potential limitations of the instrumentation and the recommended use of strategies and selected targeted infrastructure to maximise the instruments' potential.

5.3 Future technical development of low-cost instruments

The use of low-cost sensors has rapidly become widespread among the air-quality community, with relatively inexpensive sensors providing options for user-friendly, off-the-shelf particulate and gas monitoring. Most low-cost sensors have been introduced relatively recently (first patented at the end of the 20$^{\text{th}}$ Century), in comparison to the more traditional reference-grade methods of air quality monitoring. As such, the low-cost sensor market is in a near-constant state of flux as new sensor models and versions are designed, manufactured and released. This dynamic market provides frequent new opportunities for low-cost sensor networks, especially as further sensor iterations are commonly smaller and more compact, allowing increased network portability. In this section I will discuss some of the recent developments in the models of low-cost sensors used in previous chapters of this thesis. I will also discuss the likely future development of the low-cost sensor market on a wider scale and highlight some potential benefits and pitfalls to these developments.

The particulate sensors used in the PurpleAir instruments on the Island of Hawai‘i during the 2018 LERZ eruption of Kīlauea volcano were Plantower PMS5003 sensors [Section 2.3.2]. Plantower has now released a new version of the sensor, the PMS7003, which has the same particle size measurement capability (Plantower, 2016b) [Table 5.1]. The main difference between the two sensor models is the product dimensions, with the PMS7003 being approximately half the width and significantly lighter than the

PMS5003 (Plantower, 2016a; Plantower, 2022) [Table 5.1]. A recent study by Bulot et al., 2019 tested the PMS5003 and PMS7003 in an urban outdoor location for 12 months and found that the two sensor models recorded similar measurement accuracy levels [Table 5.1]. In the upgraded Plantower model, the sensor housing has been made significantly more compact, seemingly without compromising the accuracy of the sensor. A sensor upgrade which maintains instrument accuracy but halves the product dimensions could be highly useful for monitoring of both volcanic and anthropogenic particulates. The portability of the PMS7003, and required battery and control units, could allow personal particulate monitoring for urban or volcanic environments. One potential application for this could be provision of personal hand-held sensors for tourists and visitors to volcanic areas, allowing early-warning of poor air quality and the potential need to evacuate areas.

The low-cost particulate sensor used in the AQMesh pods in the environment downwind of Masaya volcano in Chapter 3 of this thesis was the OPC-N2 instrument, produced by Alphasense Ltd. In 2018, Alphasense released the OPC-N3, an updated version of the OPC-N2 (Alphasense, 2018). The two instruments are identical in terms of structure, size and weight, and the main difference in the upgraded model is the capability to monitor a wider range of particle size diameters [Table 5.1]. The OPC-N3 also features an increased number of measurement bins, 24 bins increased from 16 in the OPC-N2, allowing an enhanced investigation of particle sizes (Alphasense, 2015a; Alphasense, 2015b).

AQ-SPEC, 2022a compared both Alphasense OPC models to a reference-grade GRIMM particulate monitor in an outdoor urban environment. They found that the OPC-N3 had a better accuracy rating for fine particles in the PM_1 size range, but the OPC-N2 was more accurate for measuring $PM_{2.5}$ particles (AQ-SPEC, 2022b; AQ-SPEC, 2022c) [Table 5.1]. In this instance, the improved accuracy rating of the OPC-N3 with respect to finer PM_1 particles is beneficial for monitoring of volcanic pollution, which contain a large proportion of finer particles (Chapter 4, Ilyinskaya et al. 2021; Mason et al. 2021). However, these co-location evaluations illustrate that successive iterations of low-cost sensors may not always result in improved measurement accuracy across the sensor range. This highlights the necessity for all low-cost sensors, including iterated versions of the same model, to be carefully analysed and assessed to determine their measurement accuracy and their suitability for air quality monitoring. Following the release of the OPC-N3, the OPC-N2 version has been phased out of commercial sales and is no longer available for purchase from Alphasense Ltd. Although this is beneficial in that air quality studies using particle sensors from Alphasense are now recording measurements on the upgraded OPC-N3, it also means that previous studies of air quality using the OPC-N2 version cannot be replicated.

Table 5.1: Development of low-cost particulate sensors used in Chapters 2 and 3 of this thesis. Specifications of the models used in the thesis are compared to specifications of the upgraded models. The relative accuracy of the models is shown in comparison to reference-grade particulate monitors (GRIMM and Beta Attenuation Monitor (BAM)). Note that Ch refers to Chapter.

Manufacturer	Model Version		Size (mm)	Weight (g)	Particle diameter detection range (µm)	Model accuracy	References
Plantower	Used in Ch. 2	PMS5003	50 x 38 x 21	42	0.3 to 10	$PM_{2.5}$: R^2 0.88 (compared to BAM)	Plantower, 2016a Bulot et al., 2019
	Upgraded	PMS7003	48 x 37 x 12	27	0.3 to 10	$PM_{2.5}$: R^2 0.87 (compared to BAM)	Plantower, 2022 Plantower, 2016b Bulot et al., 2019
Alphasense	Used in Ch. 3	OPC-N2	75 x 34 x 60	105	0.38 to 17	PM_1: R^2 0.63 - 0.82; $PM_{2.5}$: R^2 0.65 - 0.8 (compared to GRIMM)	AQ-SPEC, 2022a Alphasense, 2015a
	Upgraded	OPC-N3	75 x 34 x 60	105	0.35 to 40	PM_1: R^2 0.78 - 0.82; $PM_{2.5}$: R^2 0.53 - 0.67 (compared to GRIMM)	AQ-SPEC, 2022a Alphasense, 2015b

Table 5.2: Development of low-cost SO_2 gas sensors used in Chapters 3 and 4 of this thesis. Specifications of the model used in the thesis are compared to specifications of the upgraded model. Note that Ch refers to Chapter.

Manufacturer	Model Version		Size (diameter mm)	Weight (g)	Overgas limit (ppm)	Response time (s)	References
Alphasense	Used in Ch. 2, 3	SO2-B4	32	13	200	60	Alphasense, 2021
	Upgraded	SO2-D4	13	2	50	15	Alphasense, 2022

In Chapters 3 and 4 of this thesis, the low-cost SO_2 electrochemical sensors used in the environments downwind of Masaya volcano and Fagradalsfjall volcano were SO2-B4 sensors manufactured by Alphasense Ltd [Sections 3.2.1 and 4.2.1]. These sensors have been frequently used in both urban and volcanic air quality monitoring networks with reasonable levels of measurement accuracy (Mead et al., 2013; Roberts et al., 2012; Roberts et al., 2017; Shinohara, 2005). Alphasense Ltd have recently released a new model of SO_2 electrochemical sensors, the SO2-D4 series, which is significantly smaller and lighter than the SO2-B4 series [Table 5.2]. The response time, the time in which the sensor is able to detect concentrations of SO_2, is also massively improved on the new SO2-D4 model [Table 5.2] (Alphasense, 2022). The reduction in response time is an extremely valuable improvement to the sensor capabilities as it allows short-term spikes in pollutant concentrations to be identified. Additionally, in low-cost instrument systems which monitor both PM and SO_2, such as the AQMesh pods used in Chapter 3, it is beneficial for sensors to have similar response times to reduce lag in the measurements of different pollutant types, and the necessary subsequent data processing. The OPC-N2 in the AQMesh pods have a nearly instantaneous response time (as a benefit of the optical particle operating system), and the significant reduction in response time of the SO2-D4 would improve the measurement capabilities of AQMesh pods and similar multi-pollutant monitoring systems. No research, as far as I am aware, has yet investigated the accuracy of the SO2-D4 with respect to the SO2-B4 and a reference-grade SO_2 monitor. However, the specifications of the SO2-D4 indicate that the sensor has a much lower overgas limit compared to the larger SO2-B4 model [Table 5.2], indicating that the model will be unable to cope with concentrations of SO_2 exceeding 50 ppm (Alphasense, 2022). This is not likely to be an issue in downwind volcanic environments, where SO_2 concentrations rarely exceed 1 ppm (Delmelle et al., 2002; Ilyinskaya et al., 2017b; Whitty et al., 2020), but would be a potential concern if the SO2-D4 was used for near-vent volcanic gas monitoring.

These examples of sensor development follow a continuing trend across the wider low-cost instrument market, where the specifications of the instruments are continually being improved towards a wider range of measurement possibilities and more compact instrument dimensions (Clements et al., 2017; Robinson et al., 2018). The improved portability of low-cost instruments lends itself to a wider accessibility for monitoring networks, both in terms of remote and difficult locations for downwind volcanic monitoring, and for the option of personalised air quality monitoring in urban and volcanic environments (Robinson et al., 2018). The widening scope of pollutant monitoring capabilities, such as with the OPC-N3, increases the potential uses for instruments in the air quality monitoring community. Reduced response times, as shown with the SO2-D4 series, improves the ability of the low-cost instruments to report spikes in pollutant levels.

These instrument improvements bring massive potential benefits to the use of low-cost air quality sensors and illustrate how their design and implementation may be taken forward in future years. However, the downside of such a dynamic instrument market which rapidly produces new instruments is that the research and evaluation of new sensors lags behind the market. When low-cost sensors are installed in a monitoring environment without a robust analysis of their ability to effectively monitor pollutant concentrations, the credibility of the recorded data is significantly undermined (Cross et al., 2017). It is therefore crucial that, as the low-cost sensor market develops, research and analysis of new sensors is carefully and meticulously carried out (Clements et al., 2017; Rai et al., 2017). End-users of low-cost sensors should be rigorous in researching the capability and effectiveness of sensors, and should choose sensors with the best monitoring ability for their study, even if that involves using a previous version which has undergone more vigorous evaluations.

5.4 Application of low-cost instruments

Low-cost air quality instruments, as well as becoming widespread among the scientific research community, are also becoming popular with non-scientific community groups and members of the public. One example among many are the individual public purchases and installations of low-cost PurpleAir instruments on the Island of Hawai‘i during the 2018 LERZ eruption of Kīlauea volcano [Chapter 2]. In areas where air quality measurements by reference-grade instruments are limited or non-existent, "crowed-sourced" or citizen-science data collection using low-cost instruments can be an extremely valuable source of data (Loiselle et al., 2017; Thompson, 2016). Additionally, low-cost instruments have uses as educational tools for schools, developing students' abilities in STEM (science, technology, engineering and maths) subjects and engaging them in a wider critical analysis of the world around them (Williams et al., 2014). Likewise, low-cost sensors can be used for informal air quality networks to widen awareness of air quality issues (Lewis and Edwards, 2016; Williams et al., 2014). The relatively cheap cost, ease of use and small size of low-cost sensors makes them appealing to members of the public who are interested in air quality. As a result, the proliferation of low-cost air quality sensors is increasing, with a vast array of instrument models installed around the world (Thompson, 2016).

While this instrument proliferation is ideal in providing a large volume of air quality data and a wider public awareness towards air quality, the largely-untested nature of the instruments poses significant problems. The vast majority of low-cost air quality instrumentation has not been independently evaluated for measurement accuracy and precision, resulting in questionable data outputs (Lewis and Edwards 2016, Cross et al. 2017, DEFRA, 2022a). Members of the public typically lack the technical means to verify the measurements themselves, and must trust the instrument specifications and

accuracy levels indicated by the supplier (Lewis and Edwards, 2016). This becomes a critical issue when the low-cost instrument measurements are used for decision-making on a community or personal level. For example, on the basis of measurements from a low-cost particulate sensor, children may be encouraged to play in parks near busy roads where air quality in reality is poorer than the low-cost instrument indicated. Similarly, during periods of volcanic unrest, low-cost instruments could result in a false sense of security among the public, or an unnecessary level of panic. Both end-members of the spectrum can cause harm when used in personal decision-making, in the first case by individuals not taking measures to reduce their exposure to pollutants and in the second case by isolating themselves indoors unnecessarily.

Citizen science or "crowd-sourced" low-cost networks, such as the PurpleAir instruments installed during the 2018 LERZ eruption on the Island of Hawai‘i, can provide air quality data for scientific research. There are advantages and disadvantages to using this data for scientific research. For example, instruments which are purchased and installed by members of the public tend to be located on private property, which reduces the risk of theft or vandalism that can sometimes occur with instruments installed by research groups. Instruments which are owned by members of the public are also likely to be maintained regularly. For example, batteries are likely to be replaced promptly and minor maintenance issues may be resolved quickly via the individual contacting their supplier or obtaining a new instrument. This is in contrast to some scientific networks, such as the AQMesh network downwind of Masaya volcano [Chapter 3], of which the whole network is maintained by the research group and delays in maintenance can result in periods of missing data. However, publicly owned and managed instruments can have significant disadvantages. For example, there is no information provided to establish the exact location of the low-cost instrument in the context of the environment. Members of the public may unknowingly install their instrument in a manner that compromises the accuracy of the measurements, for example, by choosing a location that is too sheltered or in proximity to a pollution source. It is therefore important that low-cost air quality instruments have clear instructions for operation, detailing the optimal installation requirements of the instrument while using language that is accessible to all potential end-users.

In instances where researchers use a network of low-cost instruments to measure air quality, it can be extremely valuable for them to provide the public with access to the measurement output in real-time. This could be achieved either by using low-cost instruments from companies providing in-built data presentation services, for example PurpleAir instruments (PurpleAir, 2019; Whitty et al., 2020) and AQMesh pods (Crilley et al., 2020; Whitty et al., 2022), or by designing and implementing custom-built data infrastructure. Provision of real-time data visualisation from low-cost instruments would allow the public to engage and benefit from the research ongoing in their local area, but

under conditions where the researchers can verify the low-cost instrument measurements and highlight levels of measurement uncertainty. This would widen the awareness of the public, both towards potential issues with air quality in their local region and towards the measurement limitations of low-cost air quality instrumentation. In such a way, real-time data visualisation benefits communities in the downwind volcanic measurement area but also benefits the researcher by contributing knowledge and providing a real-world impact through their work, which is often a requirement for research conducted under grant funding.

Low-cost sensors will inevitably spread further into the public domain as time continues and technology advances. It is therefore critical for regulators to set manufacturer guidelines to ensure that instruments are produced to a minimum standard of accuracy and with clearly-defined uncertainty levels (Lewis and Edwards, 2016). Community awareness should also be promoted, with educational programmes to inform and caution the public in their use of low-cost air quality sensors (Jiang et al. 2018, DEFRA, 2022b).

5.5 Optimised methodology for plume dispersion models

The majority of the work presented in this thesis examines volcanic SO_2 and particulate air quality using networks of reference-grade and low-cost instrumentation. However, in Chapter 4, I used outputs from the CALPUFF plume dispersion model, operated and run by the Icelandic Meteorological Office, in combination with ground-based air quality measurements to indicate the potential population exposure to volcanic SO_2. While I did not run the CALPUFF model myself, I have gained insight into the application of the model by ground-truthing the forecast outputs to instrument observations [Section 4.2.3.1]. As such, in this section I indicate potential modifications that could be made to the model constraints and inputs to reduce output errors and improve ground-truth comparisons. I discuss the recent applications of the CALPUFF model for forecasting the 2021 Fagradalsfjall eruption in Iceland and a trial implementation period at Masaya volcano in Nicaragua by the UNRESP project (Chapter 4, Barsotti et al. 2018; UNRESP 2018). In both instances, the CALPUFF model over-estimated the concentration of SO_2 at ground level, indicating that further work is required to better define the model's optimal methodology.

One of the key input parameters to the CALPUFF model is the description of the volcanic source. It is critical that the SO_2 flux, as well as the thickness of the plume and its injection height into the atmosphere, is accurately described and frequently updated to reflect the dynamic nature of the eruption (Scire et al., 2000). In the trial application of the CALPUFF plume dispersal model at Masaya volcano, the source description remained constant with a steady SO_2 flux of 250 t/d, based on previous

research at Masaya volcano (Barsotti et al., 2018; Ilyinskaya et al., 2017a). Conversely, in the application of the CALPUFF model at the 2021 Fagradalsfjall eruption, the source description input was modified, if necessary, prior to each model run [Chapter 4]. In both examples, the CALPUFF model over-estimated the concentrations of SO_2 at ground level, but the magnitude of the over-estimation varied significantly. At Masaya volcano, ground-truth comparison to observations indicated that over-estimation was by a factor of 100 (Barsotti et al., 2018), whereas during the Fagradalsfjall eruption the over-estimation was by a factor of 7 [Section 4.3.4.1]. At Masaya volcano, the SO_2 flux and plume characteristics are not monitored or reported on, making it a significant challenge to input an accurate source description to the CALPUFF model in this location. However, the variability between over-estimation levels of the CALPUFF model at Fagradalsfjall and Masaya volcano indicates that, wherever possible, accurate and frequently updated source descriptions are key to successful implementation of the CALPUFF plume dispersal model.

An additional challenge faced by the CALPUFF model at Masaya volcano was the complex small-scale meteorological dynamics. In the region frequently affected by the volcanic plume the topography varies considerably between deep valleys and high ridgelines, resulting in complicated wind shear dynamics. The close proximity of the large body of water, Laguna de Masaya, to the emission source may have also influenced the behaviour of the plume, adding complexities beyond the processing capabilities of the CALPUFF model (Barsotti et al., 2018). The meteorological inputs to the CALPUFF model were sourced from the European Centre for Medium-Range Weather Forecasts (ECMWF) with a resolution of 0.125 degrees ($\approx$ 12 km at the equator) (Barsotti et al., 2018), which may have been too coarse a resolution to accurately describe the complex atmospheric dynamics. In instances where the topography is variable around the volcanic source, and the meteorological conditions are complex or liable to alter rapidly, it would be beneficial to have meteorological observations to validate the ECMWF forecast inputs. These could be via a ground-based meteorological station or from periodic radiosonde (balloon-borne) measurements.

In Chapter 4 of this thesis, I calculated a re-scaled version of the CALPUFF model output to reduce the over-estimation of the SO_2 concentrations at ground-level [Section 4.2.3.1]. The accuracy of the re-scaled model output varied with distance from the eruption site, with a greater accuracy level within 15 km of the eruption and less accuracy at distances $>$ 15 km [Section 4.4.2]. A similar but opposite effect was found by the UNRESP project with their trial of the CALPUFF model at Masaya volcano. Here, the mismatch between the forecast and observed SO_2 concentrations was higher in locations within 10 km of the volcanic source, and a better match was achieved at distances more than 10 km from the source (Ilyinskaya et al., 2017a). The discrepancy in the CALPUFF model's prediction of SO_2 concentrations in the downwind environ-

ments could potentially be due to the user-defined values of chemical conversion between SO_2 and SO_4. The inverted findings between Iceland and Nicaragua indicate that the atmospheric conditions may play a role in the ground-truth discrepancy. For example, the high temperature and humidity conditions in Nicaragua may have resulted in a faster conversion rate of SO_2 to SO_4, resulting in an overestimation of SO_2 at near-field locations. Conversely, a slower conversion rate in the cooler Icelandic climate may have resulted in overestimation of SO_2 in locations > 15 km away from source. More research into the rates of chemical conversion across different volcanic plumes may allow greater insight into this question. In the meantime, future applications of the CALPUFF model could alter the user-defined chemical conversion inputs to determine whether small modifications in the conversion rate may result in a better comparison to pollutant observations at ground-level.

5.6 Community adaptions and involvement

Volcanic gas and aerosol emissions affect millions of people around the world, either as a result of short-term sporadic eruptions or over longer time periods resulting from prolonged eruptive activity or persistent passive degassing (Hansell and Oppenheimer, 2004). Across different cultures and societies, communities have adapted to reside in areas that are periodically or chronically affected by volcanic air pollution. It is important to observe and discuss these community adaptations to determine whether methods can be replicated from one volcanic area to another and whether the lessons learned by one community can benefit others in similar situations. Additionally, communities affected by persistent emissions can be an invaluable source of information regarding long-term volcanic emission dispersal, providing observations of potential seasonal or diurnal patterns as well as describing the impact and negative health outcomes that exposure can cause (Delmelle et al., 2002; Ilyinskaya et al., 2017a; van Manen, 2014). In almost all cases, involving communities in research can produce more meaningful and long-term impacts and benefits than would result from research where communities were not involved. In this section, I will discuss how communities across the three study sites in this thesis respond and adapt to living with volcanic air pollution, and their involvement in the monitoring of volcanic emissions.

The communities in the areas downwind of Masaya volcano, Nicaragua, clearly illustrate how societies can adapt to living with persistent volcanic air pollution. The communities use methods including cultivating specific crops (pineapples and dragon fruit) which thrive in the acidic volcanic soils, as well as using non-metal materials (cement, wood and stone blocks) to construct and maintain buildings to reduce structural damage from the corrosive volcanic emissions (Ilyinskaya et al., 2017a; Whitty et al., 2022). Farmers found that animals reared within the volcanic region were more likely to have a natural resilience to the volcanic pollutants, while animals brought in from else-

where tended to have a shorter lifespan and more prevalence of disease in the downwind volcanic areas (UNRESP, 2018). Such methods allow these communities to develop a level of resilience to the economic and practical aspects of living with persistent volcanic emissions. They can also be an example to researchers installing air quality monitoring networks in the area, indicating the need to protect instruments from the corrosive volcanic environment (Whitty et al., 2020).

Community adaptions can also help individuals, particularly those who are more vulnerable due to their age or underlying health conditions, to limit their exposure to volcanic air pollution. In Nicaragua, neighbours relay qualitative information regarding the presence and strength of volcanic pollutants, and organise farming and workloads to reduce exercise levels during periods of intense emissions (Ilyinskaya et al., 2017a). Similarly, in Hawai‘i, social media communication allows community members to highlight periods of intense volcanic air pollution, increasing the awareness of the issue across the wider community (Vog Talk, 2022).

In all three case study areas, official and unofficial advice is to remain indoors when volcanic emissions cause poor air quality in populated areas (IVHHN, 2020, IVHHN, 2022). In Iceland, buildings are typically constructed of concrete with double-glazed windows, offering good protection from outdoor air pollution. However, the cultural norm in Iceland is to let infants sleep outdoors during the day which can lead to higher potential exposure when the public is unaware of an episode of volcanic air pollution (Chapter 4, Carlsen et al. 2021b). In Hawai‘i and Nicaragua, buildings often have an open structure and are not air-tight, meaning that individuals may still be exposed to pollutants even while indoors (Horwell and Elias, 2020). Construction of air-tight buildings in Hawai‘i and Nicaragua would be impractical considering the frequently warm and humid climate, where the lack of ventilation in an air-tight building would result in uninhabitable indoor temperatures. Installation of air conditioning would solve this issue, though this would likely be cost-prohibitive in many instances. In Nicaragua, many households cook their food indoors using solid-fuel fires or stoves, meaning that air-tight buildings would result in significant indoor air pollution (Ilyinskaya et al., 2017a). It is clear that there is no one-size-fits-all solution for exposure reduction methods. Recommendations must take into account the many and varied social, cultural and economic factors as well as the concentration and frequency of volcanic air pollution episodes.

Generally, exposure reduction methods are reliant on some level of knowledge of the presence of volcanic pollutants, either via unofficial word-of-mouth or through official channels and public advisories. It is clear that development of effective volcanic pollutant monitoring and forecasting with timely communication to the public would greatly assist exposure reduction methods, therefore potentially lowering the negative health impacts within these communities. This clearly shows the critical need for permanent

air quality monitoring systems in areas where volcanic emissions are dispersed through populated areas.

One of the most consistent societal observations across the three study sites in this thesis is the interest that the communities show towards volcanic eruptions and volcanic air pollution in their region. In Iceland during the 2014 - 2015 Holuhraun eruption, there were 138 instances of members of the public self-reporting symptoms of nausea and headaches to online questionnaires provided by the Icelandic Meteorological Office (Carlsen et al., 2021a). In Nicaragua, communities in the area downwind of Masaya volcano were keen participants of the UNRESP project. Information events organised to convey scientific findings to the local communities were attended by the majority of community populations, including individuals across all generations. On the Island of Hawai'i, residents actively engage in social media groups to discuss volcanic emissions, their impact on day-to-day life and also to provide qualitative descriptions of the distribution of volcanic air pollution across the island (Vog Talk, 2022).

This level of community interest towards volcanic eruptions and volcanic air pollution can be a valuable asset to research, as communities can act as willing collaborators in data collection and provision of information. For example, during the 2018 LERZ eruption of Kīlauea volcano, community members individually purchased and installed low-cost PurpleAir particulate sensors, providing a data-set of high-resolution particulate measurements [Section 2.5.2] (Whitty et al., 2020). In Nicaragua, van Manen, 2014 used community interviews to determine the perceived risks and impacts of volcanic air pollution in the area downwind of Masaya volcano. Similarly, the UNRESP project interviewed community members to gain local knowledge of the long-term volcanic emissions from Masaya volcano. Community members conveyed that the volcanic air pollution is generally more noticeable during the rainy-season months (June to September) each year and that the water supplies in the region become affected during intense pollution episodes (Ilyinskaya et al., 2017a; UNRESP, 2018). At Masaya volcano there is no air quality monitoring network, but the high level of community engagement could be a valuable tool for hazard assessment in future if a crowd-sourced "*did you feel it*" web-server system was established. This would allow researchers to determine where and when the impact of volcanic air pollution was noticed by community members, and feed the information back to government authorities and decision makers.

5.7 Future work

In this section, I briefly outline directions for future research. I consider potential routes to improve low-cost instrument methodology and processing. I discuss how a permanent air quality monitoring network could be established in the area downwind of Masaya volcano if finances and infrastructure was available. I also discuss alternative options

which could be used as first-steps towards data-gathering and information dissemination in this area if resources were limited.

With regards to low-cost instrumentation, the following work to improve methodology and protocols would dramatically maximise the potential of these sensors:

- Design and implementation of automated data processing systems for low-cost instruments. This would include automation of user-defined validation checks and automatic calculation of humidity-correction factors for particulate measurements.
- Development of protocols for the use of low-cost instruments to better constrain how and when these instruments are appropriate to use and the level and frequency of calibration checks required to verify measurement outputs.
- Rigorous standardised evaluation of all new models and versions of low-cost sensors, including laboratory and field calibration studies with reference-grade counterparts. These studies should be widely publicised to highlight areas of concern as well as identifying specific low-cost sensors that are deemed trustworthy.
- Educational outreach programmes highlighting limitations of low-cost sensors to end-users among the public.

At Masaya volcano, Nicaragua, implementation of a permanent air quality monitoring network in the downwind area is crucial for better quantifying the level of volcanic air pollution which communities are exposed to. In an idealised scenario where funding and infrastructure were available, I would recommend the following steps towards development of a suitable air quality network and to provide more information to community residents and decision-makers.

- Installation of one or more SO_2 and particulate reference-grade monitors in the downwind area, including development of mains electricity and support infrastructure. The positioning of the reference-grade instrument(s) should be in a suitable location frequently affected by the volcanic air pollution [Section 3.4.2].
- Installation of a network of SO_2 and particulate low-cost instruments to augment the reference-grade network. The low-cost instruments should be installed following recommendations in Section 5.2.
- Establishment of an air quality index in Nicaragua to allow quantification of air quality and risk levels.
- Development of protocols for decision-making including thresholds for SO_2 concentrations at which public advisories should be issued.
- Further research into negative health impacts resulting from Masaya's volcanic air pollution, and development of official guidance towards personal exposure reduc-

tion.

Under a perhaps more realistic scenario where infrastructure and funding are limited, the following steps could be implemented in the area downwind of Masaya volcano. These steps would provide some level of information-gathering and air quality knowledge, and hopefully establish momentum to develop a more effective and comprehensive monitoring system in future.

- Development of a "*did you feel it*" web-server system using qualitative citizen-science data-gathering to determine the frequency of noticeable volcanic air pollution in communities.
- Regular meetings between community members and decision-makers to encourage communication of air quality issues, community concerns and potential hazard-mitigation steps.

5.8 Summary and conclusions

The work in this thesis is concerned with characterising the downwind SO_2 and particulate pollutants from volcanic emission sources. I examined three case studies, using a variety of instruments, methods and techniques throughout the thesis. Here in Chapter 5, I have discussed ways in which the methodology used in the research chapters could be improved to reduce instrument and network limitations and to maximise their potential. The recommendations discussed in this chapter towards development of hybrid monitoring networks, improved implementation of low-cost sensors and towards the reduction of ground-truth mismatch in applications of the CALPUFF dispersal model will hopefully assist researchers aiming to examine downwind volcanic SO_2 and particulates in future. As discussed in Sections 5.3 and 5.4, the development of low-cost sensors is likely to continue at pace, along with the proliferation of sensor installation by members of the public. These advancements lead to significant concerns regarding the lack of evaluation of instruments and validation of data outputs. I recommended that low-cost instruments be used with caution to reduce the potential for negative impacts resulting from their use for personal and community decision-making. The outlined directions for future research indicate areas of investigation which I would have liked to implement if time and resources were available.

References

Alphasense. (2015a). Alphasense User Manual OPC-N2 Optical Particle Counter [(Accessed 05/02/2020)]. *https://colandino.nl/wp-content/uploads/datasheet/072-0300_OPC-N2_manual_issue_3.pdf*.

Alphasense. (2015b). OPC-N3 Particle Monitor [(Accessed 21/07/2022)]. *https://www.alphasense.com/wp-content/uploads/2019/03/OPC-N3.pdf*.

Alphasense. (2018). New wide-ranging particulate sensor [Available at: https://www.alphasense.com/wp-content/uploads/2018/10/OPC-N3-Press-Release.pdf]. *Press Information*.

Alphasense. (2021). SO2-B4 Sulfur Dioxide Sensor Data Sheet [(Accessed 05/02/2021)]. *https://www.alphasense.com/wp-content/uploads/2019/09/SO2-B4.pdf*.

Alphasense. (2022). SO2-D4 Sulfur Dioxide Sensor Data Sheet [(Accessed 01/08/2022)]. *https://www.alphasense.com/wp-content/uploads/2020/12/SO2-D4.pdf*.

AQ-SPEC. (2022a). Air quality sensor performance evaluation centre [(Accessed 23/05/2022)]. *http://www.aqmd.gov/aq-spec/evaluations/summary-pm*.

AQ-SPEC. (2022b). Air quality sensor performance evaluation centre - OPC-N2 [(Accessed 21/07/2022)]. *http://www.aqmd.gov/docs/default-source/aq-spec/summary/alphasense-opc-n2---summary-report.pdf?sfvrsn=14*.

AQ-SPEC. (2022c). Air quality sensor performance evaluation centre - OPC-N3 [(Accessed 21/07/2022)]. *http://www.aqmd.gov/docs/default-source/aq-spec/summary/alphasense-opc-n3---summary-report.pdf?sfvrsn=20*.

Barsotti, S., Richardson, M., O'Neill, J., Ilyinskaya, E., & Strauch, W. (2018). Modelling and forecasting volcanic gas cloud dispersal from Masaya volcano: towards a warning system [DOI: http://editoria.rm.ingv.it/miscellanea/2018/miscellanea43/]. *Cities on Volcanoes Conference Abstracts*, S02.02, page 880.

Bulot, F. M., Johnston, S. J., Basford, P. J., Easton, N. H., Apetroaie-Cristea, M., Foster, G. L., Morris, A. K., Cox, S. J., & Loxham, M. (2019). Long-term field comparison of multiple low-cost particulate matter sensors in an outdoor urban environment. *Scientific reports*, *9*(1), 1–13.

Carlsen, H. K., Ilyinskaya, E., Baxter, P., Schmidt, A., Thorsteinsson, T., Pfeffer, M., Barsotti, S., Dominici, F., Finnbjornsdottir, R. G., Jóhannsson, T., Aspelund, T., Gislason, T., Valdimarsdóttir, U., Briem, H., & Gudnason, T. (2021a). Increased respiratory morbidity associated with exposure to a mature volcanic plume from a large Icelandic fissure eruption [DOI: https://doi.org/10.1038/s41467-021-22432-5]. *Nature Communications*, *12*.

Carlsen, H. K., Valdimarsdóttir, U., Briem, H., Dominici, F., Finnbjornsdottir, R. G., Jóhannsson, T., Aspelund, T., Gislason, T., & Gudnason, T. (2021b). Severe volcanic SO2 exposure and respiratory morbidity in the Icelandic population–a register study [DOI: https://doi.org/10.1186/s12940-021-00698-y]. *Environmental Health*, *20*(1), 1–12.

Chen, G., Li, S., Zhang, Y., Zhang, W., Li, D., Wei, X., He, Y., Bell, M. L., Williams, G., Marks, G. B. et al. (2017). Effects of ambient PM_1 air pollution on daily emergency hospital visits in China: An epidemiological study [DOI: https://

doi.org/10.1016/S2542-5196(17)30100-6]. *The Lancet Planetary Health*, *1*(6), e221–e229.

Clements, A. L., Griswold, W. G., Rs, A., Johnston, J. E., Herting, M. M., Thorson, J., Collier-Oxandale, A., & Hannigan, M. (2017). Low-cost air quality monitoring tools: From research to practice (a workshop summary). *Sensors*, *17*(11), 2478.

Crawford, B., Hagan, D. H., Grossman, I., Cole, E., Holland, L., Heald, C. L., & Kroll, J. H. (2021). Mapping pollution exposure and chemistry during an extreme air quality event (the 2018 Kı¯lauea eruption) using a low-cost sensor network [DOI: https://doi.org/10.1073/pnas.2025540118]. *Proceedings of the National Academy of Sciences*, *118*(27).

Crilley, L. R., Singh, A., Kramer, L. J., Shaw, M. D., Alam, M. S., Apte, J. S., Bloss, W. J., Hildebrandt Ruiz, L., Fu, P., Fu, W. et al. (2020). Effect of aerosol composition on the performance of low-cost optical particle counter correction factors [DOI: https://doi.org/10.5194/amt-13-1181-2020]. *Atmospheric Measurement Techniques*, *13*(3), 1181–1193.

Cross, E. S., Williams, L. R., Lewis, D. K., Magoon, G. R., Onasch, T. B., Kaminsky, M. L., Worsnop, D. R., & Jayne, J. T. (2017). Use of electrochemical sensors for measurement of air pollution: Correcting interference response and validating measurements [DOI: https://doi.org/10.5194/amt-10-3575-2017]. *Atmospheric Measurement Techniques*, *10*(9), 3575–3588.

Delmelle, P., Stix, J., Baxter, P., Garcia-Alvarez, J., & Barquero, J. (2002). Atmospheric dispersion, environmental effects and potential health hazard associated with the low-altitude gas plume of Masaya volcano, Nicaragua [DOI: https://doi.org/10.1007/s00445-002-0221-6]. *Bulletin of Volcanology*, *64*(6), 423–434.

Department for Environment Food and Rural Affairs. (2022a). 'Low-cost' pollution sensors - understanding the uncertainties [(Accessed 19/08/2022)]. *https://uk-air.defra.gov.uk/research/aqeg/pollution-sensors/understanding-uncertainties.php*.

Department for Environment Food and Rural Affairs. (2022b). AQEG advice on the use of 'low-cost' pollutionsensors [(Accessed 19/08/2022)]. *https://uk-air.defra.gov.uk/research/aqeg/pollution-sensors.php*.

González-Garcıá, Y., González, S., & Souto, R. (2007). Electrochemical and structural properties of a polyurethane coating on steel substrates for corrosion protection [DOI: https://doi.org/10.1016/j.corsci.2007.03.018]. *Corrosion Science*, *49*(9), 3514–3526.

Hansell, A., & Oppenheimer, C. (2004). Health hazards from volcanic gases: A systematic literature review [DOI: https://doi.org/10.1080/00039890409602947]. *Archives of Environmental Health: An International Journal*, *59*(12), 628–639.

Horwell, C. J., & Elias, T. (2020). 'This advice is absurd': issues with providing generic advice on community protection from chronic volcanic degassing [DOI: https://

doi.org/10.5194/egusphere-egu2020-16190]. *EGU General Assembly Conference Abstracts*, 16190.

Ilyinskaya, E., Mason, E., Wieser, P., Holland, L., Liu, E., Mather, T., Edmonds, M., Whitty, R., Elias, T., Nadeau, P., Schneider, D., McQuaid, J., Allen, S., Harvey, J., Oppenheimer, C., Kern, C., & Damby, D. (2021). Rapid metal pollutant deposition from the volcanic plume of Kı¯lauea, Hawai'i [DOI: https://doi.org/10.1038/s43247-021-00146-2]. *Communications Earth and Environment*.

Ilyinskaya, E., Norbert, S., Leiva, X., Francis, H., Baxter, P., Barsotti, S., & Williams, C. (2017a). Unseen but not unfelt: resilience to persistent volcanic emissions (UNRESP). Case study from Masaya volcano. *Progress report on 1st project phase*.

Ilyinskaya, E., Schmidt, A., Mather, T. A., Pope, F. D., Witham, C., Baxter, P., Jóhannsson, T., Pfeffer, M., Barsotti, S., Singh, A. et al. (2017b). Understanding the environmental impacts of large fissure eruptions: Aerosol and gas emissions from the 2014–2015 Holuhraun eruption (Iceland) [DOI: https://doi.org/10.1016/j.epsl.2017.05.025]. *Earth and Planetary Science Letters*, *472*, 309–322.

International Volcanic Health Hazard Network. (2020). The health hazards of volcanic and geothermal gases: A guide for the public [(Accessed 12/4/2021)]. *https://www.ivhhn.org/information/health-impacts-volcanic-gases#Howtolivewithvolcanicemissions*.

International Volcanic Health Hazard Network. (2022). Protect yourself from vog - Hawaii Interagency Vog Information Dashboard [(Accessed 17/8/2022)]. *https://vog.ivhhn.org/vog-protection*.

Jiang, Q., Bregt, A. K., & Kooistra, L. (2018). Formal and informal environmental sensing data and integration potential: Perceptions of citizens and experts. *Science of The Total Environment*, *619*, 1133–1142.

Lewis, A., & Edwards, P. (2016). Validate personal air-pollution sensors. *Nature*, *535*(7610), 29–31.

Lewis, A. C., Lee, J. D., Edwards, P. M., Shaw, M. D., Evans, M. J., Moller, S. J., Smith, K. R., Buckley, J. W., Ellis, M., Gillot, S. R. et al. (2016). Evaluating the performance of low cost chemical sensors for air pollution research [Available at: https://pubs.rsc.org/en/content/articlelanding/2016/FD/C5FD00201J]. *Faraday discussions*, *189*, 85–103.

Li, Z., Marston, N., & Stokes, K. (2018). Materials within geothermal environments [Available at: https://d39d3mj7qio96p.cloudfront.net/media/documents/SR393_Materials_within_geothermal_environments.pdf]. *BRANZ study report SR393*.

Liu, X., Xiong, J., Lv, Y., & Zuo, Y. (2009). Study on corrosion electrochemical behavior of several different coating systems by EIS [DOI: https://doi.org/10.1016/j.porgcoat.2008.08.012]. *Progress in Organic Coatings*, *64*(4), 497–503.

Loiselle, S. A., Frost, P. C., Turak, E., & Thornhill, I. (2017). Citizen scientists supporting environmental research priorities. *Science of the Total Environment*, *598*, 937.

Malings, C., Tanzer, R., Hauryliuk, A., Saha, P. K., Robinson, A. L., Presto, A. A., & Subramanian, R. (2019). Fine particle mass monitoring with low-cost sensors: Corrections and long-term performance evaluation [DOI: https://doi.org/10.1080/02786826.2019.1623863]. *Aerosol Science and Technology*, 1–40.

Mason, E., Wieser, P., Liu, E., Edmonds, M., Ilyinskaya, E., Whitty, R., Mather, T., Elias, T., Nadeau, P., Wilkes, T. et al. (2021). Volatile metal emissions from volcanic degassing and lava-seawater interactions at Kı¯lauea Volcano, Hawai'i [DOI: https://doi.org/10.1038/s43247-021-00145-3]. *Communications Earth and Environment*.

Mead, M., Popoola, O., Stewart, G., Landshoff, P., Calleja, M., Hayes, M., Baldovi, J., McLeod, M., Hodgson, T., Dicks, J. et al. (2013). The use of electrochemical sensors for monitoring urban air quality in low-cost, high-density networks [DOI: https://doi.org/10.1016/j.atmosenv.2012.11.060]. *Atmospheric Environment*, *70*, 186–203.

Plantower. (2016a). Digital universal particle concentration sensor PMS5003 series data manual [(Accessed 13/11/2018)]. *http://www.aqmd.gov/docs/default-source/aq-spec/resources-page/plantower-pms5003-manual_v2-3.pdf*.

Plantower. (2016b). Digital universal particle concentration sensor PMS7003 series data manual [(Accessed 01/08/2022)]. *https://download.kamami.pl/p564008-PMS7003%20series%20data%20manua_English_V2.5.pdf*.

Plantower. (2022). Laser particle sensor product display [(Accessed 01/08/2022)]. *https://www.plantower.com/products_16/*.

PurpleAir. (2019). PurpleAir: Air Quality Monitoring [(Accessed 26/10/2018)]. *https://www.purpleair.com/*.

Rai, A. C., Kumar, P., Pilla, F., Skouloudis, A. N., Di Sabatino, S., Ratti, C., Yasar, A., & Rickerby, D. (2017). End-user perspective of low-cost sensors for outdoor air pollution monitoring [DOI: https://doi.org/10.1016/j.scitotenv.2017.06.266]. *Science of The Total Environment*, *607*, 691–705.

Roberts, T., Braban, C., Oppenheimer, C., Martin, R., Freshwater, R., Dawson, D., Griffiths, P., Cox, R., Saffell, J., & Jones, R. (2012). Electrochemical sensing of volcanic gases [DOI: https://doi.org/10.1016/j.chemgeo.2012.08.027]. *Chemical Geology*, *332*, 74–91.

Roberts, T., Saffell, J., Oppenheimer, C., & Lurton, T. (2014). Electrochemical sensors applied to pollution monitoring: Measurement error and gas ratio bias — a volcano plume case study [DOI: https://doi.org/10.1016/j.jvolgeores.2014.02.023]. *Journal of volcanology and geothermal research*, *281*, 85–96.

Roberts, T. J., Lurton, T., Giudice, G., Liuzzo, M., Aiuppa, A., Coltelli, M., Vignelles, D., Salerno, G., Couté, B., Chartier, M. et al. (2017). Validation of a novel Multi-Gas sensor for volcanic HCl alongside H_2S and SO_2 at Mt. Etna [DOI: https://doi.org/10.1007/s00445-017-1114-z]. *Bulletin of volcanology*, *79*(5), 36.

Robinson, J. A., Kocman, D., Horvat, M., & Bartonova, A. (2018). End-user feedback on a low-cost portable air quality sensor system—are we there yet? *Sensors*, *18*(11), 3768.

Scire, J. S., Strimaitis, D. G., Yamartino, R. J. et al. (2000). A user's guide for the CALPUFF dispersion model [Available at: http://www.src.com/CALPUFF/download/CALPUFF_UsersGuide.pdf]. *Earth Tech, Inc*, *521*, 1–521.

Shinohara, H. (2005). A new technique to estimate volcanic gas composition: Plume measurements with a portable multi-sensor system [DOI: https://doi.org/10.1016/j.jvolgeores.2004.12.004]. *Journal of Volcanology and Geothermal Research*, *143*(4), 319–333.

Thompson, J. E. (2016). Crowd-sourced air quality studies: A review of the literature & portable sensors. *Trends in Environmental Analytical Chemistry*, *11*, 23–34.

UNRESP. (2018). Unseen but not unfelt: Resilience to persistent volcanic emissions [(accessed 12/2/2018)]. *https://unresp.wordpress.com/*.

van Manen, S. M. (2014). Perception of a chronic volcanic hazard: Persistent degassing at Masaya volcano, Nicaragua [DOI: https://doi.org/10.1186/s13617-014-0009-3]. *Journal of Applied Volcanology*, *3*(1), 9.

Vog Talk. (2022). Facebook Vog Talk Public Group [(Accessed 17/8/2022)]. *https://www.facebook.com/groups/VogTalk*.

Wang, H., Lu, F., Guo, M., Fan, W., Ji, W., & Dong, Z. (2021). Associations between PM_1 exposure and daily emergency department visits in 19 hospitals, Beijing [DOI: https://doi.org/10.1016/j.scitotenv.2020.142507]. *Science of The Total Environment*, *755*, 142507.

Whitty, R., Pfeffer, M., Ilyinskaya, E., Roberts, T., Schmidt, A., Barsotti, S., Strauch, W., Crilley, L., Pope, F., Bellanger, H., Mendoza, E., Mather, T., Liu, E., Peters, N., Taylor, I., Francis, H., Hernández Leiva, X., Lynch, D., Nobert, S., & Baxter, P. (2022). Effectiveness of low-cost air quality monitors for identifying volcanic SO_2 and PM downwind from Masaya volcano, Nicaragua [DOI: https://doi.org/10.30909/vol.05.01.3359]. *Volcanica*, *5*(1), 33–59.

Whitty, R. C. W., Ilyinskaya, E., Mason, E., Wieser, P. E., Liu, E. J., Schmidt, A., Roberts, T., Pfeffer, M. A., Brooks, B., Mather, T. A., Edmonds, M., Elias, T., Schneider, D. J., Oppenheimer, C., Dybwad, A., A, N. P., & Kern, C. (2020). Spatial and temporal variations in SO_2 and $PM_{2.5}$ levels around Kīlauea volcano, Hawai'i during 2007–2018 [DOI: https://doi.org/10.3389/feart.2020.00036]. *Frontiers in Earth Science*, *8*, 36.

Williams, R., Vasu Kilaru, E., Snyder, A., Kaufman, T., Dye, A., Rutter, A., & Russell, H. (2014). Air Sensor Guidebook [DOI: https://cfpub.epa.gov/si/si_public_record_report.cfm?Lab=NERL&dirEntryId=277996&simpleSearch=1&searchAll=air+sensor+guidebook]. *U.S. Environmental Protection Agency.*

Yang, M., Chu, C., Bloom, M. S., Li, S., Chen, G., Heinrich, J., Markevych, I., Knibbs, L. D., Bowatte, G., Dharmage, S. C. et al. (2018). Is smaller worse? new insights about associations of PM_1 and respiratory health in children and adolescents [DOI: https://doi.org/10.1016/j.envint.2018.08.027]. *Environment international*, *120*, 516–524.

Appendix A

Supplementary material for Chapter 4

Appendix figures A.1 to A.7 display the SO_2 and PM measurements from individual stations within the seven measurement groups of Chapter 4. The specific locations of the stations are shown in Figure 4.2.

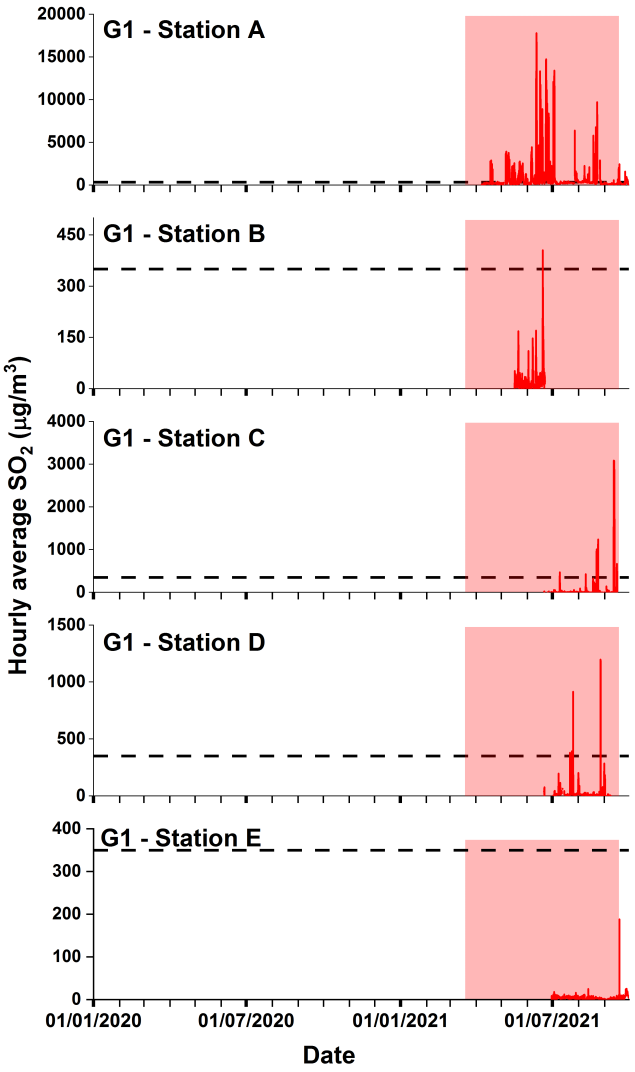

Figure A.1: Measurements from individual stations within G1. The red highlight indicates the eruption period. The horizontal black dashed line indicates the ID hourly SO_2 threshold of $350\,\mu g/m^3$.

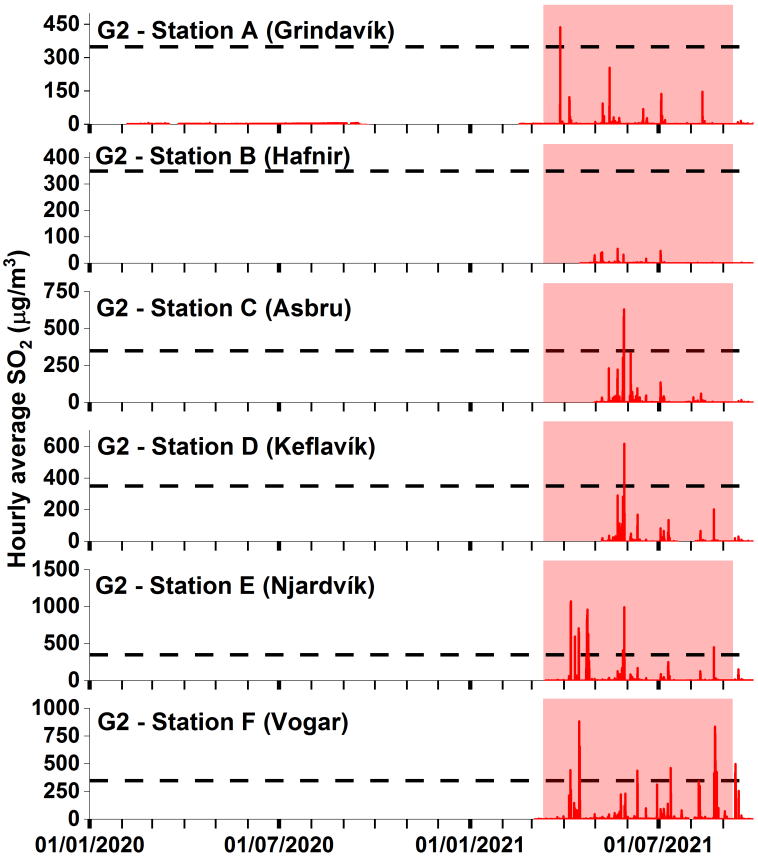

Figure A.2: Measurements from individual stations within G2. The red highlight indicates the eruption period. The horizontal black dashed line indicates the ID hourly SO_2 threshold of $350\,\mu g/m^3$.

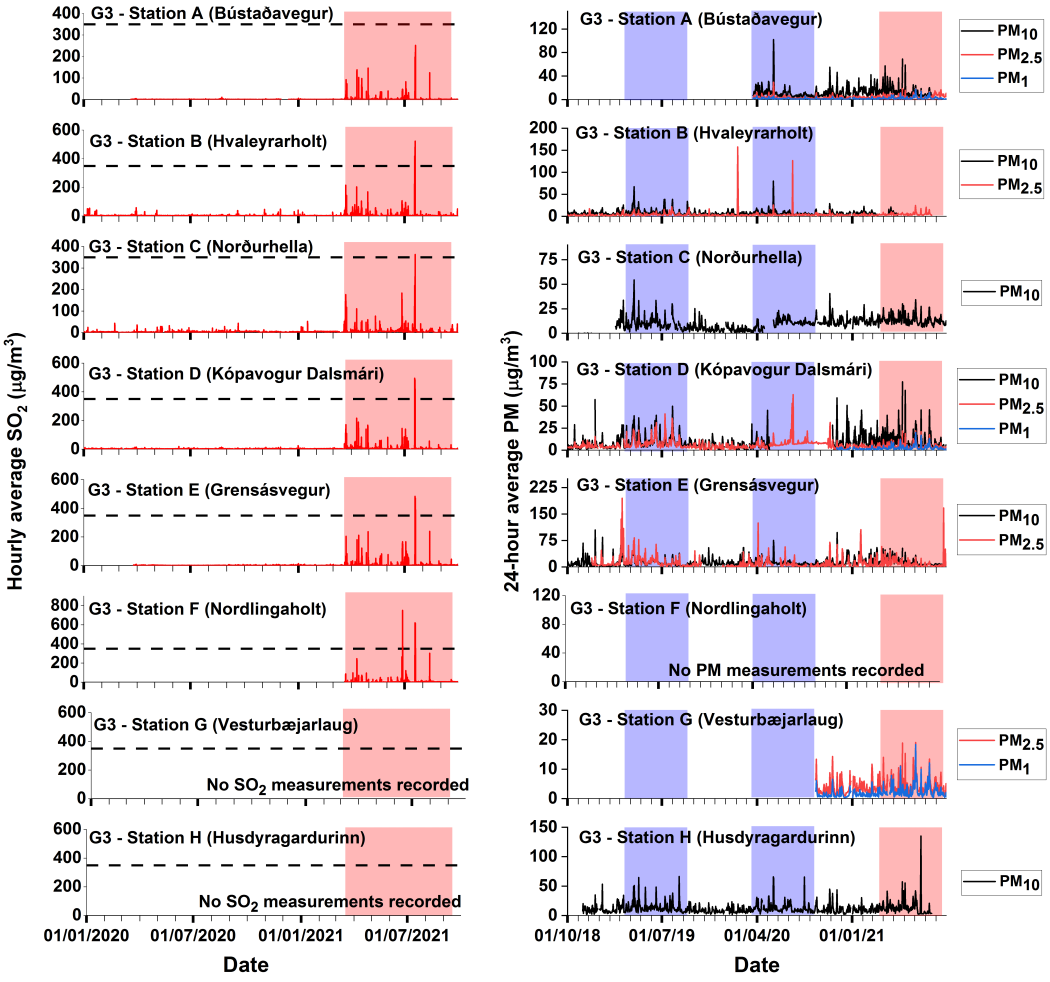

Figure A.3: Measurements from individual stations within G3. Blue highlighted periods in the PM data indicate the BG1 and BG2 background periods. The red highlight indicates the eruption period. The horizontal black dashed line indicates the ID hourly SO_2 threshold of 350 µg/m^3.

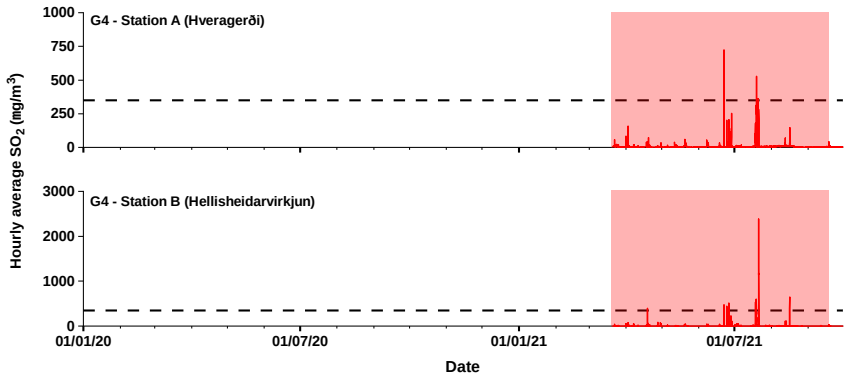

Figure A.4: Measurements from individual stations within G4. The red highlight indicates the eruption period. The horizontal black dashed line indicates the ID hourly SO_2 threshold of 350 µg/m^3.

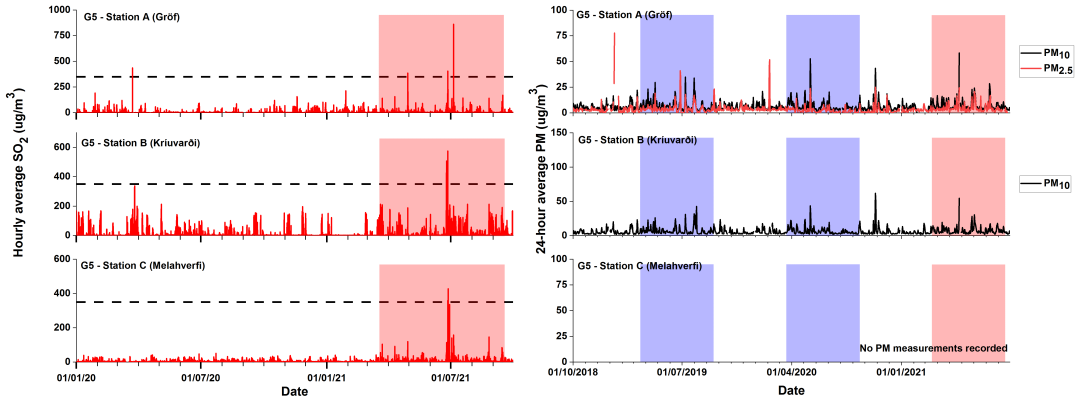

Figure A.5: Measurements from individual stations within G5. Blue highlighted periods in the PM data indicate the BG1 and BG2 background periods. The red highlight indicates the eruption period. The horizontal black dashed line indicates the ID hourly SO_2 threshold of $350\,\mu g/m^3$.

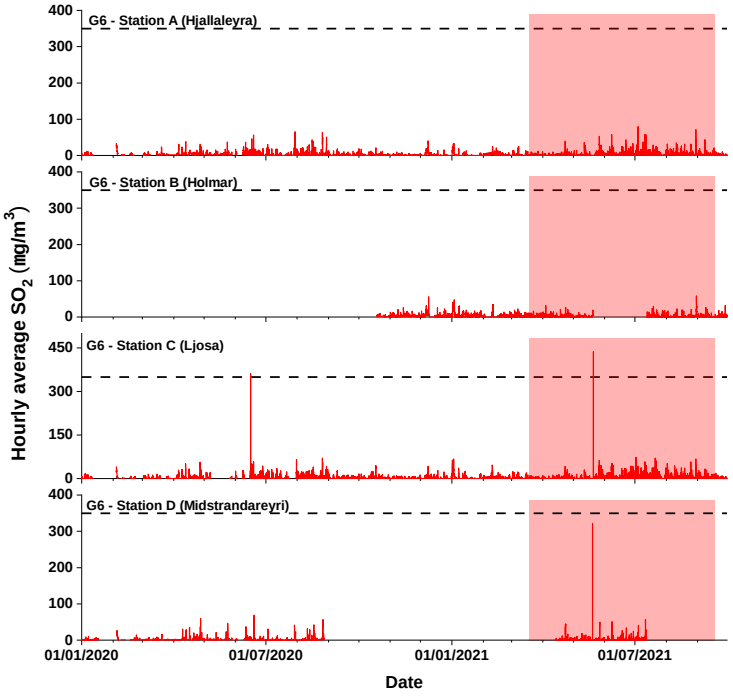

Figure A.6: Measurements from individual stations within G6. The red highlight indicates the eruption period. The horizontal black dashed line indicates the ID hourly SO_2 threshold of $350\,\mu g/m^3$.

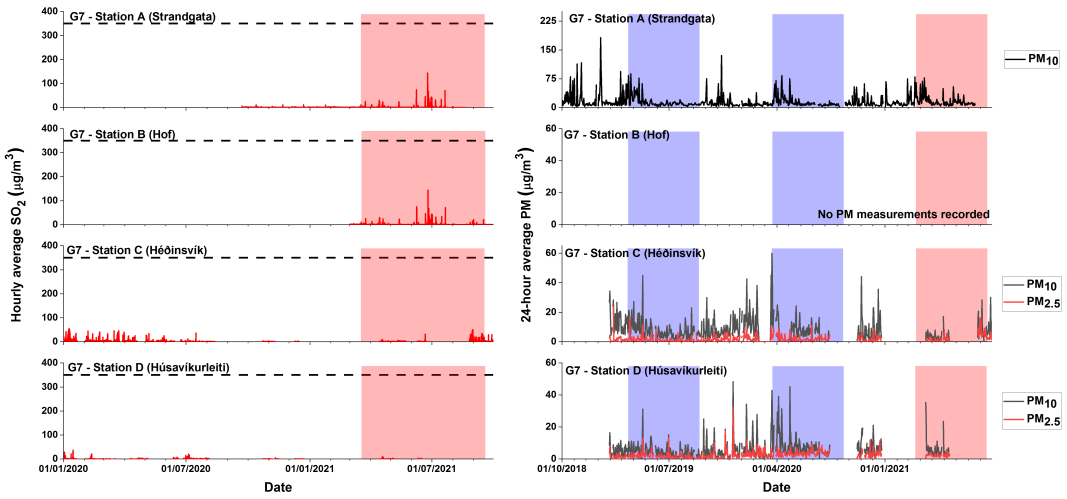

Figure A.7: Measurements from individual stations within G7. Blue highlighted periods in the PM data indicate the BG1 and BG2 background periods. The red highlight indicates the eruption period. The horizontal black dashed line indicates the ID hourly SO_2 threshold of $350\,\mu g/m^3$.